AD-A164 322 PITCH-LOCATION EFFECTS ON DYNAMIC STALL(U) AIR FORCE INST OF TECH WRIGHT-PATTERSON AFB OH SCHOOL OF ENGINEERING R L DIMMICK DEC 85 AFIT/GAE/AA/85D-4 1/2

UNCLASSIFIED F/G 20/4 NL

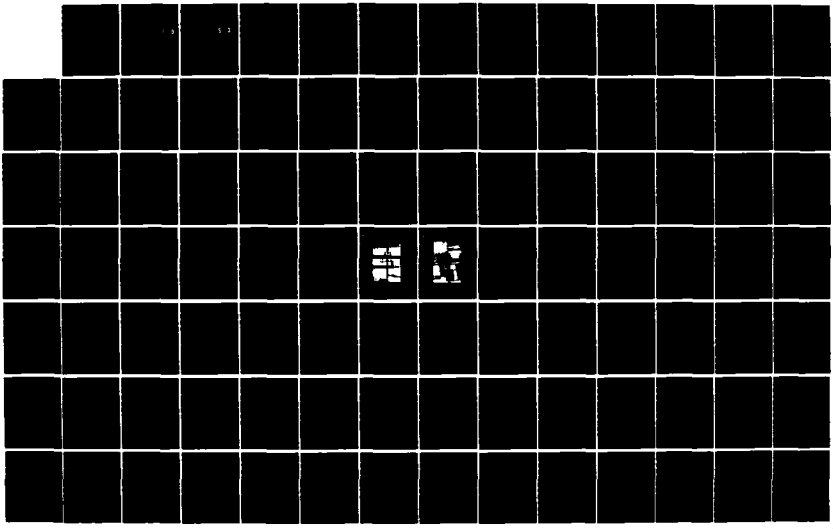

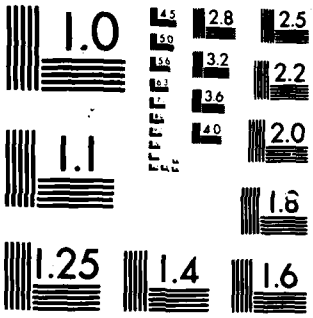

MICROCOPY RESOLUTION TEST CHART

NATIONAL BUREAU OF STANDARDS 1963-A

AD-A164 322

DTIC
ELECTE
FEB 1 8 1986
S D
D

PITCH-LOCATION EFFECTS

ON DYNAMIC STALL

THESIS

Robert L. Dimmick
Captain, USAF

AFIT/GAE/AA/85D-4

DTIC FILE COPY

DISTRIBUTION STATEMENT A
Approved for public release;
Distribution Unlimited

DEPARTMENT OF THE AIR FORCE
AIR UNIVERSITY
AIR FORCE INSTITUTE OF TECHNOLOGY

Wright-Patterson Air Force Base, Ohio

86 2 14 018

AFIT/GAE/AA/85D-4

DTIC
ELECTE
FEB 1 4 1986
S D
D

PITCH-LOCATION EFFECTS

ON DYNAMIC STALL

THESIS

Robert L. Dimmick
Captain, USAF

AFIT/GAE/AA/85D-4

Approved for public release; distribution unlimited

AFIT/GAE/AA/85D-4

PITCH-LOCATION EFFECTS ON DYNAMIC STALL

THESIS

Presented to the Faculty of the School of Engineering

of the Air Force Institute of Technology

Air University

In Partial Fulfillment of the

Requirements for the Degree of

Master of Science in Aeronautical Engineering

Accesion For

NTIS CRA&I ☑
DTIC TAB ☐
Unannounced ☐
Justification

By
Distribution /

Availability Codes

Dist	Avail and / or Special
A-1	

Robert L. Dimmick, B.S.

Captain, USAF

December 1985

Approved for public release; distribution unlimited

Acknowledgements

While performing this investigation and writing this thesis I have become indebted to numerous individuals. I would like to thank Lt Col Eric Jumper, my advisor, whose patience, reassurance, and constant guidance made this investigation possible. I would also like to thank the personnel in the AFIT model shops who helped create the experimental setup. The exceptional talents of Leroy Cannon made the electronic complexity of this experiment possible, and the willing assistance of Jay Anderson and his knowledge of digital electronics was also deeply appreciated. Nick Yardich ensured the smoke tunnel was always operational and provided assistance throughout every aspect of this work. I would like to thank Capt Wes Cox for sharing his knowledge of wind tunnels and testing procedure and providing excellent guidance during this study. Capt Scott Schreck, my predecessor in this experiment, was always willing to help and kept me out of trouble on many occasions. Finally, I would like to express my deepest appreciation to my wife, Maggie, whose constant support and continual sacrifices have made this investigation a reality.

Table of Contents

	Page
Acknowledgements	ii
List of Figures	v
List of Tables	x
List of Symbols	xi
Abstract	xii
I. Introduction	1
Background	1
Objectives	13
II. Theory and Approach	15
Dynamic Stall in Contrast to Static Stall	15
Determination of Pressure Coefficient	17
Discretization of the Pressure Distribution	21
Integration of the Pressure Distribution	22
Determination of Force Coefficients	24
The Problem of Data Acquisition	25
III. Facilities and Instrumentation	27
Smoke Tunnel	27
Velocity Measurement	27
Airfoil	28
Transducers	30
Drive Mechanism	31
Data Acquisition System	32
IV. Experimental Procedure	37
Transducer Calibration	37
Data Collection	37
Exceptions	41
Velocities and Reynolds Numbers	42

Page

V. Data Reduction and Discussion of Results . . 44

Data Reduction 44
Discussion of Results 46
Error Sources 75

VI. Conclusions and Recommendations 78

Conclusions 78
Recommendations 79

Bibliography 81

Appendix A: Transducer Calibration 84

Appendix B: Software Package 91

Appendix C: Remainder of Plotted Results 111

Vita 173

List of Figures

Figure		Page
1.	Data Summary of Deekens' and Kuebler's Results for Quarter-Chord Separation . . .	5
2.	Data Summary of Daley's Results for Quarter Chord Separation	8
3.	Data Summary of Schreck's Results and Daley's Results	12
4.	Airfoil Pressure Transducer Locations	23
5.	Airfoil Endplates and Pitch Locations	29
6.	Airfoil Drive Mechanism and Position Potentiometer Mounted on Test Stand	33
7.	Experimental Equipment and Data Acquisition System	34
8.	Airfoil Dynamic Stall Pressure Distribution (V = 29.07 fps, α = 22.1°, $\dot{\alpha}$ = 118 °/sec)	47
9.	Airfoil Dynamic Stall Pressure Distribution (V = 29.07 fps, α = 27.5°, $\dot{\alpha}$ = 118 °/sec)	48
10.	Airfoil Dynamic Stall Pressure Distribution (V = 29.07 fps, α = 30.8°, $\dot{\alpha}$ = 118 °/sec)	49
11.	Airfoil Dynamic Stall Pressure Distribution (V = 29.07 fps, α = 37.0°, $\dot{\alpha}$ = 118 °/sec)	50
12.	Airfoil Dynamic Stall Pressure Distribution (V = 29.07 fps, α = 38.8°, $\dot{\alpha}$ = 118 °/sec)	51
13.	Combined Dynamic Stall Lift Curves $\dot{\alpha}_{ND}$ = .021, .027, .036 Respectively V = 29.07, Pitch Location #3 (.50c) . . .	53
14.	Combined Dynamic Stall Drag Curves $\dot{\alpha}_{ND}$ = .021, .027, .036 Respectively V = 29.07, Pitch Location #3 (.50c) . . .	54
15.	Combined Dynamic Stall Pitching Moment Curves $\dot{\alpha}_{ND}$ = .021, .027, .036 Respectively V = 29.07, Pitch Location #3 (.50c) . . .	55

Figure		Page
16.	Data Summary for Pitch Location #1 (.08c)	58
17.	Data Summary for Pitch Location #2 (.25c)	60
18.	Data Summary for Pitch Location #3 (.50c)	63
19.	Combined Data Summary for Pitch Locations 1-3	65
20.	Data Summary for Pitch Location #4 (.61c)	68
21.	Combined Data Summary for Pitch Locations 1-4	69
22.	Data Summary for Pitch Locations 1-4 Using the Pitch Location Angular Rate (α^*)	71
23.	Data From Static Stall Lift Curve V = 30.0 fps, Pitch Location #1 (.08c)	72
24.	Combined Data From Static Stall Lift Curves Pitch Locations 1 - 4, V = 25.0 to 40.4 fps	74
25.	Pressure Transducer Calibration Chamber . . .	85
26.	Airfoil Mounted on Calibration Chamber Baseplate	87
27.	Data From Test Run 1 - 1	114
28.	Data From Test Run 1 - 2	115
29.	Data From Test Run 1 - 3	116
30.	Data From Test Run 1 - 4	117
31.	Data From Test Run 1 - 5	118
32.	Data From Test Run 1 - 6	119
33.	Data From Test Run 1 - 7	120
34.	Data From Test Run 1 - 8	121
35.	Data From Test Run 1 - 9	122
36.	Data From Test Run 1 - 10	123
37.	Data From Test Run 1 - 11	124

Figure		Page
38.	Data From Test Run 1 - 12	125
39.	Data From Static Stall Test Runs Pitch Location #1 (.08c), V = 25.0 to 37.9 fps	126
40.	Data From Test Run 2 - 1	127
41.	Data From Test Run 2 - 2	128
42.	Data From Test Run 2 - 3	129
43.	Data From Test Run 2 - 4	130
44.	Data From Test Run 2 - 5	131
45.	Data From Test Run 2 - 6	132
46.	Data From Test Run 2 - 7	133
47.	Data From Test Run 2 - 8	134
48.	Data From Test Run 2 - 10	135
49.	Data From Test Run 2 - 11	136
50.	Data From Test Run 2 - 12	137
51.	Data From Test Run 2 - 13	138
52.	Data From Test Run 2 - 14	139
53.	Data From Test Run 2 - 15	140
54.	Data From Static Stall Test Runs Pitch Location #2 (.25c), V = 25.2 to 45.0 fps	141
55.	Data From Test Run 3 - 1	142
56.	Data From Test Run 3 - 2	143
57.	Data From Test Run 3 - 3	144
58.	Data From Test Run 3 - 4	145
59.	Data From Test Run 3 - 5	146

Figure		Page
60.	Data From Test Run 3 - 7	147
61.	Data From Test Run 3 - 8	148
62.	Data From Test Run 3 - 9	149
63.	Data From Test Run 3 - 10	150
64.	Data From Test Run 3 - 11	151
65.	Data From Test Run 3 - 13	152
66.	Data From Test Run 3 - 14	153
67.	Data From Test Run 3 - 15	154
68.	Data From Test Run 3 - 16	155
69.	Data From Test Run 3 - 17	156
70.	Data From Test Run 3 - 18	157
71.	Data From Test Run 3 - 19	158
72.	Data From Static Stall Test Runs Pitch Location #3 (.50c), V = 25.6 to 44.1 fps	159
73.	Data From Test Run 4 - 1	160
74.	Data From Test Run 4 - 2	161
75.	Data From Test Run 4 - 3	162
76.	Data From Test Run 4 - 4	163
77.	Data From Test Run 4 - 5	164
78.	Data From Test Run 4 - 6	165
79.	Data From Test Run 4 - 7	166
80.	Data From Test Run 4 - 8	167
81.	Data From Test Run 4 - 9	168
82.	Data From Test Run 4 - 10	169

Figure Page

83. Data From Test Run 4 - 11 170

84. Data From Test Run 4 - 12 171

85. Data From Static Stall Test Runs
Pitch Location #4 (.61c),
V = 25.7 to 39.8 fps 172

List of Tables

Table		Page
I.	Importance of Dynamic Stall Parameters . .	16
II.	Data Summary for Pitch Location #1	57
III.	Data Summary for Pitch Location #2	60
IV.	Data Summary for Pitch Location #3	62
V.	Data Summary for Pitch Location #4	67
VI.	Transducer Calibration Sensitivities . . .	90
VII.	Summary of Test Conditions	112

List of Symbols

α	angle of attack
$\dot{\alpha}$	angle of attack angular rate
$\dot{\alpha}_{ND}$	nondimensional angular rate
$\dot{\alpha}^*$	nondimensional angular rate based on pitch location
V	freestream velocity
c	airfoil chord
$C_{LMAX\ DYN}$	maximum dynamic lift coefficient
$C_{LMAX\ ST}$	maximum static lift coefficient
$\alpha_{STALL\ DYN}$	dynamic stall angle of attack
$\alpha_{STALL\ ST}$	static stall angle of attack
C_P	pressure coefficient
P_{LOC}	airfoil local static pressure
P_∞	freestream static pressure
ΔP_{TRAN}	differential pressure sensed by transducer
P_A	ambient pressure
P_o	freestream stagnation pressure
mV	millivolts
psi	pounds per square inch
psig	pounds per square inch gage

Abstract

Experimental investigations were conducted in the AFIT Smoke Tunnel to study the effects of pitch location on dynamic stall. A NACA 0015 airfoil was rotated about four different locations at a constant angular rate and digital position and pressure information were recorded. This information was then converted into airfoil pressure distributions and integrated numerically to obtain airfoil force coefficients. Results of this investigation showed a direct relationship between the dynamic stall angle of attack and the nondimensionalized angular rotation rate, $\dot{\alpha}_{ND}$, defined as one half the airfoil chord length times the angular rate divided by the freestream velocity. Based on the three rotation points forward of the mid-chord, it was also shown that dynamic stall is delayed as the pitch location is moved aft from the leading edge. Experimental data was obtained for pitch locations of .08c, .25c, .50c and .61c and nondimensional angular rates between .011 and .065.

PITCH-LOCATION EFFECTS ON DYNAMIC STALL

I. Introduction

Background

Dynamic stall is a physical phenomenon that occurs when an airfoil undergoes a continuous, dynamic rotation through its static-stall angle of attack. During the dynamic stall event, the lift curve continues to increase beyond the static-stall point for a large range of rotation rate and freestream velocity combinations. Although it is only a transient event, the momentary increase in maximum unstalled angle of attack yields a corresponding increase in the lift generated by the airfoil. This greater lift is of sufficient magnitude to render the dynamic stall effect of some possible practical use, and therefore worthy of further investigation.

The first formal investigation of dynamic stall was conducted by Max Kramer in 1932 after pilots reported unexplained high lift values occurring while flying in turbulent air [14:1]. Kramer's experiment consisted of a wing mounted on a balance in a wind tunnel test section and a series of movable guide vanes, located upstream of the wing. By rotating the guide vanes, he created a varying freestream in the test section which

resulted in angles of attack ranging from 0 to 30 degrees [14:2-3]. Kramer conducted experiments on three airfoil shapes: the first two were Gottingen 459 airfoil cross-sections (symmetric airfoils, with different chord lengths), and the third was a Gottingen 398 airfoil cross-section (a cambered airfoil).

The results of Kramer's experiment showed a direct relationship between the maximum lift coefficient and the angular rotation rate, $\dot{a}$, and an inverse relationship to the test section velocity, V . By using a non-dimensional angular rate parameter $c\dot{a}/V$, where c is the airfoil chord length, Kramer collapsed all his data onto a single curve given by:

$$C_{L_{MAX\ DYN}} = C_{L_{MAX\ ST}} + 0.36\ c\dot{a}/V \qquad (1)$$

In the time since Kramer's experiment, a great deal of research, both analytical and experimental, has been devoted to the area of dynamic stall. However, unlike Kramer's experiment, the majority of research has involved an airfoil undergoing a dynamic angle-of-attack change in a constant-direction freestream, with the majority of this work involving a sinusoidally oscillating airfoil [16][18]. The reason dynamic stall research has taken this direction is fairly obvious.

The benefits of dynamic stall research have been most applicable to areas such as: helicopter blades, turbomachinary, and aircraft wing-flutter. In cases such as these the angle-of-attack variations are likely to be sinusoidal, or at least approximately so.

The advent of digital flight control systems promises new applications for the case of airfoils undergoing angle of attack variations described by a ramp function. A distinct advantage of the ramp angle-of-attack variation is the comparative ease and physical clarity with which a mathematical model may be developed. The mathematical model for the sinusoidal case lies in the realm of full Navier-Stokes solutions, and amounts to a very complex numerical experiment. While such an approach succeeds fairly well in modelling the results of a corresponding experiment, the sheer mathematical complexity overwhelms any attempt to generalize the solution and truly understand the physics of the phenomenon.

In 1979, Deekens and Kuebler [6] undertook an investigation of dynamic stall which evaluated the effects of constant airfoil angular rate. Smoke-trace flow visualization, in conjunction with simultaneous high speed filming, was used to characterize the dynamic stall phenomenon on an NACA 0015 airfoil, rotating about its midchord in a constant-velocity freestream. They

concluded that the increase in unstalled angle of attack for the dynamic case was directly related to airfoil anglular rate, and inversely related to the freestream velocity. Based on their findings, Deekens and Kuebler were able to accurately predict the dynamic stall angle of attack for their experiment, which covered Reynolds numbers between 14,500 and 32,500.

Introducing the same nondimensional angular rate parameter used by both Kramer and Docken, et. al., Deekens and Kuebler were able to collapse their data onto a single curve given by:

$$\alpha_{STALL\ DYN} = \alpha_{STALL\ ST} + 143.2\ \dot{\alpha}_{ND} \qquad (2)$$

where stall is defined as separation at the quarter-chord. A plot of these results, showing dynamic stall angle of attack as a function of nondimensional rotation rate parameter is shown in Fig. 1, on the following page.

By assuming the static and dynamic lift curves have the same slope and correcting that slope for the aspect ratio of Kramer's wing, Eq. 2 can be transformed into Eq. 3:

$$C_{LMAX\ DYN} = C_{LMAX\ ST} + 4.8\ \dot{\alpha}/V \qquad (3)$$

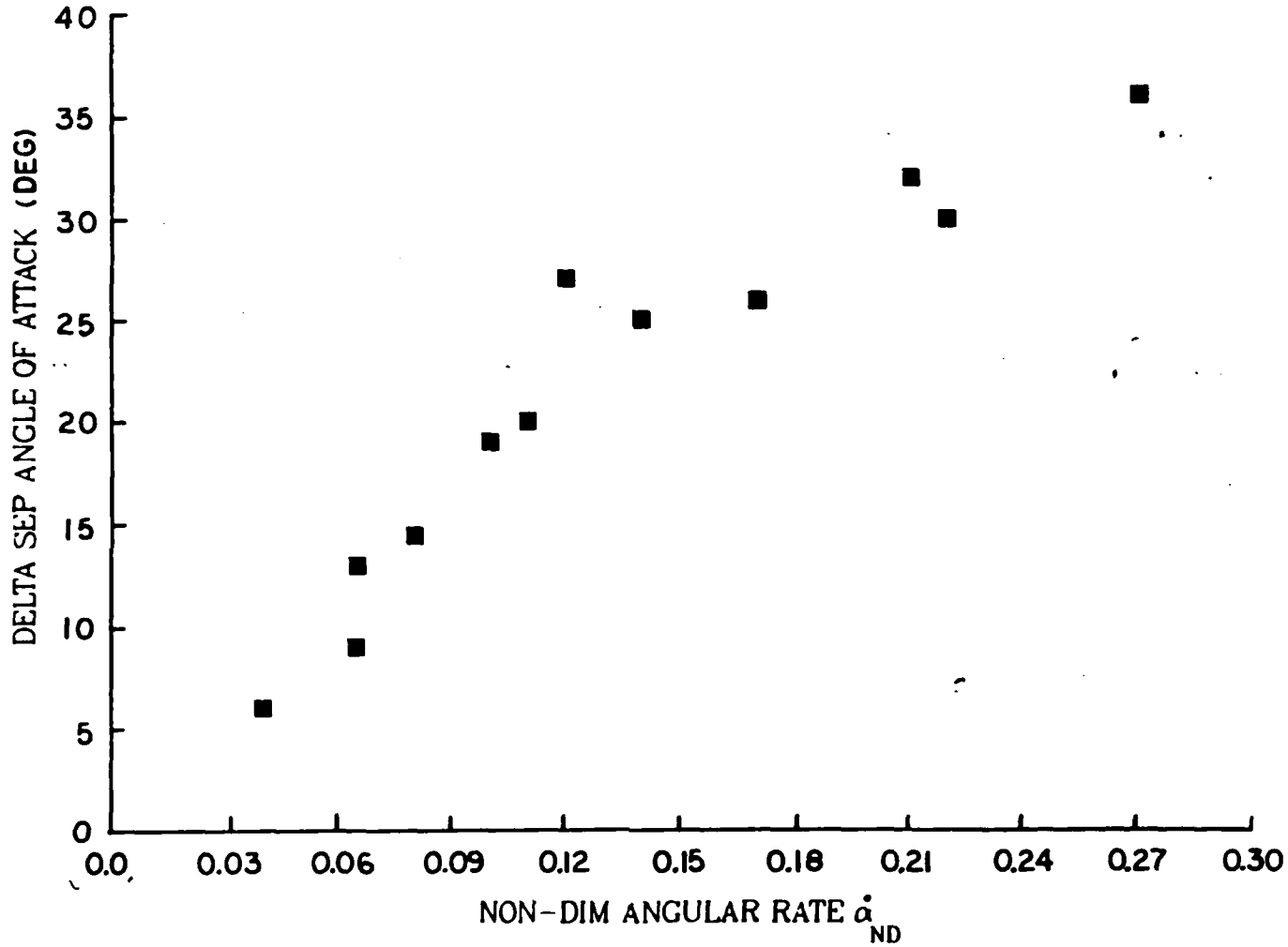

Figure 1. Data Summary of Deekens' and Kuebler's Results for Quarter Chord Separation

Comparing Eq. 1 with Eq. 3, it is immediately obvious that the dynamic lift curve slope implied by Deekens and Kuebler is significantly greater than that given by the work of either Kramer or Docken, et. al. [7]. An experimental or computational error of such magnitude to explain this apparent discrepancy can be ruled out since the results of Deekens and Kuebler are substantiated by the work of Francis, et. al. [9], and by Scheubel [22:1-4]. In addition, Kramer's work also seems to have been verified in an experiment mentioned by Scheubel [22:1].

At this point it becomes necessary to emphasize an important distinction between the work of Kramer and Deekens and Kuebler. In Kramer's experiment, as previously mentioned, the airfoil was fixed in intertial space and encountered a gust condition. Therefore, a mathematical model of the flow over the airfoil could justly assume a Newtonian, or nonaccelerating, control volume. However for the case of an airfoil rotating in a constant-velocity freestream, the airfoil is moving with respect to inertial space. In this situation, mathematical analysis of the flow over the airfoil cannot be accomplished using a Newtonian control volume. The previously mentioned order-of-magnitude disagreement between Kramer's results and those of Deekens and Kuebler could concievably be due to the effect of the

accelerating control volume.

The results of Deekens and Kuebler were again experimentally confirmed by Daley [5]. Like Deekens and Kuebler, Daley rotated a NACA 0015 airfoil section about its midchord at a constant angular rate in a constant-velocity freestream. He also used smoke-trace flow visualization in combination with high-speed motion pictures as a medium for recording and analyzing his results. However, Daley added a new dimension to the experiment by embedding four piezo- resistive pressure transducers in the airfoil quarter-chord region. This modification enabled him to simultaneously gather two types of data during the dynamic stall phenomenon. Using both movies and electronically-gathered pressure information, Daley possessed an extremely accurate and sensitive indicator of flow separation at the quarter-chord. Adopting quarter-chord flow separation as his criterion for stall, Daley proceeded to verify a major portion of Deekens and Kuebler's work. He also extended the range of results into a region of lower nondimensional angular rate, as shown in Fig. 2, and, at the same time, expanded the Reynolds number range of the experiment.

A great deal of analytical work in the field of dynamic stall was conducted during 1983 by Lawrence [15], Tupper [25], and Allaire [1]. The work of

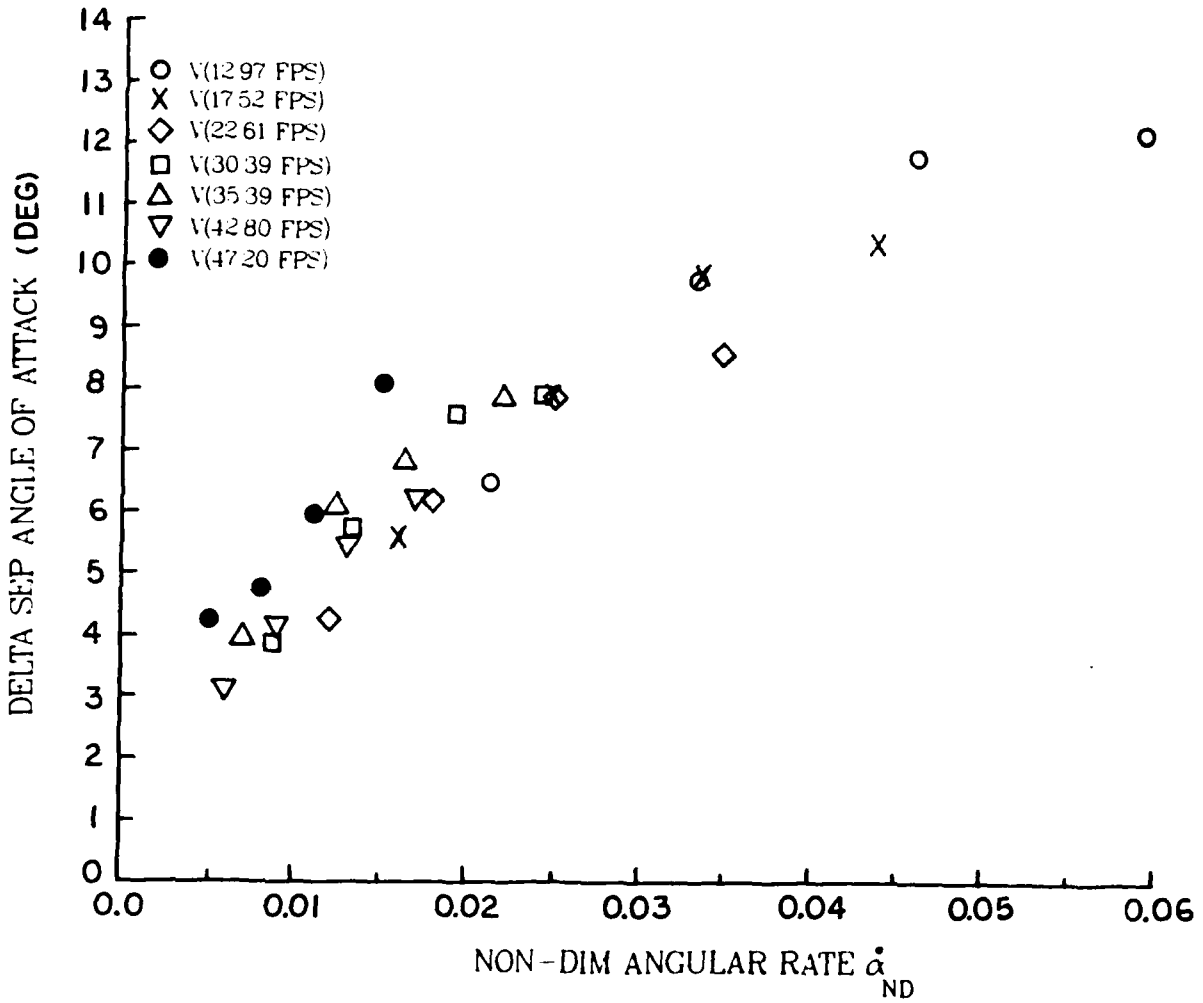

Figure 2. Data Summary of Daley's Results for Quarter Chord Separation

Lawrence was a direct continuation of Docken's [7] research. Lawrence took Docken's model and expanded it using a modified von Karman-Polhausen technique to obtain data for an airfoil rotating in inertial space. His research led to the conclusion that dynamic stall was a strong function of a non-dimensional pitch rate $\dot{\alpha}_{ND}=\frac{1}{2}c\dot{\alpha}/V$. A major factor in Lawrence's model was the introduction of a mass ingestion function. This function may be thought of as an energization of the airfoil boundary layer by mass "ingested" through the upper surface of the control volume during the rotation. Reference 13 contains a more complete description of this technique, including the appropriate mathematical development. Lawrence's work was taken one step further when Allaire used the same momentum integral method to investigate the effects of airfoil thickness, camber and pitch location on dynamic stall. At the same time that Lawrence was investigating the ability to accurately understand the phenomenon of dynamic stall using the integral method, it was obvious that something was still missing. This led Tupper to investigate the effects of trailing vortices on the production of lift for a rotating airfoil.

Tupper used a circular cylinder model which was subsequently transformed into an airfoil shape to analyze the sequence of events following the sudden

start of airfoil rotation. The results of his study produced two theoretical phenomena associated with dynamic stall. The first finding was that an airfoil undergoing a constant angular rate of change will experience a decrease in the lift curve slope. That is, the dynamic C_L vs α curve will have a slope depression when compared to the static lift curve. The second finding was that the airfoil experiences a sudden increase or "jump" condition in the C_L when rotation begins. An interesting prediction of this "jump" condition for a flat plate is:

$$\Delta C_L = 3.14\ \dot{\alpha}_{ND} \tag{4}$$

Where ΔC_L represents the sudden change in C_L when the airfoil begins its rotation. This bears a striking resemblance to the induced camber effect developed by Allaire [1:37-42] in which the effect of rotating the airfoil is equated to inducing a camber thus increasing the lift by an amount equal to:

$$\Delta C_L = \pi\ \dot{\alpha}_{ND} \tag{5}$$

Where ΔC_L represents a correction to the theroetical lift computation based on the induced camber due to rotation. One of the major problems associatated with

these theoretical predictions was the lack of high quality experimental data covering the entire process of dynamic stall.

It was this lack of experimental data that prompted Schreck [23] to begin an ambitious follow-on to the experimental work of Daley. Schreck took the same NACA 0015 airfoil used in Daley's experiment and instrumented it with sixteen miniature pressure transducers. Then, with the aid of a high speed data acquisition system, he was able to record time, position and airfoil pressure distribution measurements throughout the dynamic stall process. The results of his reduced data show a definite correlation between the increase in $\alpha_{STALL\ DYN}$ and the non-dimensional pitch rate, $\dot{\alpha}_{ND}$ as shown in Fig 3. Subsequent evaluation of Schreck's data [12] has shown a reduction in the lift curve slope, but the data scatter has prevented a conclusive evaluation of the expected results.

One more experimental investigation recently conducted by Helin and Walker [10] bears mention at this point. Helin and Walker investigated the effect various pitch locations had on the dynamic stall vortices and associated unsteady aerodynamics. This paralleled some of Allaire's theoretical work in which the airfoil rotation point was varied from the leading edge to the trailing edge. Although the general trend of increased

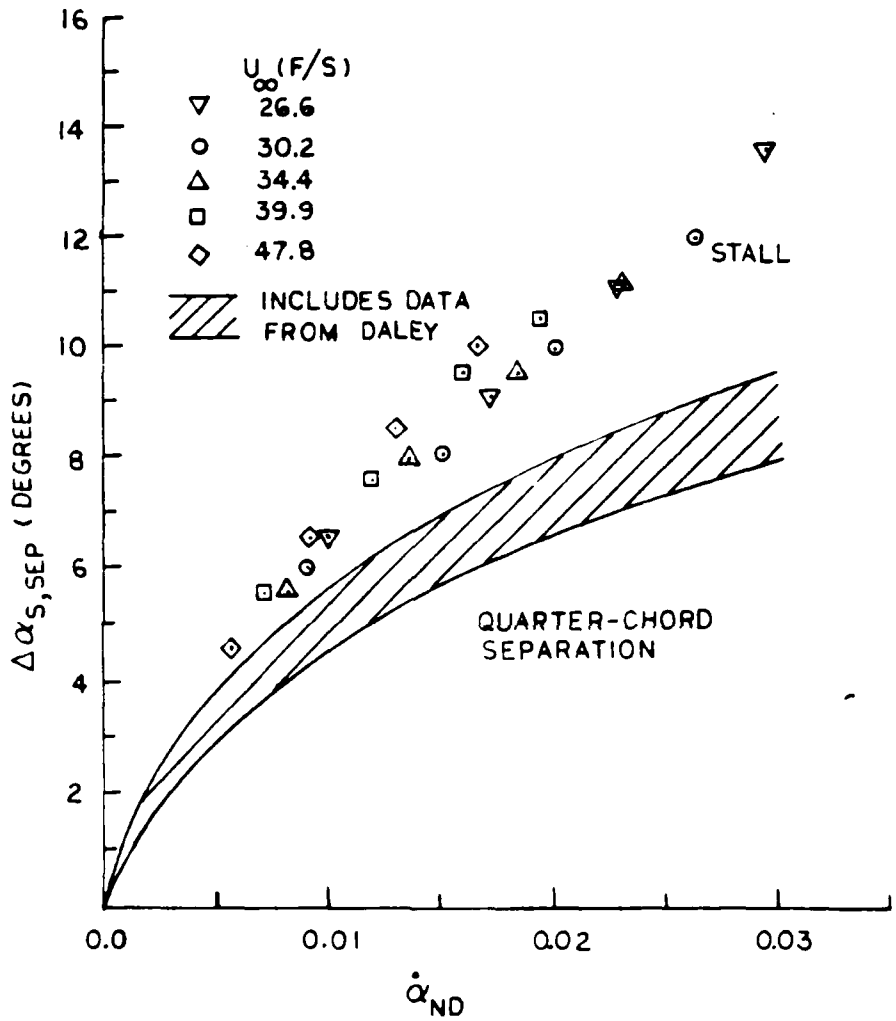

Figure 3. Data Summary of Schreck's Results and Daley's Results

leading edge velocities as the pitch location moves toward the trailing edge predicted by Allaire are present, the data is incomplete and inconclusive to make effective judgements of Allaire's methods.

Objectives

The past research in the area of dynamic stall for constant angular rotation rates is quite extensive, although most of the experiments have dealt with sinusoidal motions and fixed rotation points. These experiments create a broad base on which to conduct further investigations of the cause and effect of dynamic stall. In light of the past research, both experimental and theoretical, the objectives of this research experiment were as follows:

1. Use an existing NACA 0015 airfoil instrumented with miniature pressure transducers, and an automated data acquisition system to conduct an experimental investigation of the dynamic stall phenomenon. This investigation included a wide range of test conditions as well as varying the pitch location between the leading edge and the three-quarter chord point and attempting to increase the non-dimensional pitch rate $\dot{\alpha}_{ND}$.

2. Develop a data reduction routine to determine the airfoil force coefficients and produce high quality data output for all cases.
3. Using the reduced data from the experimental runs, determine the effect of pitch location and non-dimensional angular rate on the lift curve.

II. Theory and Approach

The following theory and approach section is composed of six subsections. Each of these subsections presents a brief discussion of the way in which previous dynamic stall theory or research influenced the experimental approach in this investigation. The first subsection provides a more detailed description of dynamic stall and the processes involved in the onset of stall. The second discusses the calculation of pressure coefficients for the airfoil. The third subsection covers discretization of the pressure distribution defined by these pressure coefficients, while the fourth describes the integration of this discretized pressure distribution. The fifth subsection considers the computation of force coefficients using the results of the integration, and the sixth presents a brief narrative concerning the problem of data acquisition.

Dynamic Stall in Contrast to Static Stall

Stall, whether static or dynamic, occurs when the surrounding flow separates from the airfoil to such a degree that any further increase in angle of attack fails to yield an increase in lift. Obviously, the boundary layer interactions for static and dynamic stall must differ significantly to produce the dramatic dis-

similarities between the two events.

In the familiar case of static stall, a boundary layer under the influence of an adverse pressure gradient eventually separates from the airfoil surface at the point where the shear stress at the wall vanishes. The point where flow separates is coincident with the point of flow reversal for static stall. Thus, the wake formed by this viscous interaction is large and appreciably distorts the potential flow field around the airfoil. For the static case, the stall angle of attack remains relatively constant, being, at most, a weak function of Reynolds number [11:248].

In dynamic stall, the boundary layer under the influence of an adverse pressure gradient also eventually separates from the airfoil. However, the similarity ends here since the point of reversed flow no longer coincides with the point of separation, but is delayed some distance downstream. The point of separation for dynamic stall is determined by the Moore-Rott-Sears (MRS) criterion [27:113-144]. This difference substantially reduces the wake size and corresponding potential flow field distortion when compared to the static case [19:294-295]. In addition to the MRS separation criterion, other effects appear to be at work [15]. It is clear that the dynamic stall process is a complex function of freestream velocity,

airfoil angular rate, and even airfoil section geometry as shown in Table I.

The fact that the wake size and corresponding potential flow field distortion associated with dynamic stall are small relative to their static-stall counterparts is favorable to this investigation. Schreck argues that tunnel wall interference effects are therefore correspondingly small compared to those encountered in the same flow regime for steady-state phenomena [23:60-63]. This implies that streamline curvature and wake blockage effects can probably be considered negligible in dynamic stall testing. McCroskey, et. al. takes a similar approach in ignoring tunnel effects for reasons of experimental data scatter and the uncertainty of determining the dynamic corrections [17]. In either case, dynamic stall tunnel effects are considered indeterminable and are subsequently ignored.

Determination of Pressure Coefficients

Because of inevitable freestream irregularities in the test section, pressure measurements at the same location on the airfoil do not remain constant in time. These irregularities can be filtered out while preserving those pressure fluctuations due only to the dynamic stall phenomenon by using ensemble-averaging. For this experiment, pressure data from five different

TABLE I

Importance of Dynamic Stall Parameters [16]

Stall Parameter	Effect
Airfoil Shape	Large in some cases
Mach Number	Small below $M \approx 0.2$ Large above $M \approx 0.2$
Reynolds Number	Small (?) at low Mach Number Unknown at high Mach Number
Reduced Frequency **	Large
Mean Angle, Amplitude	Large
Type of Motion	Virtually Unknown
Three-Dimensional Effects	Virtually Unknown
Tunnel Effects	Virtually Unknown

** The reduced frequency parameter is similar to the nondimensional pitch rate - $\dot{\alpha}_{ND}$

airfoil rotations at the same angular rate and free-stream velocity were obtained in order to generate an ensemble-averaged data set.

With the ultimate goal of determining airloads during the dynamic stall event, a method of calculating the pressure coefficient at any chord location on the airfoil was needed. This method should use physical parameters which can be readily sensed or measured as inputs. The standard equation for the pressure coefficient is given by:

$$C_P = (P_{LOC} - P_\infty) / q \qquad (6)$$

where P_{LOC} is the local static pressure at some point on the airfoil, P_∞ is the freestream static pressure, and q is the freestream dynamic pressure ($\frac{1}{2}\rho V^2$). The local pressure anywhere on the airfoil can be expressed as:

$$P_{LOC} = \Delta P_{TRAN} + P_A \qquad (7)$$

where P_{LOC} retains the same definition as in Eq. 6, P_A is some reference pressure, and ΔP_{TRAN} is the differential pressure between these two. Substituting P_{LOC} from Eq. 7 into Eq. 6 yields the relationship:

$$C_P = [(\Delta P_{TRAN} + P_A) - P_\infty] / q \qquad (8)$$

Regrouping the terms in the numerator and noting that the denominator is equivalent to $P_o - P_\infty$ following steady state resasoning for the incompressible Bernoulli equation, Eq. 8 becomes:

$$C_P = [\Delta P_{TRAN} + (P_A - P_\infty)]/[P_o - P_\infty] \qquad (9)$$

It should be noted that $q = (P_o - P_\infty)$ may not be valid under unsteady flow conditions, and this assumption can lead to pressure coefficients greater than one. However the use of the pressure coefficients in this investigation is restricted to the determination of force coefficients and the dynamic pressure term will ultimately cancel itself.

Eq. 9 requires the determination of three quantities to calculate the corresponding pressure coefficient. The first, ΔP_{TRAN}, is the difference in pressure between some constant reference pressure, P_A, and the pressure at a certain point on the surface of the airfoil. This differential pressure was sensed by a transducer mounted in the airfoil. The second, $P_A - P_\infty$, is the pressure difference between the reference pressure and test section static pressure, while the third, $P_o - P_\infty$, is the pressure difference between test section stagnation pressure and static pressure. Since

the reference pressure must be easily accessible as well as constant, ambient room pressure constituted a good choice, although any constant pressure source would have been acceptable.

Discretization of the Pressure Distribution

The mathematical procedure developed in the preceding subsection facilitates pressure coefficient determination at any transducer location on the airfoil. To minimize the error inherent in discretizing the dynamic stall pressure distribution, two basic issues had to be addressed. The first issue was to determine an acceptable number of transducers and, the second, to establish the optimum distribution of these transducers.

Obviously a greater number of transducers reduces the discretization error, however, an upper limit on this number is eventually reached. In this experiment, 16 transducers were employed in the same fashion as Schreck [23:14-16].

The requirement of accurately portraying the airfoil pressure distribution governed the placement of the 16 pressure transducers. Therefore, the transducers were concentrated in the region of the airfoil where the pressure distribution was anticipated to have the largest gradient. McCroskey, et. al. [16:3] obtained pressure distributions for an oscillating NACA 0012

airfoil that provided a useful guide for locating the transducers. Accordingly, the transducers were distributed most densely on the upper surface of the airfoil and near the leading edge, as shown in Fig. 4.

The fact that there was no transducer at the trailing edge of the airfoil meant there was no direct means of determining the pressure at the trailing edge. However, McCroskey, et. al., obtained results using an airfoil with the rearmost pressure transducer located at the 98 percent chord position [16:4]. They reasoned that the trailing edge pressure coefficient can be approximated through extrapolation of the rearmost two transducers on the airfoil upper surface.

Integration of the Pressure Distribution

The discretized pressure distributions were integrated numerically to obtain the corresponding force coefficients. McCroskey, et. al., found that cubic and variable power splines applied to the discrete data points did not yield acceptable accuracy. The spline fits caused large overshoots that made this method unsatisfactory in general application [17:3]. Therefore, all integration in this investigation was accomplished using the trapezoidal rule following the method of McCroskey, et.al.

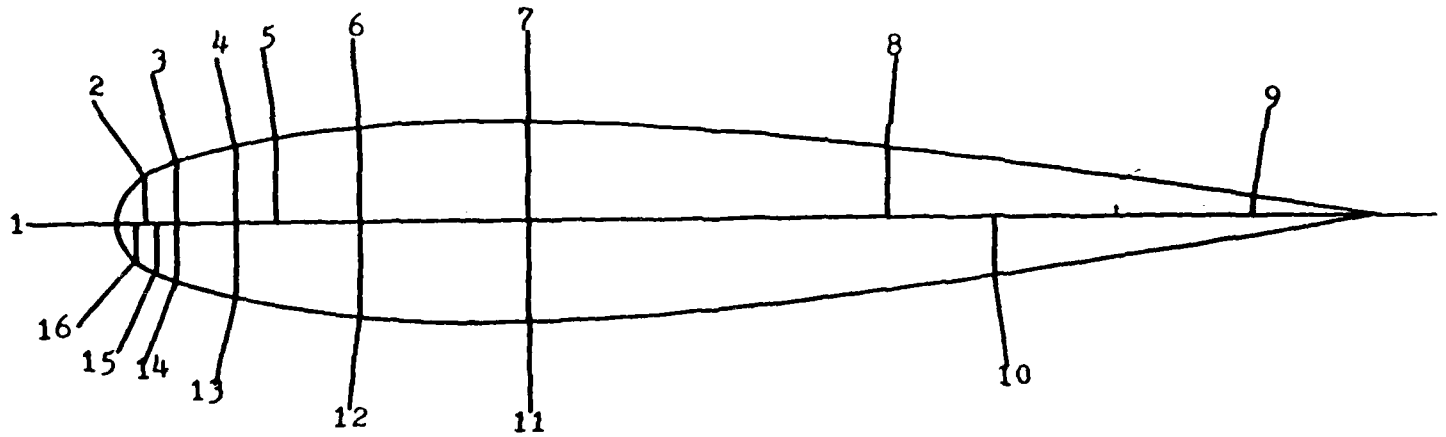

Point	(X/C)	(Y/C)	Point	(X/C)	(Y/C)
1	0.000	0.0000	9	0.902	0.0178
2	0.025	0.0327	10	0.697	0.0461
3	0.049	0.0440	11	0.328	0.0743
4	0.098	0.0581	12	0.197	0.0714
5	0.131	0.0637	13	0.098	0.0581
6	0.197	0.0714	14	0.049	0.0440
7	0.328	0.0743	15	0.033	0.0364
8	0.615	0.0554	16	0.016	0.0262

Figure 4. Airfoil Pressure Transducer Locations

Determination of Force Coefficients

A major factor in this investigation was the determination of the force and moment coefficients for the airfoil. These coefficients were obtained through integration of the pressure distribution as follows [3]:

$$C_N = -\int C_P \, d(x/c) \tag{10}$$

$$C_C = \int C_P \, d(y/c) \tag{11}$$

where C_N is the normal force coefficient, C_C is the chord force coefficient and C_P is the surface pressure coefficient. The quantities d(x/c) and d(y/c) represent the differential lengths in the x and y directions referenced to the airfoil chord length.

$$C_M = \int C_P \, (0.25 - x/c) \, d(x/c) \tag{12}$$

where C_M is the quarter-chord moment coefficient, C_P is the surface pressure coefficient and x/c is the chord-wise location on the airfoil.

The results of these integrations were then combined to form the lift and drag coefficients [21]:

$$C_L = C_N \cos(\alpha) \tag{13}$$

$$C_D = C_N \sin(\alpha) + C_C \cos(\alpha) \qquad (14)$$

Since viscous forces were not measured, the chord force is incomplete and should be regarded as only the pressure drag portion of the airfoil drag. Further, it is recognized that the spacing of the pressure transducers was such that the C_C should be treated as far less representative of the actual chord force than C_N is representative of the normal force. For this reason, an additional term of $C_C \sin(\alpha)$ was not included in Eq. 13.

The Problem of Data Acquisition

Measurement of the physical parameters associated with dynamic stall presents a unique problem due to the transient nature of the phenomenon. The measurement system had to be not only accurate, but relatively fast. The solution to this problem has taken many forms, with many advances resulting from the current state of digital electronics. Kramer used a balance system to measure and record the aerodynamic forces on the wing as the freestream flow was rotated past it. Deekens and Kuebler used high-speed cinematography of smoke traces to ascertain airfoil rotation rate and dynamic separation angle of attack. Daley also used movies of smoke traces, but simultaneously gathered digital position and

pressure data using four transducers embedded in the quarter-chord region of the airfoil. McCroskey, et.al., used an airfoil equipped with 16 pressure transducers, and collected analog electronic position and pressure data.

In this investigation, following Schreck's methods [23], digital position and pressure information was collected using an airfoil instrumented with 16 pressure transducers (c.f. above). In any dynamic measurement system, sample rate is a crucial factor in determining the resolution capability of the measurements. In this case, the absolute lower threshold on sample rate was approximately 300 data samples per second [4:7]. The data acquisition system used in this investigation had the capability to meet and exceed this criterion by a wide margin (c.f. below).

III. Facilities and Instrumentation

Smoke Tunnel

This investigation was conducted in the AFIT smoke tunnel located in Building 640, Area B, Wright-Patterson AFB, Ohio. The test section measures 59 inches long, 39.5 inches high, and 2.75 inches deep. The smoke tunnel is capable of test section velocities between, approximately, 10 and 45 feet per second. This facility, its capabilities and limitations, are further described by Sisson [24], and Baldner [2]. Since this experiment did not involve flow visualization, the smoke generation rake was removed from the tunnel. Shreck suggested that this modification would improve test section flow characteristics and improve data quality [23:55], although this may not have been the case (c.f. below).

Velocity Measurement

Test section static and total pressure were measured using a standard hemispherical-head Pitot-static probe in conjunction with a Dwyer Portable inclined manometer, model 102. These pressures were used to establish the test section velocity during data collection and recorded for later use during data reduction to determine pressure coefficients. Based on

Schreck's investigation of the test section flow characteristics, the pitot-static probe was located at a point 31 inches from the start of the test section [23:64-69]. This afforded the most accurate measurement of test section pressures while minimizing the mutual interference between the airfoil and probe.

Airfoil

The NACA 0015 airfoil used in this experiment measured 12.2 inches chord and 2.63 inches span. It consisted of a hollow mahogany shell closed on both sides by aluminum endplates, which were sealed to the shell with silicone rubber adhesive sealant. Figure 5 shows the four different rear endplates that were constructed to allow the airfoil pitch location to vary between the leading edge and three-quarter chord point. The rear endplate was rigidly attached to a 14 inch tubular aluminum shaft with an outside diameter of .75 inches. This aluminum shaft had a slot at its midpoint which allowed ambient atmospheric pressure into the interior of the airfoil. The airfoil shell had 16 transducer ports drilled into it at the locations shown in Figure 4.

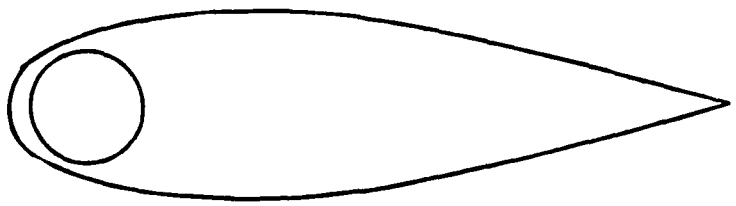

a) Pitch Location #1 - .08c

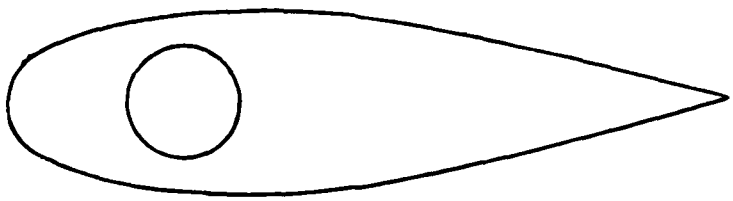

b) Pitch Location #2 - .25c

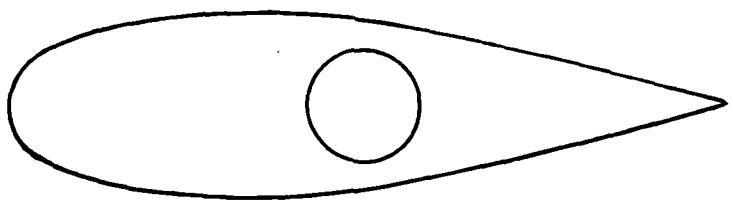

c) Pitch Location #3 - .50c

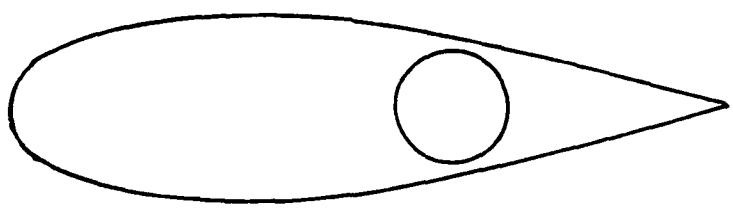

d) Pitch Location #4 - .61c

Figure 5. Airfoil Endplates and Pitch Locations

Transducers

The transducers used in this experiment were Endevco 8506-2 and 8507-2 miniature piezo-resistive pressure transducers. The only difference between the two models was the type of mounting fixture used. Both transducers had a maximum range of plus or minus 2 psig, and required an excitation voltage of 10.00 volts DC. This excitation voltage was provided by a Kepco KB 25 DC Power Supply, and monitored by a Hewlett-Packard 34701A DC voltmeter with a 34740A digital display insert, allowing voltage readings to three decimal places. Resonant frequency for both types of transducers was 45,000 Hertz. Thus, the transducer frequency response had a negligible effect on the results obtained in this investigation.

The transducers were mounted in the ports of the airfoil according to the specifications provided by Endevco [8] using Silastic 732 RTV silicone rubber adhesive as the bonding agent. The transducer leads were soldered into a 40 pin connector which remained within the airfoil and facilitated the easy change of airfoil endplates. After completing the electrical connections between the transducers and the micro-computer, the transducers were calibrated as described in Appendix A.

Drive Mechanism

The airfoil was rotated using a TRW Globe Model 5A2298-4 12 volt DC, constant-speed planetary gearmotor with a 525:1 reduction ratio. The motor was further geared at the output shaft in a 2:1 ratio to obtain higher rotation rates. The motor voltage source was the Hewlett-Packard 6205C Dual DC Power Supply. By adjusting the input voltage, the motor produced constant rotation rates. An experimental test of the airfoil drive mechanism under static conditions found the motor response to be linear with no more than 0.5% deviation. The high reduction ratio of this motor provided a high output torque, which, in turn, spun the output shaft up to constant speed in less than .01 seconds. This start up time was negligible when compared to the time required to reach the dynamic stall angle of attack. A spring-loaded double-pole, double-throw toggle switch was used to control the motor and allowed both positive and negative rotations of the airfoil.

The airfoil angle-of-attack transducer consisted of a Spectrol 80059 1000 ohm, ten-turn potentiometer which was coupled to the airfoil shaft through a gear train having a 33:1 ratio. This allowed approximately 100 degrees of airfoil rotation for the full ten turns of the potentiometer. The potentiometer was excited at 10 volts DC using the Hewlett-Packard 6205C Dual DC Power

Supply and the output was fed into the microcomputer to provide airfoil position information. A calibration of the potentiometer found a linear response with a maximum deviation less than 0.4% full scale. Figure 6 shows the entire assembly in place on the test stand which was mounted on the rear side of the tunnel.

Data Acquisition System

The microcomputer system consisted of a Heathkit H-29 terminal, a Tarbell Model VDS-IId dual eight-inch floppy disk drive, and an Electronic Control Technology S-100 bus equipped with an SD Systems SBU-100 Single Board Computer, SD Systems Expandoram II board, and an MD2022 Tarbell Disk Controller board. Figure 7 shows the entire system in position next to the smoke tunnel. This system was augmented with two Dual Systems Control Corporation AIM-12 analog input module boards to perform the digital data gathering function.

The AIM-12 is a high speed, multiplexed analog-to-digital data acquisition module compatible with the standard S-100 bus. The AIM-12 employs a sample/hold mechanism which, combined with the multiplexer, allows maximum throughput operation for analog-to-digital (A/D) conversions. The board is capable of making a complete data pass through all sixteen transducers in less than 4 milliseconds. The analog-to-digital conversion sub-

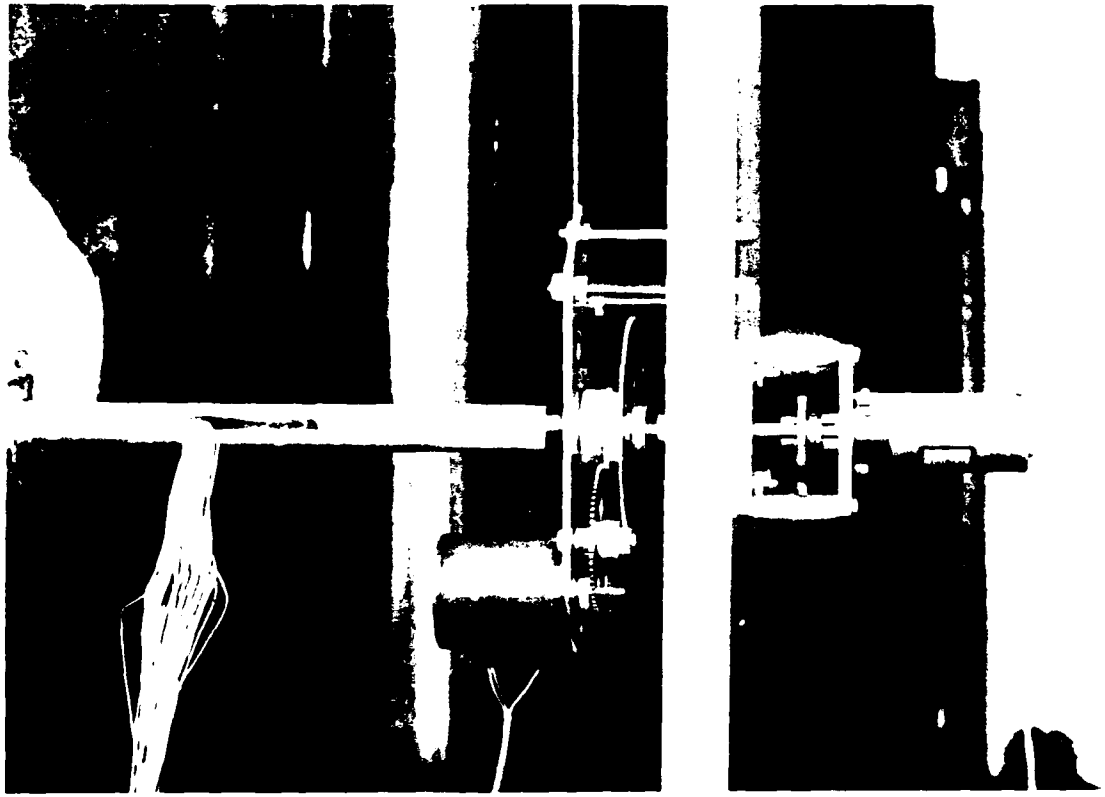

Figure 6. Airfoil Drive Mechanism and Position Potentiometer Mounted on Test Stand

Figure 7. Experimental Equipment and Data Acquisition System

system on the board operates in either bipolar or unipolar mode. The unipolar mode requires the input voltage to the A/D converter be within the range of 0 to 10 volts, while the bipolar mode accepts input voltages from -5 volts to +5 volts. The AIM-12 board also has a preconditioning subsystem consisting of a multiplexed, precision instrumentation amplifier with variable gains between 1 and 100. Operation in the bipolar, or differential, mode takes advantage of the amplifier's high common mode rejection ratio, which is a maximum of 114 decibels with the gain set at 100.

As mentioned previously, the data acquistion system used two AIM-12 boards. The board responsible for collection and digitization of the pressure transucer signals was configured for bipolar A/D conversion and amplifier gain of 100. Due to the small pressures being sensed by the transducers, the electrical signals originating at the pressure transducers had a magnitude of approximately 15 millivolts. Although the gain of 100 resulted in no more than 30 percent of full-scale on the A/D converter, the high common mode rejection ratio was very effective in cancelling noise in the system and the resulting in good overall system accuracy.

The second AIM-12 board was responsible for the collection and digitization of the position potentiometer signal, which varied between 0 and 10 volts.

This board was configured for unipolar A/D conversion and amplification gain of 1. It should be noted that the second AIM-12 board used only one of the 16 availble channels, thus the experimental configuration has further growth potential.

IV. Experimental Procedure

Transducer Calibration

All 16 transducers in the airfoil were statically calibrated prior to the first data collection run. This calibration procedure was repeated at the completion of all data gathering and the results compared to the initial calibration run. A complete description of the transducer calibration procedure is presented in Appendix A.

Data Collection

To prepare the system for a data collection run, all three voltmeters, both power supplies, and the computer were allowed to warm up for a minimum of one hour before any data was taken. This procedure allowed any large electrical transients in the system to die out and insured nearly steady-state operation during data collection.

The first step in making a data collection run was to execute the data acquisition program, TESTRUN (see Appendix B). This program controlled the remainder of the experimental procedure by requesting input or providing instructions concerning equipment operation. The following discussion constitutes a summary of the data collection sequence.

The first set of inputs to the computer included date, time, temperature, and barometric pressure. These values were then echoed back to the operator for verification before writing them to the disk file. The program then obtained zero-input readings for the 16 transducers, displayed them on the terminal screen, and wrote the values to disk. At this point the program instructed the operator to turn on the tunnel motors and obtain the desired test section velocity.

The next set of inputs consisted of the two different inclined manometer readings, the airfoil drive motor voltage and the potentiometer voltages corresponding to the 90 and 0 degree angle-of-attack positions. The first manometer reading was the difference between ambient pressure and test section static pressure ($P_A - P_\infty$). This was obtained by connecting the pitot-static probe static port to one leg of the manometer and leaving the other leg open to ambient air. The second manometer reading was the difference between the test section total and static pressures ($P_o - P_\infty$), and was obtained by connecting the tube from the probe total pressure port to the other leg of the manometer.

The voltages corresponding to 90 and 0 degrees angle-of-attack were determined using a digital voltmeter connected to the position potentiometer. The 90

and 0 degree positions were indicated by markers attached to the back glass wall of the test section. After inputing the position voltages, the motor voltage was entered, and all input values were echoed at the terminal screen for verification.

The next phase of the program involved the actual dynamic stall data collection for five consecutive airfoil rotations. The operator would first input the number of samples to be taken and choose either manual or automatic trigger for the data collection routine. The number of samples and trigger method remained consistent for the five consecutive rotations to avoid difficulty during data reduction. After rotating the airfoil through dynamic stall and returning it to zero angle-of-attack, the computer would output the number of samples actually taken and the computed angular rotation rate in degrees per second. The data set was then scanned for obvious cases of non-linear motor response. At this point the operator decided whether to write the data set to disk, or repeat the rotation. The data set was repeated if the rotation rate was not within two degrees per second of the previous angular rotation rates or if it was judged that the rotation rate was not constant. The operator repeated this process for a total of five airfoil rotations.

After obtaining five satisfactory dynamic stall data files, a static lift curve was determined for the same test section velocity. This part of the program first instructed the operator to position the airfoil at the desired static angle-of-attack. The static angle of attack was estimated using a protractor taped to the back wall of the test section. Then, at the command of the operator, the transducers were sampled 180 times, and the resulting normal force coefficient was computed and displayed at the terminal. The position potentiometer voltage and transducer values were recorded on disk and the procedure was repeated a sufficient number of times at successively higher angles of attack to define a static lift curve. After obtaining enough samples to determine the static lift curve, the data collection program, TESTRUN, was terminated and the tunnel shut down until the next run.

After completing all the data runs for a given pitch location, the airfoil model was removed from the tunnel. The rear endplate was then removed and the transducer leads were disconnected from the computer. The endplate was exchanged for one with a new pitch location and the transducer leads were reconnected to the computer. After a quick check to determine the transducers were still functioning properly, the airfoil was sealed using RTV adhesive and returned to the tunnel

test section. The entire test procedure was then repeated for the new pitch location.

Exceptions

During the course of the experimental runs, certain events differed from the procedures outlined above. The first exception involved data runs with pitch locations forward of the mid-chord. Due to large aerodynamic forces, the airfoil failed to rotate beyond approximately 50 degrees angle-of-attack. A plot of time versus position for the airfoil rotation showed a constant angular rate up to 50 degrees. Since the dynamic stall event is usually complete by the 35 degree position and the rotation rate was constant throughout that range, this condition did not affect the experimental results. Another problem with airfoil rotation was discovered during the rotations about the three-quarter chord point. The rotation motor could not supply enough torque to rotate the airfoil from the zero angle of attack position through dynamic stall. This condition necessitated the procedure of pitch down for these test runs. Being a symmetric airfoil, the aerodynamic forces, in principal, are the same for a given angle-of-attack, whether positive or negative. This fact combined with a relatively symmetric distribution of pressure transducers implies that pitch up or pitch

down should, theoretically, have little effect as long as the rotation rate is constant; in practice, however, there may have been some differences (c.f. discussion after Eq. 18, below). The third exception involved the change of transducer number seven. This transducer became errratic and failed to respond accurately during a change of endplates. The old transducer was replaced with another Endevco 8507-2 and the transducer leads were wired into the connector pin. The new transducer required minor modifications to the experiment software to reflect the new transducer sensitivity.

Velocities and Reynolds Numbers

Using the procedure outlined above, test runs were conducted at test section velocities ranging between 25 and 45 feet per second. Although the smoke tunnel was capable of test section velocities as low as 10 feet per second, any data gathered at velocities below approximately 25 feet per second was assumed unacceptable for two reasons. First, the magnitude of the resulting signal was small enough to fall within the noise range of the transducer. Second, the resulting angalog-to-digital resolution was unacceptable due to the small percent of full scale output at the analog-to-digital converter. Velocities above 40 feet per second were attempted, but the results were suspect and suggest the

existence of large scale tunnel turbulence discovered during Sisson's investigation [24]. At each test section velocity, five data runs were accomplished for three different motor voltages, giving a total of 60 test conditions, or 300 total dynamic data runs. The resulting Reynolds numbers, based on airfoil chord-length, ranged from 14,700 to 26,700. As such, all data was collected in a flow regime generally accepted as laminar, based on Reynolds number.

V. Data Reduction and Discussion of Results

Data Reduction

The data reduction process for this experiment was a two step process. The first step was accomplished on the experimental mini-computer using a heavily modified version of Schreck's data reduction program. The program used the five raw pressure data files generated during the experimental runs and produced a data file that contained time, position, pressure coefficient and aerodynamic force coefficient data. The program first computed the experimental test conditions using the temperature, barometric pressure and manometer readings taken during the test runs. These data were used to compute the test section velocity and Reynolds number based on airfoil chord for the experiment. The program then cycled through all five data runs, using the recorded digital voltages to compute airfoil angle of attack and pressures. Because the transducer sampling was not simultaneous, a linear interpolation was performed on all transducer data in order to reference the airfoil pressure distribution to a time of interest. The subsequent pressure distribution was then converted into pressure coefficients using Eq. 9, and integrated using the trapezoidal rule to obtain airfoil normal force, chord force and pitching moment about the quarter-

chord. Finally, the force data were converted to lift and drag coefficients using Eqs. 13 and 14. The reduced data file was then written to disk for later use. This file consisted of heading information, including test conditions, and five sets of data runs, each containing 200 data points.

The static data was similarly reduced, except there was no linear interpolation of pressure data since these runs were conducted at static angles-of-attack. This program also introduced the computed wind tunnel correction factors for blockage and streamline curvature. Schreck [23:60-63] developed the correction factors for this experimental setup based on the discussion by Pankhurst and Holder. These values were recomputed to confirm their accuracy and then applied to the static data.

The rough static and dynamic stall data files were then transferred to the Aeronautical Systems Division CDC Cyber computer for further manipulation and plotting. The dynamic data files were reduced further by using the DATRED program. This program took all five data runs and performed an ensemble averaging routine based on one degree blocks of angle-of-attack to produce the final dynamic stall data sets. This program also took the time and position data and computed the average rotation rate for the data set using a linear least

squares fit. The maximum deviation from a linear response was computed and data sets that varied by more than five percent were identified as non-linear. A similar averaging routine was performed on the static stall data runs and all files were stored for future use.

After performing the averaging routines, the final data files were printed and used in conjunction with the rough data files to determine the dynamic stall angle of attack. A similar procedure was followed for the static stall curves and these data were used to compute the $\Delta\alpha_{STALL}$ information listed in the results section. The final step in the data reduction was to generate the plots shown in the results section using the PLOTM routines on the Cyber computer. A copy of each program is provided in the Computer Software Appendix B.

Discussion of Results

The details of the dynamic stall event have been described in numerous works [9],[18], [26], and this experiment found the same tendencies in the dynamic stall lift curves. In all cases, the lift curve extended beyond the point of static stall and the airfoil lift continued to increase to a point at which catastrophic stall occurred. This is most easily seen in Figures 8-12 which show the pressure distribution

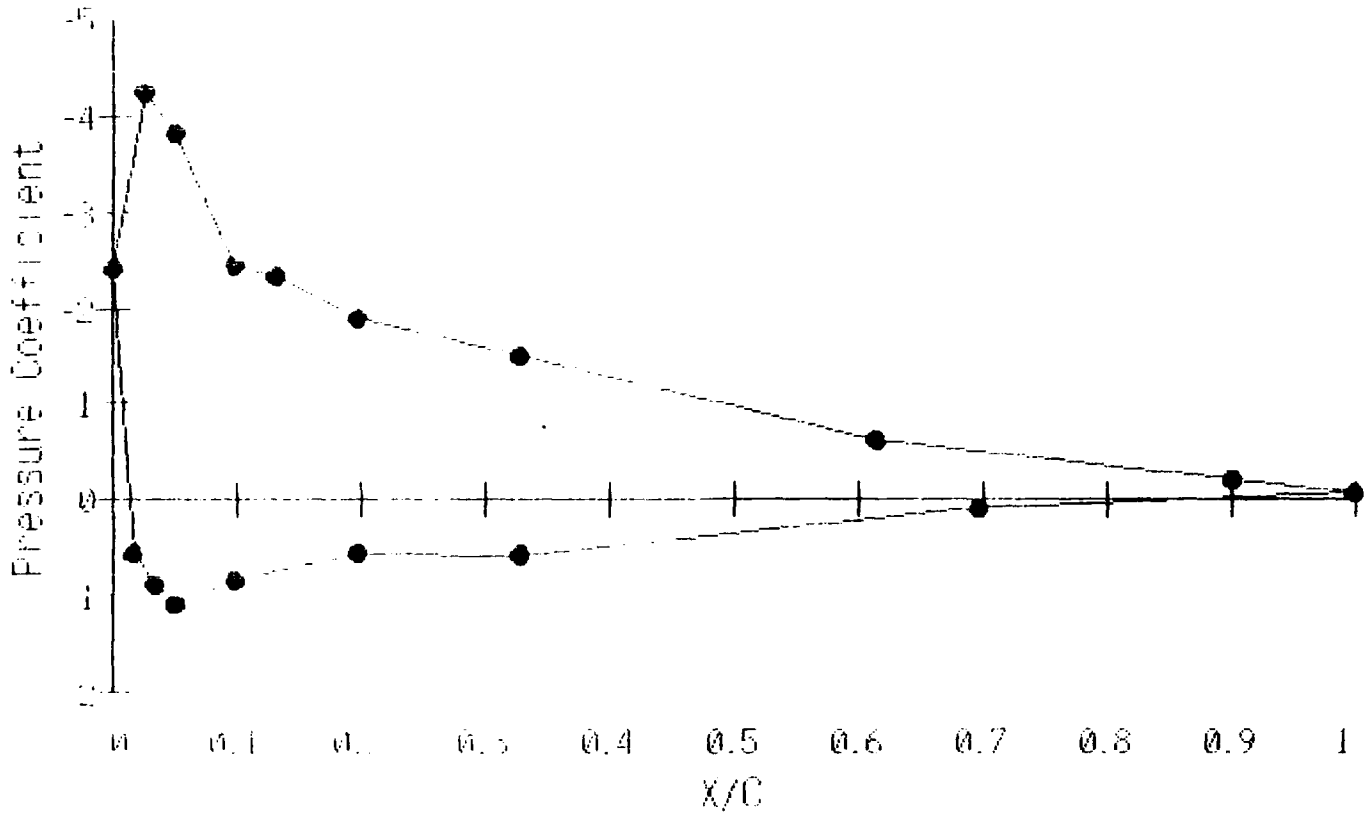

Figure 8. Airfoil Dynamic Stall Pressure Distribution
V = 29.1 fps, α = 22.1 deg, $\dot{\alpha}$ = 118.8 deg/sec

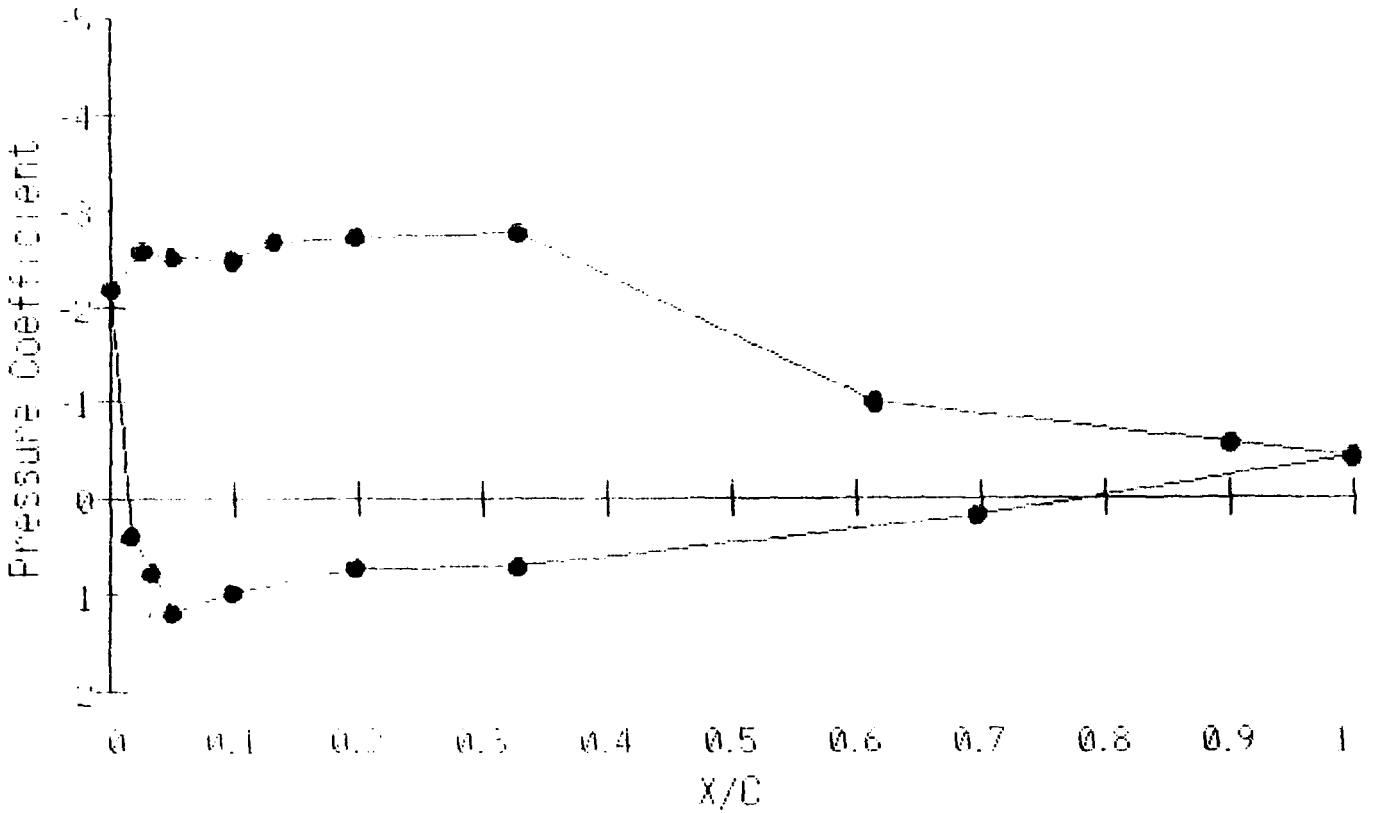

Figure 9. Airfoil Dynamic Stall Pressure Distribution
V = 29.1 fps, α = 27.5 deg, $\dot{\alpha}$ = 118.8 deg/sec

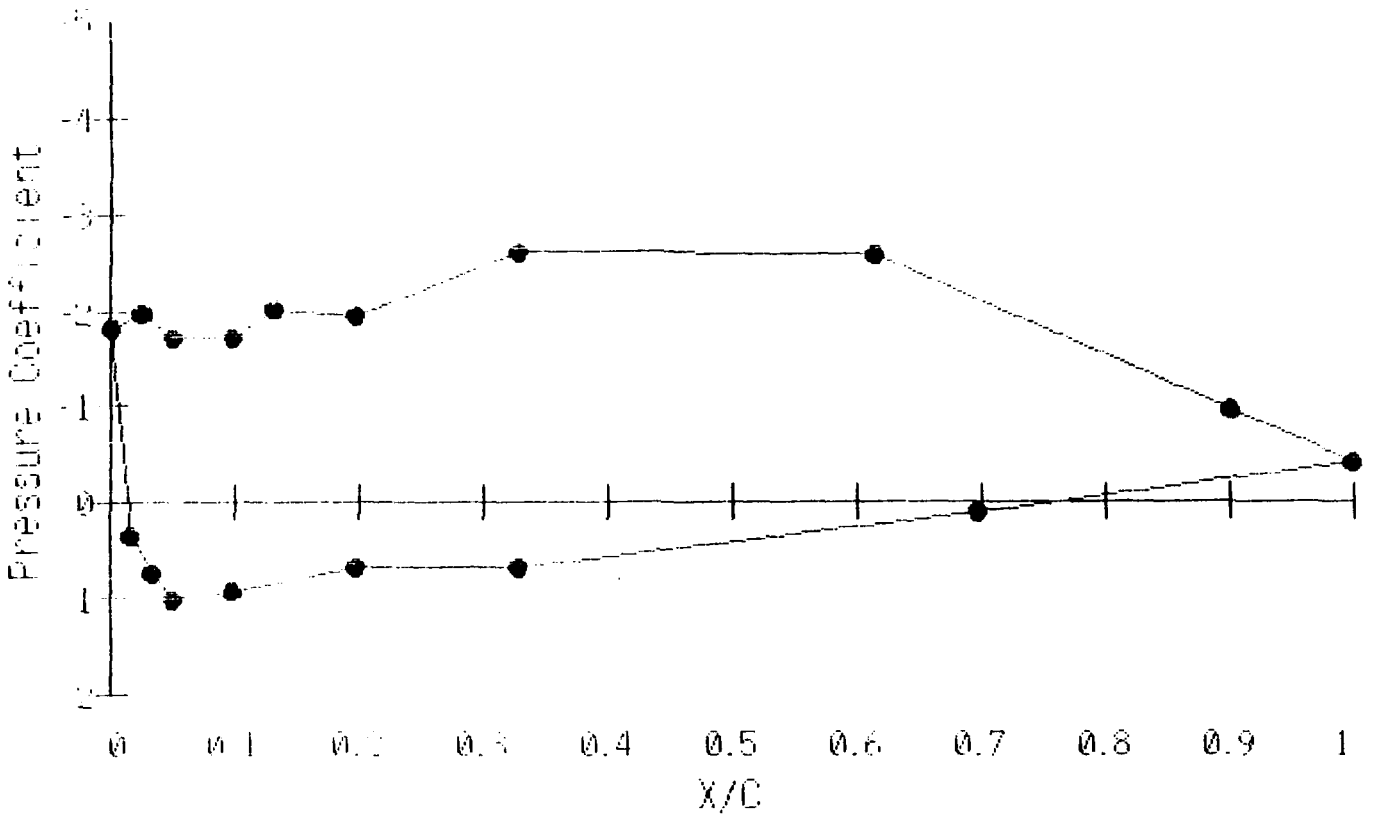

Figure 10. Airfoil Dynamic Stall Pressure Distribution
V = 29.1 fps, α = 30.8 deg, $\dot{\alpha}$ = 118.8 deg/sec

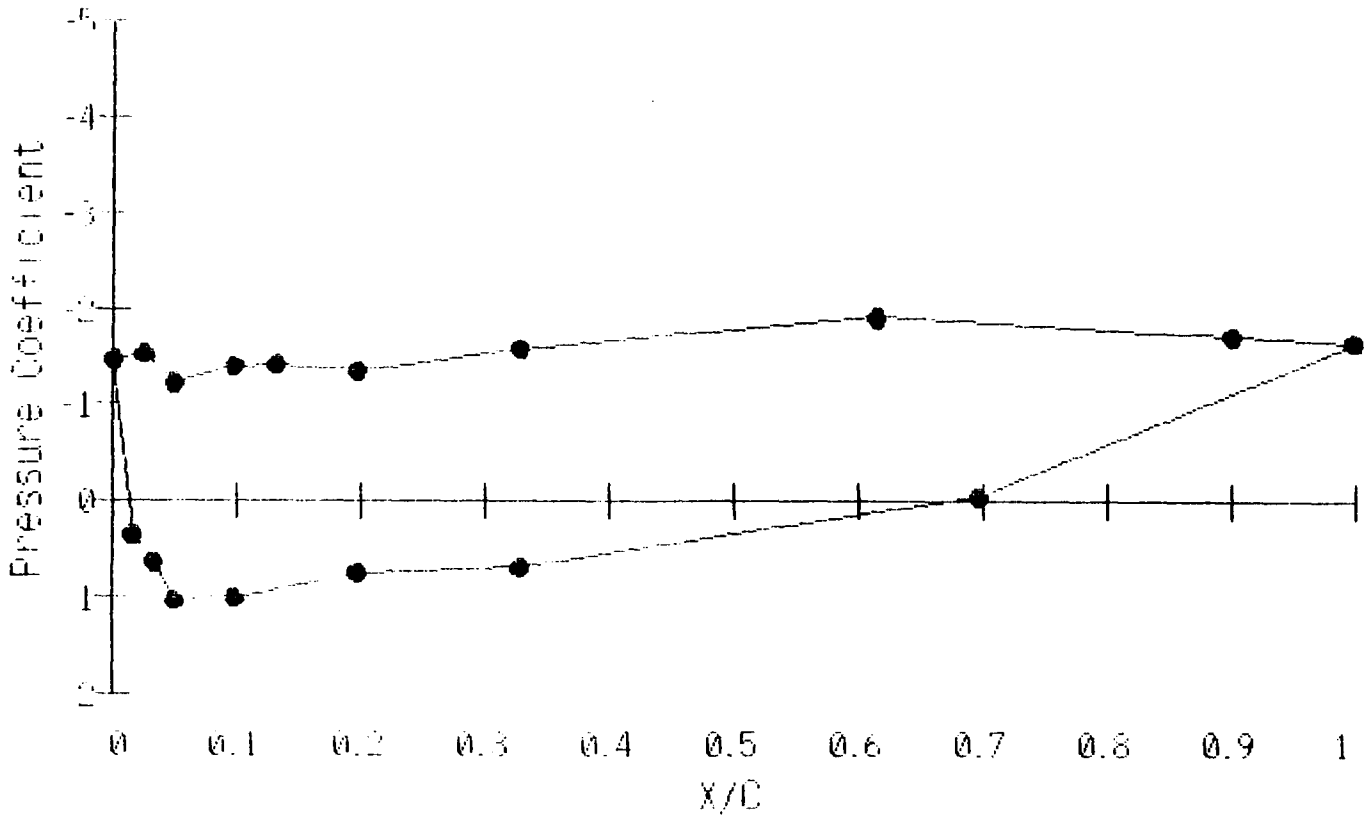

Figure 11. Airfoil Dynamic Stall Pressure Distribution
V = 29.1 fps, α = 37.0 deg, $\dot{\alpha}$ = 118.8 deg/sec

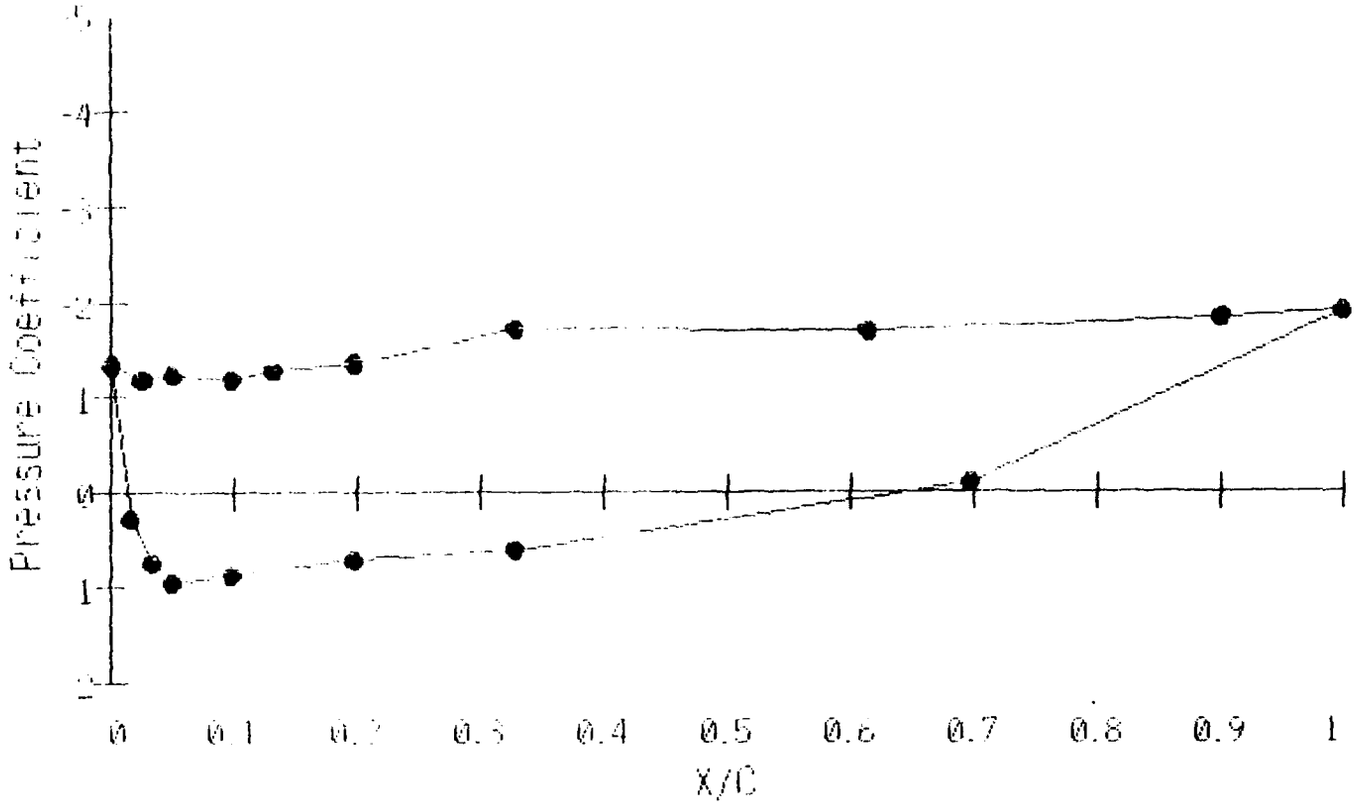

Figure 12. Airfoil Dynamic Stall Pressure Distribution
V = 29.1 fps, α = 38.8 deg, $\dot{\alpha}$ = 118.8 deg/sec

around the airfoil at points before and after dynamic stall. The dynamic stall event begins with a large build-up of pressure near the leading edge of the airfoil. Just after quarter-chord separation (c.f. introduction), this pressure spike begins to flatten and move toward the trailing edge. As the pressure spike moves off the airfoil, there is a catastrophic collapse of the pressure distribution resulting in the deep dynamic stall condition. The physical explanation for this sequence shows that the flattening and movement of the pressure spike is caused by the formation and subsequent shedding of a strong vortex from the airfoil leading edge. Reference 10 and reference 26 have excellent smoke flow visualization pictures substantiating this argument.

As with the past research, a strong correlation exists between the non-dimensional rate parameter ($\dot{\alpha}_{ND}$) and the increased stall angle-of-attack. Figure 13 shows this result by plotting three cases of increasing $\dot{\alpha}_{ND}$ for dynamic stall lift curves. In each case, the dynamic stall point is delayed due to the increase in pitch rate. This study also introduced the determination of airfoil drag and moment coefficients. The same effect found in the lift curve data also is found in the drag and moment data. As $\dot{\alpha}_{ND}$ increases there is a corresponding increase in drag coefficient and a delay

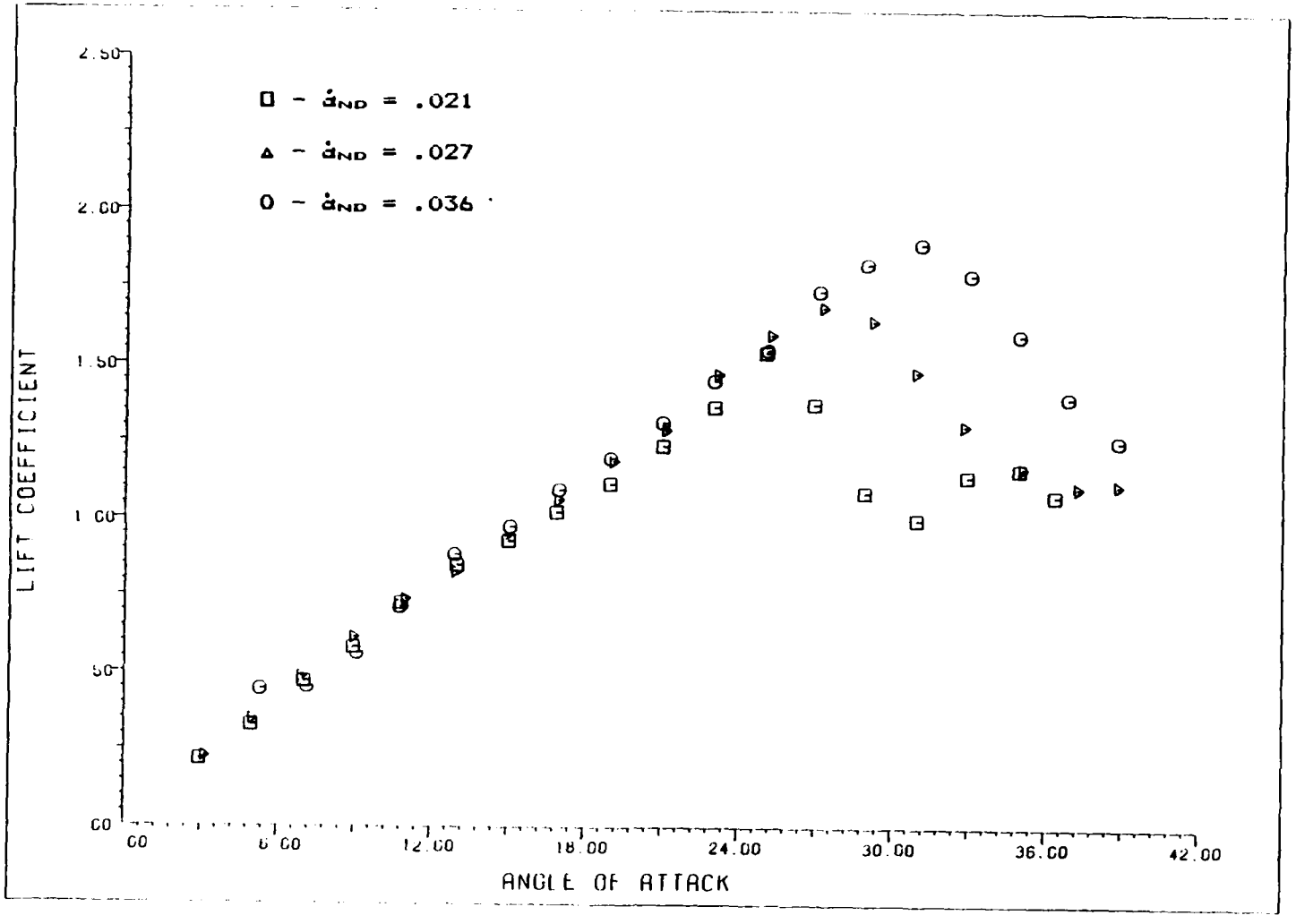

Figure 13. Combined Dynamic Stall Lift Curves
$\dot{\alpha}_{ND}$ = .021, .027, .036 Respectively
V = 29.07, Pitch Location #3 (.50c)

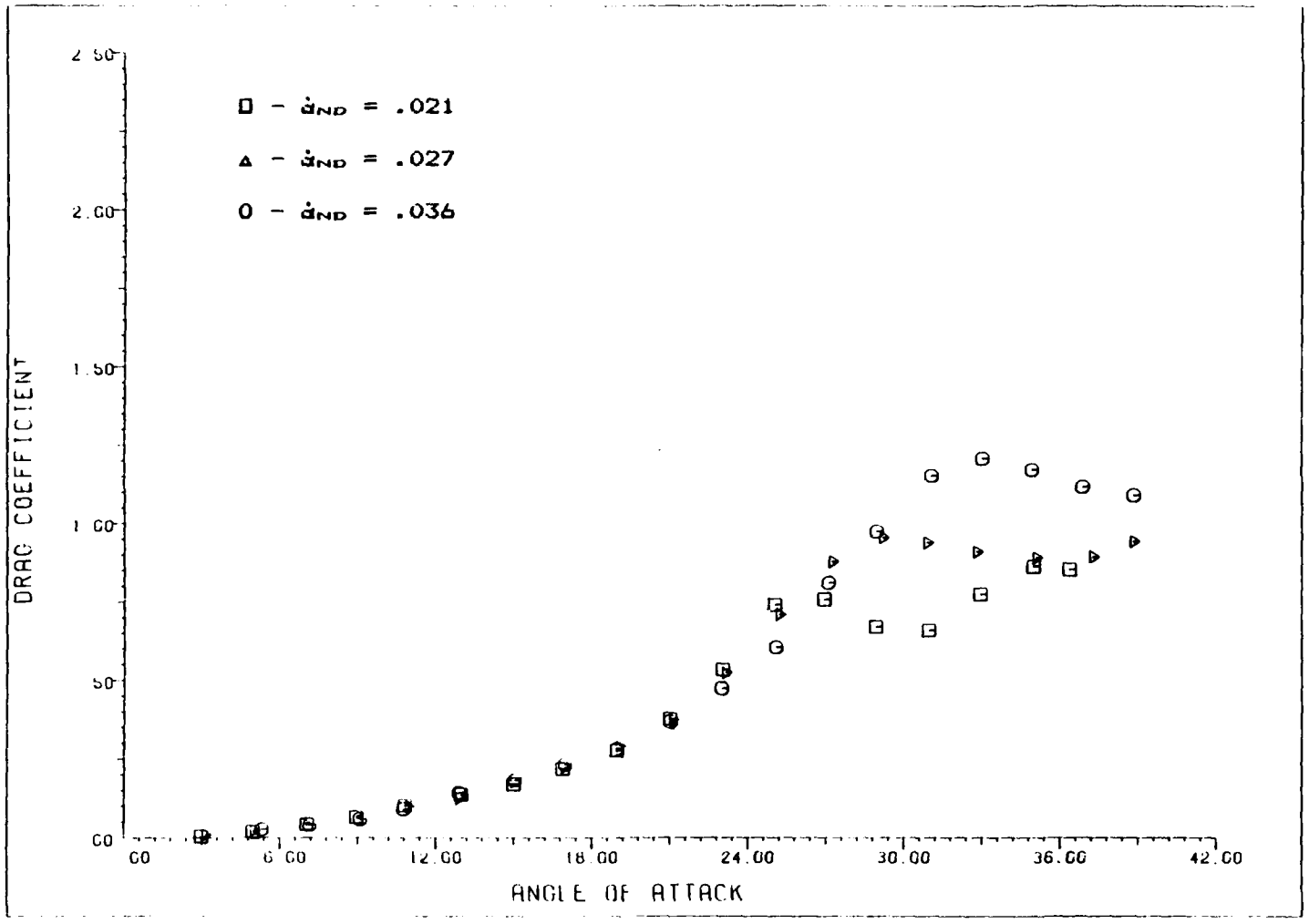

Figure 14. Combined Dynamic Stall Drag Curves
$\dot{\alpha}_{ND}$ = .021, .027, .036 Respectively
V = 29.07, Pitch Location #3 (.50c)

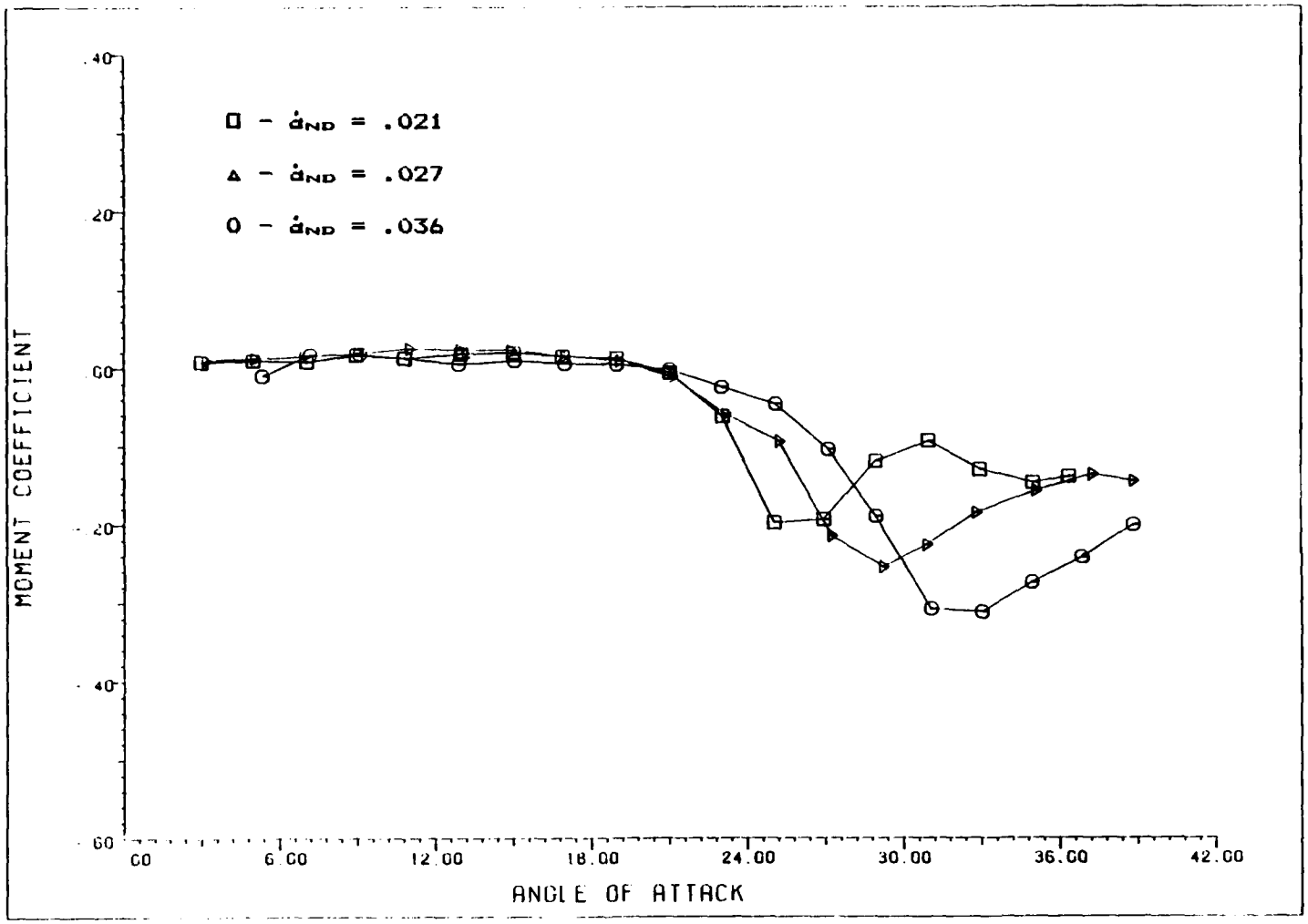

Figure 15. Combined Dynamic Stall Pitching Moment Curves
$\dot{\alpha}_{ND}$ = .021, .027, .036 Respectively
V = 29.07, Pitch Location #3 (.50c)

in the stall angle of attack, as shown in Fig 14. The moment coefficient was calculated for the airfoil quarter-chord point. Fig 15 shows the moment to be fairly constant through the initial part of the dynamic stall rotation followed by an abrupt increase with a large pitch down moment. This tendency was also noted by McCroskey, et. al. in their experimental investigations. Thus it appears that the non-dimensional angular rate has a direct impact on all airfoil aerodynamic forces.

The results of the experimental runs at pitch location number one (pitching about the .08 chord position) are provided in Table II. These data show a consistent trend of increased stall angle of attack with increased $\dot{\alpha}_{ND}$. Fig 16 shows this data plotted in the form developed by Deekens and Kuebler [6] where the change in stall angle of attack ($\Delta\alpha_{STALL}$) is plotted versus non-dimensional angular rate. As expected this shows a linear tendency between increased stall angle of attack and non-dimensional pitch rate. A linear least squares curve was fit through the data with the resulting equation:

$$\Delta\alpha_{STALL} = 5.06 + 173.89\ \dot{\alpha}_{ND} \qquad (15)$$

Where $\Delta\alpha_{STALL}$ is expressed in degrees. Although the

TABLE II

Data Summary for Pitch Location #1 - .08c

Test Run	Tunnel Velocity (ft/sec)	Rotation Rate (deg/sec)	α_{STALL} Static (degrees)	α_{STALL} Dynamic (degrees)	$\dot{\alpha}_{ND}$
1-1	25.43	85.95	16	26.4	.030
1-2	25.43	N/L	16	10.6	
1-3	24.97	183.17	16	31.5	.065
1-4	30.05	N/L	16	21.5	
1-5	30.03	112.84	16	27.1	.033
1-6	30.02	183.02	16	31.1	.054
1-7	35.64	44.19	16	22.5	.011
1-8	35.64	98.39	16	25.0	.024
1-9	35.32	129.16	16	27.0	.032
1-10	37.87	N/L	16	22.6	
1-11	37.57	95.16	16	24.6	.022
1-12	37.59	133.89	16	26.9	.031

Note: N/L means the rotation was non-linear

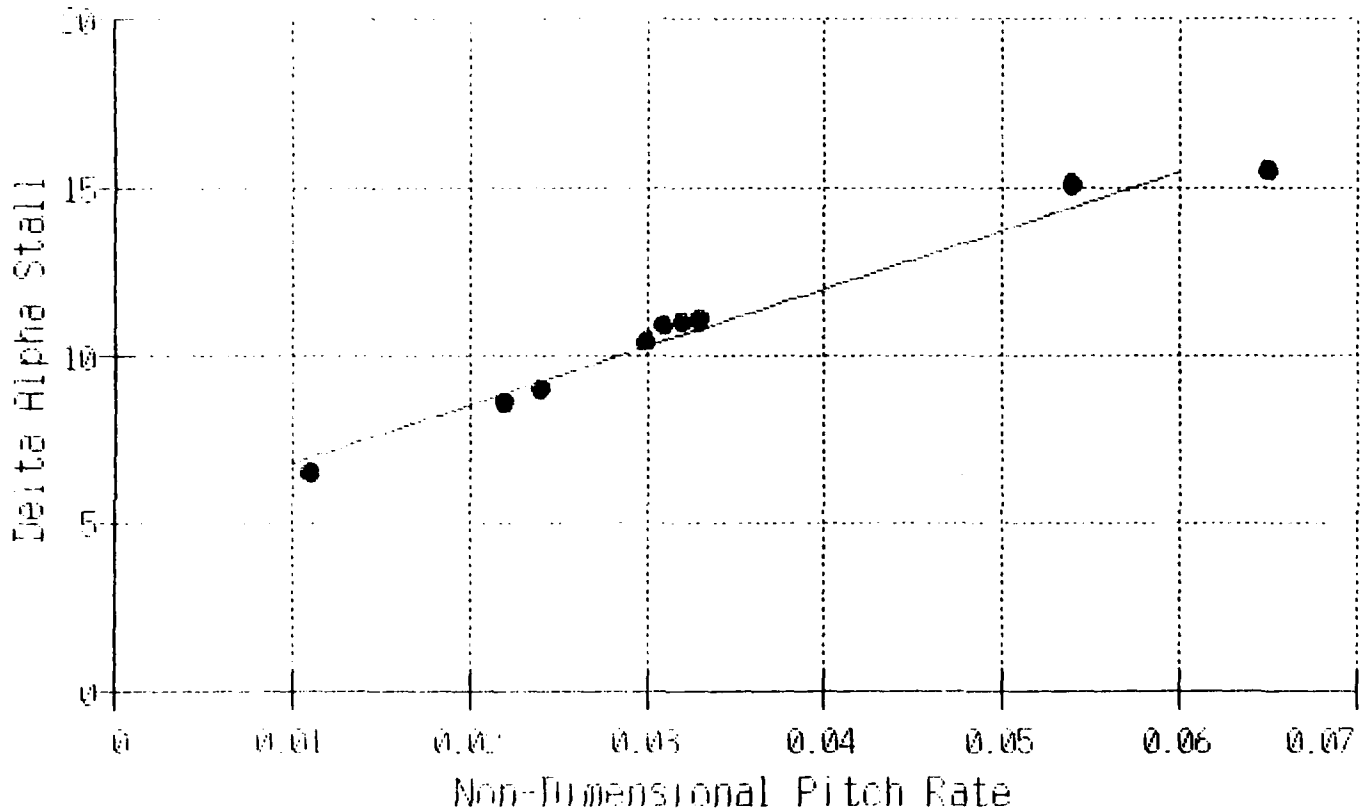

Figure 16. Data Summary for Pitch Location #1 (.08c)

correlation factor is high for this data, visual inspection suggests the possibility of a curve with decreasing slope as α_{ND} increases beyond about .05. This type of curve would be consistent with the findings of Daley and Deekens and Keubler for quarter-chord separation as shown in Fig. 3 (c.f. Introduction). However, there were insufficient data points at the higher nondimensional rates to substaintiate this idea.

The results of the experimental runs at the second pitch location (rotation about the .25 chord point) are given in Table III. Again the trends of increased stall angle of attack with increased pitch rate are present. Fig 17 shows the change in stall angle of attack versus non-dimensional pitch rate and the relationship again appears fairly linear. A least squares fit of this data yields the equation:

$$\Delta\alpha_{STALL} = 4.48 + 240.06\ \dot{\alpha}_{ND} \qquad (16)$$

The results of the experimental runs for pitching about the airfoil mid-chord are given in Table IV. These data should be directly comparable with the data of Schreck who also pitched about the mid-chord point. A comparison of Schreck's data and the results of this experiment is provided in Fig 18. A least squares fit of the mid-chord pitching data has the equation:

TABLE III

Data Summary for Pitch Location #2 - .25c

Test Run	Tunnel Velocity (ft/sec)	Rotation Rate (deg/sec)	α_{STALL} Static (degrees)	α_{STALL} Dynamic (degrees)	$\dot{\alpha}_{ND}$
2-1	25.57	74.04	15.5	25.1	.025
2-2	25.83	145.24	15.5	31.6	.049
2-3	25.20	175.61	15.5	33.6	.062
2-4	29.68	90.56	15.5	26.2	.027
2-5	29.68	117.02	15.5	29.4	.035
2-6	29.30	148.63	15.5	32.5	.045
2-7	35.23	N/L	15.5	26.5	
2-8	35.76	N/L	15.5	31.5	
2-9		DISK ERROR - DATA LOST			
2-10	40.38	59.29	15.5	23.1	.013
2-11	38.89	133.66	15.5	27.2	.030
2-12	39.21	170.13	15.5	29.4	.038
2-13	44.50	N/L	15.5	22.6	
2-14	45.03	101.53	15.5	24.3	.020
2-15	44.84	N/L	15.5	26.9	

Note: N/L means the rotation was non-linear

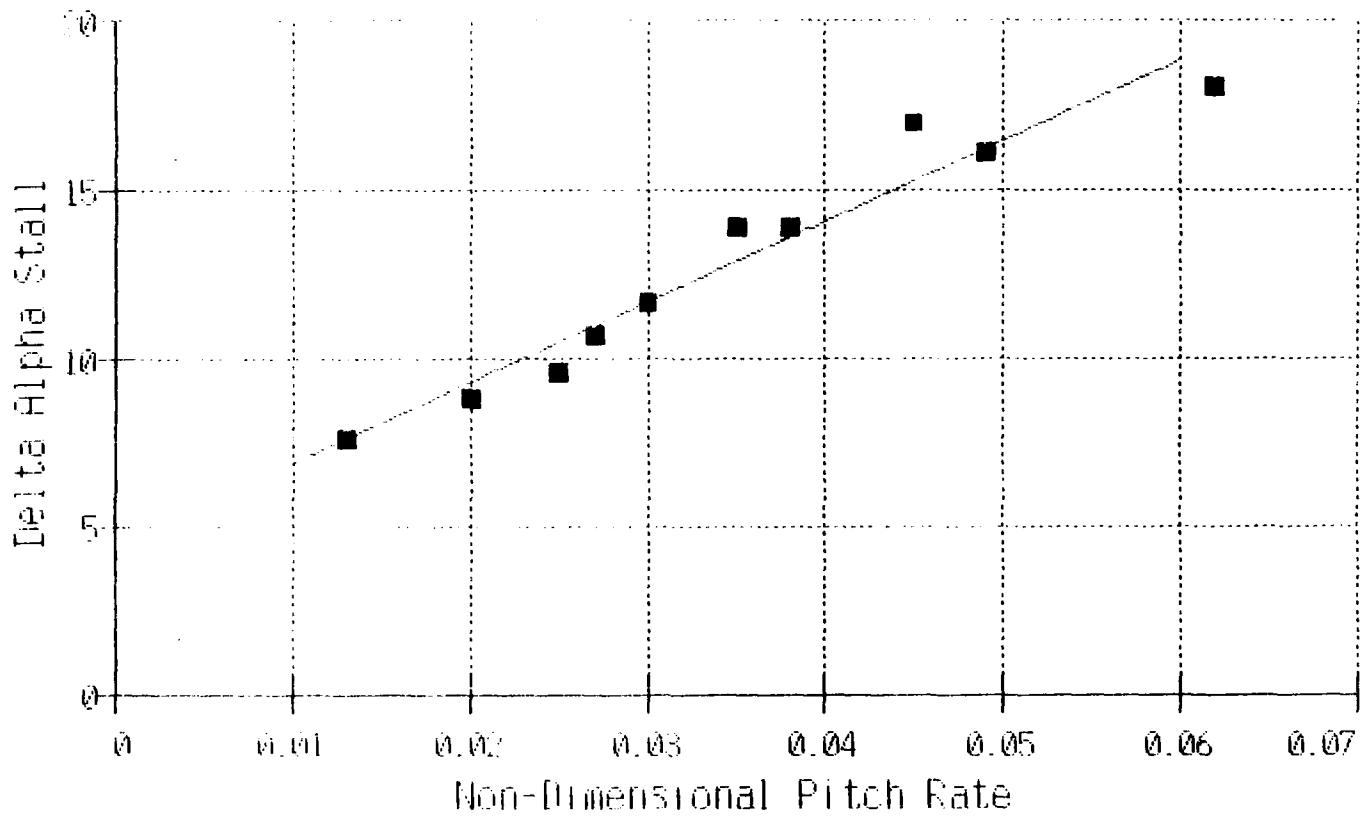

Figure 17. Data Summary for Pitch Location #2 (.25c)

TABLE IV

Data Summary for Pitch Location #3 - .50c

Test Run	Tunnel Velocity (ft/sec)	Rotation Rate (deg/sec)	α_{STALL} Static (degrees)	α_{STALL} Dynamic (degrees)	$\dot{\alpha}_{ND}$
3-1	25.77	83.07	15.8	28.5	.028
3-2	25.61	102.70	15.8	32.5	.036
3-3	25.86	N/L	15.8	34.4	
3-4	26.41	109.72	15.8	32.6	.037
3-5	29.16	69.01	15.8	25.5	.021
3-6		DISK ERROR - DATA LOST			
3-7	29.07	116.89	15.8	31.1	.036
3-8	31.52	97.70	15.8	28.5	.027
3-9	34.16	N/L	15.8	28.6	
3-10	35.92	N/L	15.8	30.4	
3-11	34.04	114.26	15.8	29.6	.030
3-12		DISK ERROR - DATA LOST			
3-13	39.55	74.57	15.8	23.2	.016
3-14	39.96	102.21	15.8	27.0	.022
3-15	39.09	N/L	15.8	32.5	
3-16	40.38	N/L	15.8	31.5	
3-17	44.04	N/L	15.8	28.5	
3-18	44.15	N/L	15.8	29.5	
3-19	43.90	N/L	15.8	29.6	

Note: N/L means the rotation was non-linear

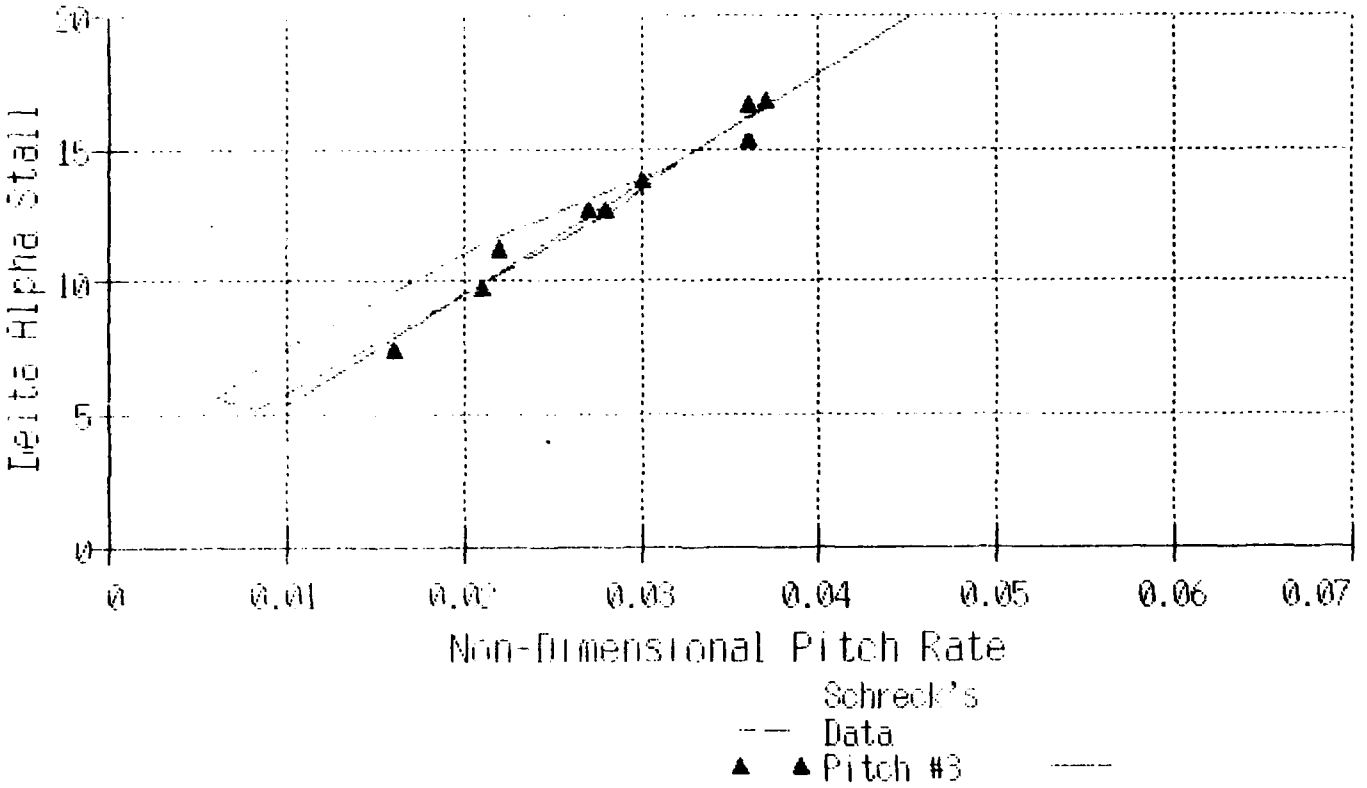

Figure 18. Data Summary for Pitch Location #3 (.50c) Including Schreck's Data

$$\Delta\alpha_{STALL} = 1.16 + 418.34\ \dot{\alpha}_{ND} \qquad (17)$$

These results tend to verify the findings of Schreck and increase the range of data into a higher non-dimensional pitch rate area. Thus the expected response of increased stall angle of attack with increased pitch rate seems to be confirmed.

When the results from the three pitch locations are combined into one graph, as shown in Fig 19, a definite trend exists between pitch location and change in stall angle of attack. This trend was predicted by Allaire who showed that the change in quarter chord separation angle of attack would increase as the pitch location moved from the leading edge to the trailing edge. The reasoning behind this argument points to the increased leading edge velocity induced during the rotation. As the rotation point moves backward along the airfoil, the stream velocity induced by the pitching motion is increased, thus for the same α_{ND} the leading edge velocity will increase as the pitch location moves aft. This increased velocity will increase the "mass ingestion" into the boundary layer and tend to help keep the flow attached to the wing for a longer period of time. Assuming that quarter chord separation is a precursor of airfoil stall, it is logical to extend the argument to

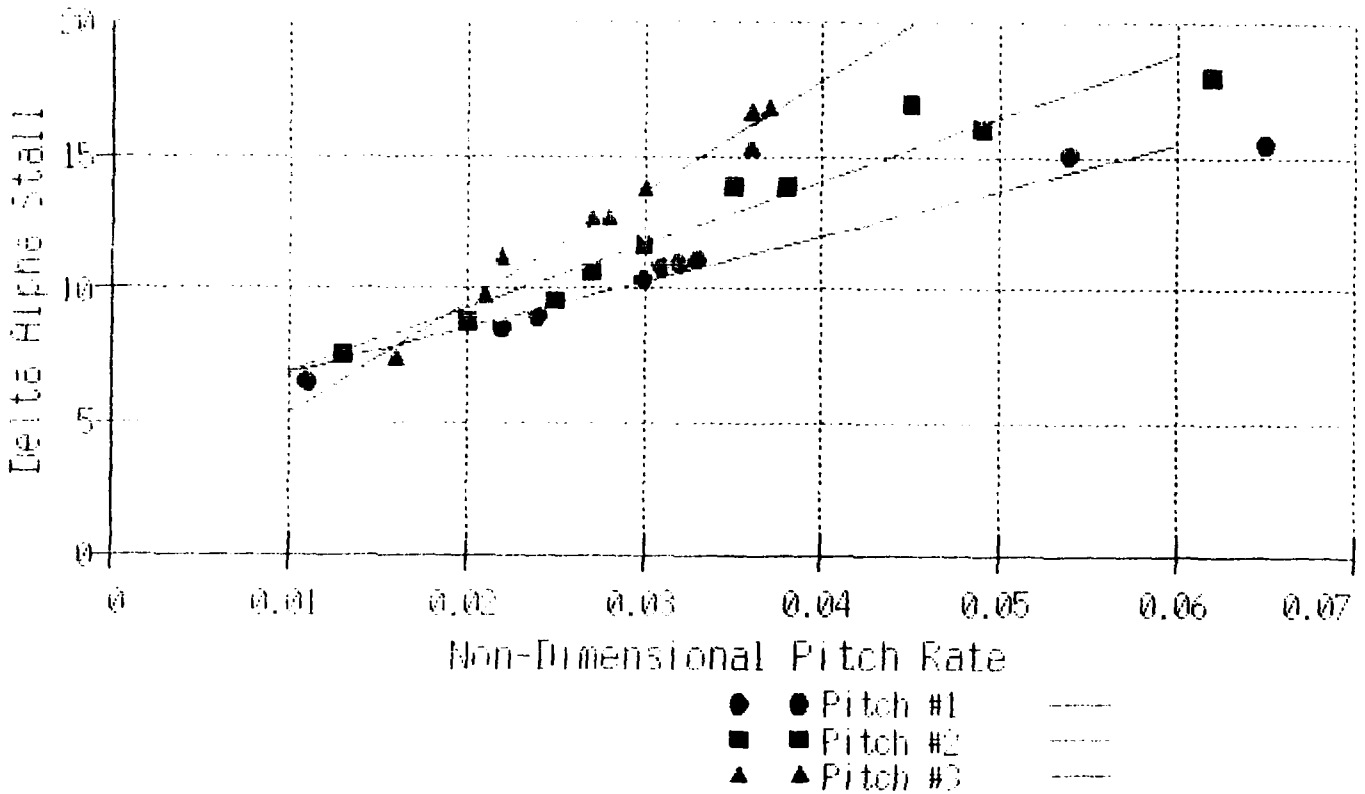

Figure 19. Combined Data Summary for Pitch Locations 1 - 3

include dynamic stall. Thus, moving the pitch location aft should have the same tendency as increasing the non-dimensional pitch rate, delaying stall and increasing the maximum lift.

The data from airfoil rotations about the fourth pitch location were not included in the previous discussion due to the change in experimental conditions. Table V lists the results of these test runs and the same tendency to a linear relationship between delta alpha stall and pitch rate exists in the data. A least squares fit of the data generates the equation:

$$\Delta\alpha_{STALL} = 2.52 + 329.42\,\dot{\alpha}_{ND} \qquad (18)$$

Fig 20 shows these results, however, when compared to the other pitch location data, as shown in Fig 21, it is seen that pitching about the .61 chord position brought a decrease in the change in stall angle of attack versus angular rate. Although this decreased slope may be an actual physical occurance, there seems to be no theoretical explanation for it. Another possible explanation for the discrepancy between experiment and theory falls in the realm of experimental procedure. Although the airfoil is symmetric and the pressure transducers are fairly evenly distributed near the leading edge, a disparity between upper and lower surface transducers

TABLE V

Data Summary for Pitch Location #4 - .61c

Test Run	Tunnel Velocity (ft/sec)	Rotation Rate (deg/sec)	α_{STALL} Static (degrees)	α_{STALL} Dynamic (degrees)	$\dot{\alpha}_{ND}$
4-1	25.75	82.45	15.5	26.5	.028
4-2	25.75	120.68	15.5	31.6	.041
4-3	26.17	139.43	15.5	33.6	.047
4-4	30.98	71.34	15.5	24.5	.020
4-5	28.66	118.84	15.5	30.6	.037
4-6	30.95	135.95	15.5	31.1	.039
4-7	36.46	61.92	15.5	23.0	.015
4-8	36.13	102.28	15.5	26.5	.025
4-9	33.54	135.95	15.5	30.5	.036
4-10	38.02	80.86	15.5	24.5	.019
4-11	38.01	157.60	15.5	29.4	.037
4-12	39.80	203.27	15.5	32.6	.045

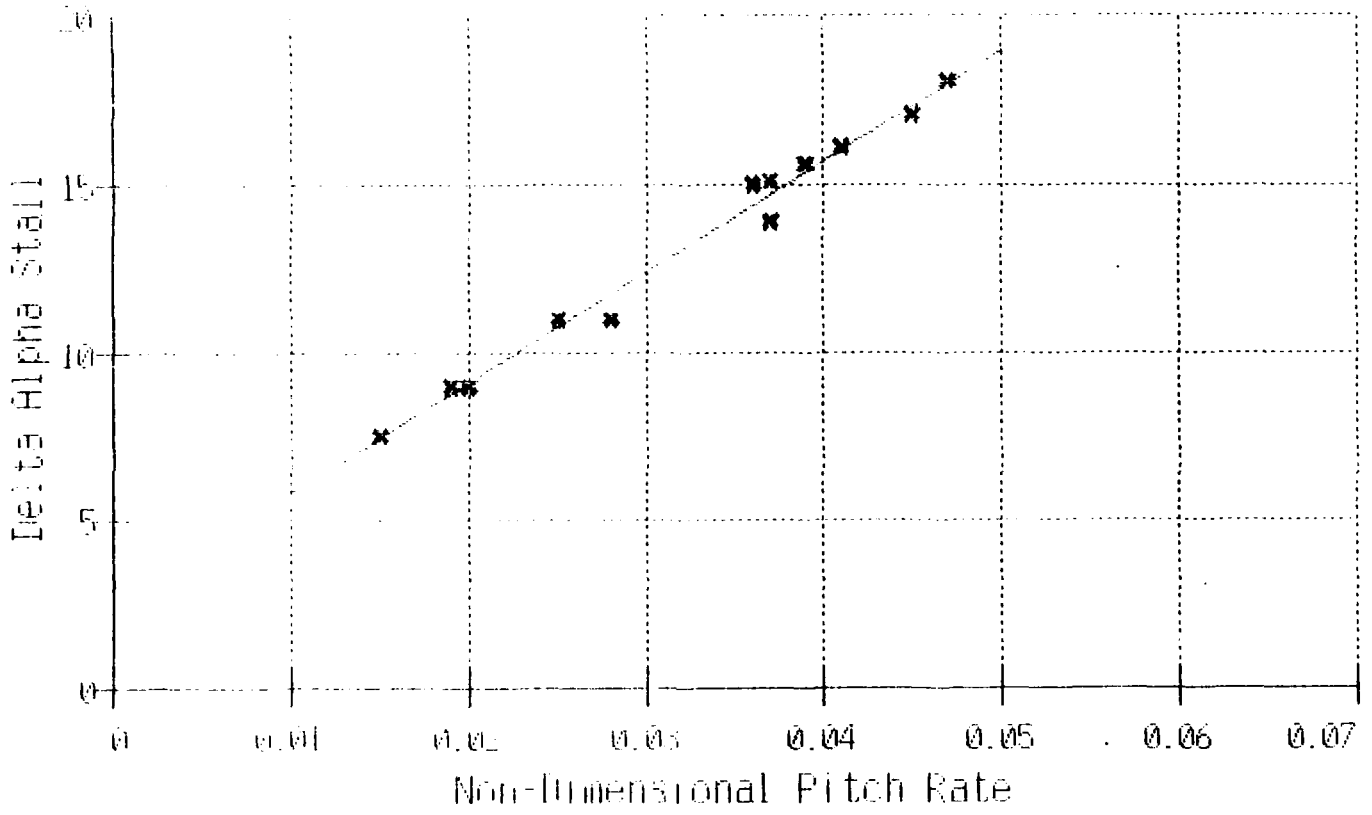

Figure 20. Data Summary for Pitch Location #4 (.61c)

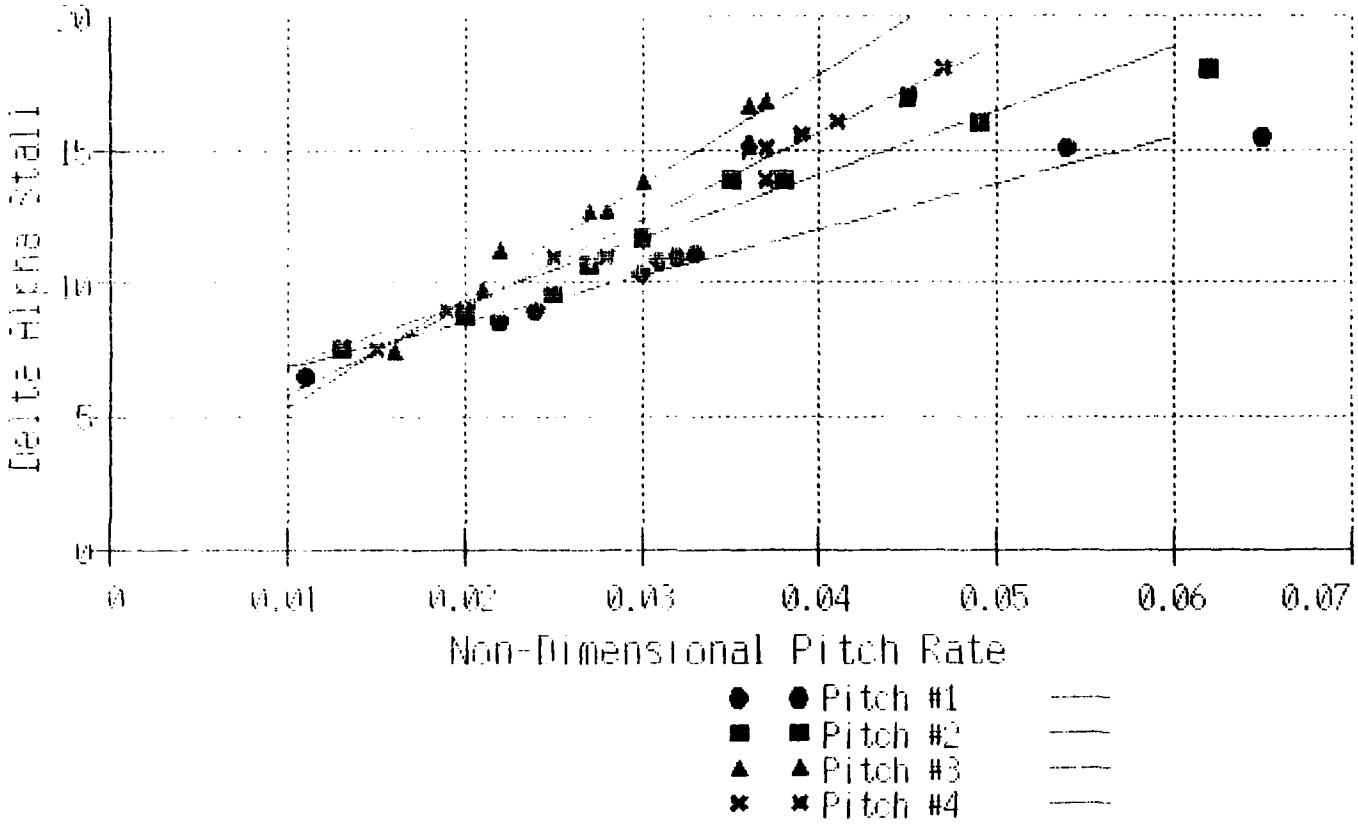

Figure 21. Combined Data Summary for Pitch Locations 1 - 4

exists in the aft portion of the airfoil. As mentioned previously, the vortex formed during dynamic stall eventually moves aft and departs the airfoil. The number of transducers and their location on the aft part of the airfoil strongly influences the ability of the data system to record and analyze the effects of this vortex. It is therefore assumed that the disparity in transducer locations led to the lower slope in Fig 20.

The idea of an effective pitch rate due to the location of the rotation point led to Fig 22. In this figure, α_{ND} was replaced by an $\dot{\alpha}^*$ in which $\dot{\alpha}^* = (PL)c\dot{\alpha}/V$, where PL is the airfoil pitch location expressed in terms of percent chord. For this experiment PL was equal to .08, .25, .50 and .61 respectively. As Fig 22 shows, the results discount the thought that dynamic stall data can be collapsed into one curve based on an effective non-dimensional pitch rate. Further attempts to collapse the pitch location data onto a single curve proved unsuccessful, although the existence of some universal length scale seems possible.

Another area of questionable results occurs in the static lift curves. When compared to the data presented in reference 11, there are obvious differences. The most notable being the zero lift point. For the NACA 0015, zero lift should occur at the zero angle of attack point, however, this was not the case as shown in Fig 23.

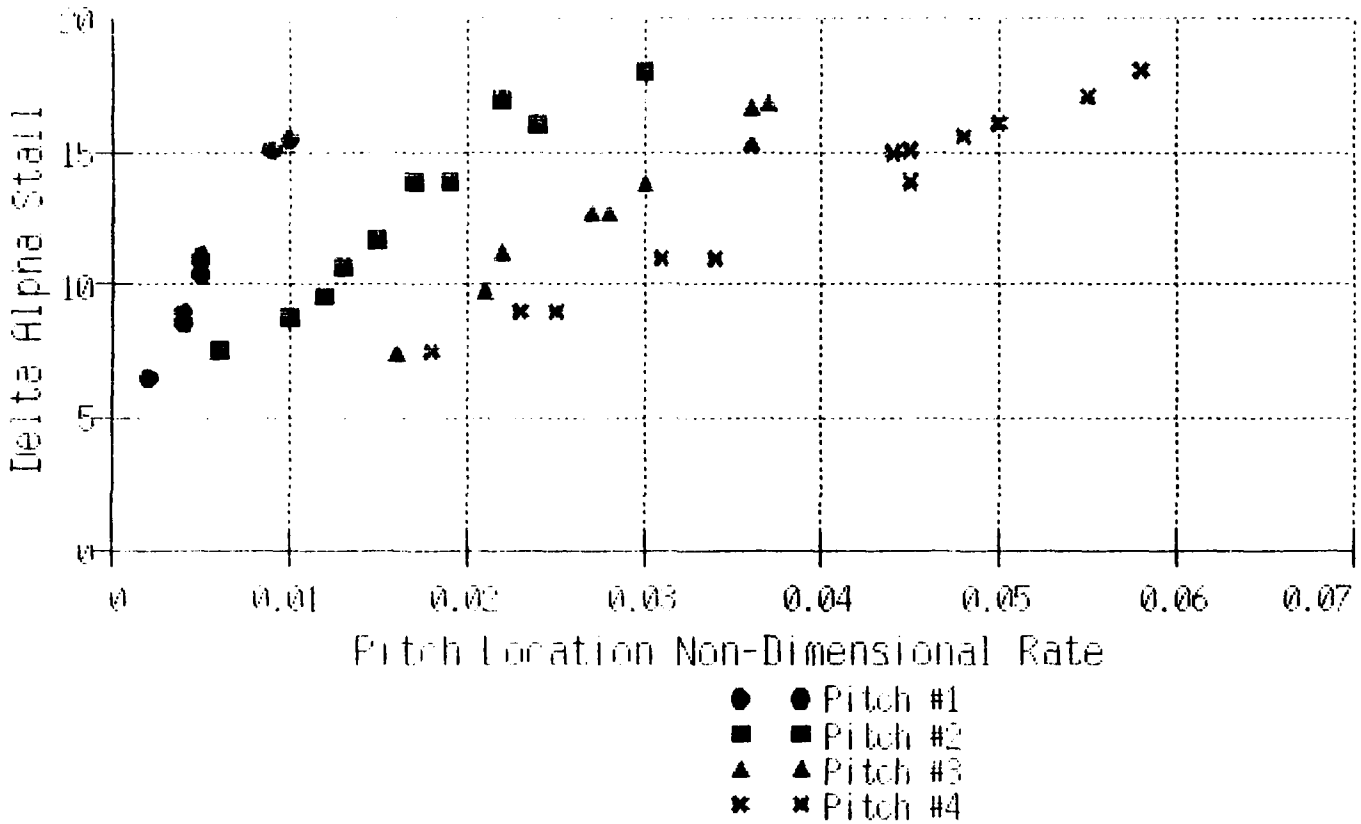

Figure 22. Combined Data Summary for Pitch Locations 1 - 4 Using the Pitch Location Non-Dimensional Rate ($\dot{\alpha}^*$)

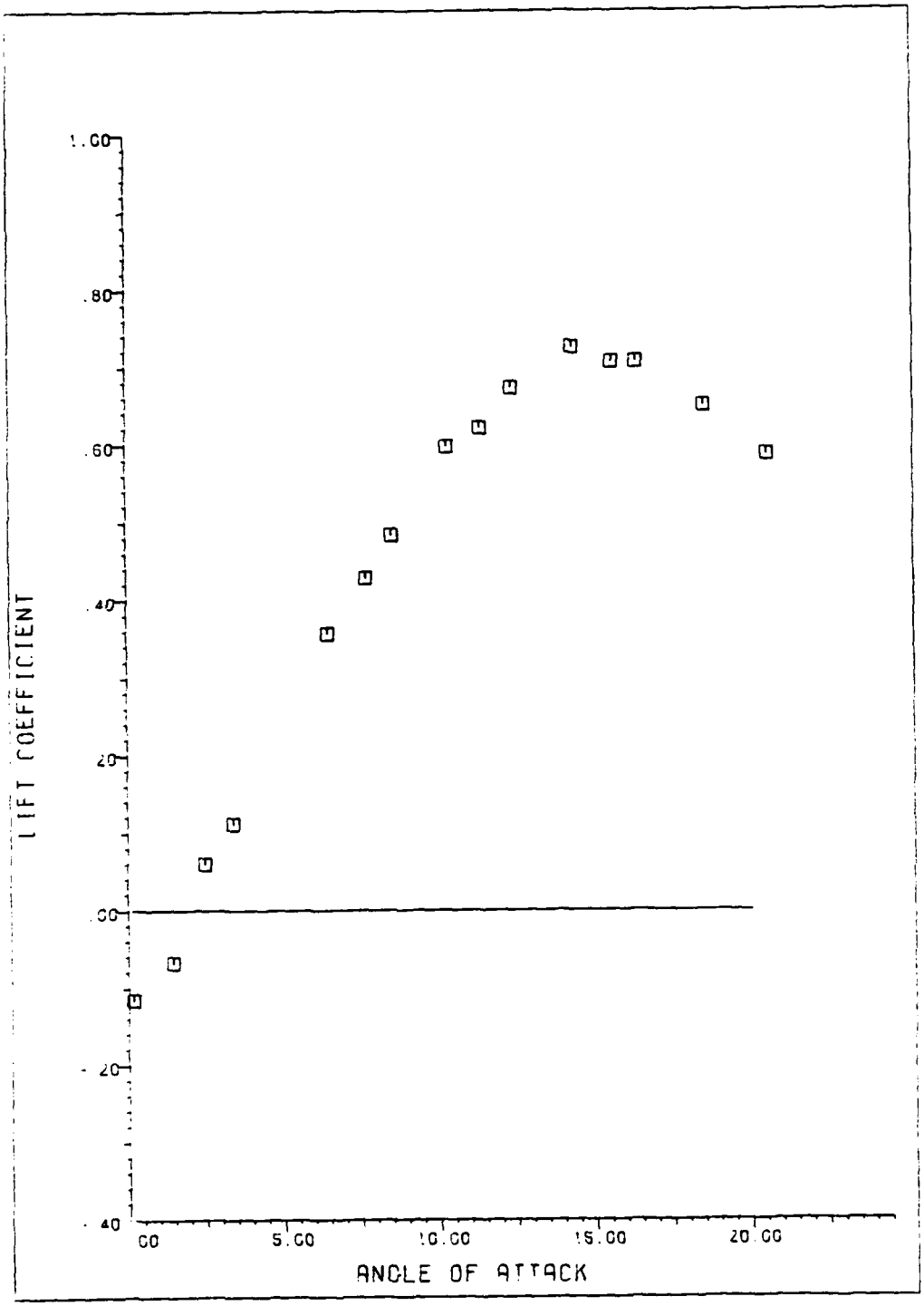

Figure 23. Data From Static Stall Lift Curve
V = 30.0 fps, Pitch Location #1 (.08c)

In order to make all references to static data consistent with the experimental procedure during the dynamic testing the static stall curve for pitch location four was obtained with downward rotation. The sign convention associated with this system would be equivalent to negative lift and negative angle of attack when compared to the other static lift curves. When this sign convention is adopted, the static lift data can be collapsed into Fig 24. The fact that the data from pitch location four represents a continuation of the upper lift curve leads to the conclusion that some form of flow angularity exists in the smoke-tunnel test section. If the flow angularity effects are corrected in the static data, the data compare favorably with that of reference 11. The existence of a flow angularity would also help explain the discrepancies that Schreck found in his static lift data [23:33-40]. Although this anglularity tends to skew the data, the overall effect on the results presented in this report is insignificant. This is due to the fact that the data is presented as a change in stall angle of attack and not as a representative angle of attack. Therefore, any angularity effects in the dynamic data should be cancelled by the equivalent angularity effect in the static data.

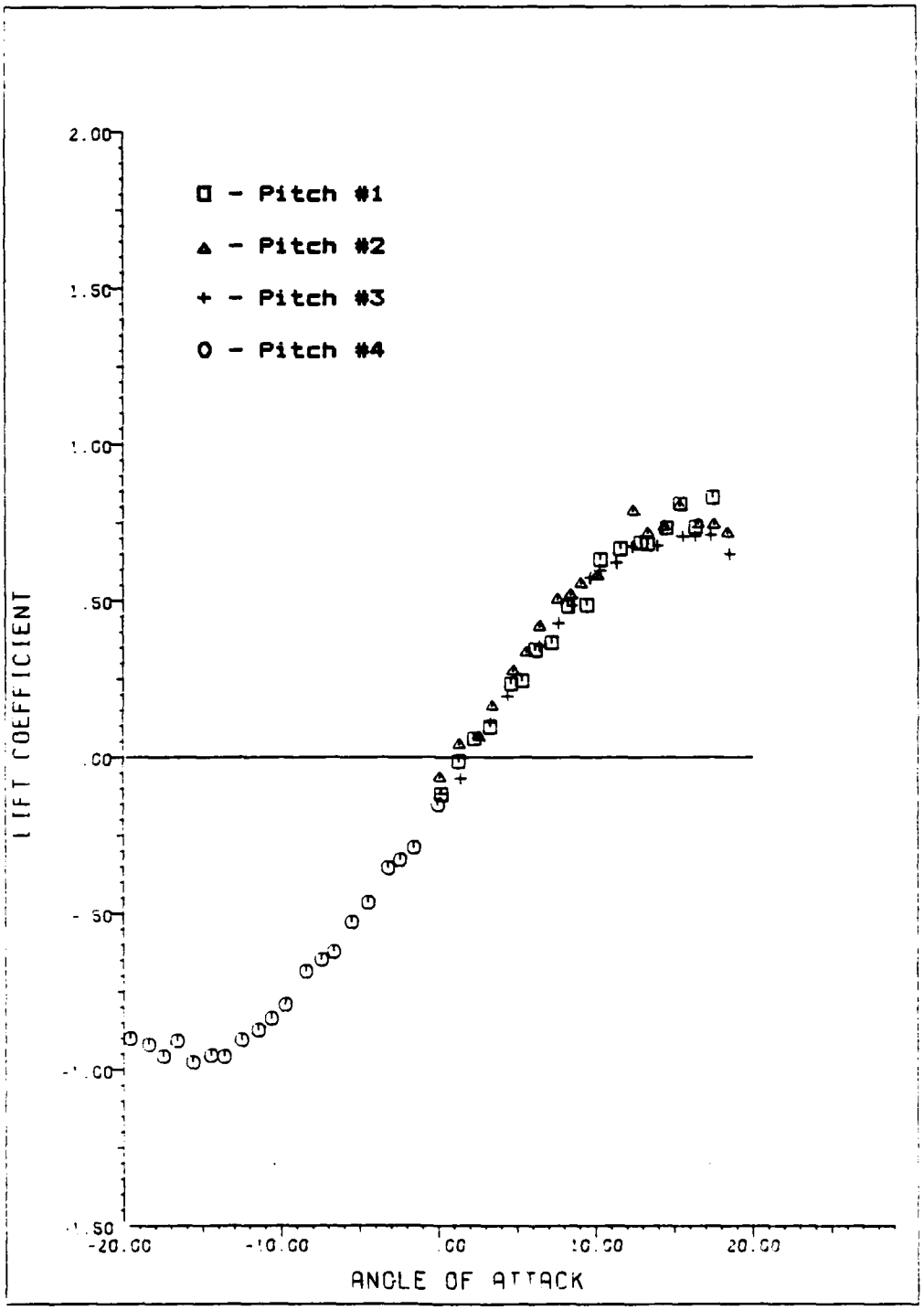

Figure 24. Combined Data From Static Stall Lift Curves Pitch Locations 1 - 4, V = 25.0 to 40.4 fps

Error Sources

As in any experimental investigation, the accuracy of the results depends on the amount of error introduced during the experimental process. Probably the largest problem in this investigation was maintaining a constant pitch rate throughout the dynamic stall event. As the data summary tables indicated, some test cases were eliminated due to a non-linear airfoil rotation. The necessity to eliminate these runs comes from the fact that most of the theoretical work in dynamic stall has dealt with a constant pitch rate. The addition of an angular acceleration would greatly complicate the problem and creates unpredictalbe results. As a result of these peculiarities, careful analysis of time versus angle of attack was performed for all experimental cases. One possible cause for the non-linear motion was the additional gearing placed on the existing rotation motor. This gearing was probably the reason that pitch down was required to obtain the data for pitch location four. Another possible source of error was frictional effects between the airfoil endplates and the test section walls. Although a good seal between the airfoil and the tunnel walls is desired to produce good two dimensional flow, this seal may have caused more error in the motor response. In either case, a non-linear motor response was not acceptable for representative

data.

Other sources of error in the data center on the tunnel test section and its flow qualities. As previously discussed, a flow angularity has been discovered although its effect on the experimental results was inconsequential. The possibility of three dimensional flow effects also exists in the test section. This condition could be caused by an interaction between the airfoil and the boundary layer formed along the test section walls [23:39]. Schreck tried to quantify these effects, but a true understanding is only possible through a careful experimental investigation involving the tunnel and the airfoil together. Tunnel flow quality is another area of concern in this experiment. There have been numerous modifications to the smoke tunnel since Baldner and Sisson performed their investigations during the initial tunnel setup. Turbulence level in the test section is one area that might play a large factor in the ultimate test results, leading to an increased angle of attack for both separation and stall. However, this effect should tend to cancel with the data representation assuming the tunnel turbulence level remained fairly constant. Finally, the tunnel inter-

ference effects of blockage and streamline curvature could have had a larger influence than previously anticipated. Without a large-scale test of the tunnel flow qualities, an accurate understanding of exactly what occurs in the test section will not exist.

VI. Conclusions and Recommendations

Conclusions

There are three major conclusions that can be drawn based on this experimental work. The first conclusion is that the dynamic stall effects are directly related to the non-dimensional pitch rate, $\dot{\alpha}_{ND}$. This can be seen through the fact that increasing $\dot{\alpha}_{ND}$ delays the point of airfoil stall and increases the maximum lift coefficient. The non-dimensional pitch rate also affects the airfoil drag and quarter chord pitching moment in a similar manner. As $\dot{\alpha}_{ND}$ increases, the maximum drag also increases and the airfoil pitching moment becomes more severe at the point of dynamic stall. The second conclusion concerns the effect of pitch location on dynamic stall. Based on the data from the pitch locations before the mid-chord, the effect of moving the pitch location aft of the leading edge is to in- crease the the dynamic stall angle of attack. This effect was accurately predicted by Allaire. The final conclusion stems from the static angle-of-attack data. Based on the information obtained during these tests, there is strong evidence that some form of flow angu- larity or disturbance exists in the smoke tunnel test section. This angularity appears to be on the order of two to two and a half degrees of flow misalignment.

Recommendations

There is still a great deal of research necessary before the entire dynamic stall phenomenon is completely understood. Although this work has tended to substantiate the predicted effects of pitch location, further work is necessary to completely determine pitch location effects on dynamic stall. The following are some of the recommendations for future research in dynamic stall:

First, re-investigate the effects of pitching the airfoil at locations beyond the mid-chord position. The results of this study were inconclusive in this area due to differences in test equipment and procedures. This investigation could be aided by returning to a direct drivesystem on the drive motor in order to provide the capability to rotate the airfoil in a pitch up motion.

Second, a major investigation of the smoke tunnel test section flow quality is a necessity. In order to effectively use this tunnel for testing two-dimensional aerodynamics, the test section flow characteristics must be known. It has become evident that some form of flow irregularity does exist and the cause of this problem should be discovered before future investigations are attempted.

Third, although the methods used in this study failed to collapse the non-dimensional pitch data into

one curve, the existence of an appropriate scaling factor is presumed. Further attempts to scale the data are necessary and may provide an insight into the pitch location effect on dynamic stall.

Finally, further experiments in dynamic stall are still in order. Although the data acquisition system has proven itself effective throughout this investigation, its abilities are limited by the model characteristics. Therefore, a larger model with more interior room is recommended. This larger model would allow for more transducers and help to eliminate some of the error introduced during the pressure distribution discretization process. Another recommendation for the new model would be to supply ambient pressure to the reference pressure ports of the transducers, thus eliminating the need to seal the interior airfoil chamber. This would greatly faciltate model changes and help reduce damage to the model. Finally, if a larger model is created, the experiment will need to be moved to a larger tunnel to avoid large tunnel errors due to blockage and streamline curvature. Although the benefits of a two dimensional flow would be lost, the AFIT five foot wind tunnel could provide the necessary test section qualities to continue the investigation of dynamic stall.

Bibliography

1. Allaire, Andre J. S., "Investigation of Potential and Viscous Flow Effects Contributing to Dynamic Stall," Master's Thesis, AFIT/GAE/AA/84S-1, Air Force Institute of Technology, 1984.

2. Baldner, J. L., "Completion of the Development of the AFIT Smoke Tunnel," Master's Thesis, AFIT/GAE-2, Air Force Institute of Technology, 1959.

3. Clancy, L. J. Aerodynamics. New York: John Wiley and Sons, 1975.

4. Daley, D. C., "Experimental Investigation of Dynamic Stall," Master's Thesis, AFIT/GAE/AA/82D-6, Air Force Institute of Technology, July 1983.

5. Daley, D. C. and Jumper, E. J., "Experimental Investigation of Dynamic Stall for a Pitching Airfoil," Journal Of Aircraft, 21, October 1984, pp. 831-832.

6. Deekens, A. C., and Kuebler, W. R., "A Smoke Tunnel Investigation of Dynamic Separation," Air Force Academy Aeronautics Digest - Fall 1978, 2-16, USAFA-TR-79-1 (February 1979).

7. Docken, R. G. Jr., Jumper, E. J., and Hitchcock, J. E. "Theoretical Gust Response Prediction of a Joukowski Airfoil," Proceedings of the Ninth Annual AIAA (Dayton-Cincinnati) Mini-Symposium, AIAA(DAY/CIN) 83-1 3-2-1-3-2-3 (February 1983).

8. Endevco Corporation. Series 8507 Miniature Piezo-resistive Pressure Transducers. San Juan Capistrano, California: Endevco Corp.

9. Francis, M. S., Keese, J. E., and Retelle, J. P. Jr. "An Investigation of Airfoil Dynamic Stall With Large Amplitude Motions," F. J. Seiler Research Laboratory, FJSRL-TR-83-0010 (October 1983).

10. Helin, Hank E. and Walker, John M., "Interrelated Effects of Pitch Rate and Pivot Point on Airfoil Dynamic Stall," AIAA 23rd Aerospace Sciences Meeting, Reno, NV, January 1985. AIAA 85-0130.

11. Jacobs, Eastman N., and Sherman, Albert. "Airfoil Section Characteristics as Affected by Variation of the Reynolds Number. NACA Report 586, 1937.

12. Jumper, E. J., Schreck, S. J., and Dimmick, R. L., "Lift Curve Characteristics for an Airfoil Pitching at Constant Rate," AIAA paper number AIAA-86-0117.

13. Jumper, E. J., "Mass Ingestion: A Perturbation Useful in Analyzing Some Boundary Layer Problems," work in progress.

14. Kramer, Von M., "Die Zunahme des Maximalauftriebes von Tragflugeln bie plotzlicher Anstellwinkel-vergro Berung (Boeneffekt)," Zeitschrift fur Flugtechnik und Motorluftschiffahrt, 7, 14 April 1932, pp. 185-189

15. Lawrence, John S., "Investigation of Effects Contributing to Dynamic Stall Using A Momentum-Integral Method," Master's Thesis, AFIT/GAE/AA/83D-12, Air Force Institute of Technology, 1983.

16. McCroskey, W. J., McAlister, K. W., Carr, L. W., and Pucci, S. L. "An Experimental Study of Dynamic Stall on Advanced Airfoil Sections," Vol. 1, July 1982, NASA TM-84245.

17. McCroskey, W. J., McAlister, K. W., Carr, L. W., and Pucci, S. L. "An Experimental Study of Dynamic Stall on Advanced Airfoil Sections," Vol. 2, July 1982, NASA TM-84245.

18. McCroskey, W. J. "The Phenomenon of Dynamic Stall," March 1981, NASA TM-81264.

19. McCroskey, W. J., "Unsteady Airfoils," Annual Review of Fluid Mechanics, 1982, pp. 285-311.

20. Pankhurst, R. C. and Holder, D. W. Wind Tunnel Technique. London: Sir Isaac Pittman and Sons, Ltd., 1954.

21. Rae, William H. Jr. and Pope, Alan. Low Speed Wind Tunnel Testing, 2nd ed. New York: John Wiley and Sons, 1984.

22. Scheubel, N. "Some Tests on the Increase of the Maximum Lift of Aerofoils Whose Angle of Incidence Changes at Constant Angular Velocity", Mitt deut Akad Luftfahrt-Forsch, 1, 39-45, (1942).

23. Schreck, Scott J., "Continued Experimental Investigation of Dynamic Stall," Master's Thesis, AFIT/GAE/AA/83D-21, Air Force Institute of Technology, 1983.

24. Sisson, F. E. II, "Completion of the AFIT Smoke Tunnel," Master's Thesis, AFIT/GAE-12, Air Force Institute of Technology, 1957.

AD-A164 322 PITCH-LOCATION EFFECTS ON DYNAMIC STALL(U) AIR FORCE INST OF TECH WRIGHT-PATTERSON AFB OH SCHOOL OF ENGINEERING R L DIMMICK DEC 85 AFIT/GAE/AA/85D-4 2/2

UNCLASSIFIED F/G 20/4 NL

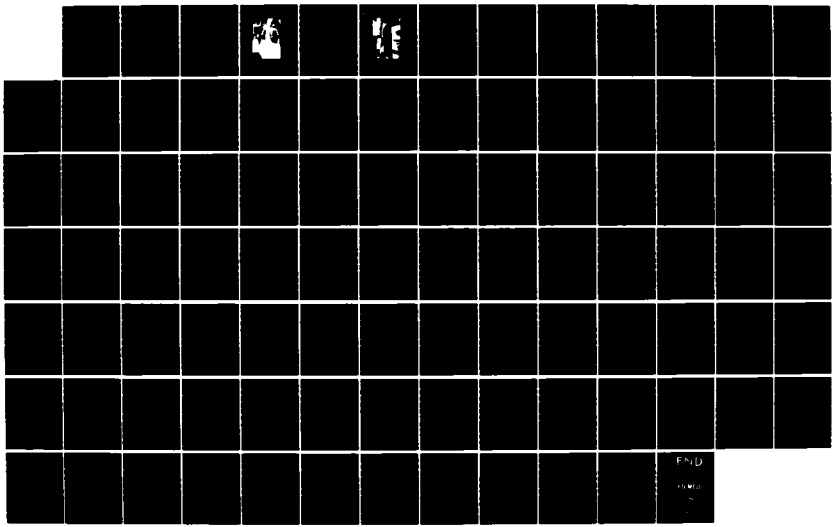

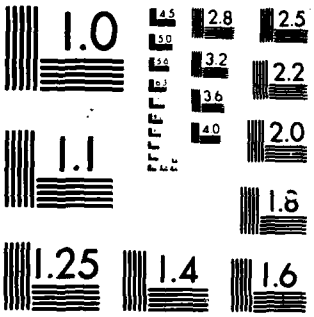

MICROCOPY RESOLUTION TEST CHART

NATIONAL BUREAU OF STANDARDS 1963 A

25. Tupper, Kenneth W., "The Effect of Trailing Vortices on the Production of Lift on an Airfoil Undergoing a Constant Rate of Change of Angle of Attack," Master's Thesis, AFIT/GAE/AA/83D-26, Air Force Institute of Technology, 1983.

26. Walker, J. M., Helin, H. E., and Strickland, J. H., "An Experimental Investigation of an Airfoil Undergoing Large Amplitude Pitching Motions," Air Force Academy Aeronautics Digest, April 1985. USAFA TR-85-2.

27. Williams, James C. III. "Incompressible Boundary-Layer Separtation," Annual Review of Fluid Mechanics, 9, 113-144 (1977).

APPENDIX A

Transducer Calibration

Introduction

Even though each transducer came from Endevco complete with its own factory calibration, all 16 transducers were recalibrated prior to their use in this experiment. As Table VI shows, most transducer sensitivities changed only slightly between the last known calibration and the pre-test calibration conducted for this investigation. Calibration of the transducers was subsequently repeated at the completion of the data collection. Comparison of the pre- and post-test calibrations shows no transducer undergoing a sensitivity change greater than approximately two percent.

Apparatus

A simpler and more accurate method of calibrating the transducers was one of the goals of this continuation study. Schreck used a complicated process to calibrate each transducer individually using a suction cup apparatus [23:70-75]. In order to simplify the calibration, a means of supplying the same calibration pressure to all 16 transducers simultaneously was necessary. This requirement led to the construction of the calibration chamber shown in Fig 25. Due to the

Figure 25. Pressure Transducer Calibration Chamber

use of electronic pin connectors and the redesigned tunnel mounting fixture, the airfoil could be removed from the tunnel and placed in the calibration chamber with only minor difficulty. The chamber consisted of a baseplate and a large bell jar. The base plate was constructed from 1/2 inch Aluminum and had three holes drilled into it. The large center hole permitted the airfoil rotation shaft to protrude from the plate and used a collar attached to the shaft to hold the airfoil in place and form a seal. The airfoil was mounted so that the slot in the rotation shaft was outside the chamber, allowing ambient air into the airfoil shell. The two other holes were used for supply and measurement of the calibration pressure and had quarter-inch fittings for tygon tubing. One tube led to a Meriam A-937 water micromanometer and the other went to a hand vacuum pump. The vacuum pump was used to create the calibration pressure and the micromanometer was used to measure the pressure within the chamber. With the airfoil mounted to the baseplate, as shown in Fig 26, the bell jar was placed over it to form an airtight chamber.

Calibration Procedure

The computer, the transducer power supply and voltmeter were powered up and allowed to warm up for one hour before the actual calibration began. A light

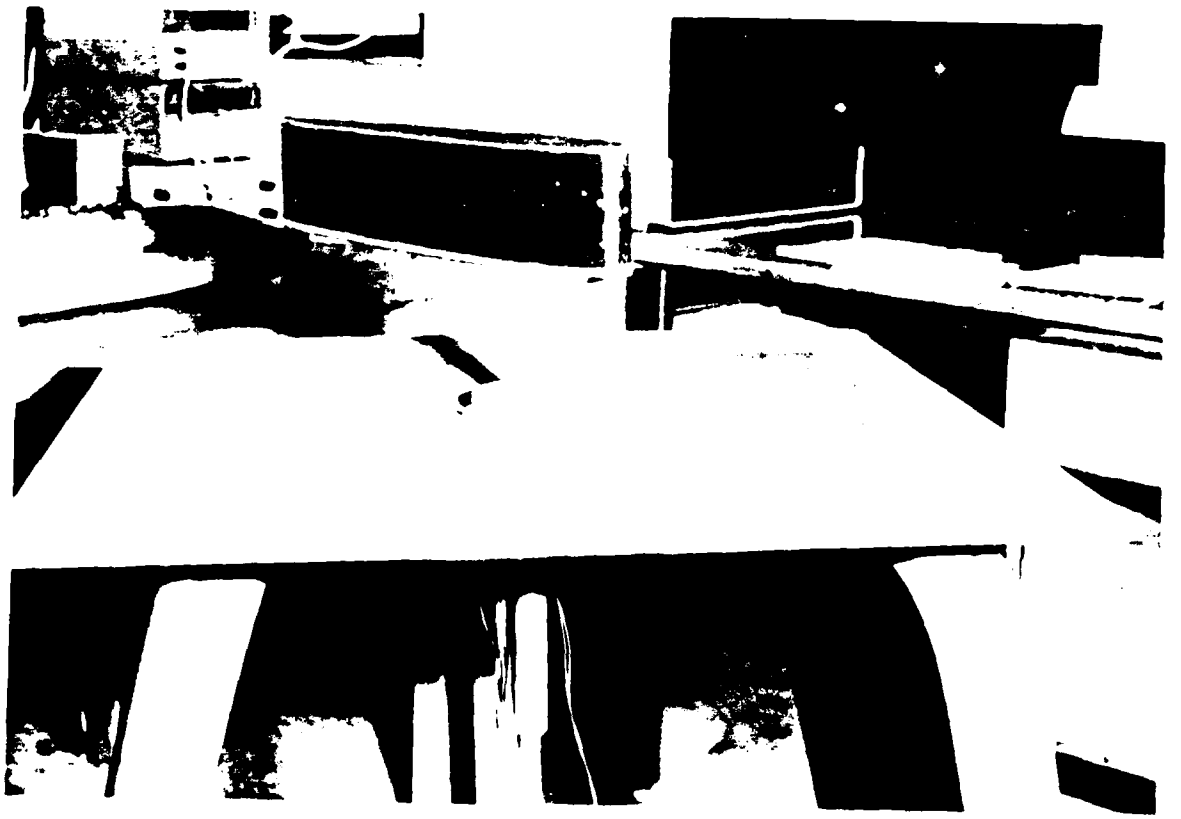

Figure 26. Airfoil Mounted on Calibration Chamber Baseplate

coating of silicon vacuum grease was applied to the bell jar and it was placed on top of the baseplate. The micromanometer was zeroed and then set to the desired calibration pressure. Using the hand pump, the chamber pressure was lowered until it read the value set on the micromanometer. Next, the calibration program, CALTRAN, was initiated. After applying a calibration pressure to the chamber the program would continuously sample all 16 transducers and determine an average digital reading based on 100 samples. The transducer data and calibration pressure were then written to disk for later use.

A total of five successively lower water column heights were used in calibrating the transducers. These heights ranged between zero and minus four inches, spaced at one inch intervals. This calibration process was repeated five times giving a total of twenty five data points for each transducer. These data points were then plotted on a graph having the pressure input to the transducer in inches of water on its horizontal axis and the pressure reading from the transducer in digital counts on the horizontal axis. In all cases the data proved to be linear and a least squares fit was accomplished to determine the slope of the calibration curve. The transducer sensitivity was then calculated by taking the calibration curve slope in digital counts per inch of water and converting it

to units of millivolts per psi (pounds per square inch) using the following formula:

$$\frac{mV}{psi} = \frac{digital\ ct}{inch\ H_2O} \times \frac{100\ mV}{4096\ digital\ ct} \times \frac{27.68\ inch\ H_2O}{psi}$$

The calculated transducer sensistivities were then used in the experimental software for both data collection and data reduction.

A repeat of the entire calibration process at the conclusion of all data gathering showed no appreciable difference in the transducer calibrations as shown in Table VI. The only exception being transducer 7 A which was damaged during the change of airfoil end-plates. This transducer could not be recalibrated, although based on the response of the other transducers it would be expected that there was no significant change in transducer response.

TABLE VI

Transducer Calibration Sensitivities

Transducer	Last Known Calibration (mV/psi)	Pre-test Calibration (mV/psi)	Post-test Calibration (mV/psi)
1	196.2	202.5	204.6
2	168.4	172.3	173.3
3	173.5	176.3	174.9
4	226.4	231.7	234.5
5	203.8	204.6	205.4
6	200.1	204.6	202.1
7 A		116.2	*****
7 B		189.5	190.8
8	208.8	216.4	212.5
9	170.9	174.0	175.2
10	113.9	113.8	114.0
11	119.3	114.4	115.2
12	112.3	113.6	112.1
13	139.2	136.6	137.9
14		165.3	167.0
15	217.4	219.6	220.8
16	217.2	222.8	221.2

Note: Transducer 7A was damaged during the experiment and therefore a post-test calibration was not possible.

Appendix B

Software Package

The following appendix contains copies of the pertinent software written for this experiment. Permanent copies of all programs used during this experiment have been archived on floppy disks and are located in Room 142, Bldg 640, Wright-Patterson AFB.

The following programs are listed in this appendix:

TESTRUN - This is the data collection and storage program. The program requests the experimental conditions, collects the experimental time, position, and pressure data in digital form, and stores the data to disk. Finally, the program collects pressure and position data for the static stall data base.

DOS2A - This is the main data reduction program. The program reads the data files created by the TESTRUN program and then converts the pressure data into pressure coefficients. These pressure coefficients are integrated numerically to obtain aerodynamic force and moment coefficients. This program creates a reduced data output file REDUDATA.DAT which contains experimental conditions, time, position, pressure coefficients, and lift, drag, and moment coefficients for the five airfoil rotations.

DATRED - This is the final data averaging program. The REDUDATA.DAT file created by DOS2A is read and the position and force coefficients are used to form an ensemble averaged data set for the test condition. The time and position data are also used to determine an average angular rotation rate and linearity of the airfoil drive motor. The output file from this program contains airfoil rotation rate, position, and lift, drag and moment coefficients.

```
      PROGRAM TESTRUN
C ----  To gather and store data for further processsing
C ----  Link:  TESTRUN,STCLK,GETTIM,ADIO,FORLIB/S,TESTRUN/N/E
C
      IMPLICIT INTEGER (A-Z)
      REAL AVSTAT(16),STATIC(16),BAROM,TEMP,MANOM1,MANOM2,TUNVEL
      REAL MOTVOL,P90,PO,RHO,DTIM,DPOSV,DPOSD,ROTRAT,VPD
      REAL PORTU(10),PORTL(10),SENS(16),CPU(10),CPL(10)
      REAL IDATAT(16),NORMCO,PRESS,STICKY
      REAL CP(16),AREAUT,AREALT,LNGTHU,LNGTHL,AREAU,AREAL,INTU,INTL
      INTEGER IDATA(3960),HOUR,CHECK,CHAN,DAY,MONTH,YEAR,XX
      INTEGER VALUE,CHEK,NS,N,A,DI,K,J,B,AA,L,C,KOUNT,S,T,U,DD,EE,ZZ
      INTEGER DIFANG,INK,RUNS,XXX,YYY,RRR,ZERANG,SNAP,SELECT
      INTEGER CHECK,CHEK,CHAN,VALUE,KOUNT,Z,W,S,CCC
      INTEGER II,JJ,KK,WW,DD,X,V,Y,TT,ZZZ
      INTEGER SDATA(5,18)
      REAL CNORM
C
C ---- Load transducer sensitivities (millivolts/psi)
      DATA SENS/202.5,172.3,176.3,231.7,204.6,204.6,189.5,
     +216.4,174.0,113.8,114.4,113.6,136.6,165.3,219.6,222.8/
C
C ---- Load transducer locations on upper surface (percent chord)
      DATA PORTU/0.0,0.0242,0.0484,0.0969,0.129,0.194,0.323,0.605,
     +0.888,1.000/
C
C ---- Load transducer locations on lower surface (percent chord)
      DATA PORTL/0.0,0.0161,0.0319,0.0484,0.0969,0.194,0.323,
     +0.686,1.000/
C
C ----  Initialize count of passes to zero.
C
 10   KOUNT=0
C
C ----  Input date, time, barometer, and room temperature
C ----  for experimental records.
C
      WRITE (1,15)
 15   FORMAT (' ENTER DAY, MONTH, YEAR SEPERATED BY COMMAS',/)
      READ (1,20)DAY,MONTH,YEAR
 20   FORMAT (I3,I3,I3)
      WRITE (1,25)
 25   FORMAT ('  ENTER TIME (MILITARY: XXXX HOURS)',/)
      READ (1,30)HOUR
 30   FORMAT (I5)
      WRITE (1,35)
 35   FORMAT (' ENTER BAROMETER (INCHES OF MERCURY)',/)
      READ (1,40)BAROM
 40   FORMAT (F7.2)
      WRITE (1,45)
 45   FORMAT (' ENTER ROOM TEMPERATURE (DEGREES FAHRENHEIT)',/)
      READ (1,50)TEMP
 50   FORMAT (F6.1)
C
```

```
C ----  Echo date, time, barometer, and room temperature for
C ----  verification.  Offer option to correct faulty input.
C
        WRITE (1,55)DAY,MONTH,YEAR
 55     FORMAT (' DAY:',I3,'    MONTH:',I3,'    YEAR:',I3)
        WRITE (1,60)HOUR
 60     FORMAT (' TIME:',I5)
        WRITE (1,65)BAROM
 65     FORMAT (' BAROMETER:',F7.2,' INCHES OF MERCURY')
        WRITE (1,70)TEMP
 70     FORMAT (' ROOM TEMPERATURE:',F6.1,' DEGREES FAHRENHEIT')
        WRITE (1,75)
 75     FORMAT (///,'                    ARE THE INPUTS, ECHOED ABOVE,')

        WRITE (1,80)
 80     FORMAT ('                    CORRECT?  IF SO, ENTER A 1',/)
        READ (1,85)CHECK
 85     FORMAT (I1)
        IF (CHECK.NE.1) GO TO 10
C
C ----  Following part of program calculates an average zero-input
C ----  reading for each transducer.  Average is obtained from 100
C ----  readings of each transducer.
C
        WRITE (1,90)
 90     FORMAT (///,' THIS PART OF THE PROGRAM OBTAINS AVERAGE')
        WRITE (1,95)
 95     FORMAT (' TRANSDUCER ZERO-INPUT READINGS.  WHEN TEST-')
        WRITE (1,100)
 100    FORMAT (' SECTION VELOCITY IS ZERO, HIT RETURN KEY')
        WRITE (1,102)
 102    FORMAT (' IN RESPONSE TO "PAUSE" ',///)
        PAUSE
C
C       Initialize all array elements to zero.
C
 110    CONTINUE
        DO 120 Z=1,16
        AVSTAT(Z)=0.0
 120    CONTINUE
C
C ----  Take 100 readings from each transducer, average them as shown
C ----  below. then write these averages to terminal. Also offer the
C ----  option to retake the average zero-input readings.
C
        DO 150 S=1,100
        DO 160 T=1,16
        CHAN=T-1
        CALL AD(VALUE,CHAN,80)
        AVSTAT(T)=AVSTAT(T)+(VALUE/100.0)
 160    CONTINUE
 150    CONTINUE
C
C
```

```
      WRITE (1,155)
 155  FORMAT (' AVERAGE ZERO-INPUT READINGS FOLLOW',/)
C
      DO 180 W=1,16
      WRITE (1,165)W,AVSTAT(W)
 165  FORMAT (' TRANSDUCER',I3,' AVERAGE STATIC READING:',F6.0)
 180  CONTINUE
      WRITE (1,177)
 177  FORMAT (///,' TO PROCEED WITH THE PROGRAM, ENTER A 1',/)
      READ (1,178)XX
 178  FORMAT (I2)
      IF (XX.NE.1) GO TO 110
C
C
C ----  Enter manometer reading, motor voltage, and 90 and 0
C ----  degree angle of attack voltages for experimental records.
C ----  Test-section velocity is also computed as shown below.
C
C
      WRITE (1,185)
 185  FORMAT (//////,'*****************************NOW TURN ON THE
     + TUNNEL***************************',//////)
 187  WRITE (1,190)
 190  FORMAT (' ENTER ROOM PRESS. MINUS TUNNEL STAT. PRESS.
     + (INCHES OF WATER)',/)
      READ (1,195)MANOM1
 195  FORMAT (F8.4)
      WRITE (1,200)
 200  FORMAT (' ENTER TUNNEL TOTAL PRESS. MINUS TUNNEL STATIC PRESS.
     + (INCHES OF WATER)',/)
      READ (1,195)MANOM2
 205  FORMAT (F8.4)
      WRITE (1,210)
 210  FORMAT (' ENTER MOTOR VOLTAGE (VOLTS)',/)
      READ (1,215)MOTVOL
 215  FORMAT (F6.2)
      WRITE (1,220)
 220  FORMAT (' ENTER 90 AND 0 DEGREE VOLTAGES, RESPECTIVELY',/)
      READ (1,225)P90,P0
 225  FORMAT (2F7.4)
      RHO=(BAROM*70.45)/(1716.0*(460.0+TEMP))
      TUNVEL=SQRT((2.0*(5.204*MANOM2))/RHO)
C
C ----  Echo manometer readings, tunnel velocity, motor voltage and
C ----  90 and 0 degree angle of attack voltages for verification.
C ----  offer option to correct faulty input.
C
      WRITE (1,230)MANOM1
 230  FORMAT (' MANOMETER ONE: ',F8.4,' INCHES OF WATER')
      WRITE (1,233)MANOM2
 233  FORMAT (' MANOMETER TWO: ',F8.4,' INCHES OF WATER')
      WRITE (1,235)TUNVEL
 235  FORMAT (' TUNNEL VELOCITY: ',F7.2,' FT/SEC')
      WRITE (1,240)MOTVOL
```

```
 240    FORMAT (' MOTOR VOLTAGE: ',F6.2,' VOLTS')
        WRITE (1,245)P90,PO
 245    FORMAT (' P90: ',F7.4,' VOLTS      PO: ',F7.4,' VOLTS')
        WRITE (1,75)
        WRITE (1,80)
        READ (1,85)CHEK
        IF (CHEK.NE.1) GO TO 187
C
C ----  The following part of the program writes pertinent
C ----  information to file RAWDATAODAT on disk.
C
        CALL OPEN (3,'RAWDATAODAT',2)
        WRITE (3,500)
 500    FORMAT (' DAY',10X,'MONTH',9X,'YEAR',9X,'TIME')
        WRITE (3,510)DAY,MONTH,YEAR,HOUR
 510    FORMAT (I3,11X,I3,11X,I3,9X,I5,/)
        WRITE (3,520)
 520    FORMAT (' TEMPERATURE',14X,'BAROMETER')
        WRITE (3,530)TEMP,BAROM
 530    FORMAT (2X,F6.1,18X,F7.2,/)
        WRITE (3,540)
 540    FORMAT (' MANOMETER 1',22X,'MANOMETER 2')
        WRITE (3,545)MANOM1,MANOM2
 545    FORMAT (2X,F8.4,25X,F8.4,/)
        WRITE (3,550)
 550    FORMAT (' TUNNEL VELOCITY',22X,'MOTOR VOLTAGE')
        WRITE (3,555)TUNVEL,MOTVOL
 555    FORMAT (4X,F7.2,31X,F6.2,/)
        WRITE (3,560)
 560    FORMAT (' 90 DEG. VOLTAGE',16X,'0 DEG. VOLTAGE')
        WRITE (3,570)P90,PO
 570    FORMAT (5X,F7.4,23X,F7.4,/)
        WRITE (3,580)
 580    FORMAT (' NUMBER OF PASSES',10X,'NUMBER OF IDATA ELEMENTS')
        WRITE (3,590)
 590    FORMAT (5X,'(KOUNT)',26X,'(N)')
        KOUNT=200
        N=3600
        WRITE (3,600)KOUNT,N
 600    FORMAT (3X,I6,26X,I6,//)
        WRITE (3,610)
 610    FORMAT (' AVERAGE ZERO-INPUT READINGS GIVEN BELOW',/)
        WRITE (3,620)AVSTAT(1),AVSTAT(2),AVSTAT(3),AVSTAT(4)
        WRITE (3,620)AVSTAT(5),AVSTAT(6),AVSTAT(7),AVSTAT(8)
        WRITE (3,620)AVSTAT(9),AVSTAT(10),AVSTAT(11),AVSTAT(12)
        WRITE (3,620)AVSTAT(13),AVSTAT(14),AVSTAT(15),AVSTAT(16)
 620    FORMAT (F9.3,5X,F9.3,5X,F9.3,5X,F9.3)
        WRITE (3,660)
 660    FORMAT (///)
        ENDFILE 3
C
C ----  Offer option to conduct only static runs
C
        WRITE (1,247)
```

```
 247    FORMAT (//,' DO YOU WANT TO MAKE 1=DYNAMIC OR 2=STATIC RUNS?',/)
        READ(1,85)CHEK
        IF (CHEK.EQ.2) GOTO 2345
C
C ----  Initialize number or runs to zero, and then increment this
C ----  number by one each run thereafter.
C
        RUNS=0
 250    CONTINUE
        RUNS=RUNS+1
 255    CONTINUE
C
        WRITE (1,257)RUNS
 257    FORMAT (////,' ********RETURN AIRFOIL TO ZERO ANGLE OF
     + ATTACK IN PREPARATION FOR RUN',I2,'********',////)
        NS=0
        KOUNT=0
        WRITE (1,260)
 260    FORMAT (' ENTER NUMBER OF SAMPLES (MULTIPLE OF 18,
     + 5040 MAXIMUM)',/)
        READ (1,265)NS
 265    FORMAT (I5)
        WRITE (1,270)NS
 270    FORMAT (//,' ',25X,'NS:',I5,//)
C
C ----  In the next segement, the operator is given the choice
C ----  between manual and automatic trigger.
C
        WRITE (1,273)
 273    FORMAT (' DO YOU WANT MANUAL OR AUTOMATIC TRIGGER?
     + (1=AUTO, 2=MANUAL)',/)
        READ (1,277)SELECT
 277    FORMAT (I2)
        IF (SELECT.NE.2) GO TO 281
        PAUSE
        GOTO 285
C
C ----  The program segement below is the automatic trigger.
C ----  The program stays in the 280 loop below until ZERANG
C ----  and VALUE differ by 2 or more digital counts.
C ----  When this occurs, due to rotation of the airfoil, the
C ----  program continues on to line number 285.
C
 281    CALL AD(VALUE,0,84)
        ZERANG=VALUE
 280    CALL AD(VALUE,0,84)
        SNAP=IABS(VALUE-ZERANG)
        IF (SNAP.LE.1) GO TO 280
C
C ----  STCLK, below, will count up to 32,768 time clicks, each click
C ----  being .0010046 seconds long. Therefore, STCLK can only time
C ----  an event that lasts for no more than about 32 seconds.
C
 285    CALL STCLK
```

```
C
C ----  The following part of the program reads and stores the time
C ----  obtained from subroutine GETTIM, as well as position and
C ----  pressure information obtained from the potentiometer and
C ----  pressure transducers, respectively.  This position and pressure
C ----  information is obtained through subroutine ADIO.
C
        WRITE(1,290)
 290    FORMAT(///,' ',20X,'STARTING TO TAKE DATA',///)
        DO 320 J=1,NS,18
        KOUNT=KOUNT+1
        CALL GETTIM(TIME)
        IDATA(J)=TIME
        CHAN=0
        CALL AD(VALUE,CHAN,84)
        IDATA(J+1)=VALUE
        DO 300 K=1,16
        CHAN=K-1
        CALL AD(VALUE,CHAN,80)
        DI=K+J+1
        IDATA(DI)=VALUE
 300     CONTINUE
 320     CONTINUE
        WRITE (1,330)RUNS
 330     FORMAT (' ',15X,'DATA GATHERING COMPLETE FOR RUN',I2,//)
        WRITE (1,340)KOUNT
 340     FORMAT (' NUMBER OF PASSES = ',I6,//)
         N=KOUNT*18
        WRITE (1,343)N
 343    FORMAT (' NUMBER OF IDATA ELEMENTS= ',I6,//)
        VPD=(P90-P0)/90.0
        DTIM=(IDATA(2701)-IDATA(901))*(0.0010046)
        DPOSV=((IDATA(2702)-IDATA(902))/4096.0)*10.0
        DPOSD=DPOSV/VPD
        ROTRAT=DPOSD/DTIM
        WRITE (1,410)ROTRAT
 410    FORMAT (' AIRFOIL AVERAGE ROTATION RATE:',F6.2,' DEG/SEC',////)
C
C ----  Options are now offered to list the IDATA array at the
C ----  terminal, to write this array to disk, and to repeat the
C ----  data run.
C
 344    WRITE(1,345)
 345     FORMAT(' DO YOU WANT TO LIST THE IDATA ARRAY?(Y=1)',//)
        READ(1,347)AA
 347    FORMAT (I2)
        IF (AA.NE.1)GO TO 350
        DO 420 XXX=180,N,180
        YYY=XXX-179
        WRITE (1,360)(IDATA(L),L=YYY,XXX)
 360    FORMAT (9I7)
 420    CONTINUE
        GOTO 344
        WRITE (1,351)
```

```
 351    FORMAT (//)
 350    WRITE(1,355)
 355    FORMAT(' DO YOU WANT TO WRITE TO DISK?(Y=1)',//)
        READ (1,347)B
        IF (B.EQ.1) GO TO 390
 374    WRITE (1,375)RUNS
 375    FORMAT (' DO YOU WANT TO REPEAT RUN',I2,'? (Y=1)',//)
        READ (1,380)C
 380    FORMAT (I2)
        IF (C.EQ.1) GO TO 255
        IF (C.EQ.2) GO TO 4800
        GOTO 374
 390    CONTINUE
C
C ----  The part of the program below writes the collected data
C ----  to disk, in unformatted form, under the filename
C ----  RAWDATA1DAT, RAWDATA2DAT, . . . . . , RAWDATA5DAT, depending
C ----  on the value of the variable RUNS. To view the data files
C ----  that are in unformatted form, use program LOOK.
C
        IF (RUNS.EQ.1) GO TO 710
        IF (RUNS.EQ.2) GO TO 720
        IF (RUNS.EQ.3) GO TO 730
        IF (RUNS.EQ.4) GO TO 740
        IF (RUNS.EQ.5) GO TO 750
C
 710    CONTINUE
        CALL OPEN (4,'RAWDATA1DAT',2)
        WRITE (4)(IDATA(L),L=1,N)
        GO TO 760
 720    CONTINUE
        CALL OPEN (5,'RAWDATA2DAT',2)
        WRITE (5)(IDATA(L),L=1,N)
        GO TO 760
 730    CONTINUE
        CALL OPEN (6,'RAWDATA3DAT',2)
        WRITE (6)(IDATA(L),L=1,N)
        GO TO 760
 740    CONTINUE
        CALL OPEN (7,'RAWDATA4DAT',2)
        WRITE (7)(IDATA(L),L=1,N)
        GO TO 760
 750    CONTINUE
        CALL OPEN (8,'RAWDATA5DAT',2)
        WRITE (8)(IDATA(L),L=1,N)
        GO TO 760
 760    CONTINUE
        IF (RUNS.NE.5) GO TO 250
        ENDFILE 4
        ENDFILE 5
        ENDFILE 6
        ENDFILE 7
        ENDFILE 8
```

```
 2345   CONTINUE
        WRITE (1,2346)
 2346   FORMAT (/////,' FOLLOWING PART OF PROGRAM GIVES STATIC
     + NORMAL COEFF. FOR STATIC ALPHA',//////)
        CALL OPEN(9,'RAWDATA6DAT',2)
        CALL OPEN(10,'STATICCNDAT',2)
C
C ----  The remaining portion of the program takes and processes
C ----  data for static angle of attack lift-curves.
C
 2400   CONTINUE
        WRITE (1,2450)
 2450   FORMAT (' ENTER NS (MULTIPLE OF 18, LESS THAN OR
     + EQUAL TO 5040)',/)
        READ (1,2150)NS
 2150   FORMAT (I4)
        KOUNT=0
        CNORM=0
        DO 5000 ZZZ=1,5
        KOUNT=0
        WRITE (1,2000)
 2000   FORMAT (////,' HIT RETURN TO START DATA COLLECTION',/)
C
C ----  STCLK, below, will count up to 32,768 time clicks, each click
C ----  being .0010046 seconds long. Therefore, STCLK can only time
C ----  an event that lasts for no more than about 32 seconds.
C
        CALL STCLK
C
        WRITE(1,2100)
 2100   FORMAT(///,' ',20X,'STARTING TO TAKE DATA',///)
        DO 2200 J=1,NS,18
        KOUNT=KOUNT+1
        CALL GETTIM(TIME)
        IDATA(J)=TIME
        CHAN=0
        CALL AD(VALUE,CHAN,84)
        IDATA(J+1)=VALUE
        DO 2300 K=1,16
        CHAN=K-1
        CALL AD(VALUE,CHAN,80)
        DI=K+J+1
        IDATA(DI)=VALUE
 2300   CONTINUE
 2200   CONTINUE
        N=KOUNT*18
        WRITE (1,2500)N
 2500   FORMAT (' NUMBER OF IDATA ELEMENTS= ',I6,//)
C
C ----  Time-average data
C
        DO 2550 S=1,16
        IDATAT(S)=0.0
 2550   CONTINUE
```

```
      DO 2600 II=1,N,18
      DO 2700 JJ=3,18
      TT=II+JJ
      IDATAT(JJ-2)=((IDATA(TT-1))/KOUNT)+IDATAT(JJ-2)
 2700 CONTINUE
 2600 CONTINUE
C
C ---- Compute the pressure coefficients
C
      DO 2800 KK=1,16
      STICKY=AVSTAT(KK)-2048.0
      PRESS=(((IDATAT(KK)-STICKY)-2048.0)/2048.0)*(50.0/SENS(KK))
      CP(KK)=(PRESS+(MANOM1/27.68))/(MANOM2/27.68)
 2800 CONTINUE
C
C ---- The next loop defines the pressure distribution on the upper
C ---- surface of the airfoil, leading edge to trailing edge.
C ---- Pressure coefficient is assumed to be zero at the trailing edge.
C
      WRITE (1,2900)
 2900 FORMAT (' UPPER SURFACE PRESSURE COEFFICIENTS,
     + L.E. TO T.E., ARE GIVEN BELOW',)
      DO 3000 V=1,9
      CPU(V)=CP(V)
 3000 CONTINUE
      CPU(10)=0.0
      DO 3100 V=1,10
      WRITE (1,3200)V,CPU(V)
 3200 FORMAT (' CPU',I3,'=',F8.4)
 3100 CONTINUE
C
      WRITE (1,3300)
 3300 FORMAT (/,' LOWER SURFACE PRESSURE COEFFICIENTS,
     + L.E. TO T.E., ARE GIVEN BELOW')
      CPL(1)=CP(1)
      DO 3400 W=2,8
      DD=18-W
      CPL(W)=CP(DD)
 3400 CONTINUE
      CPL(9)=CPU(10)
      DO 3500 W=1,9
      WRITE (1,3600)W,CPL(W)
 3600 FORMAT (' CPL',I3,'=',F8.4)
 3500 CONTINUE

C
C ---- The following loop integrates the upper pressure
C ---- distribution using the trapezoidal rule.
C
      AREAUT=0.0
      DO 3700 X=1,9
      LNGTHU=PORTU(X+1)-PORTU(X)
      IF ((ABS(CPU(X+1)-CPU(X))).GT.(ABS((0.01)*CPU(X)))) GO TO 3800
      AREAU=(0.5)*(CPU(X+1)+CPU(X))*LNGTHU
```

```
 3800   IF ((ABS(CPU(X+1)-CPU(X))).LE.(ABS((0.01)*CPU(X)))) GO TO 4000
        INTU=(PORTU(X)-PORTU(X+1))*CPU(X)/(CPU(X+1)-CPU(X))
        IF (INTU.LT.LNGTHU) GO TO 3900
        AREAU=(.5)*(CPU(X+1)+CPU(X))*LNGTHU
        IF ((INTU).GE.(LNGTHU)) GO TO 4000
 3900   AREAU=((.5)*INTU*CPU(X))+
      +                 ((.5)*(LNGTHU-INTU)*CPU(X+1))
 4000   AREAUT=AREAUT+AREAU
 3700   CONTINUE
C
C ---- The following loop integrates the lower pressure
C ---- distribution using the trapezoidal rule.
C
        AREALT=0.0
        DO 4100 Y=1,8
        LNGTHL=PORTL(Y+1)-PORTL(Y)
        IF ((ABS(CPL(Y+1)-CPL(Y))).GT.(ABS((0.01)*CPL(Y)))) GO TO 4200
        AREAL=(.5)*(CPL(Y+1)+CPL(Y))*LNGTHL
        IF ((ABS(CPL(Y+1)-CPL(Y))).LE.(ABS((0.01)*CPL(Y)))) GO TO 4400
 4200   INTL=(PORTL(Y)-PORTL(Y+1))*CPL(Y)/(CPL(Y+1)-CPL(Y))
        IF ((INTL).LT.(LNGTHL)) GO TO 4300
        AREAL=(.5)*(CPL(Y+1)+CPL(Y))*LNGTHL
        IF ((INTL).GE.(LNGTHL)) GO TO 4400
 4300   AREAL=((.5)*INTL*CPL(Y))+
      +                 ((.5)*(LNGTHL-INTL)*CPL(Y+1))
 4400   AREALT=AREALT+AREAL
 4100   CONTINUE
C
        NORMCO=AREALT-AREAUT
        CNORM=CNORM+NORMCO/5.
C
        WRITE (1,4500)NORMCO
 4500   FORMAT (/,' NORMAL FORCE COEFFICIENT=',F8.5,/)
C
C ----  Option now offered to write to disk and continue run
C
         DO 4550 J=1,16
 4550    IDATA(J+2)=IDATAT(J)
         DO 4560 J=1,18
 4560    SDATA(ZZZ,J)=IDATA(J)
 5000    CONTINUE
         WRITE(1,4570)CNORM
 4570    FORMAT(//,' AVERAGED NORMAL COEFFICIENT=',F8.5,/)
         WRITE(1,4575)
 4575    FORMAT(/,' DO YOU WANT TO WRITE TO DISK (Y=1) ')
         READ(1,4700)CHEK
         IF (CHEK.NE.1) GOTO 4599
         DO 4577 ZZZ=1,5
 4577    WRITE(9,360) (SDATA(ZZZ,L),L=1,18)
         WRITE(10,4580)IDATA(2),NORMCO
 4580    FORMAT(I5,F8.5,/)
 4599    WRITE (1,4600)
 4600    FORMAT (' DO YOU WANT TO CONTINUE THE RUN?  (Y=1)',/)
         READ (1,4700)CCC
```

```
4700    FORMAT (I2)
        IF (CCC.EQ.1) GO TO 2400
        IF (CCC.NE.2) GOTO 4599
4800    CONTINUE
        STOP
        END
```

```
      PROGRAM DOS2A
      INTEGER IDATA2(3600),NJ
      INTEGER N,R,X,Y,V,W,S,I,J,L,AA,PP,QQ
      INTEGER RR,SS,TT,UU,VV,WW,XX,YY,ZZ,RUN,TRAP,PAZZ,DIV,NUMEL
      INTEGER ELEM1,ELEM2,DAY,MONTH,YEAR,HOUR,CHANG1,CHANG2
      INTEGER DD,EE,FF,HH,LL,NN,MOOCOW,JJJ,ZOO
      REAL PORTX(20),PORTY(20),CP(16),CPU(20),SENS(16)
      REAL PRESS(16),REDAT(40),P90,PO,TEMP,BAROM,MANOM1,MANOM2
      REAL TUNVEL,MOTVOL,AVSTAT(16),ARNORM,ARMOM,RE,RHO,MU
      REAL VPD,AOA,AOAR,CL,CD,CNORM,CCHORD,TUNQ,LNGTHU,LNGTHL
      REAL AREAU,AREAL,DTIM,DPOSD,DPOSV,ROTRAT,NDRATE
      REAL REDATC(40),CMOM,ARN,ARM,ARC,ARCHOR
      REAL DETAN,DETBN,INCPL,INCPN,PI
C
C ---- Load transducer sensitivities (millivolts/psi)
      DATA SENS/202.5,172.3,176.3,231.7,204.6,204.6,116.2,
     +216.4,174.0,113.8,114.4,113.6,136.6,165.3,219.6,222.8/
C
C ---- Load transducer locations for normal force (percent chord)
      DATA PORTX/0.0,0.0250,0.0490,0.0980,0.131,0.197,0.328,0.615,
     +0.902,1.000,0.697,0.328,0.197,0.0980,0.0490,0.0330,0.016,0.0/
C
C ---- Load transducer locations for chord force (percent chord)
      DATA PORTY/0.0,0.0327,0.0440,0.0581,0.0637,0.0714,.0743,
     +0.0554,0.0178,0.0,0.0461,0.0743,0.0714,0.0581,0.0440,
     +0.0364,0.0262,0.0/
      WRITE (1,5)
    5 FORMAT (///,' *****THE DATA FILES TO BE REDUCED MUST BE ON
     + DISK DRIVE B AND MUST BE NAMED*****')
      WRITE (1,6)
    6 FORMAT (' *************RAWDATA0.DAT, RAWDATA1.DAT,. . . . . . .,
     + RAWDATA5.DAT*************',///)
C
C ---- Read raw data from RAWDATA0DAT on drive B.
      CALL OPEN(3,'RAWDATA0DAT',2)
      READ (3,10)DAY,MONTH,YEAR,HOUR
   10 FORMAT (/,I3,11X,I3,11X,I3,9X,I5)
      READ (3,20)TEMP,BAROM
   20 FORMAT (//,2X,F6.1,18X,F7.2)
      READ (3,30)MANOM1,MANOM2
   30 FORMAT (//,2X,F8.4,25X,F8.4)
      READ (3,40)TUNVEL,MOTVOL
   40 FORMAT (//,4X,F7.2,31X,F6.2)
      READ (3,50)P90,PO
   50 FORMAT (//,5X,F7.4,23X,F7.4)
      READ (3,60)KOUNT,N
   60 FORMAT (///,3X,I6,26X,I6)
      READ (3,70)AVSTAT(1),AVSTAT(2),AVSTAT(3),AVSTAT(4)
      READ (3,75)AVSTAT(5),AVSTAT(6),AVSTAT(7),AVSTAT(8)
      READ (3,75)AVSTAT(9),AVSTAT(10),AVSTAT(11),AVSTAT(12)
      READ (3,75)AVSTAT(13),AVSTAT(14),AVSTAT(15),AVSTAT(16)
   70 FORMAT (////,F9.3,5X,F9.3,5X,F9.3,5X,F9.3)
   75 FORMAT (F9.3,5X,F9.3,5X,F9.3,5X,F9.3)
      ENDFILE 3
```

```
      VPD=(P90-P0)/90.0
C
      RUN=0
 470  CONTINUE
      RUN=RUN+1
      WRITE(1,5000) RUN
 5000 FORMAT('  RUN = ',I3)
      IF (RUN.EQ.1) GO TO 490
      IF (RUN.EQ.2) GO TO 510
      IF (RUN.EQ.3) GO TO 525
      IF (RUN.EQ.4) GO TO 535
      IF (RUN.EQ.5) GO TO 545
 490  CONTINUE
      CALL OPEN(4,'RAWDATA1DAT',2)
      READ(4)(IDATA2(L),L=1,N)
      ENDFILE 4
      GO TO 550
 510  CONTINUE
      CALL OPEN(5,'RAWDATA2DAT',2)
      READ(5)(IDATA2(L),L=1,N)
      ENDFILE 5
      GO TO 550
 525  CONTINUE
      CALL OPEN(6,'RAWDATA3DAT',2)
      READ(6)(IDATA2(L),L=1,N)
      ENDFILE 6
      GO TO 550
 535  CONTINUE
      CALL OPEN(7,'RAWDATA4DAT',2)
      READ(7)(IDATA2(L),L=1,N)
      ENDFILE 7
      GO TO 550
 545  CONTINUE
      CALL OPEN(8,'RAWDATA5DAT',2)
      READ(8)(IDATA2(L),L=1,N)
      ENDFILE 8
 550  CONTINUE
C
 850  CONTINUE
C
C ---- The steps below compute Reynolds number, tunnel "Q"
C ---- and volts per degree for the run.
C
      IF (RUN.GT.1) GOTO 895
      RHO=(BAROM*70.45)/(1716.0*(460+TEMP))
      MU=(2.270*(10.0**(-8.0))*((460.0+TEMP)**1.5))/(460.0+TEMP+198.6)
      RE=(RHO*TUNVEL*1.016)/MU
      TUNQ=(0.5)*RHO*(TUNVEL**2)
C
C ---- The following writes pertinent information to disk file
C ---- REDUDATADAT as a heading.
C
      CALL OPEN(10,'REDUDATADAT',2)
      WRITE (10,800)
```

```
 800    FORMAT (' DAY',10X,'MONTH',9X,'YEAR',9X,'TIME')
        WRITE (10,810)DAY,MONTH,YEAR,HOUR
 810    FORMAT (I3,11X,I3,11X,I3,9X,I5,/)
        WRITE (10,820)
 820    FORMAT (' TEMPERATURE',14X,'BAROMETER')
        WRITE (10,830)TEMP,BAROM
 830    FORMAT (2X,F6.1,18X,F7.2,/)
        WRITE (10,840)
 840    FORMAT (' MANOMETER 1',22X,'MANOMETER 2')
        WRITE (10,845)MANOM1,MANOM2
 845    FORMAT (2X,F8.4,25X,F8.4,/)
        WRITE (10,850)
 850    FORMAT (' TUNNEL VELOCITY',22X,'MOTOR VOLTAGE')
        WRITE (10,855)TUNVEL,MOTVOL
 855    FORMAT (4X,F7.2,31X,F6.2,/)
        WRITE (10,880)
 880    FORMAT (' REYNOLDS NUMBER',25X,'TUNNEL "Q"')
        WRITE (10,890)RE,TUNQ
 890    FORMAT (4X,E11.4,30X,F6.3,/)
        DO 895 HH=1,16
        WRITE (10,897)HH,AVSTAT(HH)
 897    FORMAT (' AVERAGE ZERO-INPUT READING, TRANSDUCER',I3,' =',F6.0)
 895    CONTINUE
        WRITE(10,1100)
C
C ---- One pass through the DO 100 J=1,N,18 loop computes one
C ---- point in the CN (normal force coefficient) versus ALPHA curve.
C
        DO 1000 J=1,100
        NJ=(J-1)*18
        DO 100  I=1,18
        NN=I+NJ
        REDAT(I)=IDATA2(NN)
        REDAT(I+18)=IDATA2(NN+18)
 100    CONTINUE
C
C ---- The loop below subtracts the average zero input readings
C ---- (AVSTAT) from each appropriate IDATAT element.
C
        DO 200 I=3,18
        REDAT(I)=REDAT(I)-(AVSTAT(I-2)-2048.0)
        REDAT(I+18)=REDAT(I+18)-(AVSTAT(I-2)-2048.0)
 200    CONTINUE
C
C ---- Operations in the following loop correct for the finite
C ---- time between samples using a linear interpolation. Time
C ---- between passes must be sufficiently small or the linear
C ---- interpolation will be invalid.
C
        DO 300 R=1,18
        REDATC(R)=REDAT(R+18)-(REDAT(R+18)-REDAT(R))*(R-1)/18.0
 300    CONTINUE
C
C ---- The following loop converts digital quantities to degrees
```

```
C ---- (angle of attack) and psi (sensed differential pressure).
C
C ---- The AOA conversion below assumes the A/D board is strapped
C ---- for the 0-10 volt unipolar input range. The amp on the
C ---- board is set for a gain of 1, so any input to the board
C ---- greater than 10 volts will saturate the A/D conversion system.
C
      AOA=(((REDATC(2)/4096.0)*10.0)-PO)/VPD
      TIME=REDATC(1)
C
C ---- The PRESS conversion below assumes the A/D board is strapped
C ---- for the (-5)-(+5) volt bipolar input range, where the input
C ---- (from the transducers) is first amplified through an
C ---- amplifier of gain 100. So any input greater than +/-50 milli-
C ---- volts will saturate the A/D conversion system.
C
      DO 400  S=1,16
      PRESS(S)=((REDATC(S+2)-2048.0)/2048.0)*50.0/SENS(S)
      CP(S)=(PRESS(S)+(MANOM1/27.68))/(MANOM2/27.68)
 400  CONTINUE
C
C ---- The next loop defines the pressure distribution on the
C ---- airfoil, leading edge to trailing edge, and back to leading
C ---- edge.
C
      DO 405  V=1,9
      CPU(V)=CP(V)
 405  CONTINUE
C
      CPU(10)=CPU(9)+(CPU(9)-CPU(8))/.287*.098
C
      DO 410  V=10,16
      CPU(V+1)=CP(V)
 410  CONTINUE
C
      CPU(18)=CPU(1)
C
      CP4=CPU(4)
      CP6=CPU(6)
      CP7=CPU(7)
C
C ---- The following loop integrates the normal force and moment
C ---- distribution using the trapezoidal rule.
C
      ARNORM=0.0
      ARMOM=0.0
C
C
      DO 2000  I=1,9
      ARN=.5*(PORTX(I+1)-PORTX(I))*(CPU(I)+CPU(I+1))
      ARM=.5*(PORTX(I+1)-PORTX(I))*(PORTX(I)*CPU(I)+PORTX(I+1)*
     +  CPU(I+1))
C
      ARNORM=ARNORM-ARN
```

```
      ARMOM=ARMOM-ARM
 2000 CONTINUE
C
C
      DO 2500  I=10,17
      ARN=.5*ABS(PORTX(I+1)-PORTX(I))*(CPU(I)+CPU(I+1))
      ARM=.5*ABS(PORTX(I+1)-PORTX(I))*(PORTX(I)*CPU(I)+PORTX(I+1)*
     +  CPU(I+1))
C
      ARNORM=ARNORM+ARN
      ARMOM=ARMOM+ARM
 2500 CONTINUE
C
      CNORM=ARNORM
      CMOM=-ARMOM+0.25*CNORM
C
C ---- The following loop integrates the chord force
C ---- distribution using the trapezoidal rule.
C
      ARCHOR=0.00
C
      DO 3000  I=1,6
      ARC=.5*(PORTY(I+1)-PORTY(I))*(CPU(I)+CPU(I+1))
      ARCHOR=ARCHOR+ARC
 3000 CONTINUE
C
      DO 3500  I=7,10
      ARC=.5*ABS(PORTY(I+1)-PORTY(I))*(CPU(I)+CPU(I+1))
      ARCHOR=ARCHOR-ARC
 3500 CONTINUE
C
      DO 3750  I=11,17
      ARC=.5*ABS(PORTY(I+1)-PORTY(I))*(CPU(I)+CPU(I+1))
      ARCHOR=ARCHOR+ARC
 3750 CONTINUE
C
C
      CCHORD=ARCHOR
C
      PI=3.14159
      AOAR=AOA*PI/180.0
      CD=CNORM*SIN(AOAR)+CCHORD*COS(AOAR)
      CL1=CNORM*COS(AOAR)
      WRITE(10,900)TIME,AOA,CP4,CP6,CP7,CL1,CD,CMOM
 900  FORMAT(F5.0,8F9.4)
 1000 CONTINUE
      WRITE(10,1100)
 1100 FORMAT(//)
      IF(RUN.LT.5) GO TO 470
      STOP
      END
```

```
      PROGRAM DATRED(INPUT,OUTPUT,TAPE7,TAPE8,TAPE9)
C
C  THIS PROGRAM READS A DYNAMIC STALL DATA FILE AND THEN
C  PERFORMS AN ENSEMBLE AVERAGE OF THE DATA POINTS
C  OUTPUT IS WRITTEN TO THE FILES TAPE8, AND TAPE9
C
      DIMENSION DYN(9,600),ENS(7,50),ADOT(2,50)
      REAL NUMBER
      REWIND7
      REWIND8
      REWIND9
      REWIND10
      WRITE(9,*)' DATA FROM '
C
C  READ THE DYNAMIC STALL DATA FILE
C
      DO 100  J=1,600
 50   READ (7,110,END=500) (DYN(I,J),I=1,8)
      IF (DYN(1,J) .EQ. 0.0) GOTO 50
 100  CONTINUE
 110  FORMAT(F5.0,8F9.4)
C
C
 500  JMAX=J-1
C
C  ENSEMBLE AVERAGE THE TIME AND POSITION DATA
C
      DO 900  N=1,46
      TOTTIM=0.
      TOTAOA=0.
      NUMBER=0.
C
        DO 1000  J=1,JMAX
        TIME=60.0+FLOAT(N)*5.
      IF (DYN(1,J).LT.TIME .OR. DYN(1,J).GE.(TIME+5.)) GOTO 1000
        TOTTIM=TOTTIM+DYN(1,J)
        TJTAOA=TOTAOA+DYN(2,J)
        NUMBER=NUMBER+1.0
 1000   CONTINUE
C
      AVGTIM=TOTTIM/NUMBER
      AVGAOA=TOTAOA/NUMBER
      ADOT(1,N)=AVGTIM
      ADOT(2,N)=AVGAOA
 900  CONTINUE
C
C  ENSEMBLE AVERAGE FORCE AND PRESSURE DATA
C
      DO 2000  N=1,20
      NUMBER=0.
      TOTAOA=0.
      TOTCP4=0.
      TOTCP6=0.
      TOTCP7=0.
```

```
      TOTCL=0.
      TOTCD=0.
      TOTCM=0.
        DO 1900  J=1,JMAX,2
        ANGLE=0.0+FLOAT(N-1)*2.0
      IF (DYN(2,J).LT.ANGLE .OR. DYN(2,J).GE.(ANGLE+2.))
     +  GOTO 1900
        NUMBER=NUMBER+1.
        TOTAOA=TOTAOA+DYN(2,J)
        TOTCP4=TOTCP4+DYN(3,J)
        TOTCP6=TOTCP6+DYN(4,J)
        TOTCP7=TOTCP7+DYN(5,J)
         TOTCL=TOTCL+DYN(6,J)
         TOTCD=TOTCD+DYN(7,J)
         TOTCM=TOTCM+DYN(8,J)
 1900   CONTINUE
C
      IF (NUMBER.EQ.0) NUMBER=1.
      AVGAOA=TOTAOA/NUMBER
      AVGCP4=TOTCP4/NUMBER
      AVGCP6=TOTCP6/NUMBER
      AVGCP7=TOTCP7/NUMBER
       AVGCL=TOTCL/NUMBER
       AVGCD=TOTCD/NUMBER
       AVGCM=TOTCM/NUMBER
      ENS(1,N)=AVGAOA
      ENS(2,N)=AVGCP4
      ENS(3,N)=AVGCP6
      ENS(4,N)=AVGCP7
      ENS(5,N)=AVGCL
      ENS(6,N)=AVGCD
      ENS(7,N)=AVGCM
 2000 CONTINUE
C234567
C
C  COMPUTE AOA SLOPE AND CORRELATION COEFFICIENT
C
      DO 2600  J=1,3
      X=0.
      Y=0.
      AN=0.
      XX=0.
      XY=0.
      YY=0.
      DO 2500  N=1,46
      IF(ADOT(2,N).LT.FLOAT(J)*5. .OR. ADOT(2,N).GT.30. ) GOTO 2500
        X=X+ADOT(1,N)
        Y=Y+ADOT(2,N)
       XX=XX+ADOT(1,N)**2
       YY=YY+ADOT(2,N)**2
       XY=XY+ADOT(1,N)*ADOT(2,N)
       AN=AN+1.
 2500  CONTINUE
       IF (X.EQ.0.) GOTO 2600
```

```
      B1=(AN*XY-X*Y)/(AN*XX-X**2)*(1./.0010046)
      R1=(AN*XY-X*Y)/SQRT((AN*XX-X**2)*(AN*YY-Y**2))
      WRITE(*,10)B1,R1
      WRITE(9,10)B1,R1
   10 FORMAT('ROTATION RATE = ',F8.3,'   CORR = ',F10.8)
 2600 CONTINUE
C
C  FIND MAX PRESSURE COEFFICIENTS
C
      CP4MAX=0.
      CP7MAX=0.
      CP6MAX=0.
      DO 2900  I=5,20
      IF(ENS(2,I).LT.CP4MAX) CP4MAX=ENS(2,I)
      IF(ENS(3,I).LT.CP6MAX) CP6MAX=ENS(3,I)
      IF(ENS(4,I).LT.CP7MAX) CP7MAX=ENS(4,I)
 2900 CONTINUE
      PRINT*,' CP4MAX = ',CP4MAX
      PRINT*,' CP6MAX = ',CP6MAX
      PRINT*,' CP7MAX = ',CP7MAX
C
C  WRITE ENSEMBLE AVERAGED DATA TO FILES
C
      DO 4000  N=1,20
      WRITE(9,4100)  (ENS(I,N),I=1,7)
 4100 FORMAT(7F9.4)
 4000 CONTINUE
C
      DO 5000 N=5,20
      ENS(2,N)=ENS(2,N)/CP4MAX
      ENS(3,N)=ENS(3,N)/CP6MAX
      ENS(4,N)=ENS(4,N)/CP7MAX
 5000  CONTINUE
      DO 5100  N=5,20
      WRITE(10,4100)  (ENS(I,N),I=1,7)
 5100 CONTINUE
C
      STOP
      END
```

APPENDIX C

Remainder of Plotted Results

The plotted results are presented in test number order. A summary of the test numbers and associated test conditions is provided in Table VII. The following legend applies to all test data in this appendix:

LEGEND	
□ - Lift Coefficient	C_L
O - Drag Coefficient	C_D
▲ - Moment Coefficient	C_M

Figure . DATA FROM TEST RUN 1-1

The first digit in the test run number represents the pitch location and the second digit represents the test number.

TABLE VII

Summary of Test Conditions

Test Run	Tunnel Velocity (ft/sec)	Rotation Rate (deg/sec)	$\dot{\alpha}_{ND}$	Figure Number
1-1	25.43	85.95	.030	27
1-2	25.43	N/L		28
1-3	24.97	183.17	.065	29
1-4	30.05	N/L		30
1-5	30.03	112.84	.033	31
1-6	30.02	183.02	.054	32
1-7	35.64	44.19	.011	33
1-8	35.64	98.39	.024	34
1-9	35.32	129.16	.032	35
1-10	37.87	N/L		36
1-11	37.57	95.16	.022	37
1-12	37.59	133.89	.031	38
2-1	25.57	74.04	.025	40
2-2	25.83	145.24	.049	41
2-3	25.20	175.61	.062	42
2-4	29.68	90.56	.027	43
2-5	29.68	117.02	.035	44
2-6	29.30	148.63	.045	45
2-7	35.23	N/L		46
2-8	35.76	N/L		47
2-10	40.38	59.29	.013	48
2-11	38.89	133.66	.030	49
2-12	39.21	170.13	.038	50
2-13	44.50	N/L		51
2-14	45.03	101.53	.020	52
2-15	44.84	N/L		53
3-1	25.77	83.07	.028	55
3-2	25.61	102.70	.036	56
3-3	25.86	N/L		57
3-4	26.41	109.72	.037	58
3-5	29.16	69.01	.021	59
3-7	29.07	116.89	.036	60
3-8	31.52	97.70	.027	61
3-9	34.16	N/L		62
3-10	35.92	N/L		63
3-11	34.04	114.26	.030	64
3-13	39.55	74.57	.016	65
3-14	39.96	102.21	.022	66
3-15	39.09	N/L		67
3-16	40.38	N/L		68
3-17	44.04	N/L		69
3-18	44.15	N/L		70
3-19	43.90	N/L		71

Test Run	Tunnel Velocity (ft/sec)	Rotation Rate (deg/sec)	$\dot{\alpha}_{ND}$	Figure Number
4-1	25.75	82.45	.028	73
4-2	25.75	120.68	.041	74
4-3	26.17	139.43	.047	75
4-4	30.98	71.34	.020	76
4-5	28.66	118.84	.037	77
4-6	30.95	135.95	.039	78
4-7	36.46	61.92	.015	79
4-8	36.13	102.28	.025	80
4-9	33.54	135.95	.036	81
4-10	38.02	80.86	.019	82
4-11	38.01	157.60	.037	83
4-12	39.80	203.27	.045	84

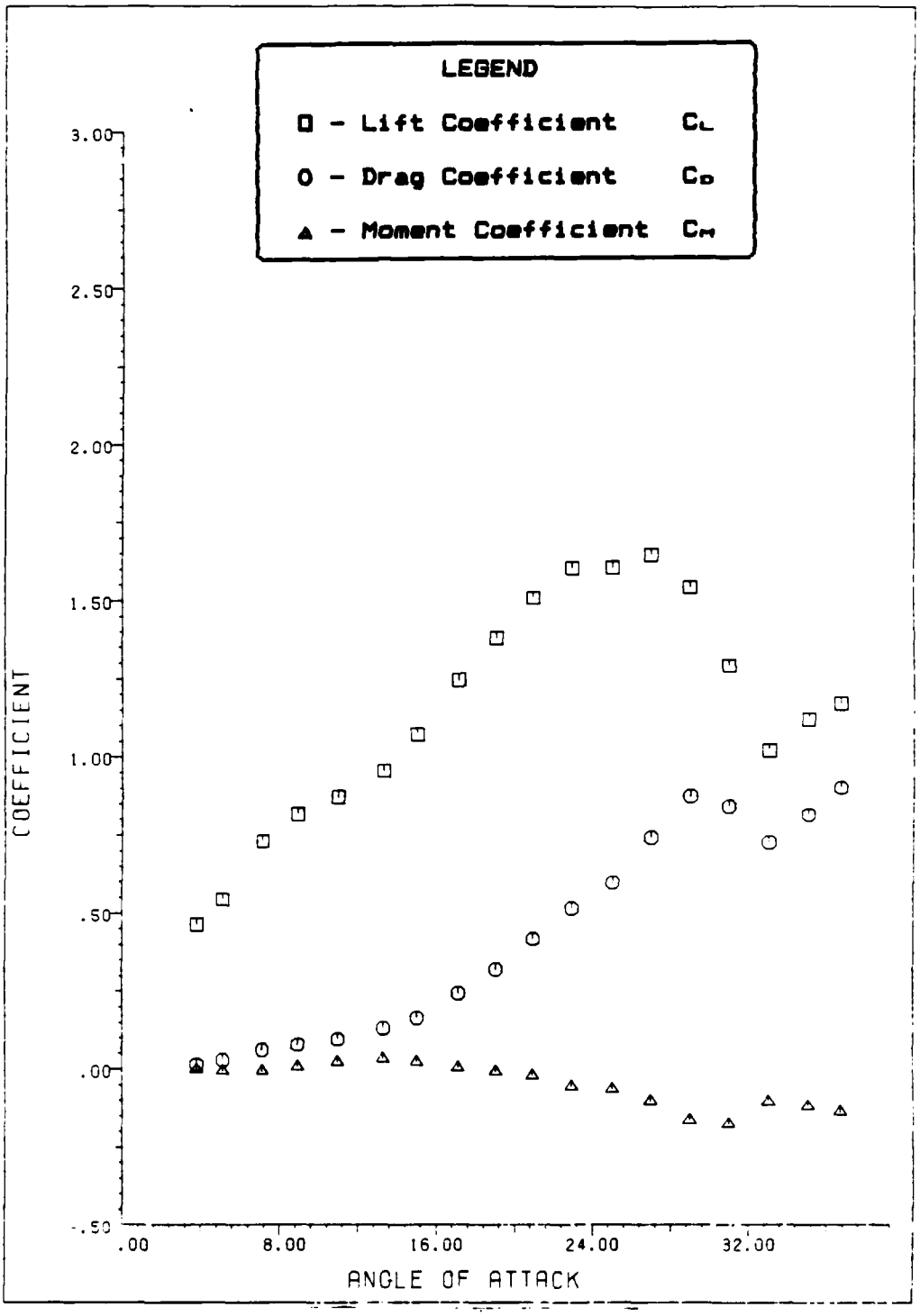

Figure 27. Data From Test Run 1 - 1

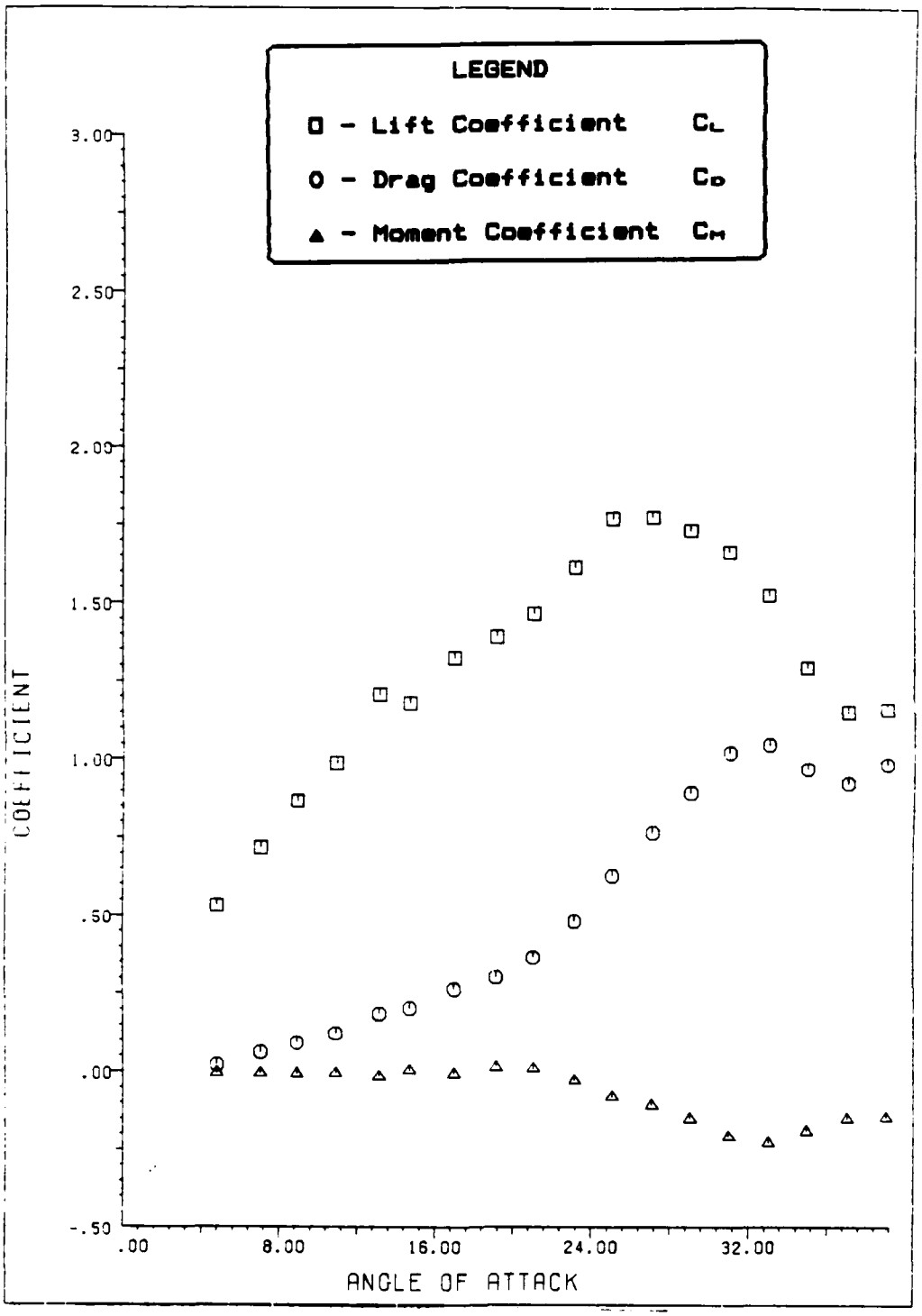

Figure 28. Data From Test Run 1 - 2

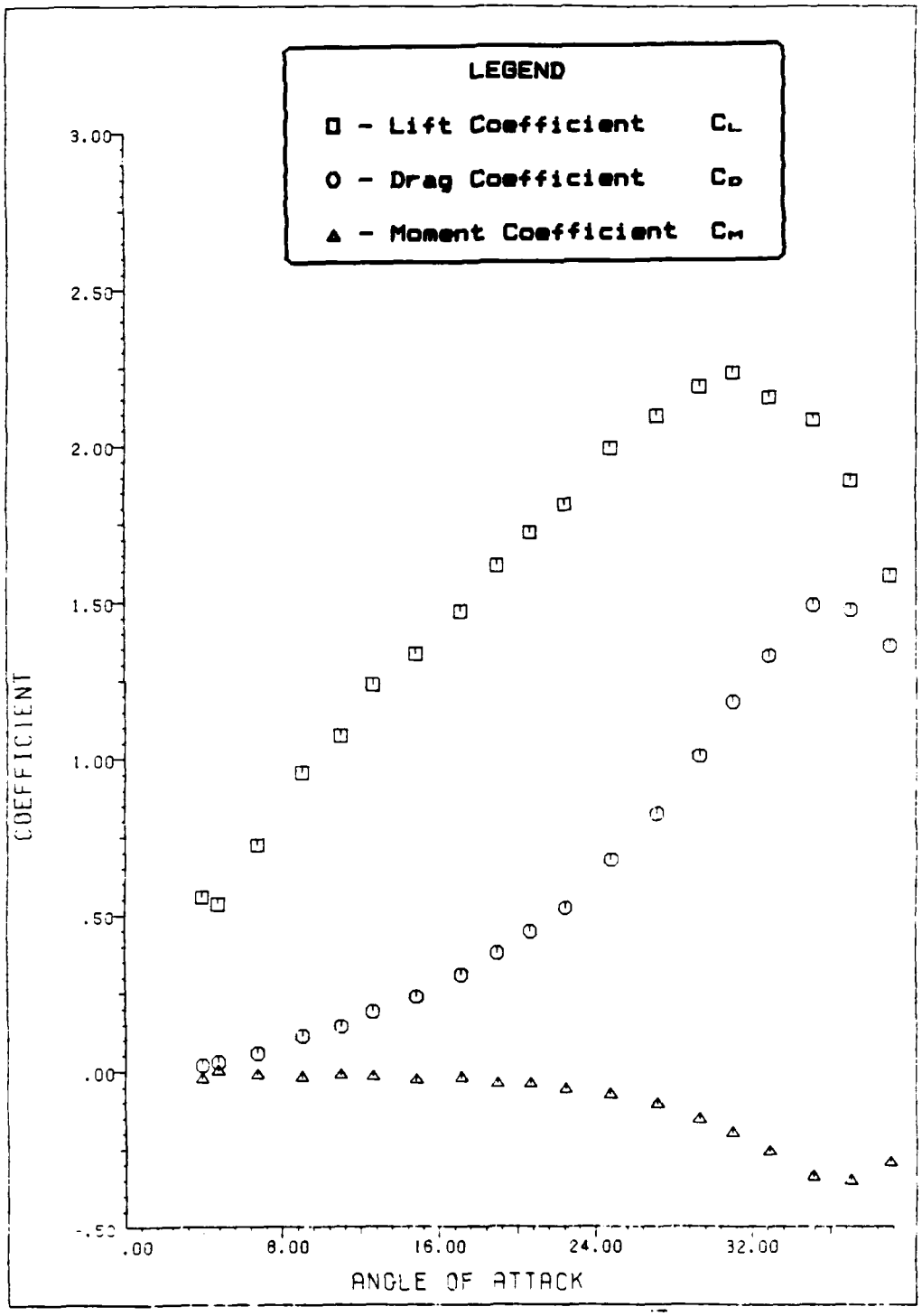

Figure 29. Data From Test Run 1 - 3

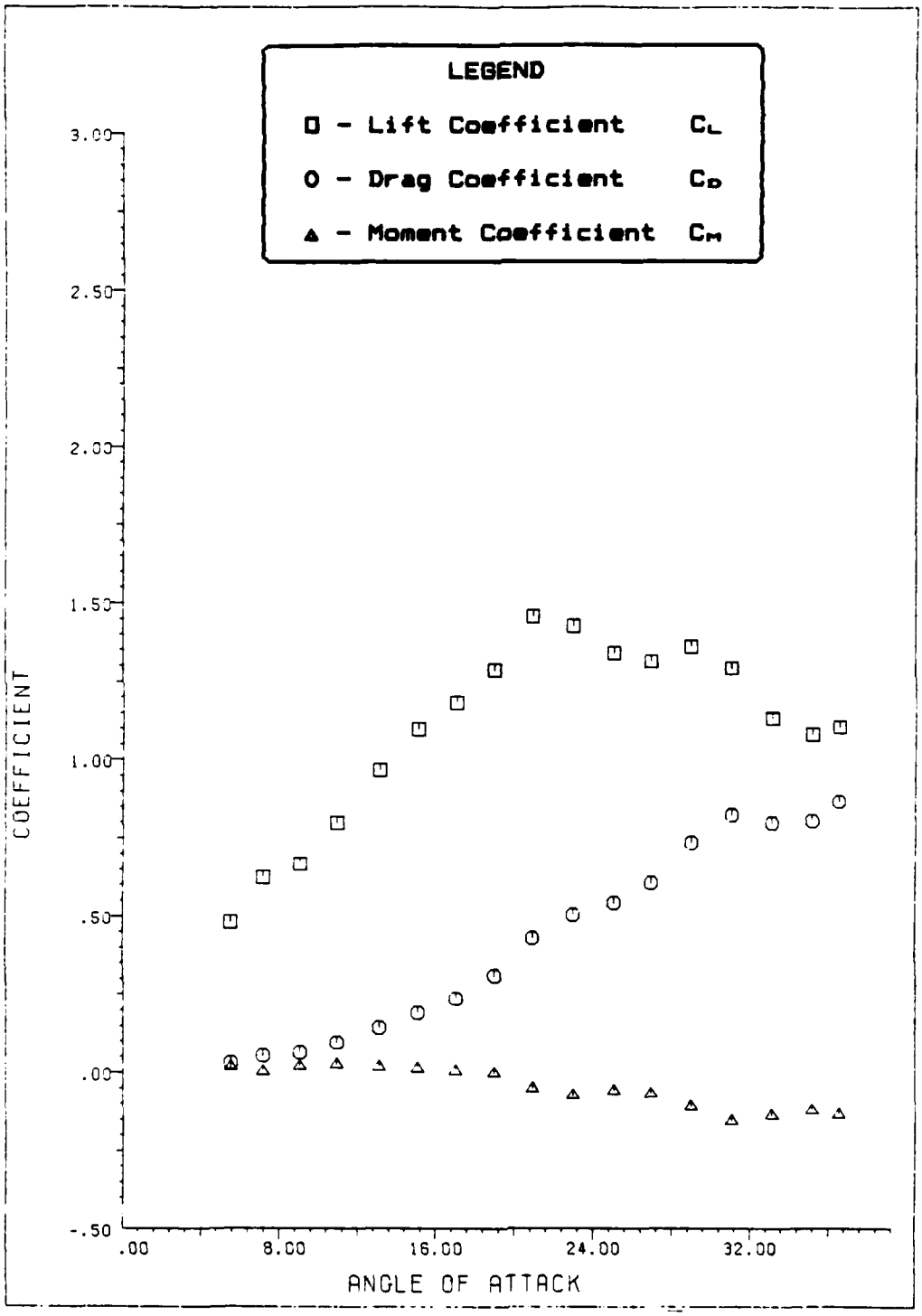

Figure 30. Data From Test Run 1 - 4

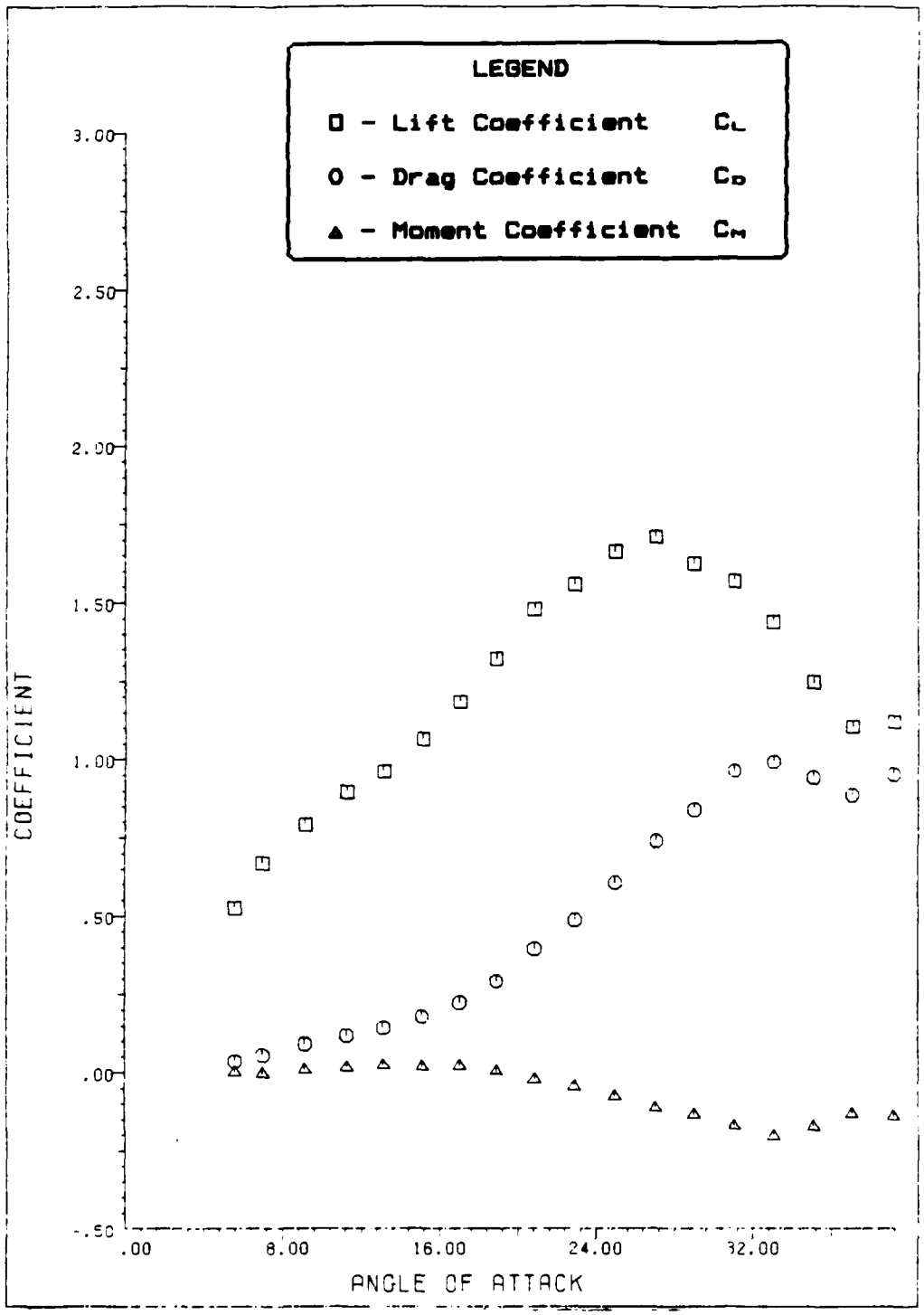

Figure 31. Data From Test Run 1 - 5

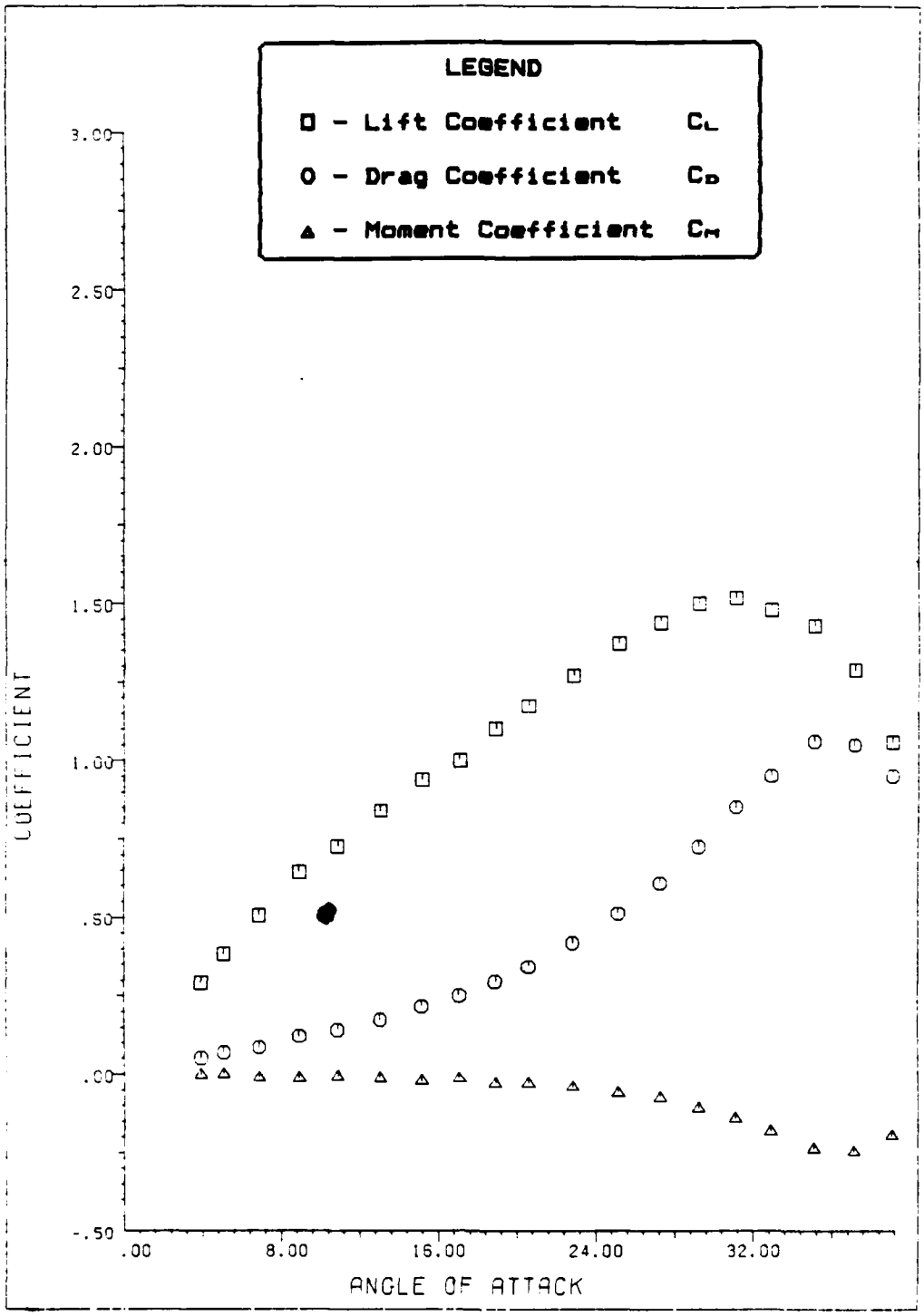

Figure 32. Data From Test Run 1 - 6

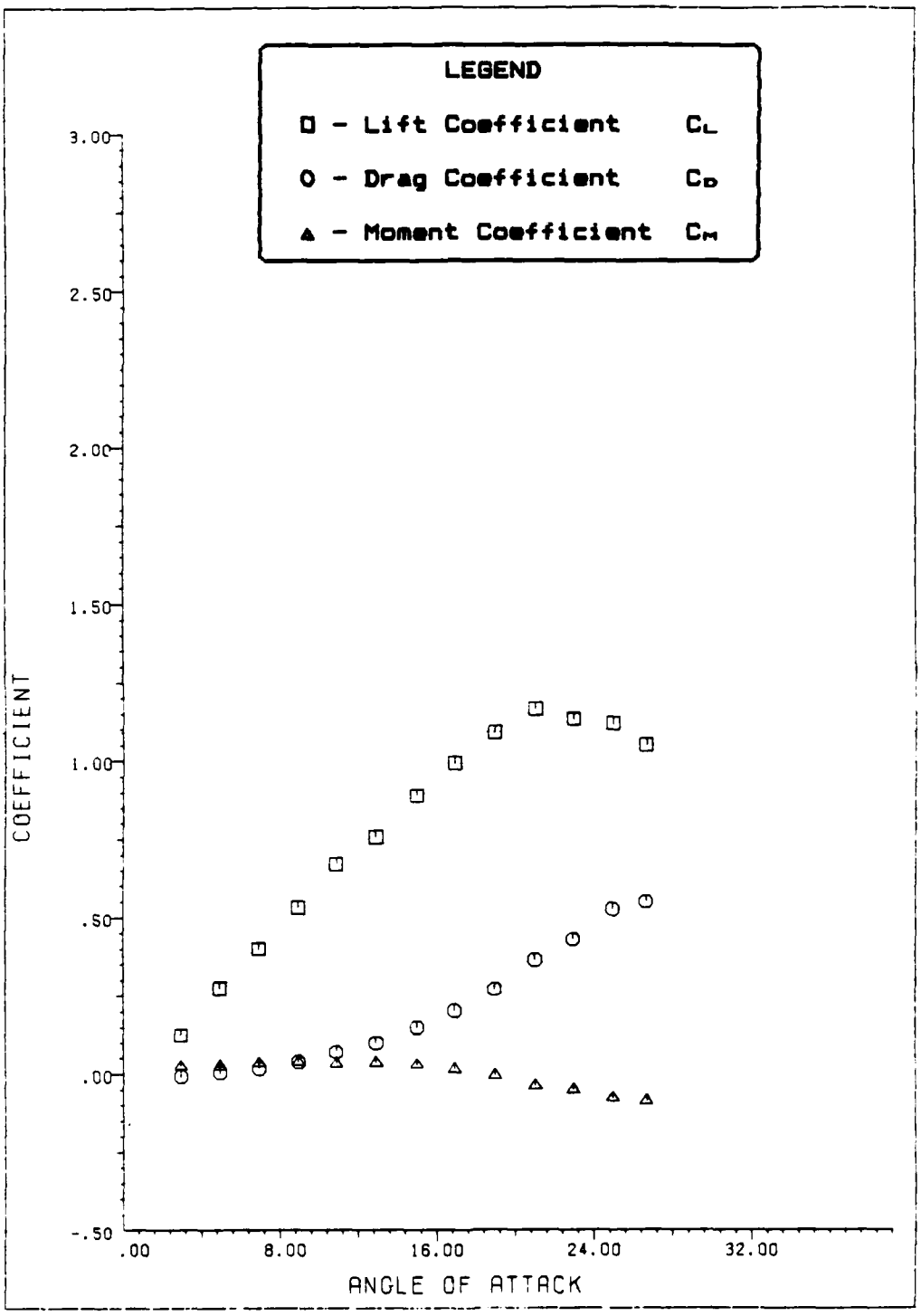

Figure 33. Data From Test Run 1 - 7

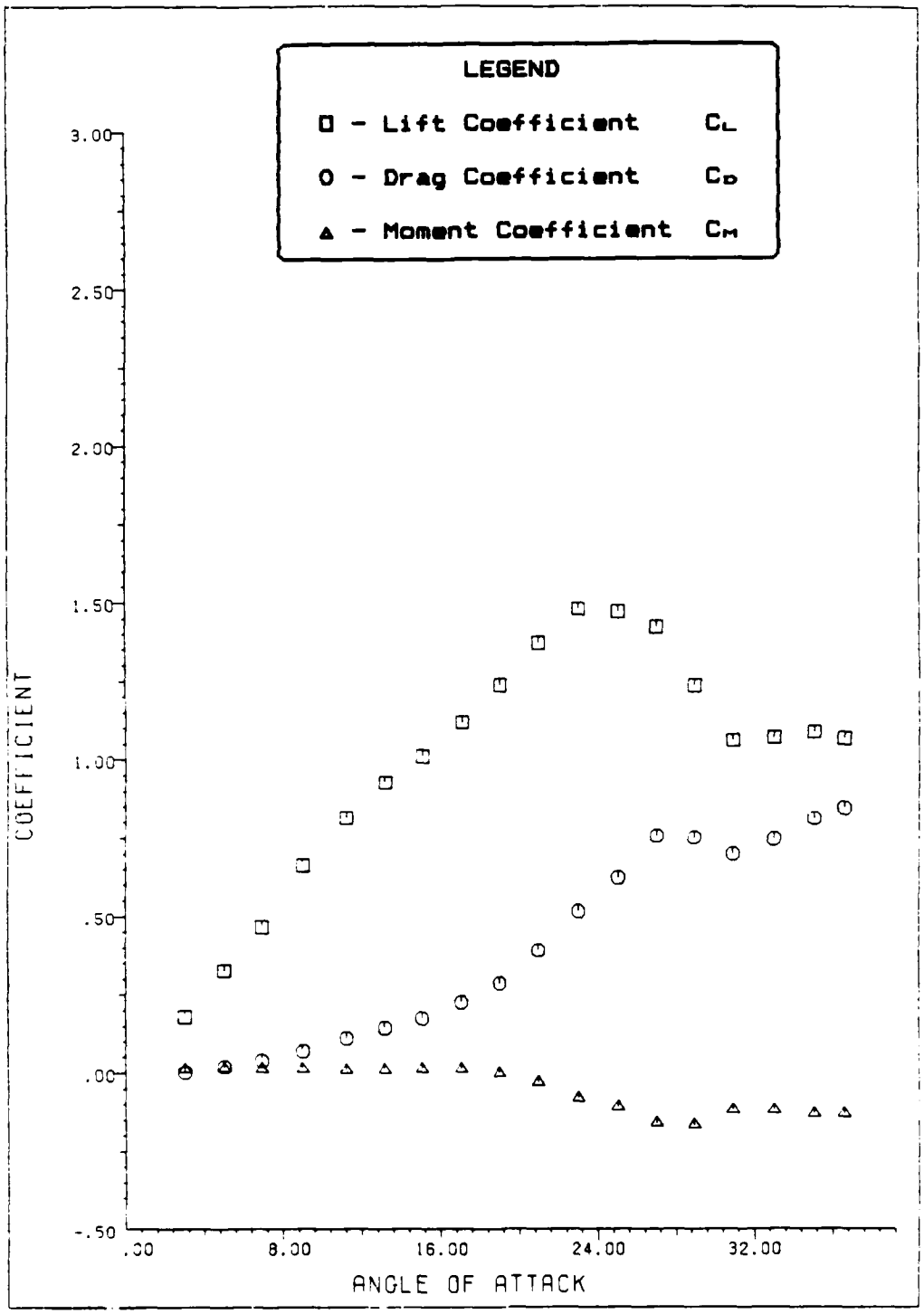

Figure 34. Data From Test Run 1 - 8

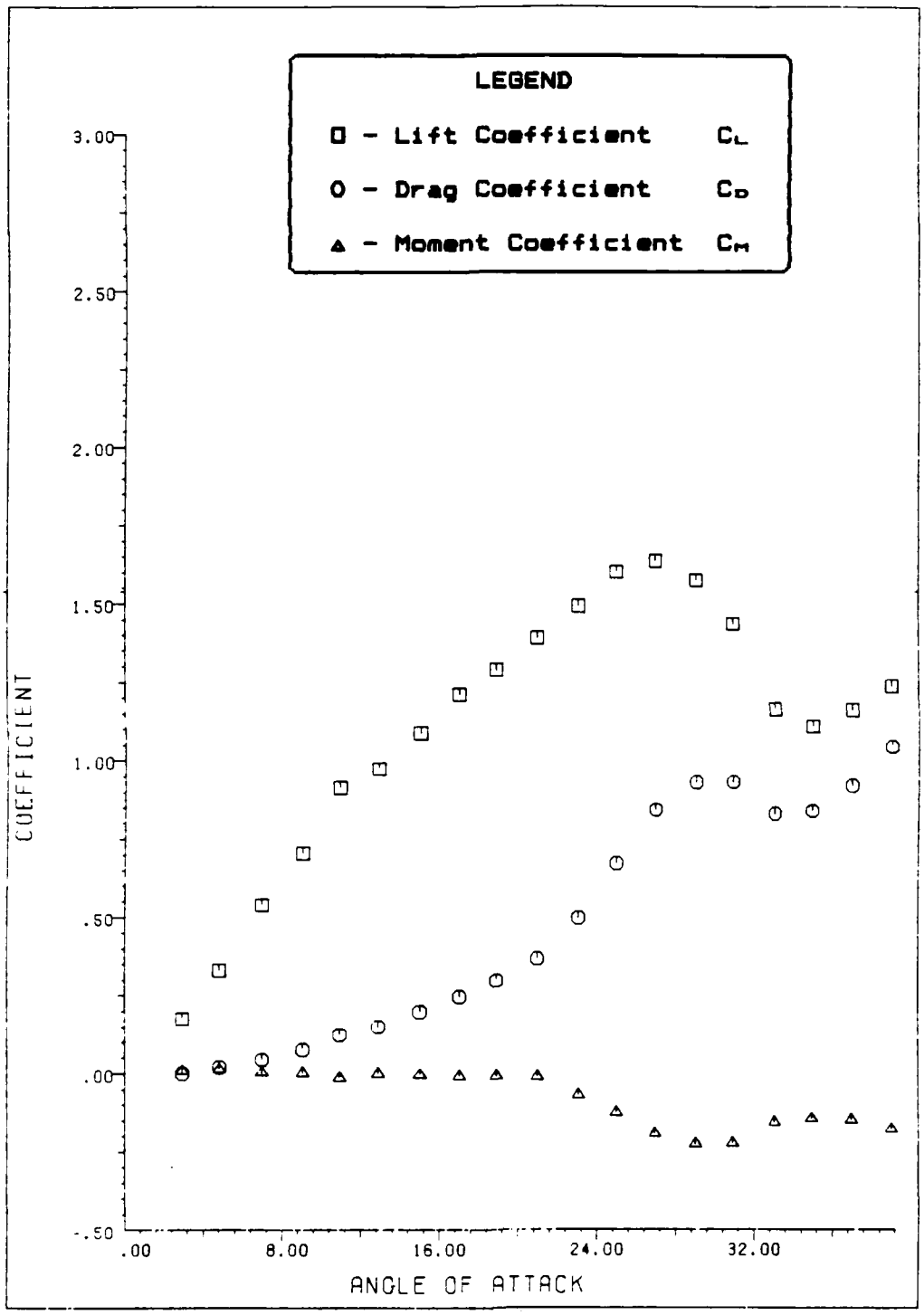

Figure 35. Data From Test Run 1 - 9

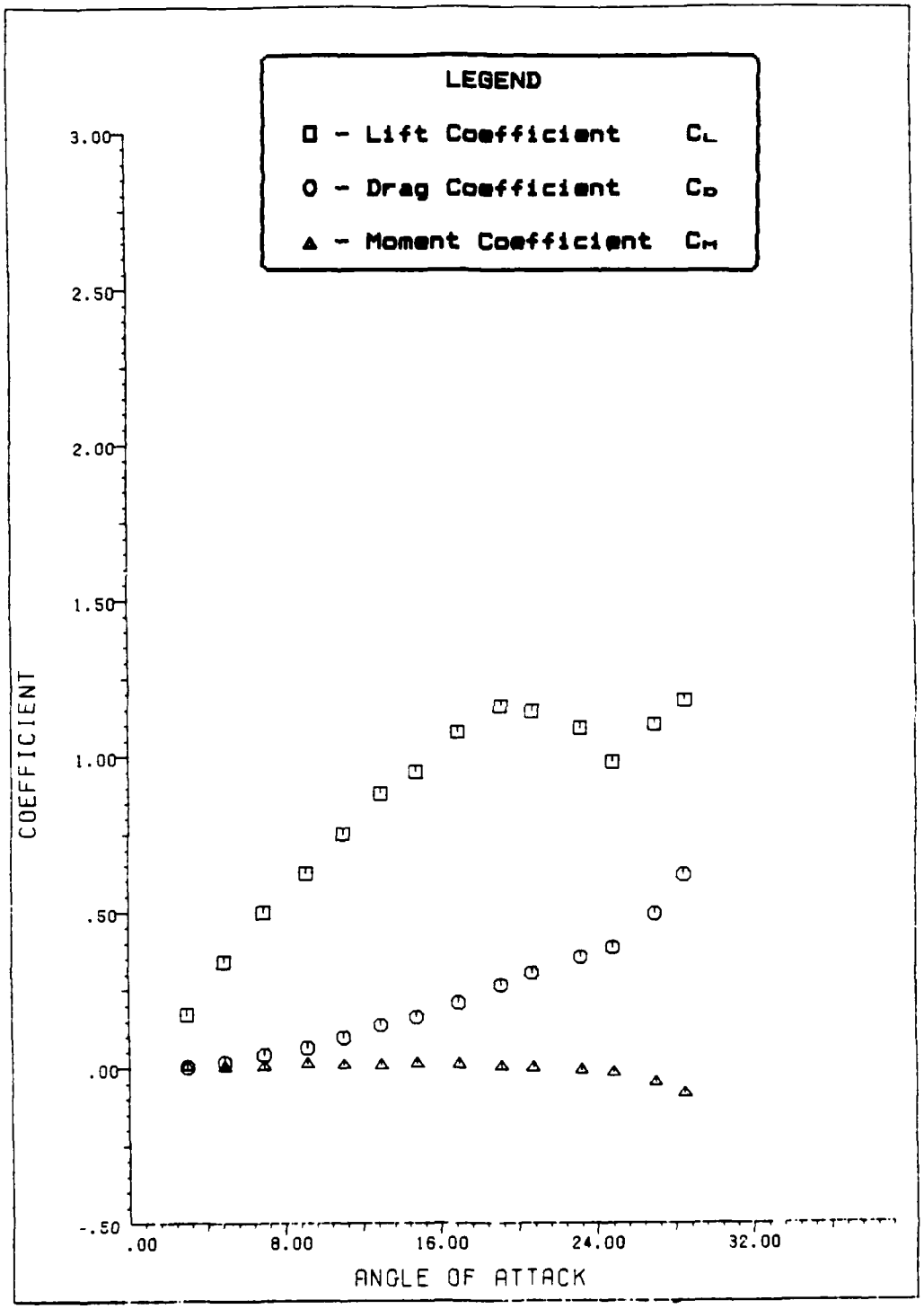

Figure 36. Data From Test Run 1 - 10

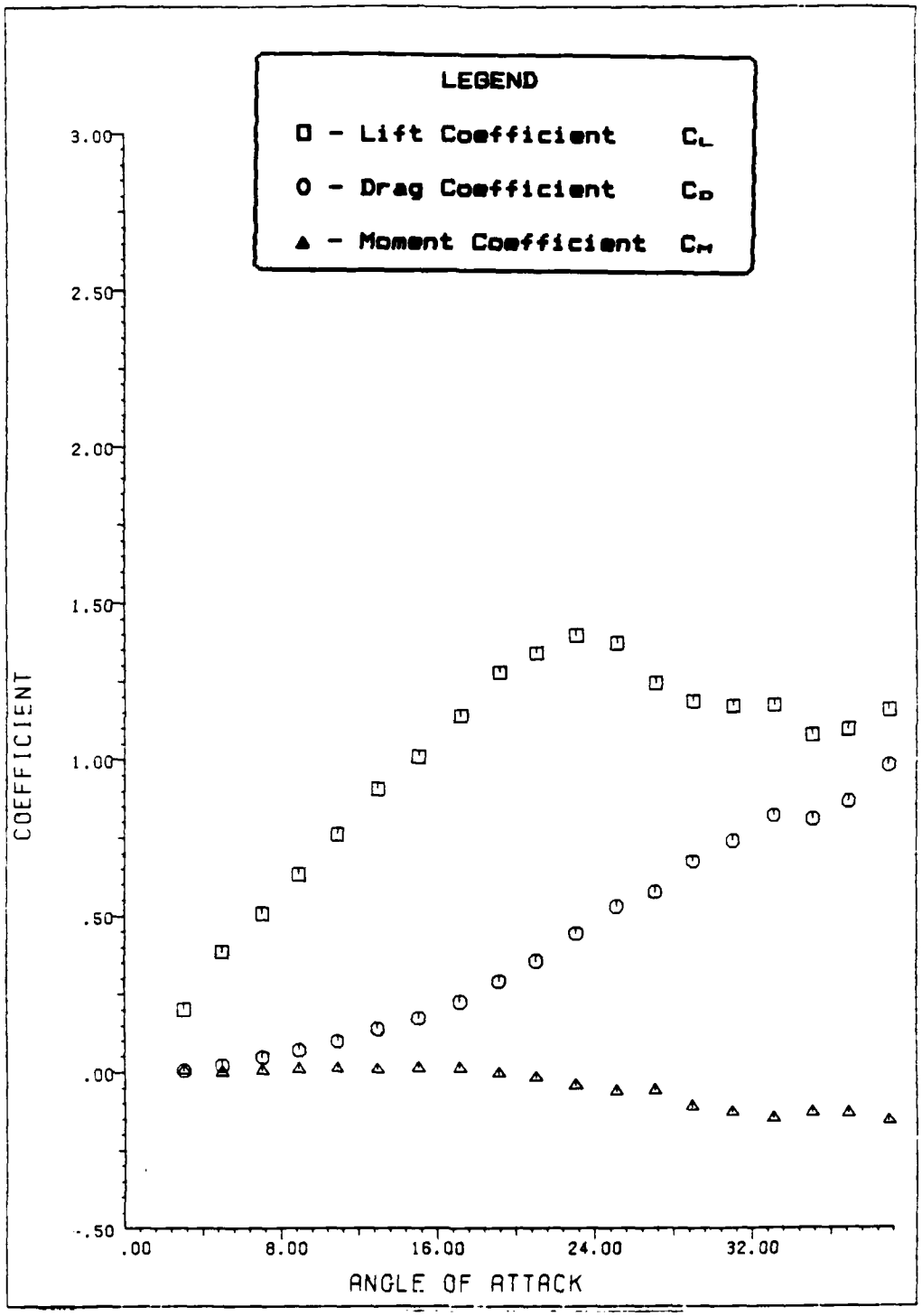

Figure 37. Data From Test Run 1 - 11

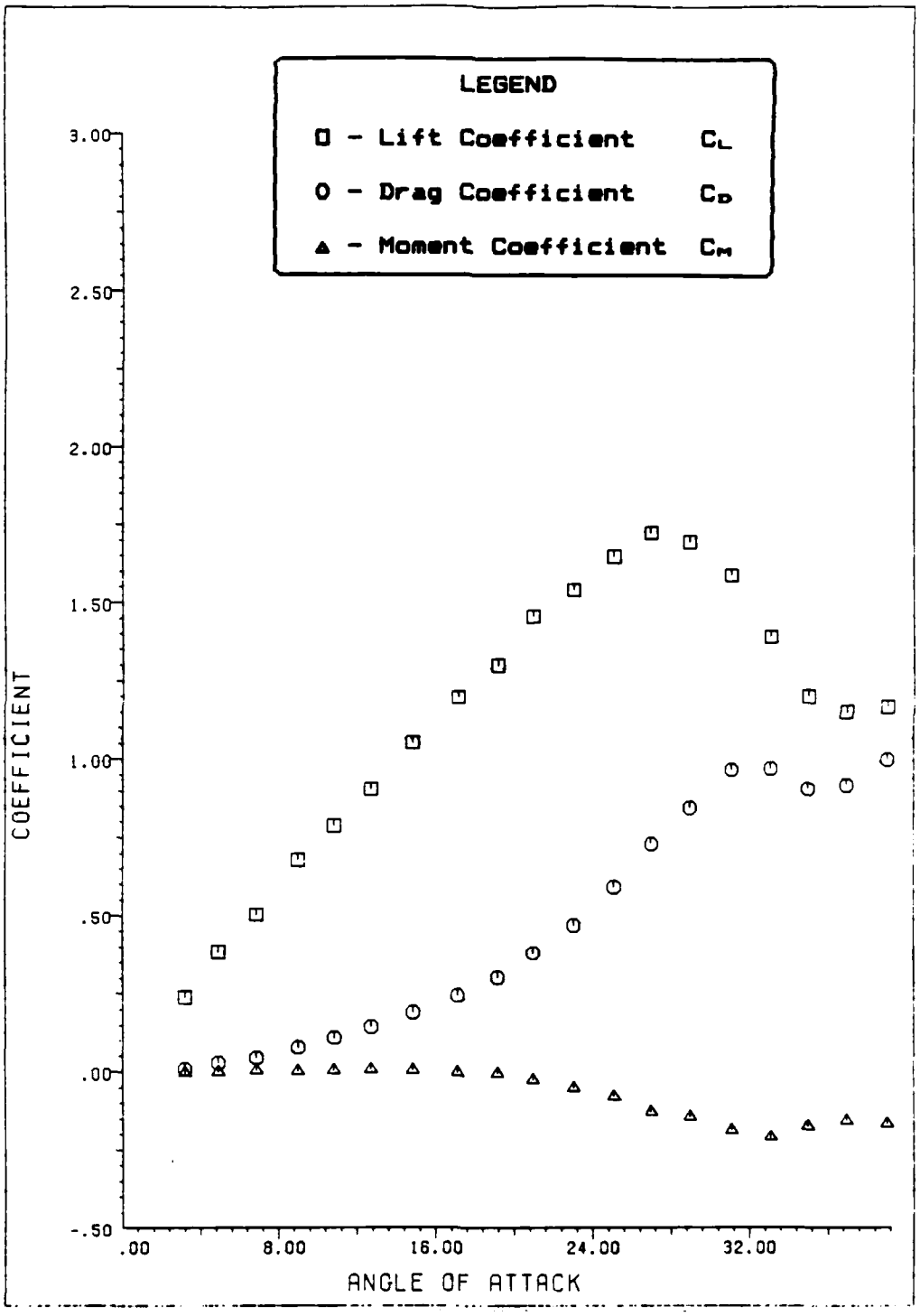

Figure 38. Data From Test Run 1 - 12

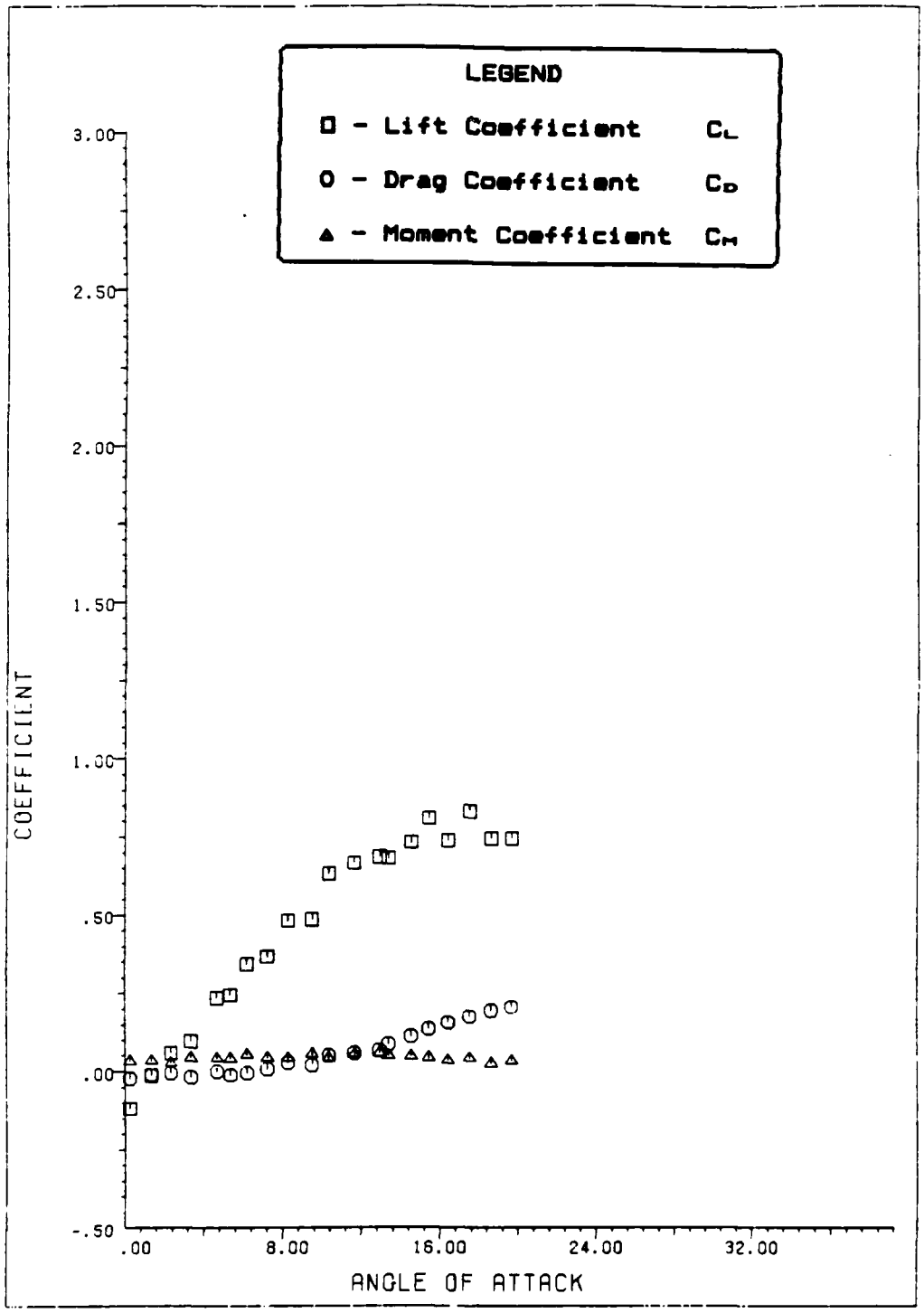

Figure 39. Data From Static Stall Test Runs Pitch Location #1 (.08c), V = 25.0 to 37.9 fps

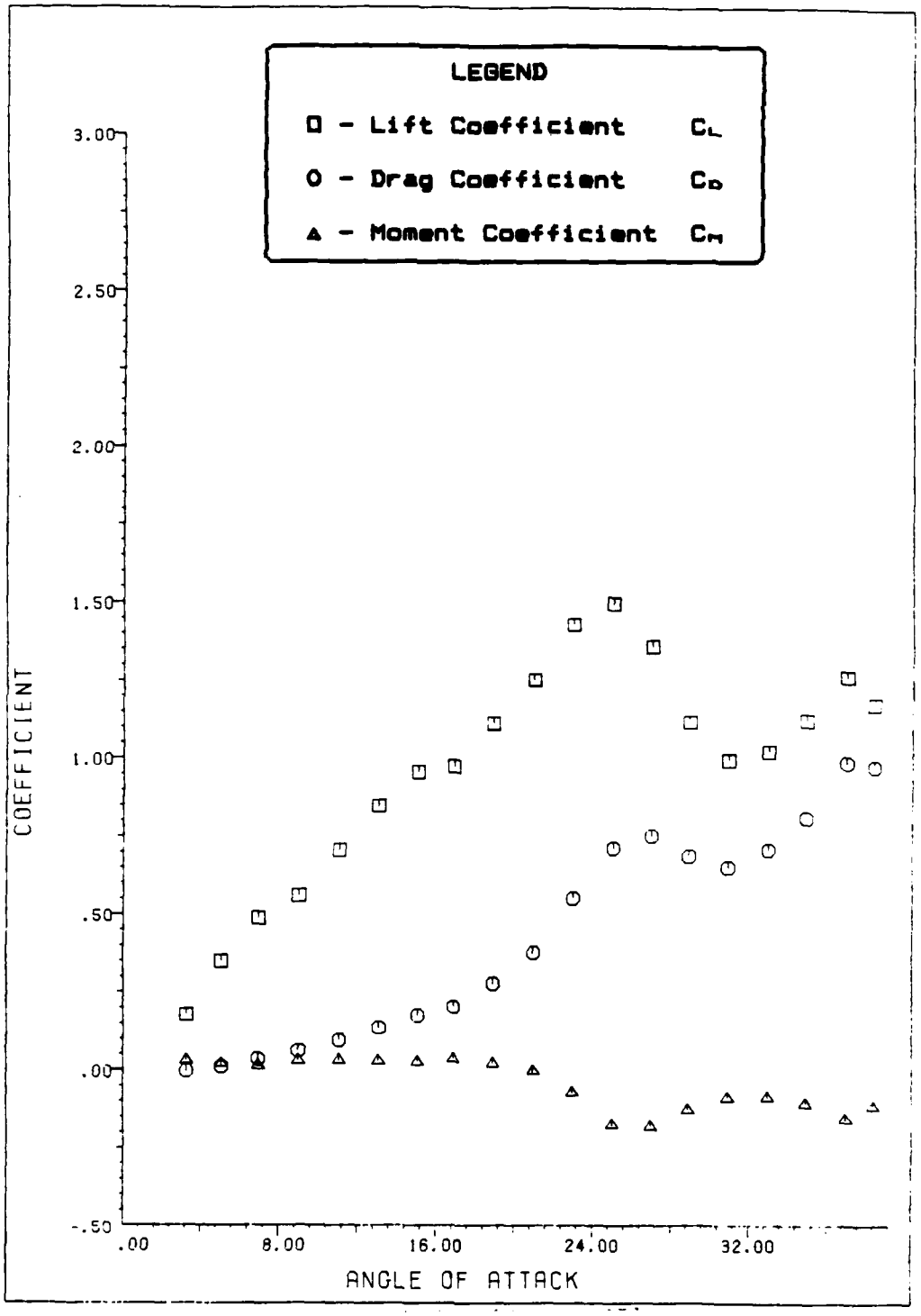

Figure 40. Data From Test Run 2 - 1

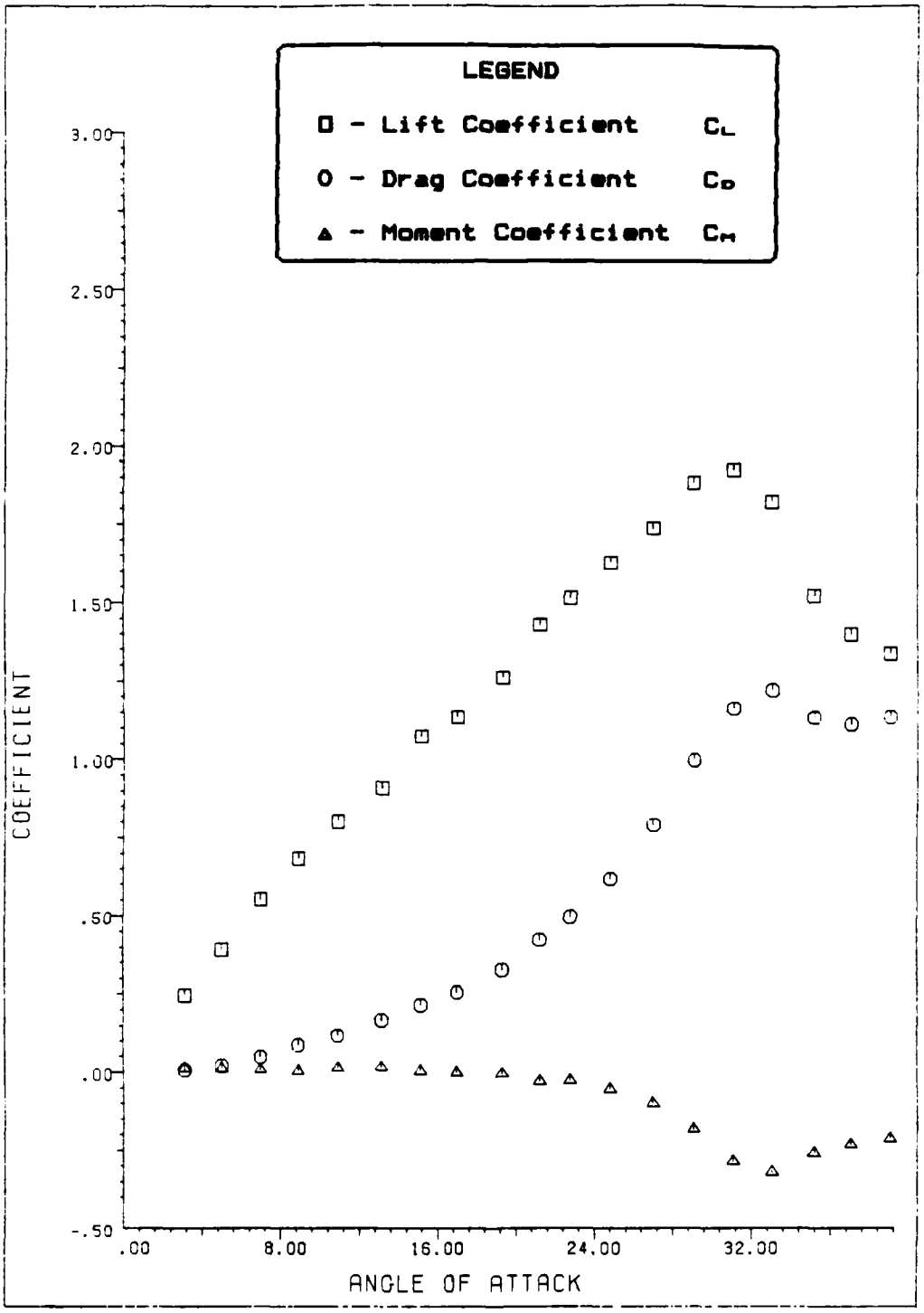

Figure 41. Data From Test Run 2 - 2

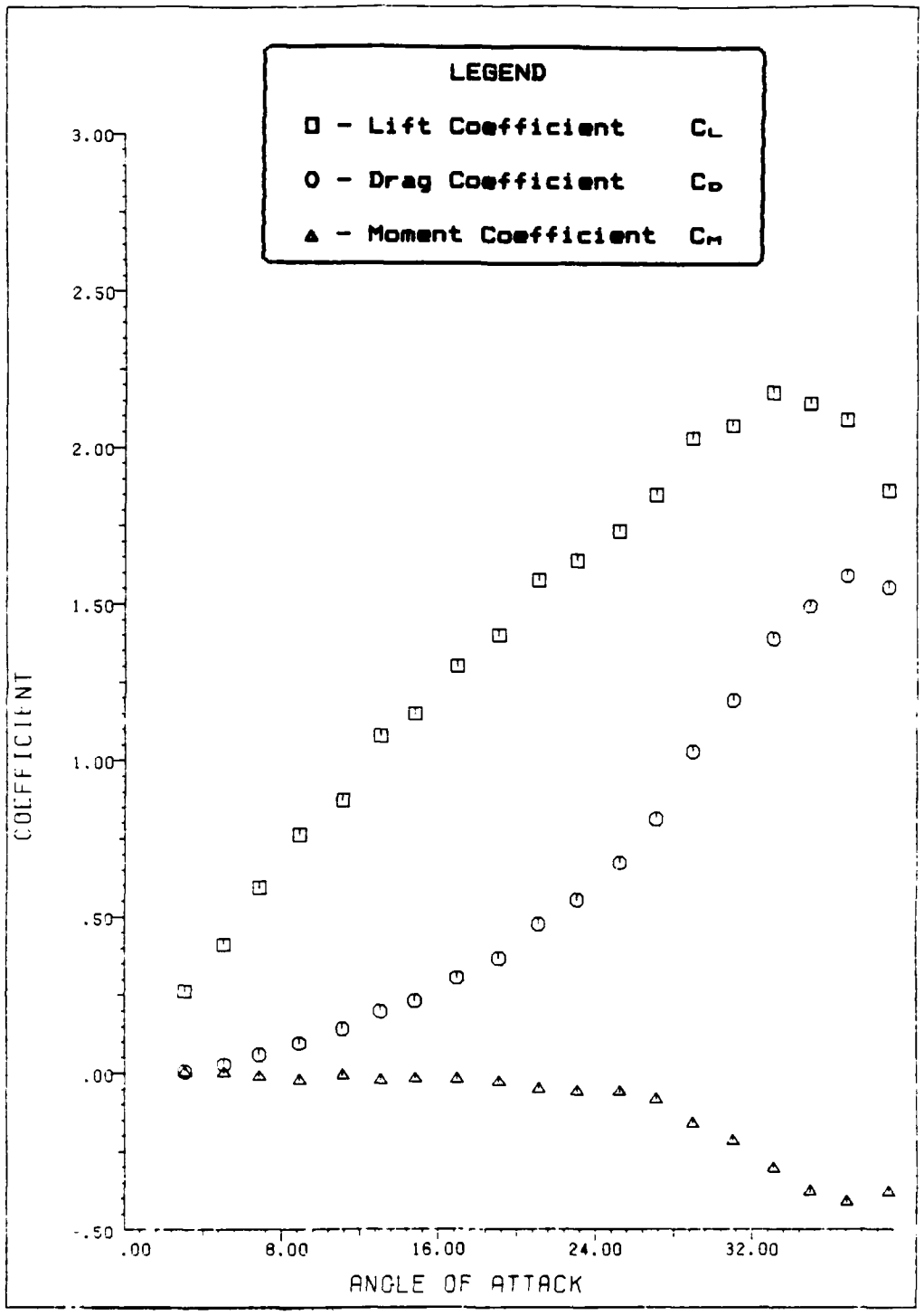

Figure 42. Data From Test Run 2 - 3

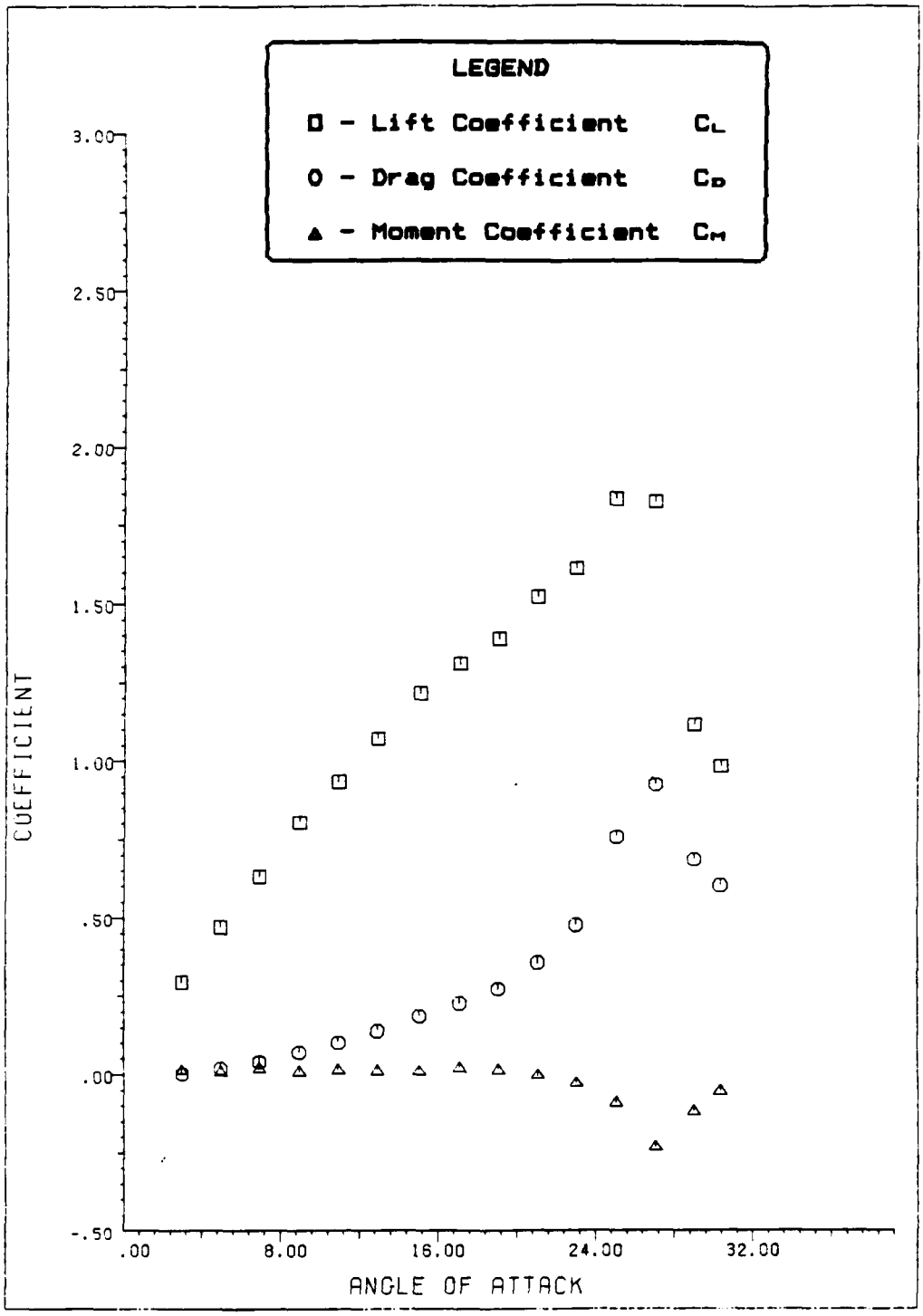

Figure 43. Data From Test Run 2 - 4

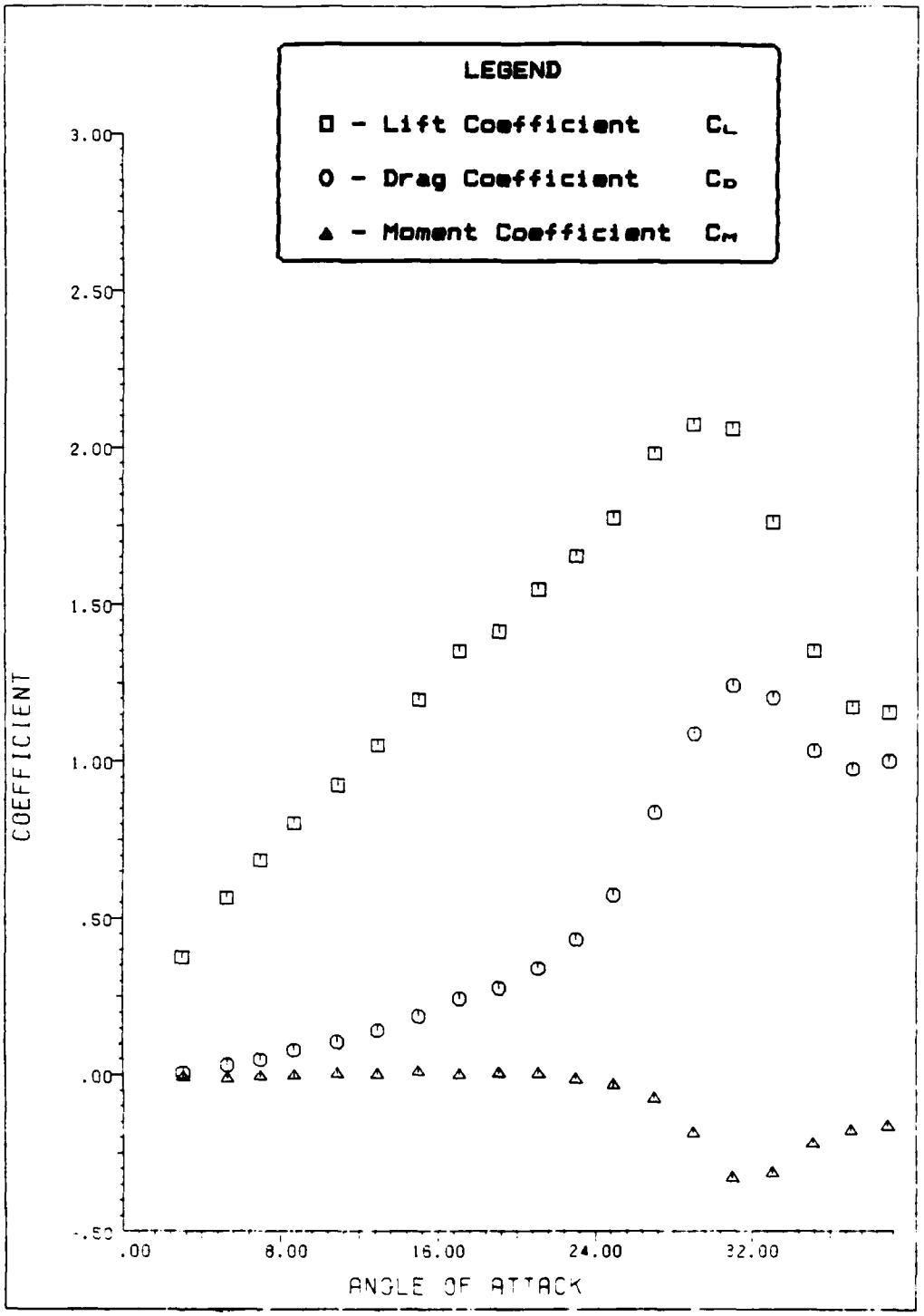

Figure 44. Data From Test Run 2 - 5

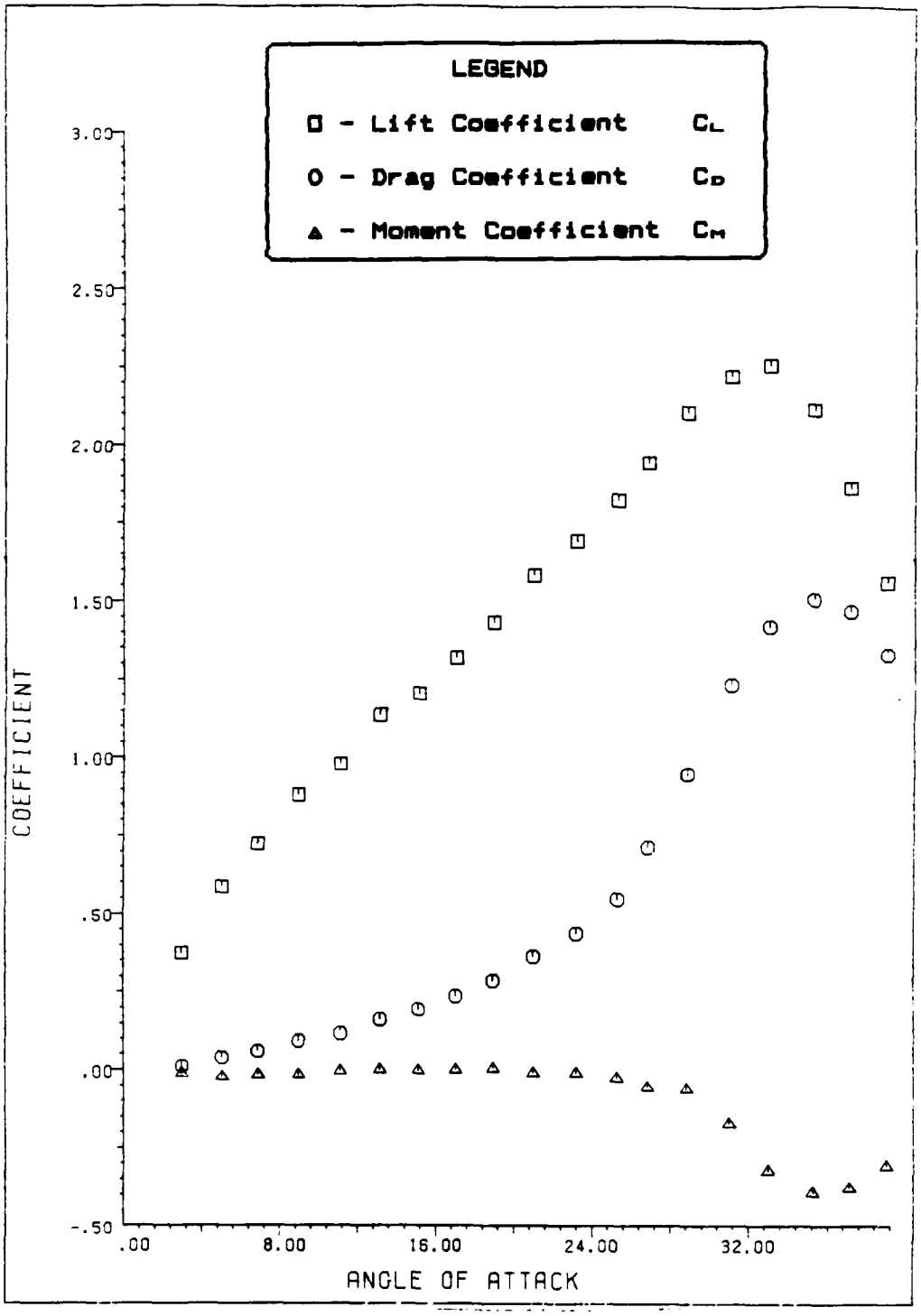

Figure 45. Data From Test Run 2 - 6

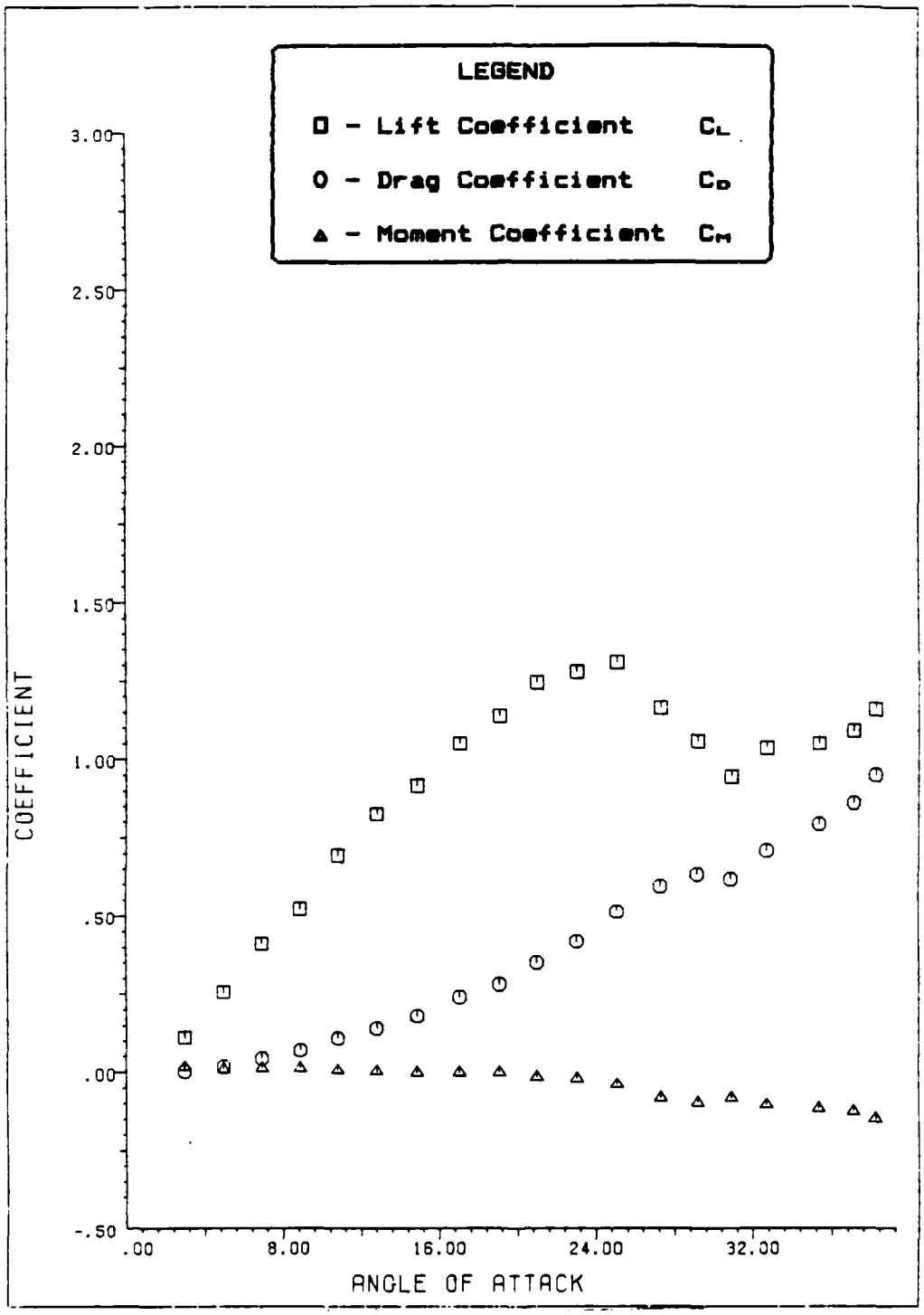

Figure 46. Data From Test Run 2 - 7

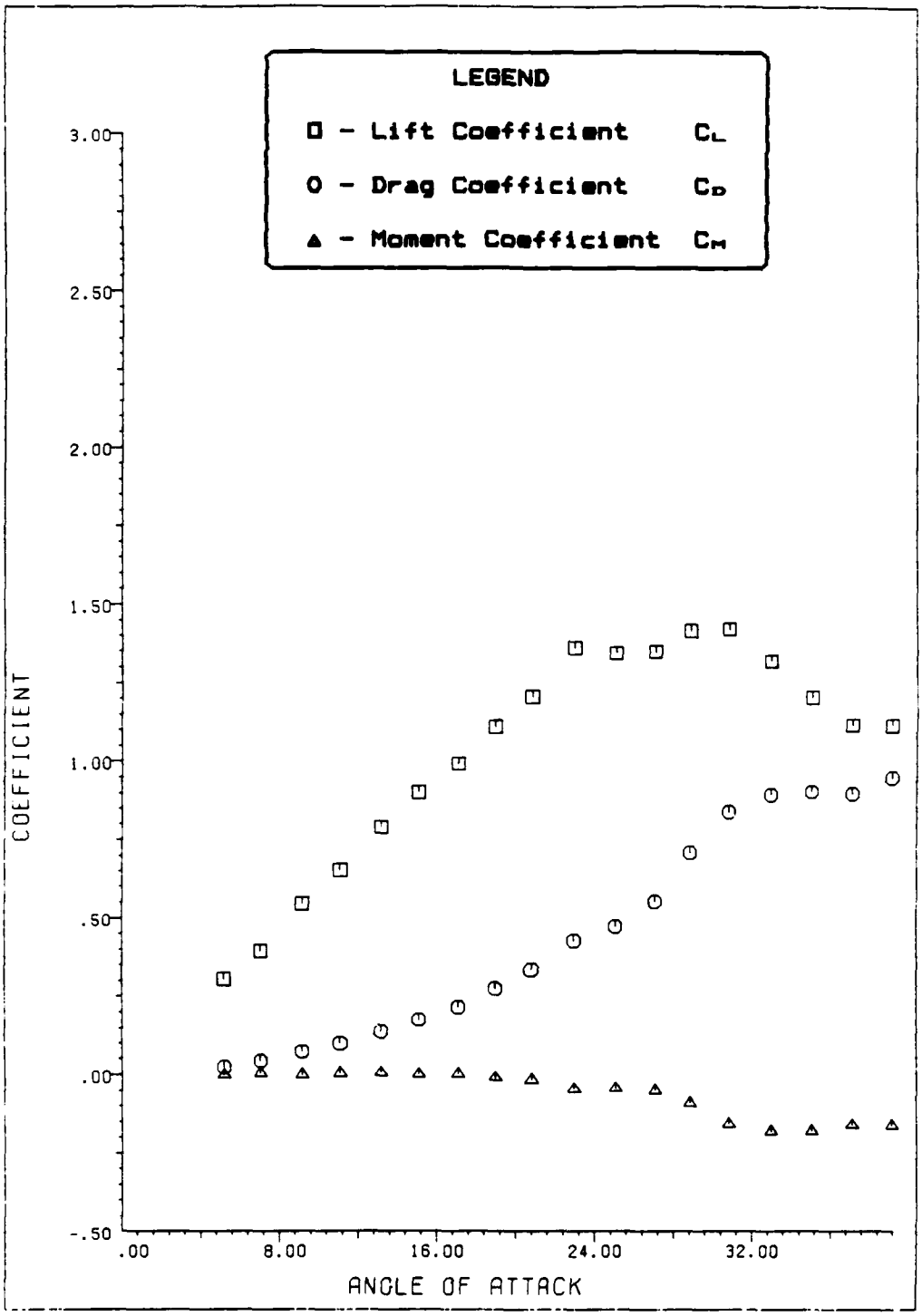

Figure 47. Data From Test Run 2 - 8

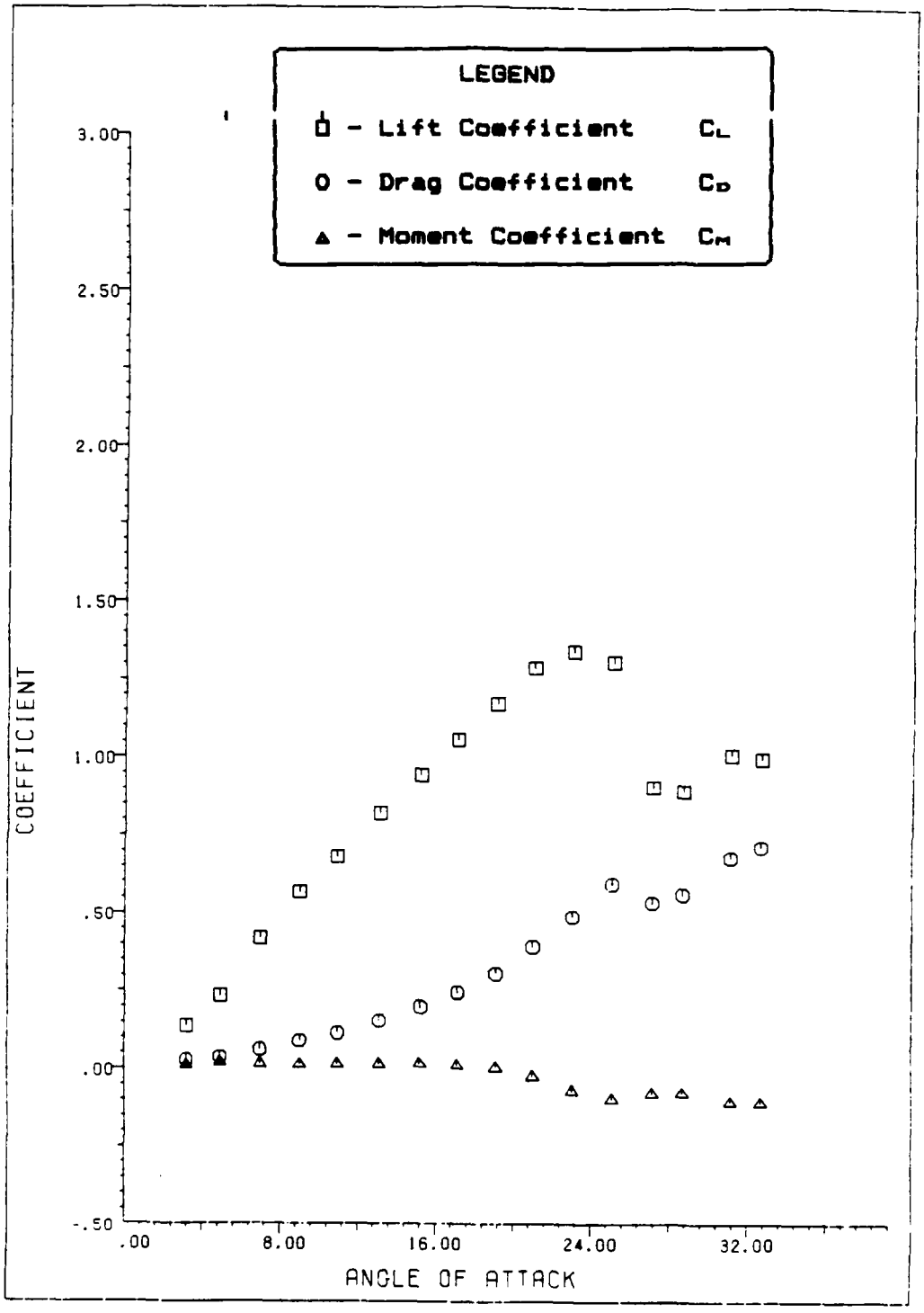

Figure 48. Data From Test Run 2 - 10

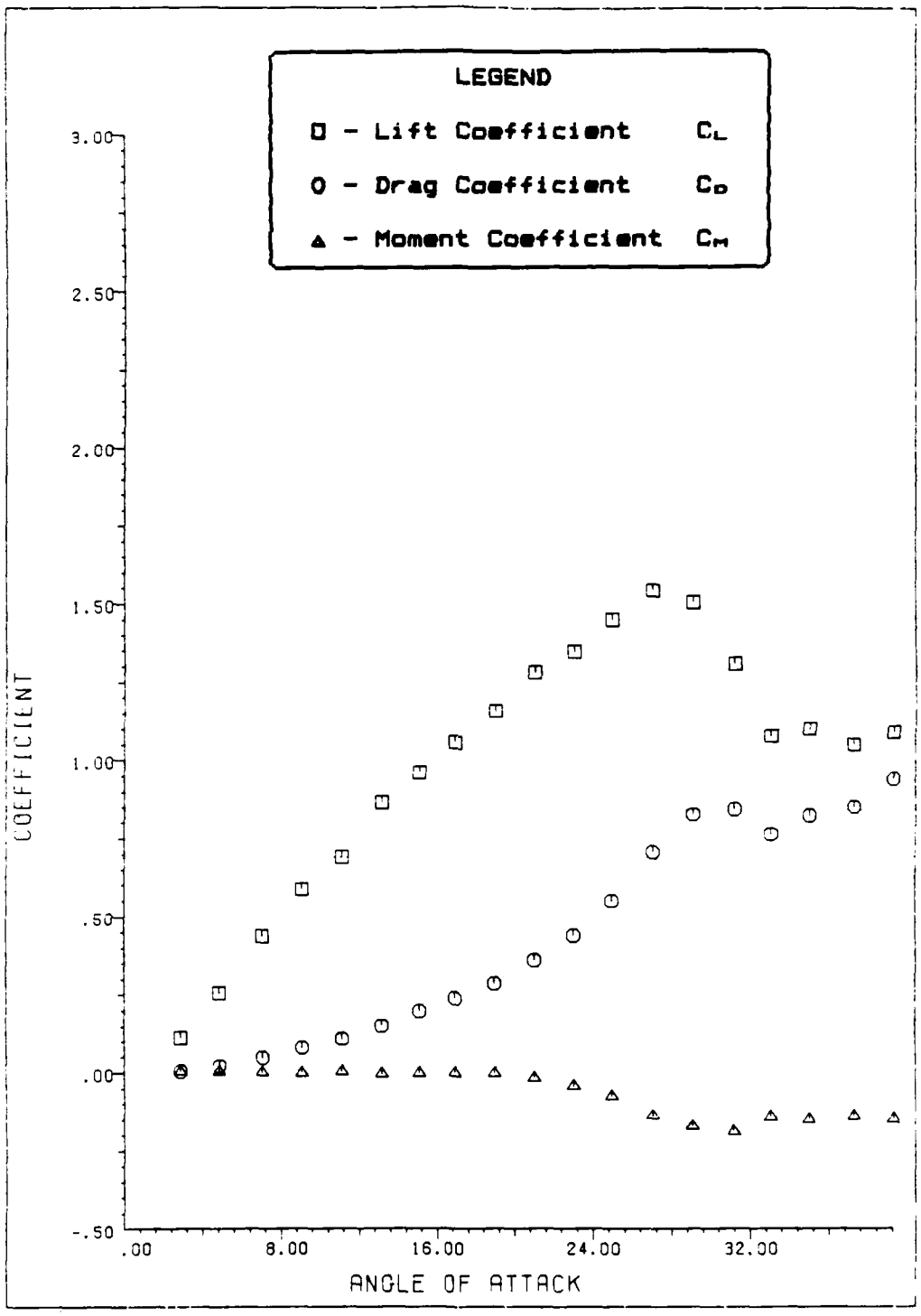

Figure 49. Data From Test Run 2 - 11

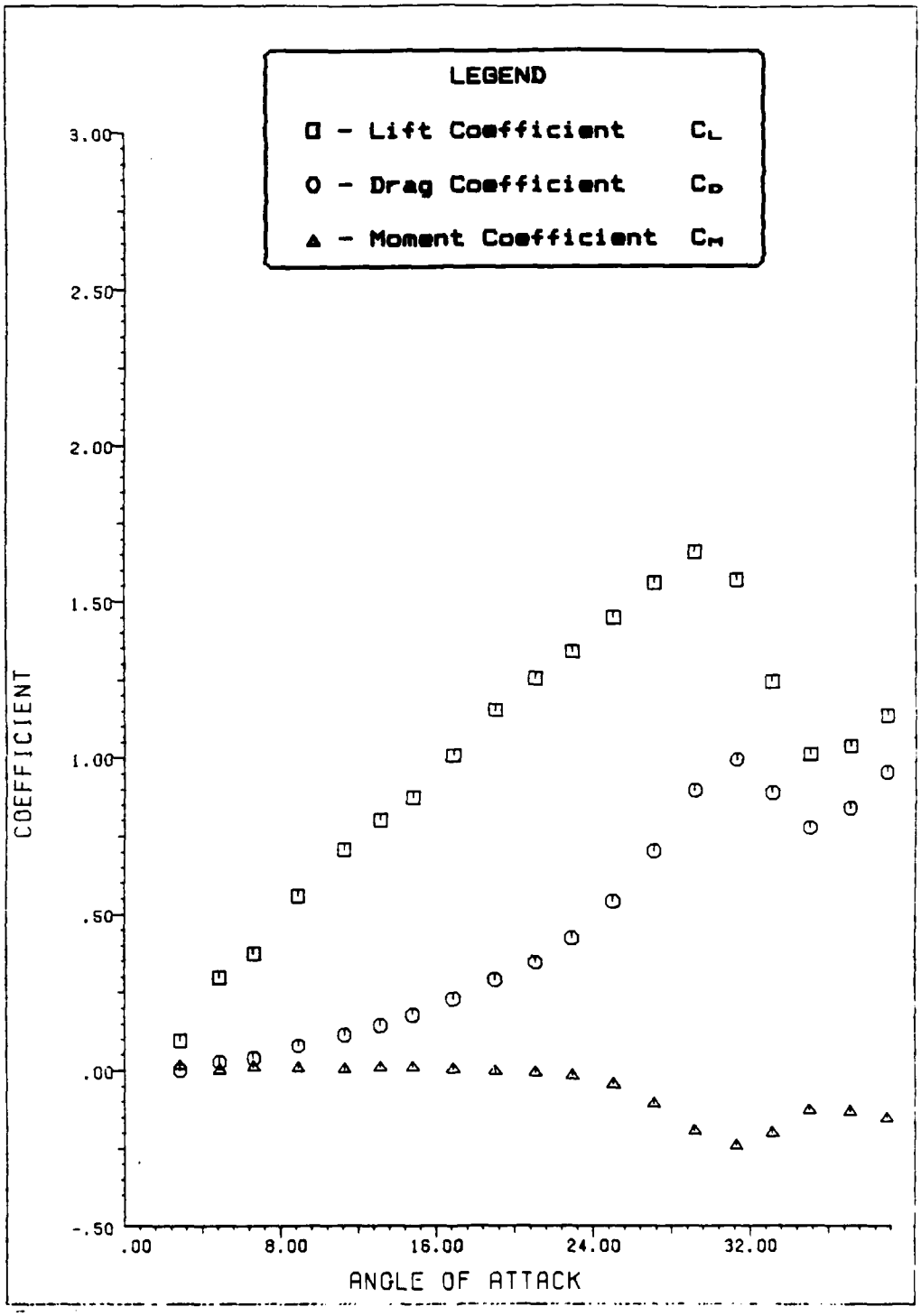

Figure 50. Data From Test Run 2 - 12

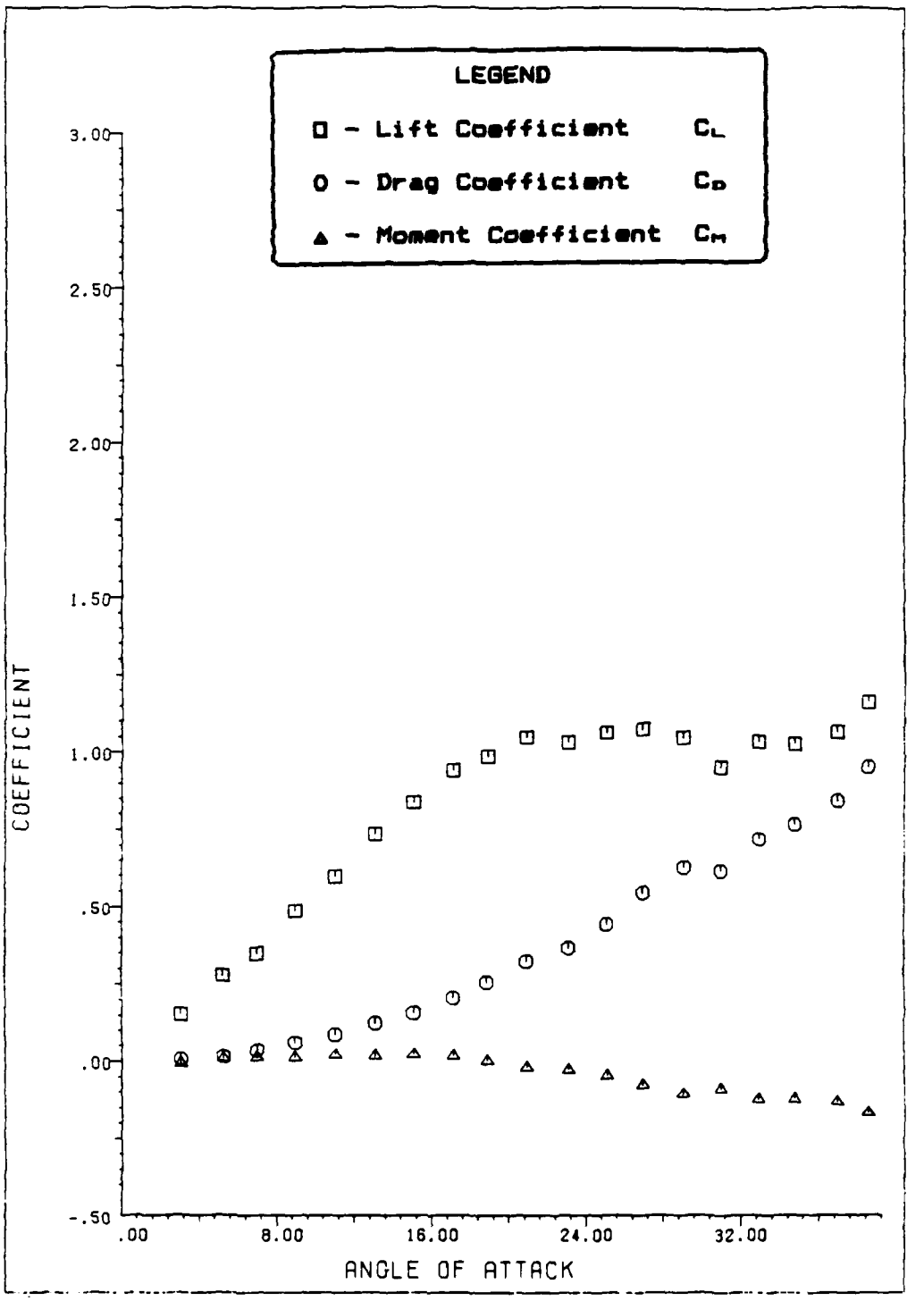

Figure 51. Data From Test Run 2 - 13

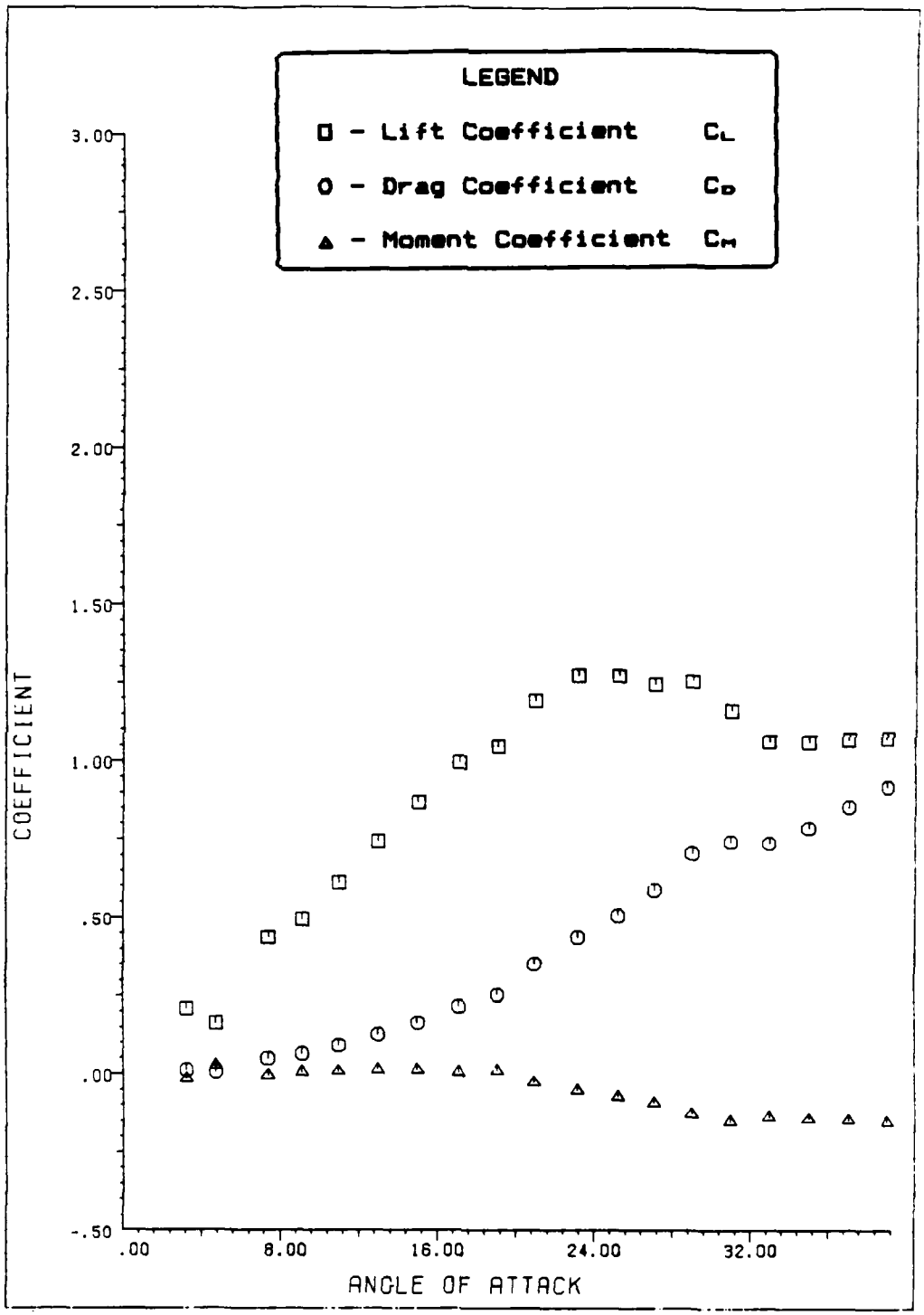

Figure 52. Data From Test Run 2 - 14

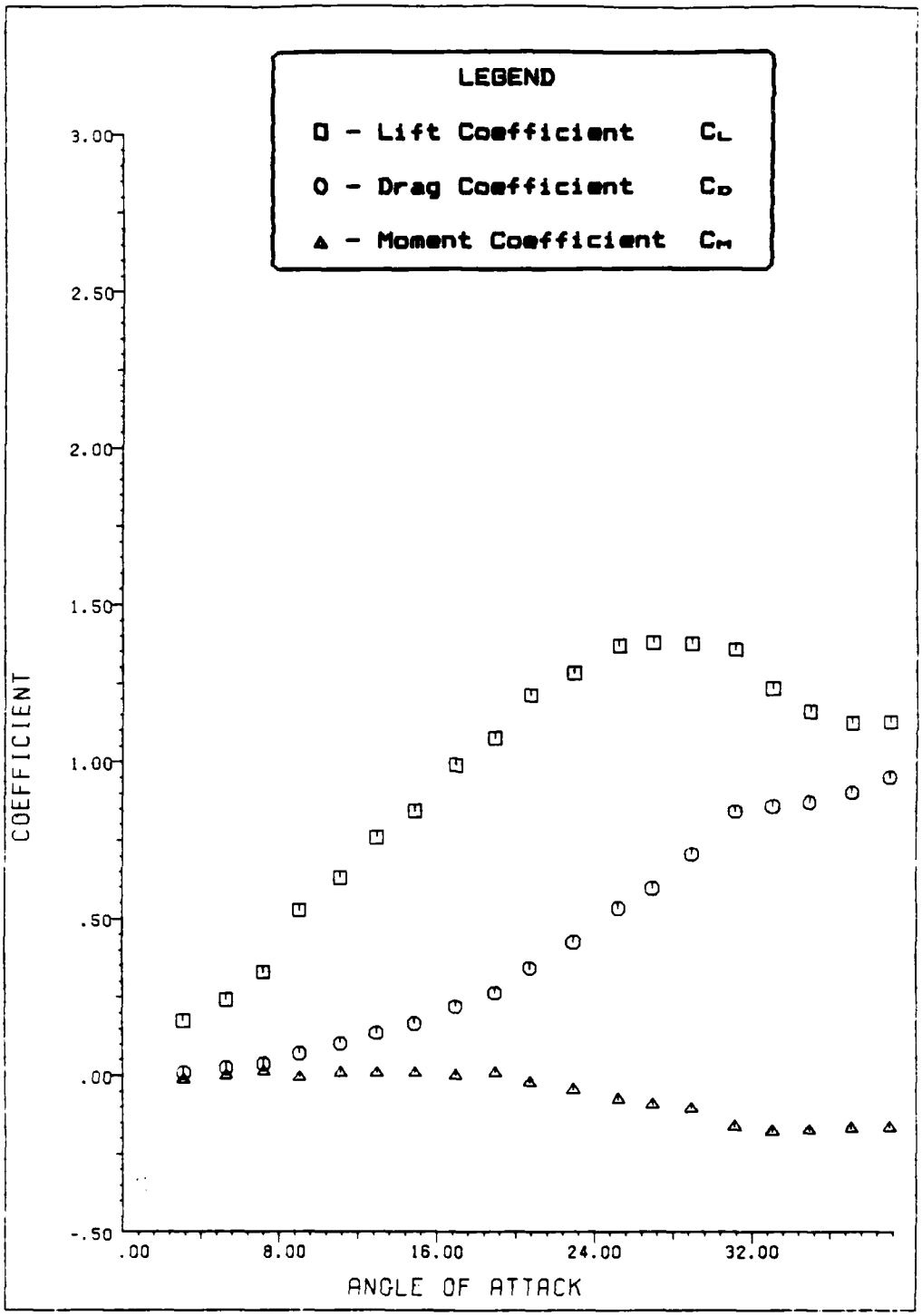

Figure 53. Data From Test Run 2 - 15

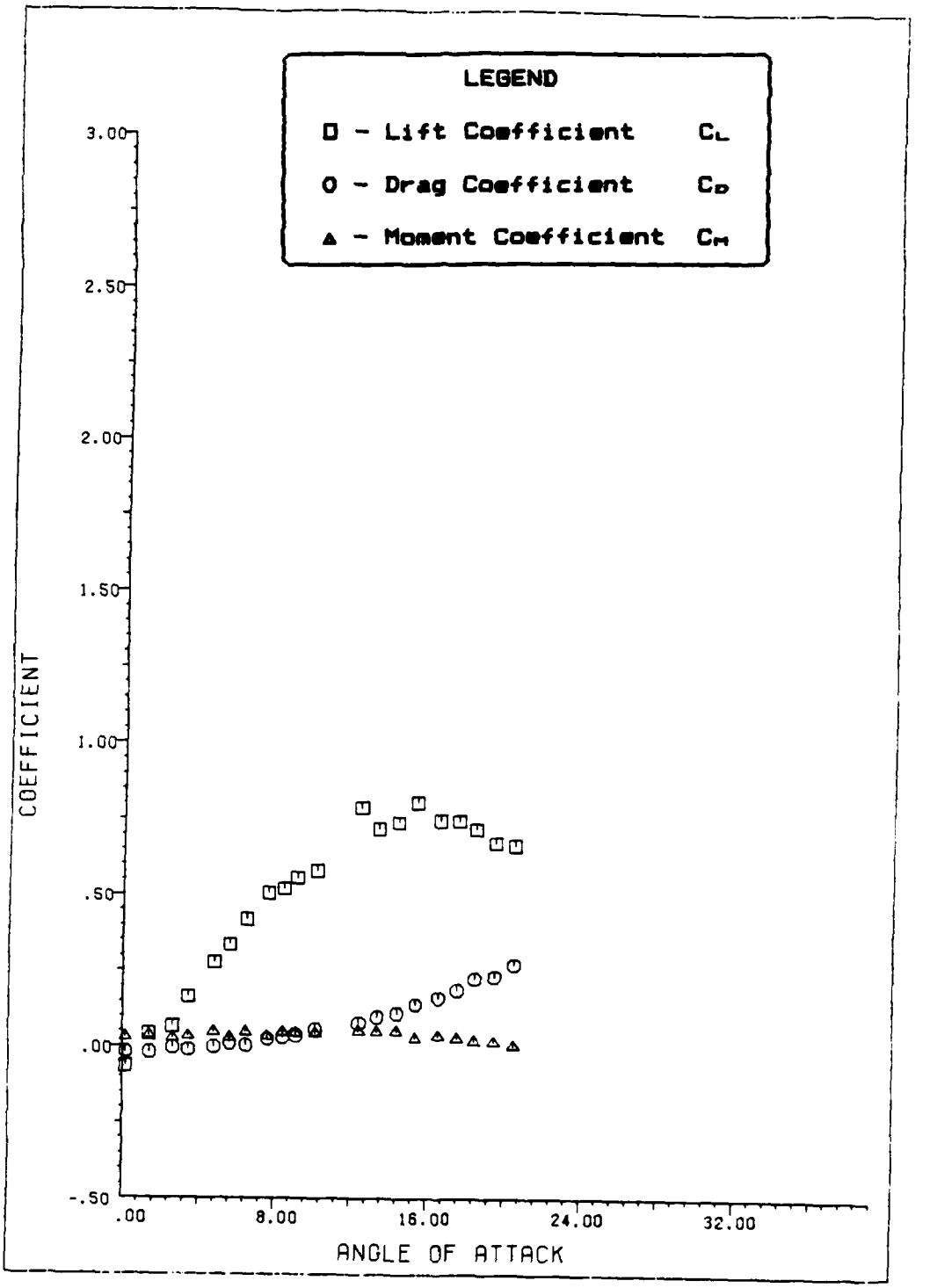

Figure 54. Data From Static Stall Test Runs
Pitch Location #2 (.25c), V = 25.2 to 45.0 fps

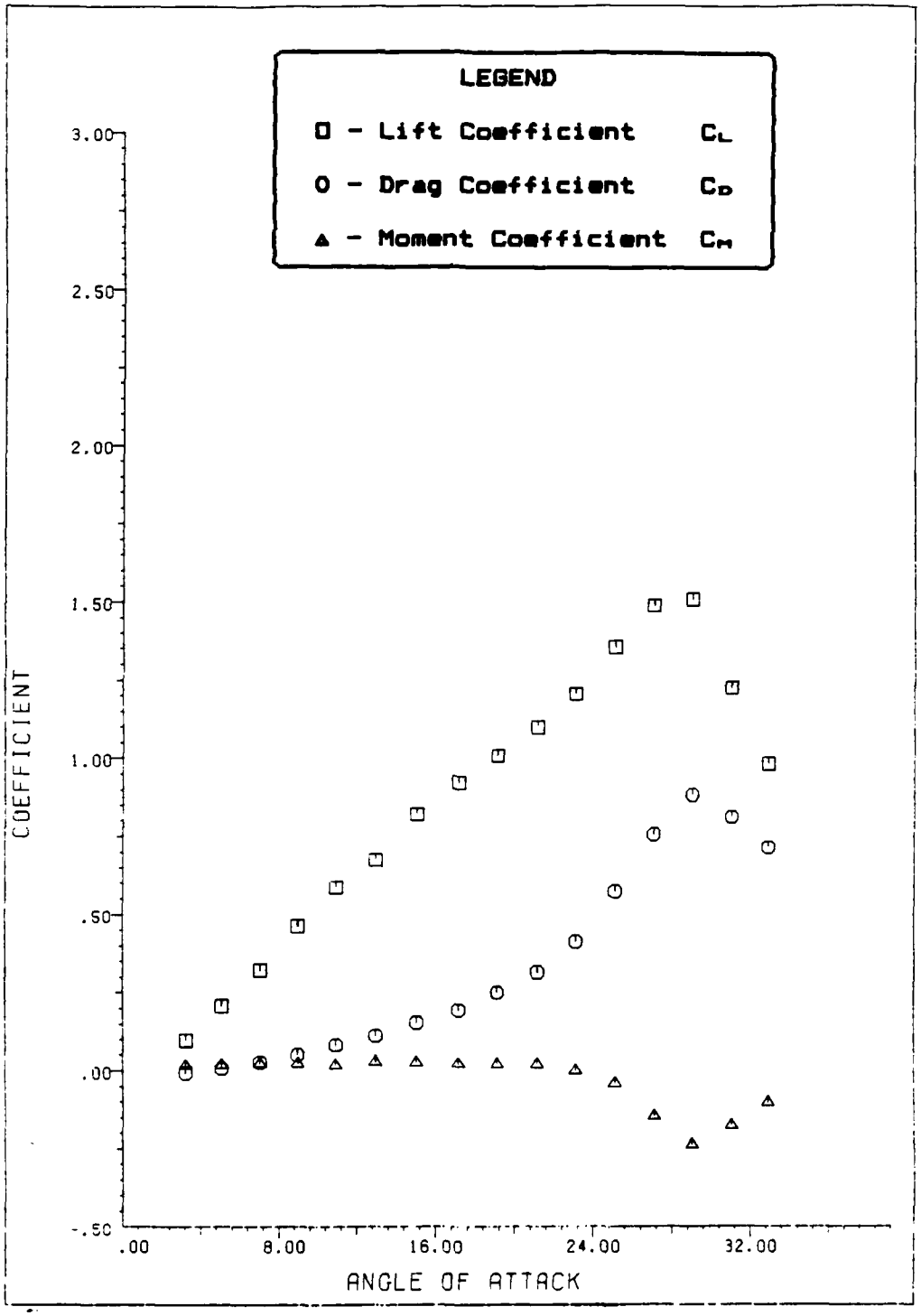

Figure 55. Data From Test Run 3 - 1

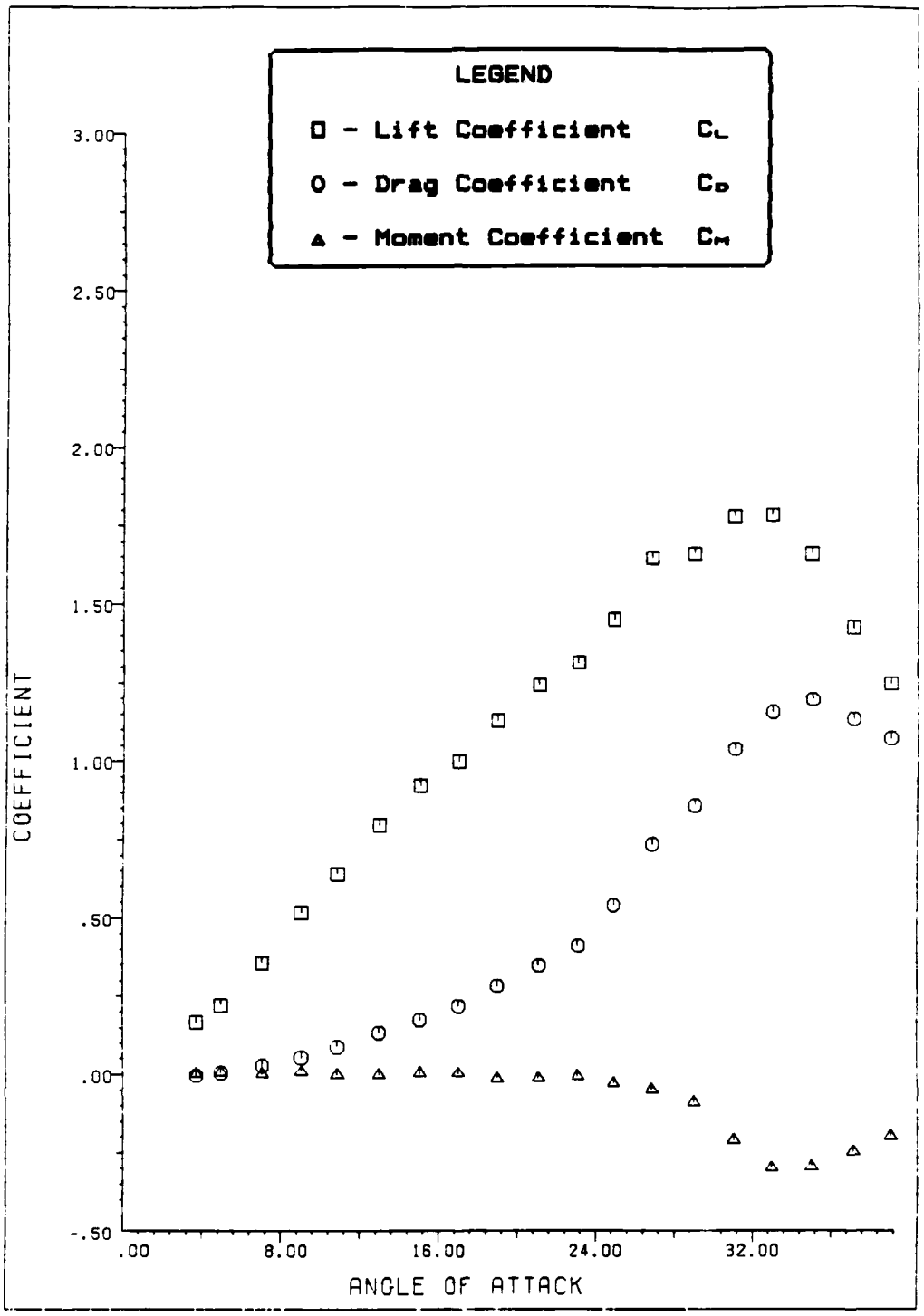

Figure 56. Data From Test Run 3 - 2

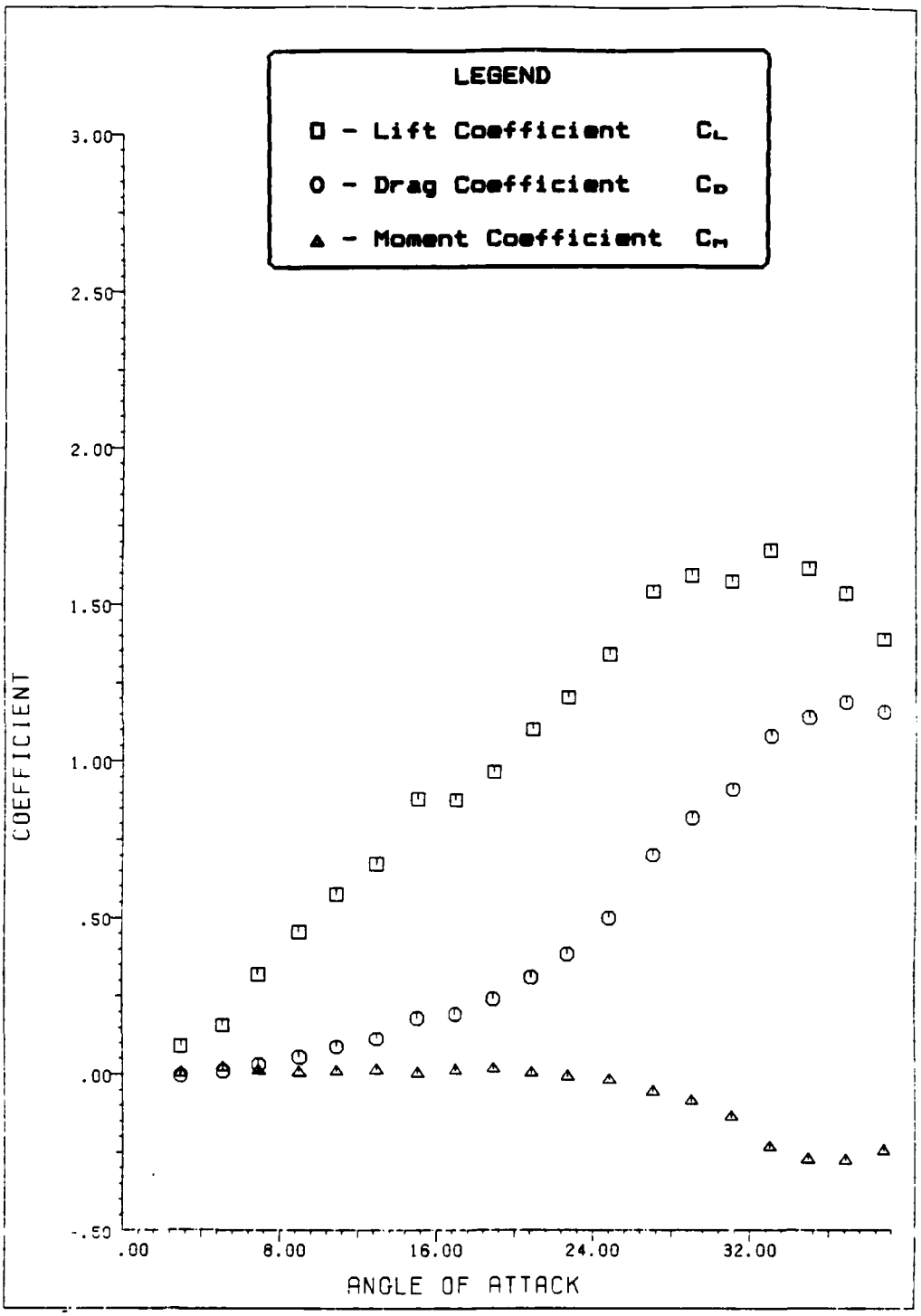

Figure 57. Data From Test Run 3 - 3

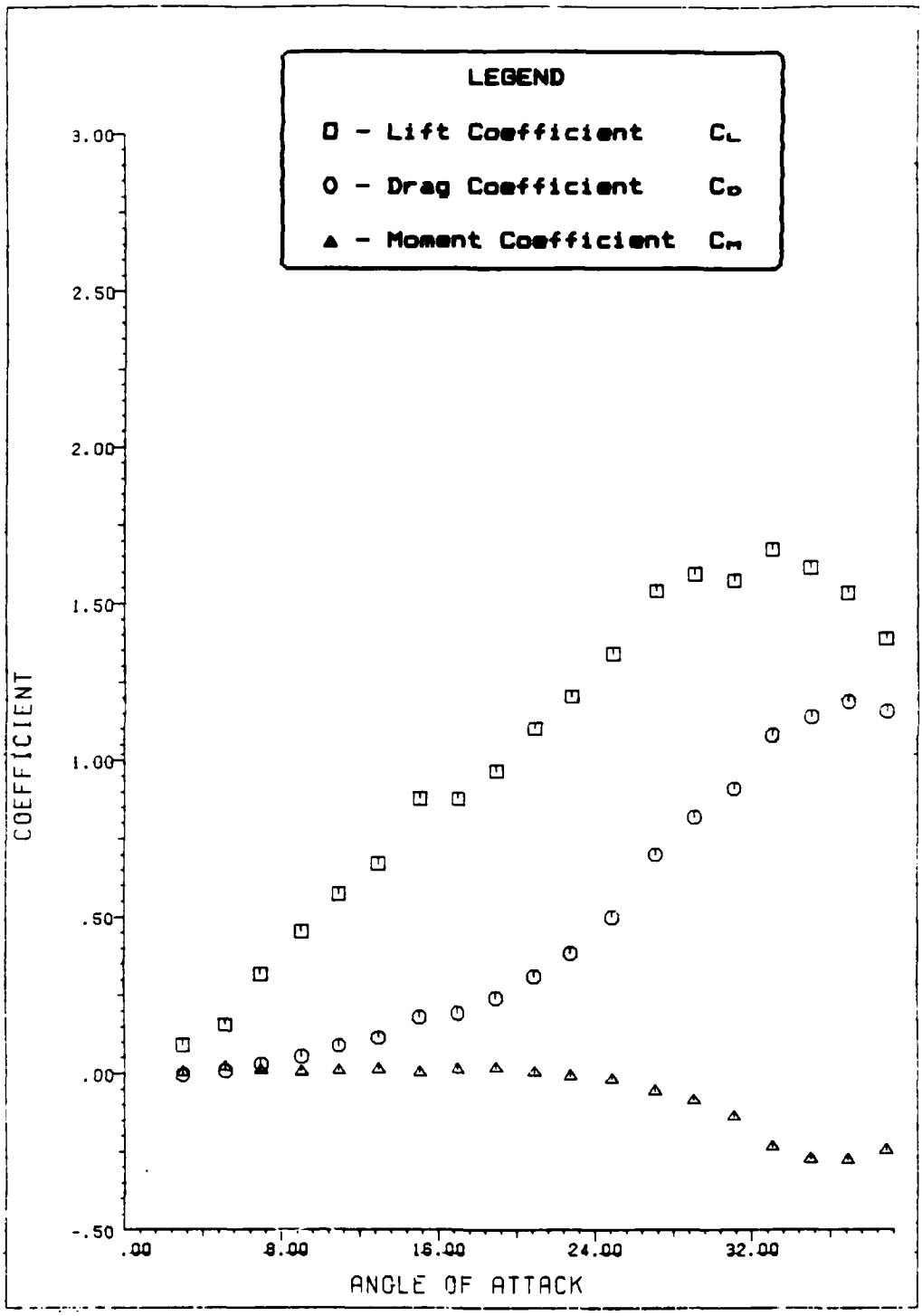

Figure 58. Data From Test Run 3 - 4

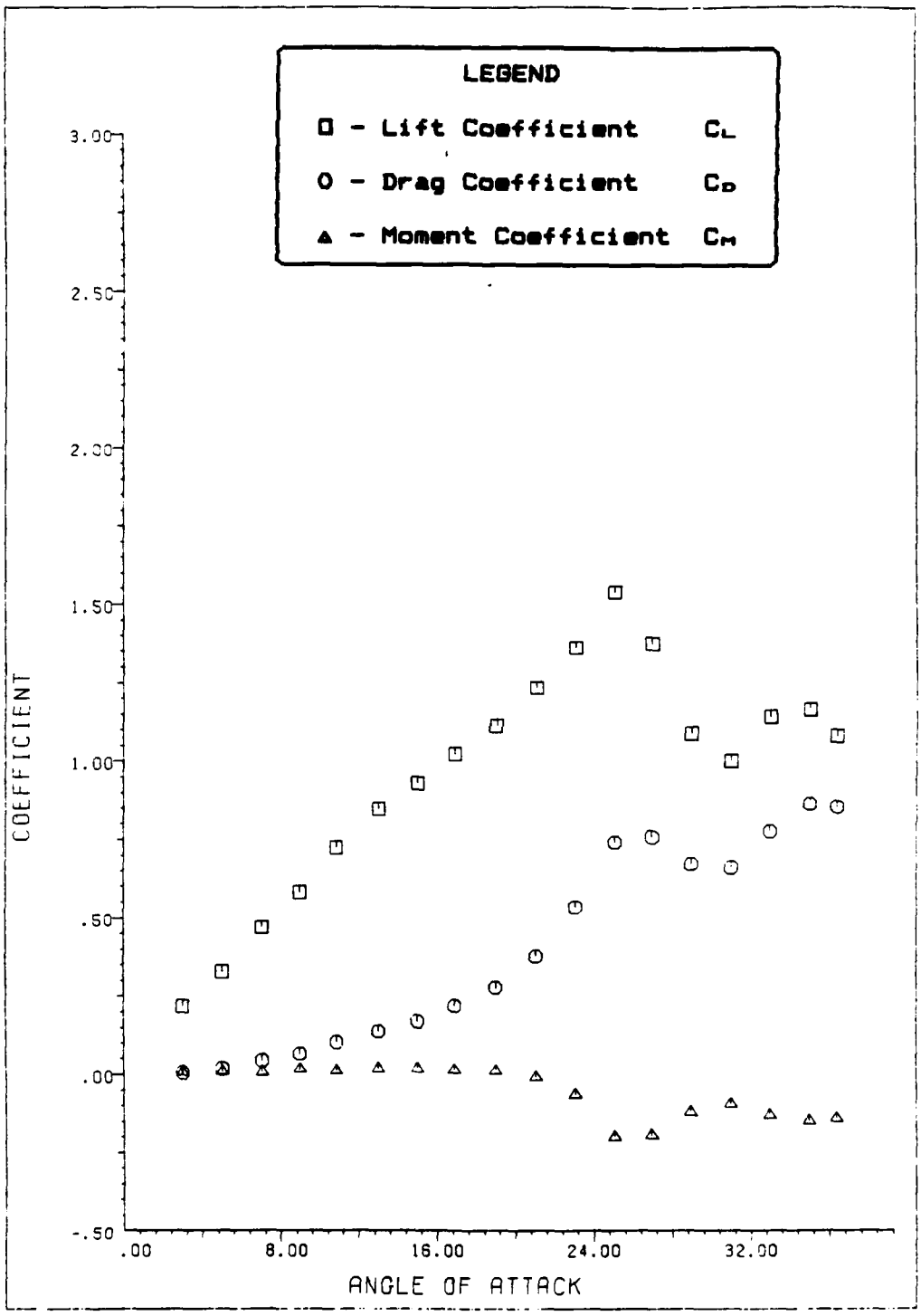

Figure 59. Data From Test Run 3 - 5

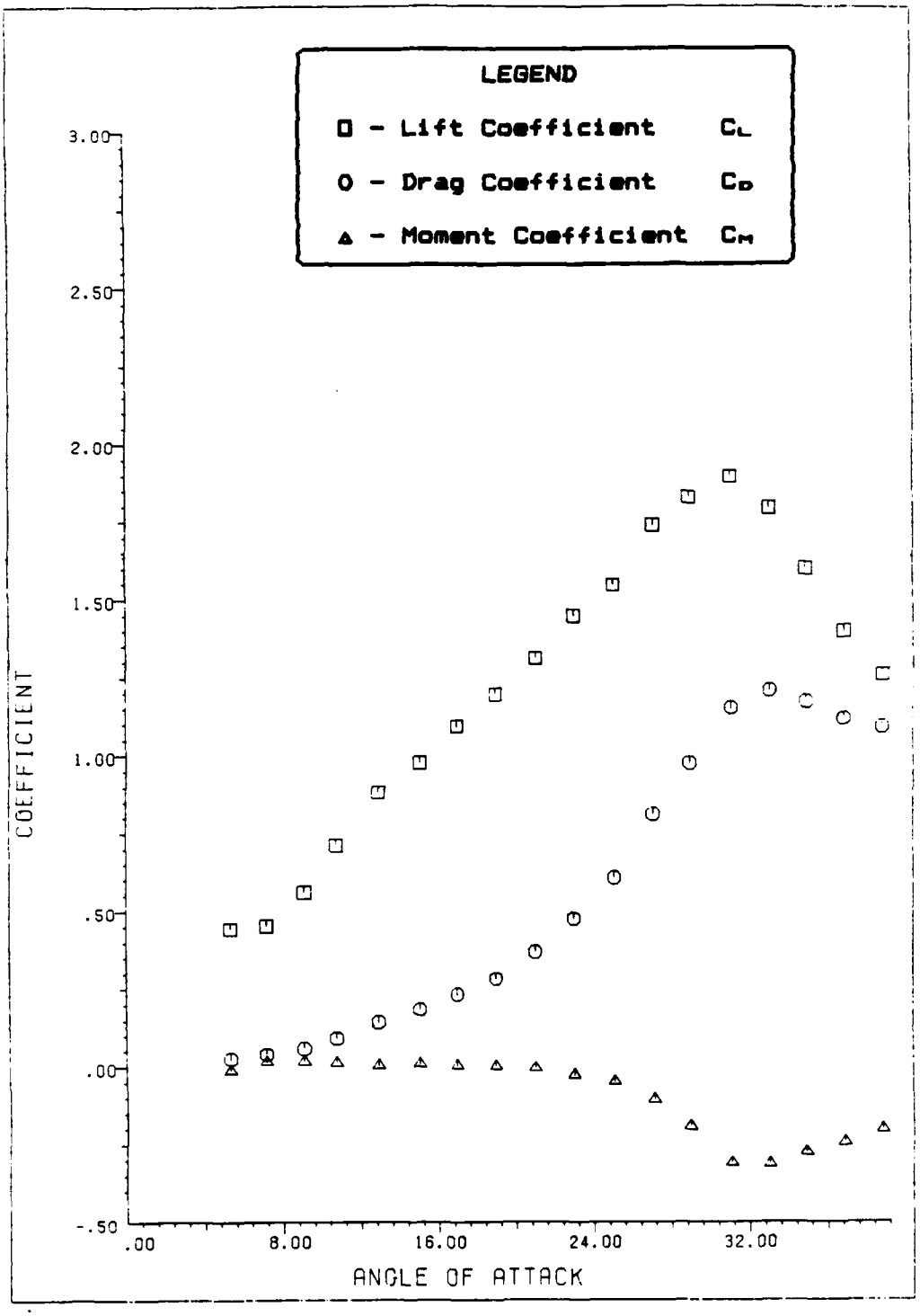

Figure 60. Data From Test Run 3 - 7

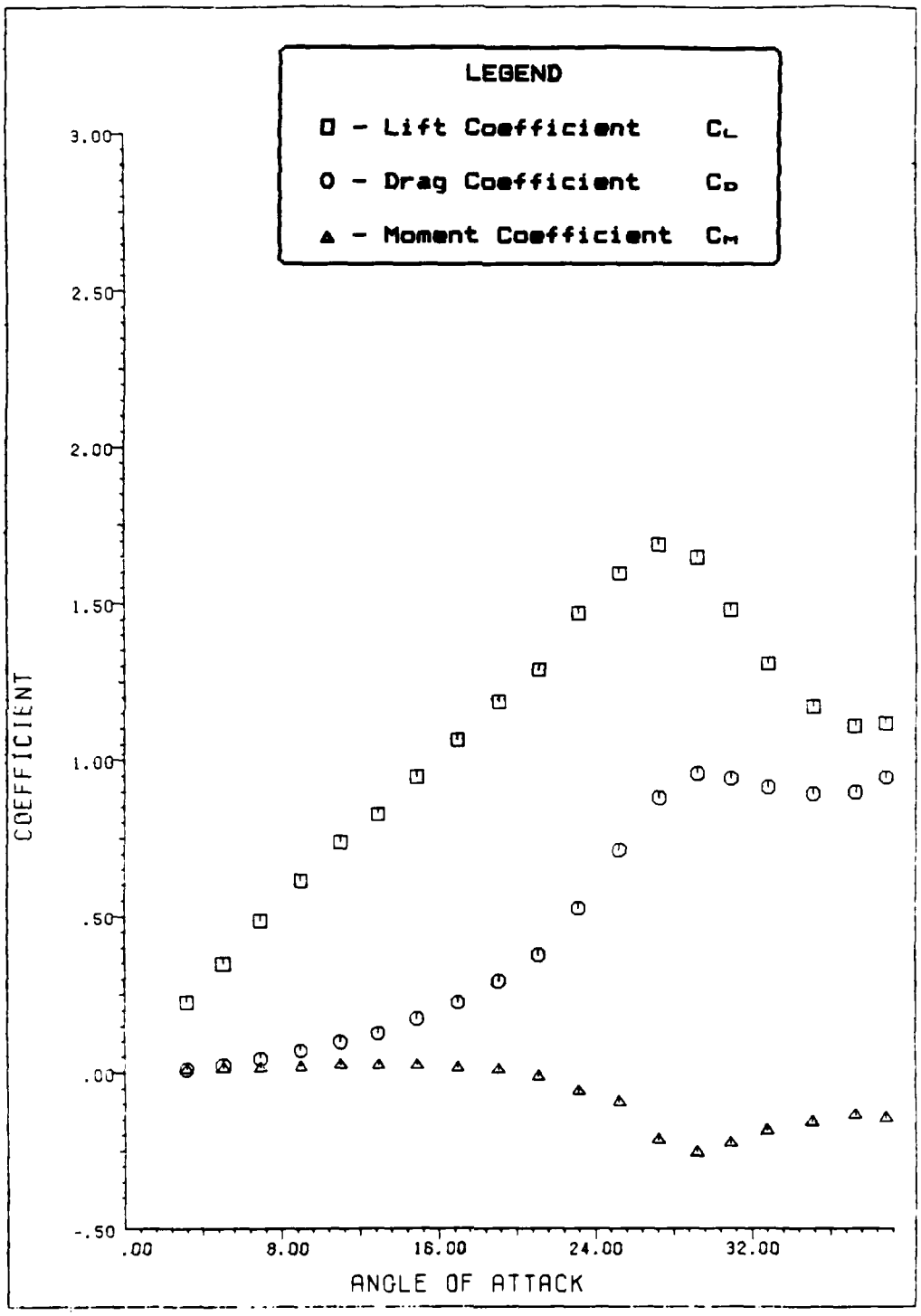

Figure 61. Data From Test Run 3 - 8

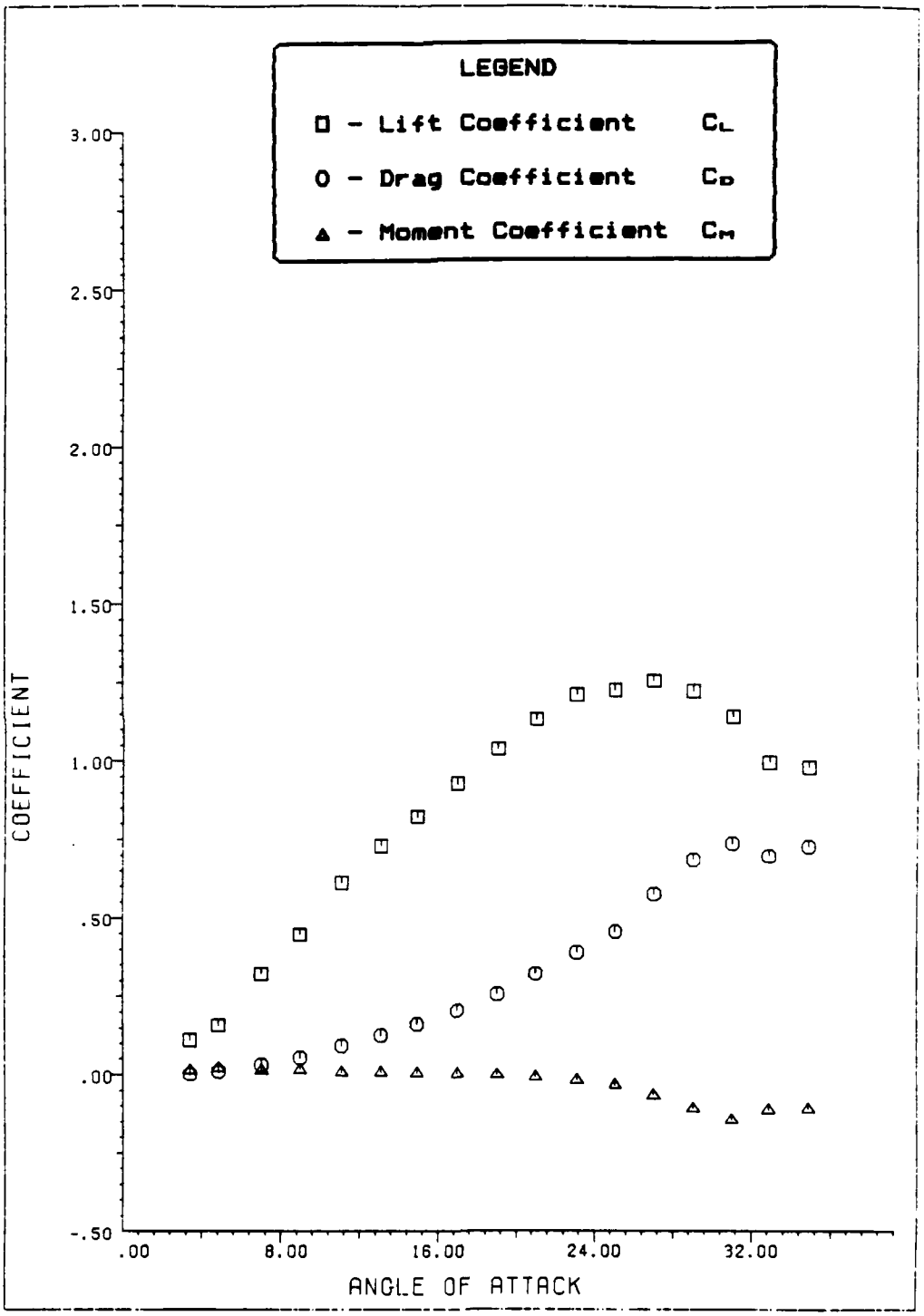

Figure 62. Data From Test Run 3 - 9

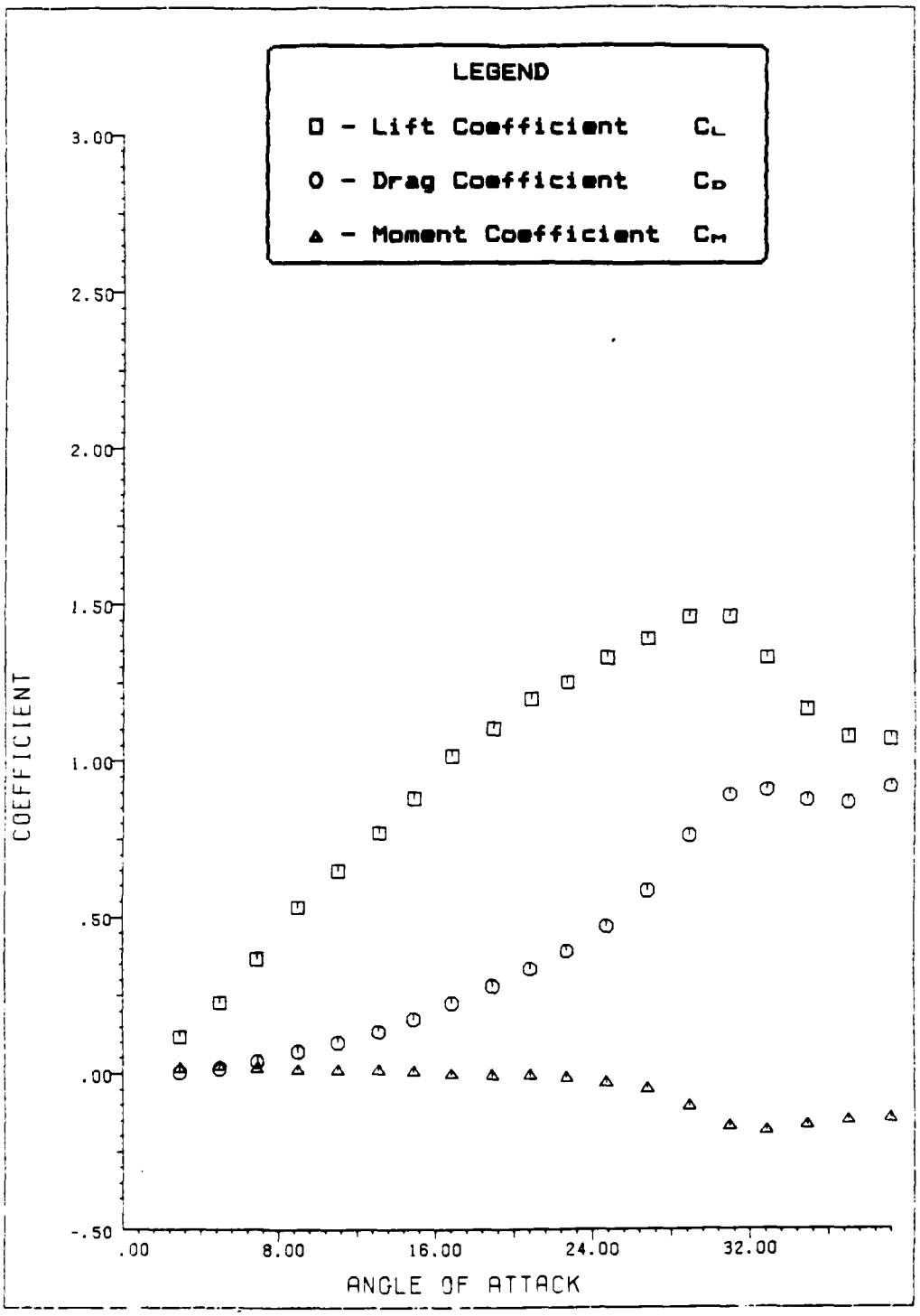

Figure 63. Data From Test Run 3 - 10

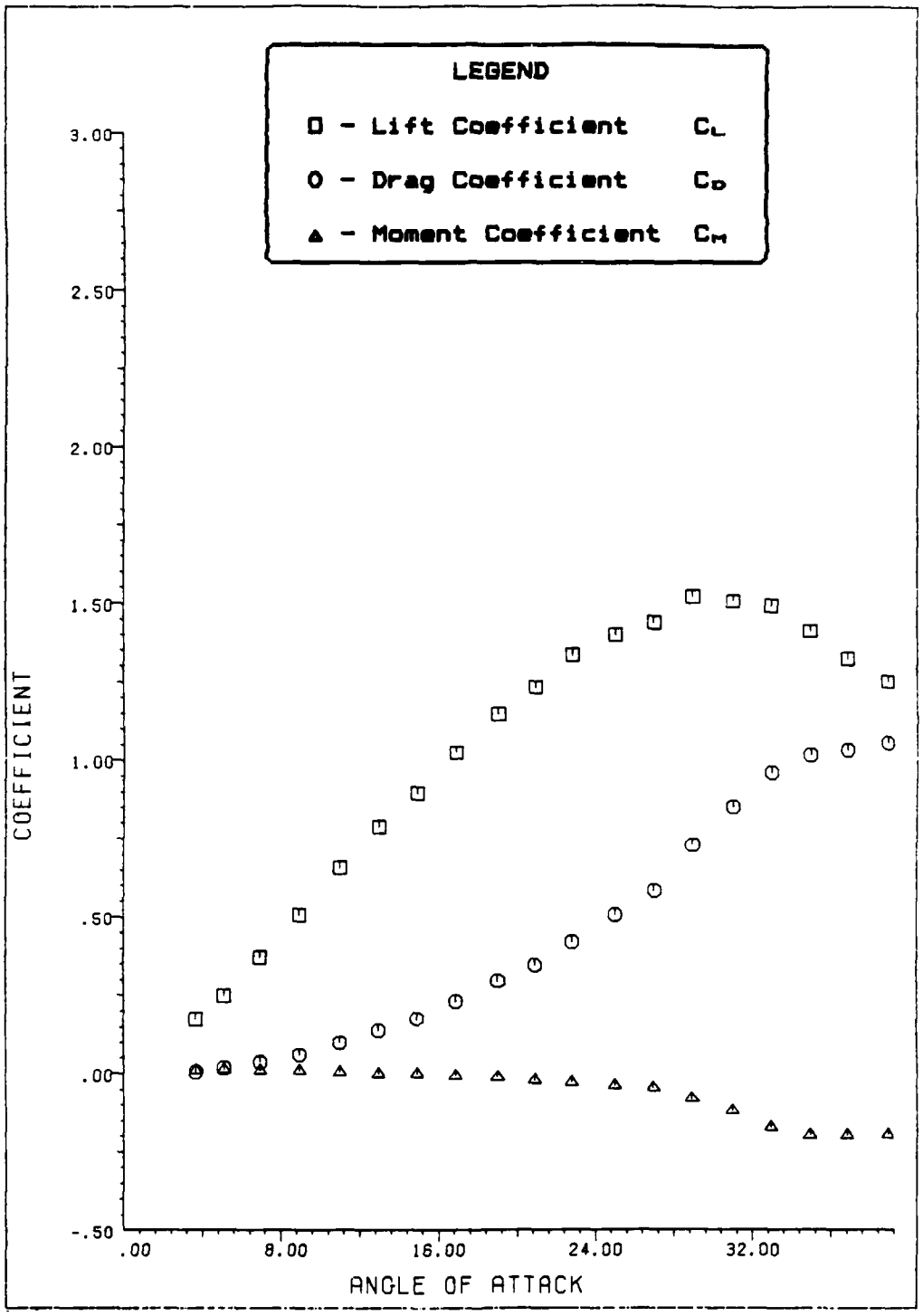

Figure 64. Data From Test Run 3 - 11

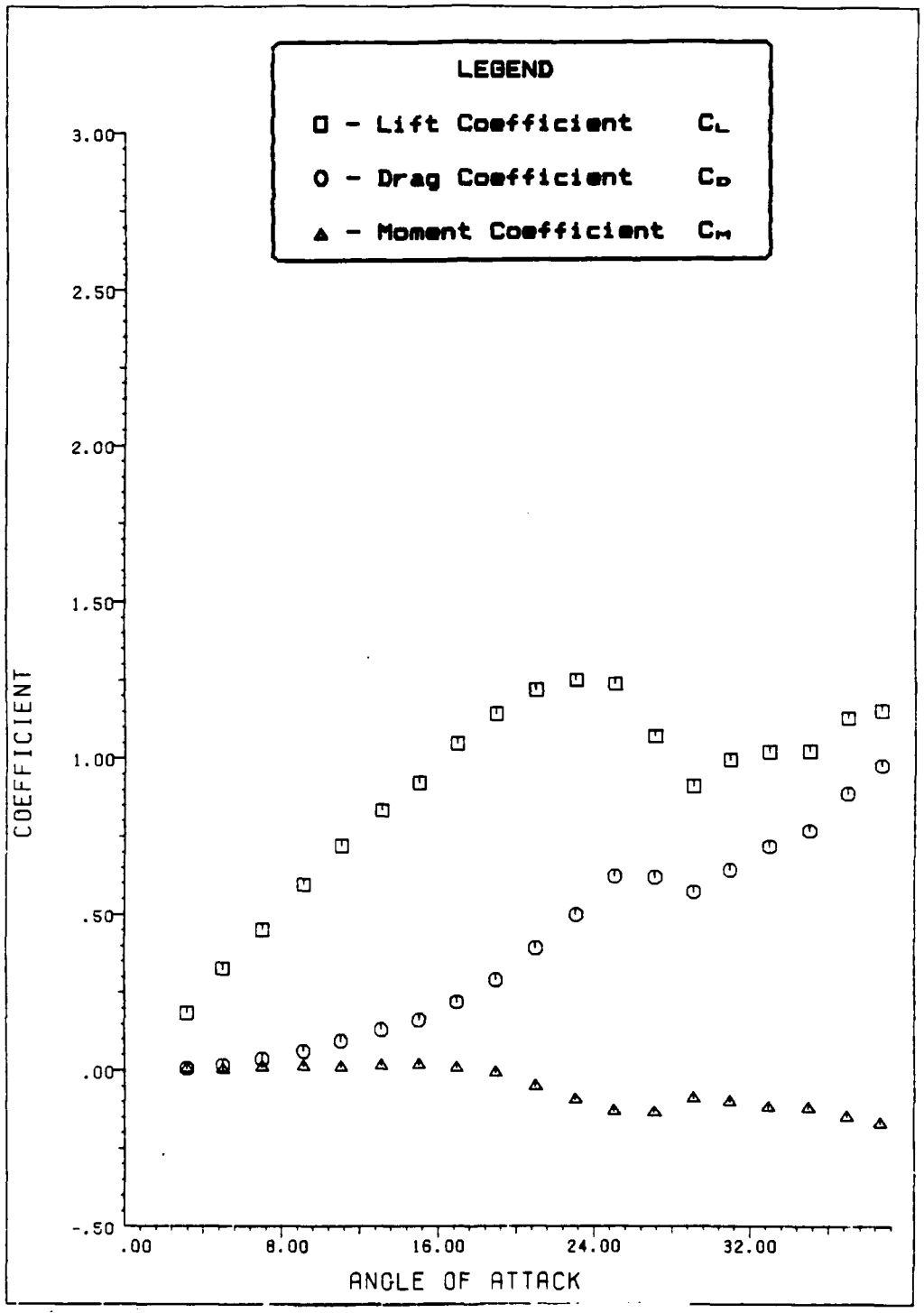

Figure 65. Data From Test Run 3 - 13

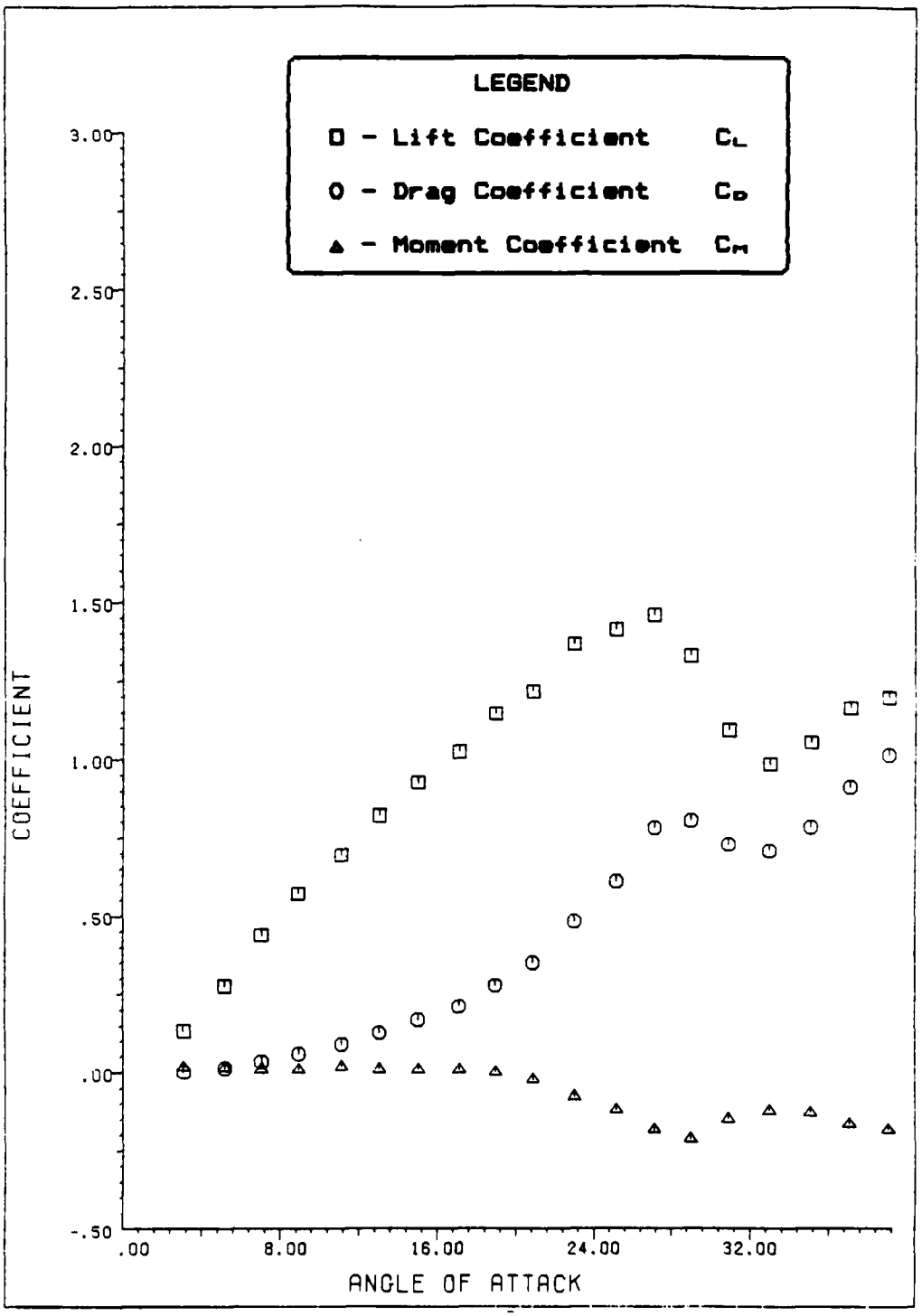

Figure 66. Data From Test Run 3 - 14

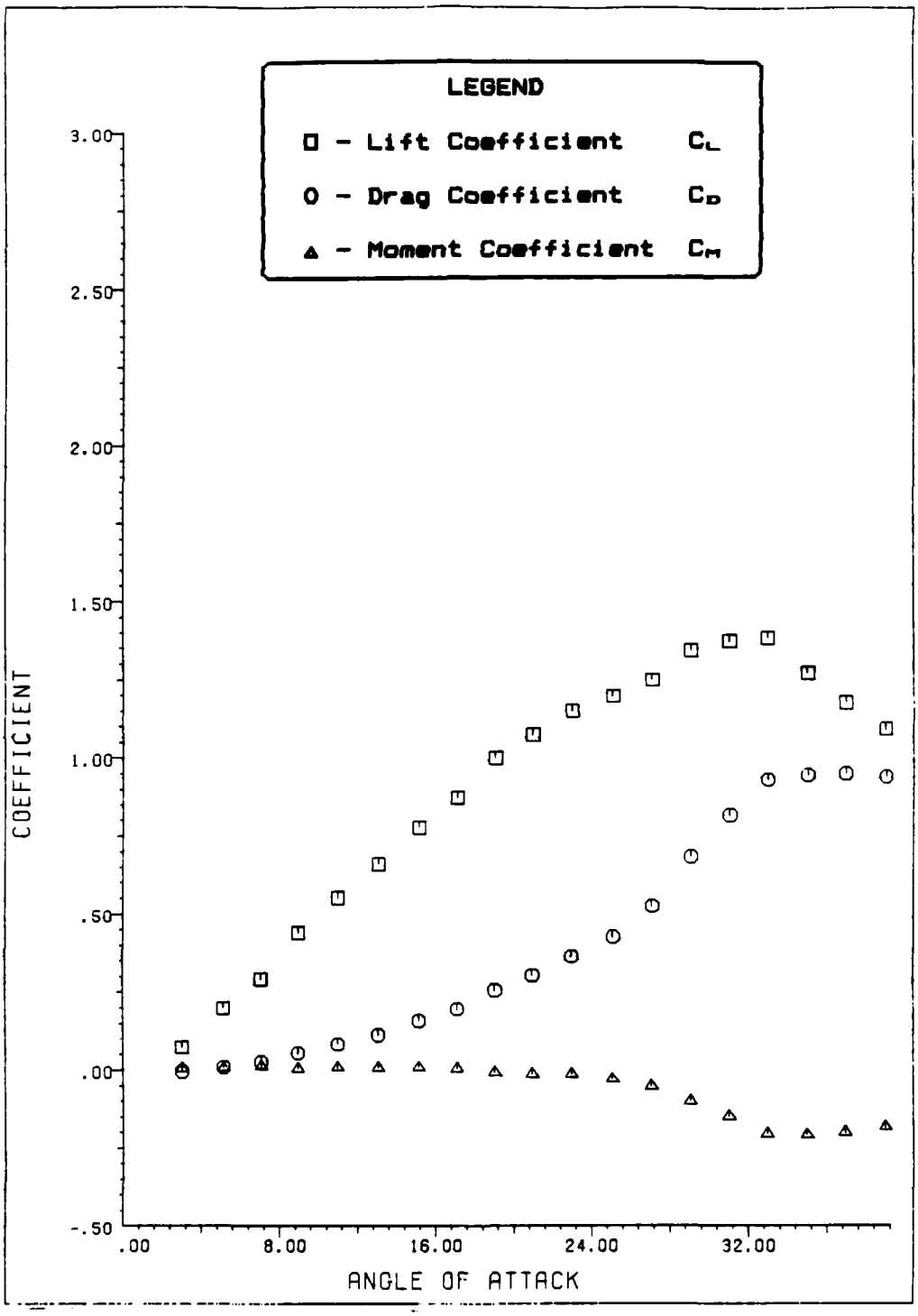

Figure 67. Data From Test Run 3 - 15

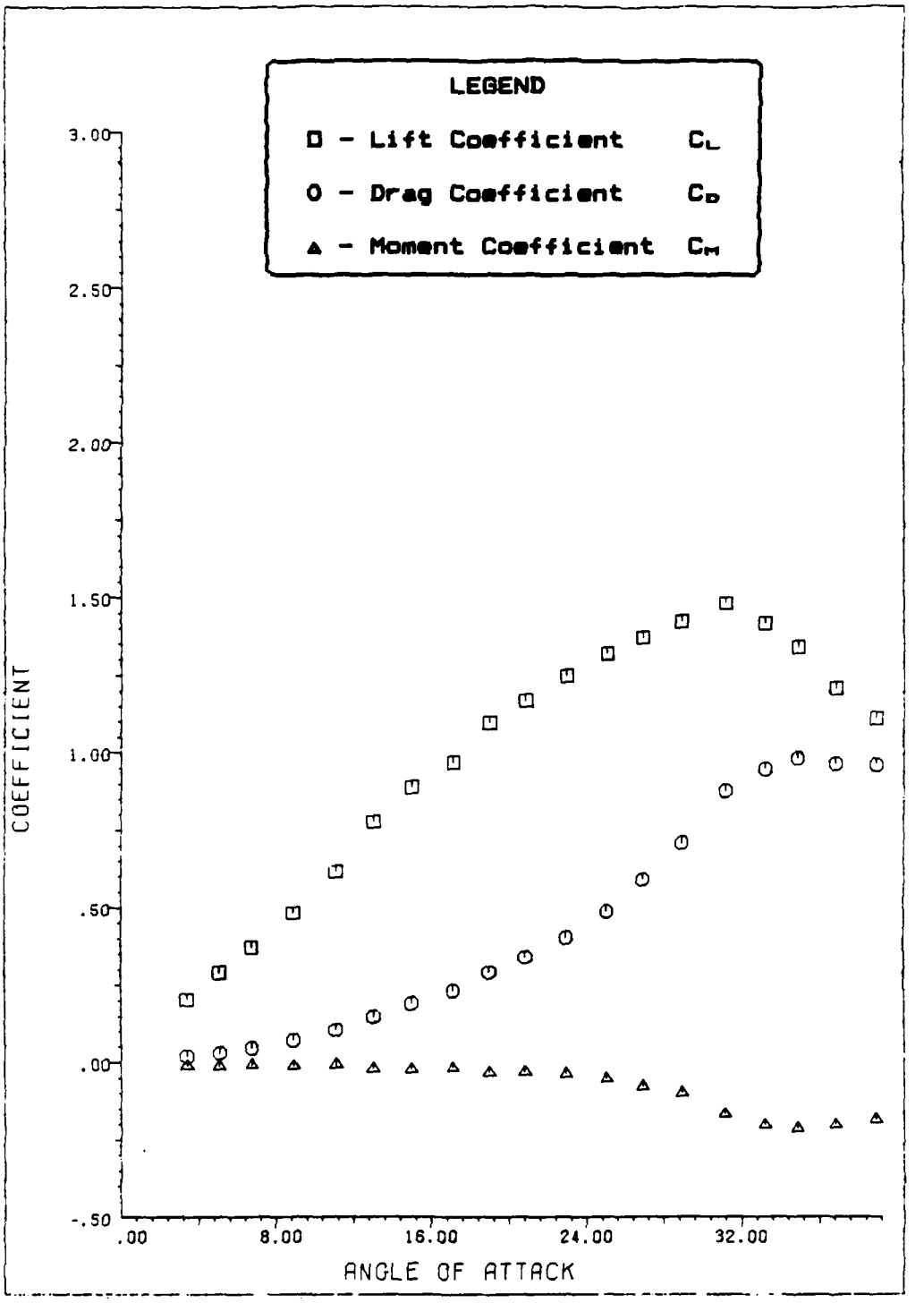

Figure 68. Data From Test Run 3 - 16

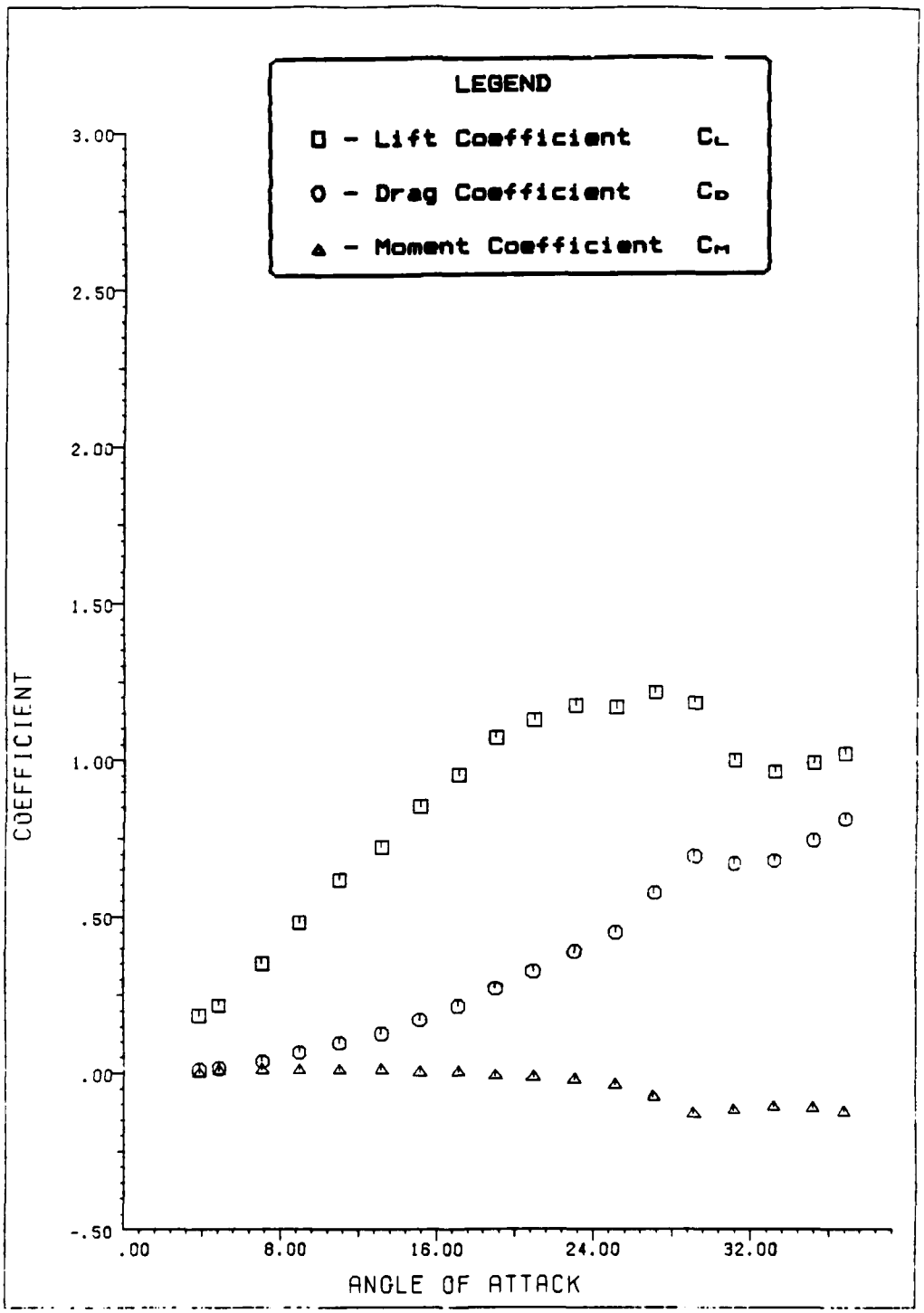

Figure 69. Data From Test Run 3 - 17

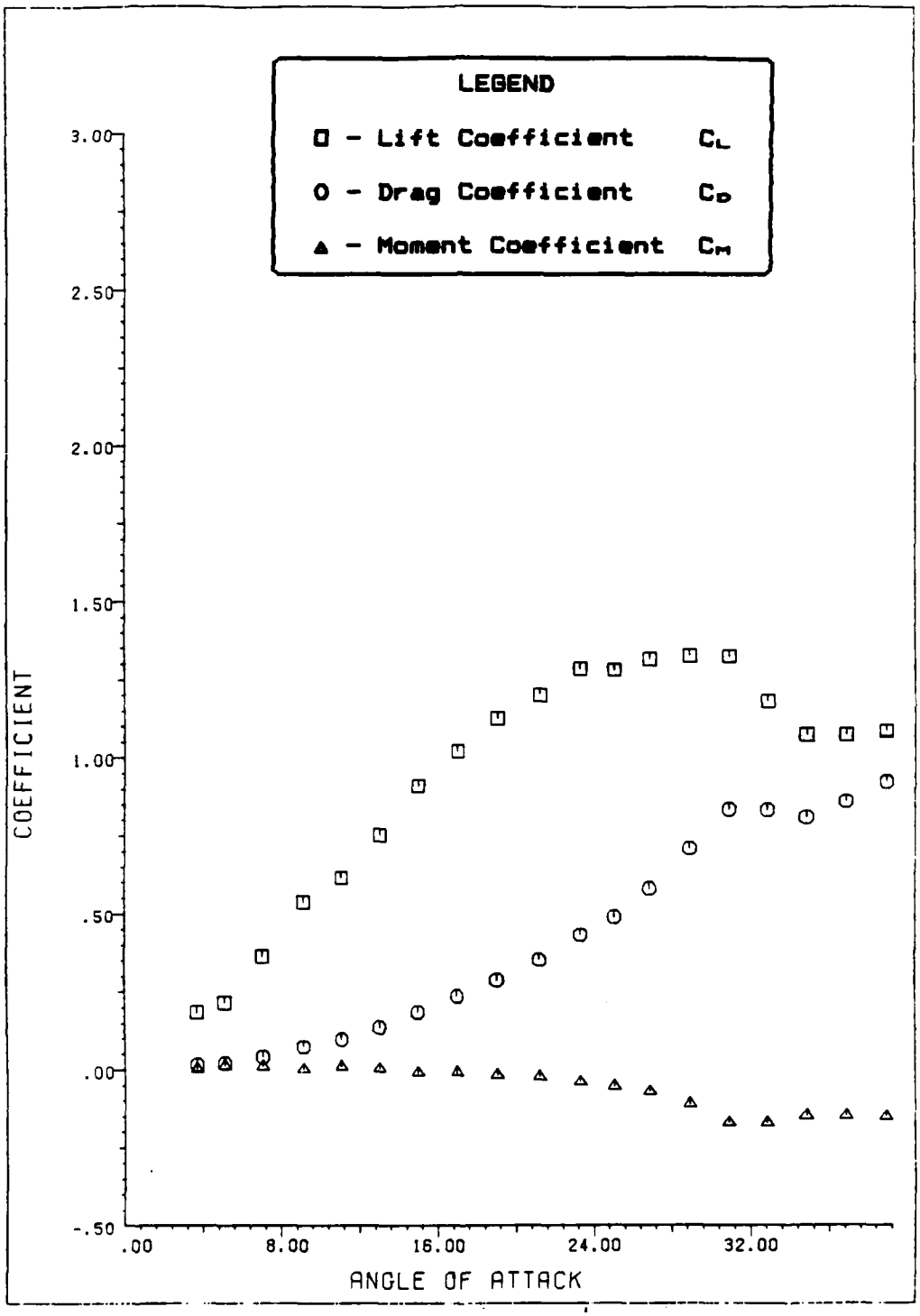

Figure 70. Data From Test Run 3 - 18

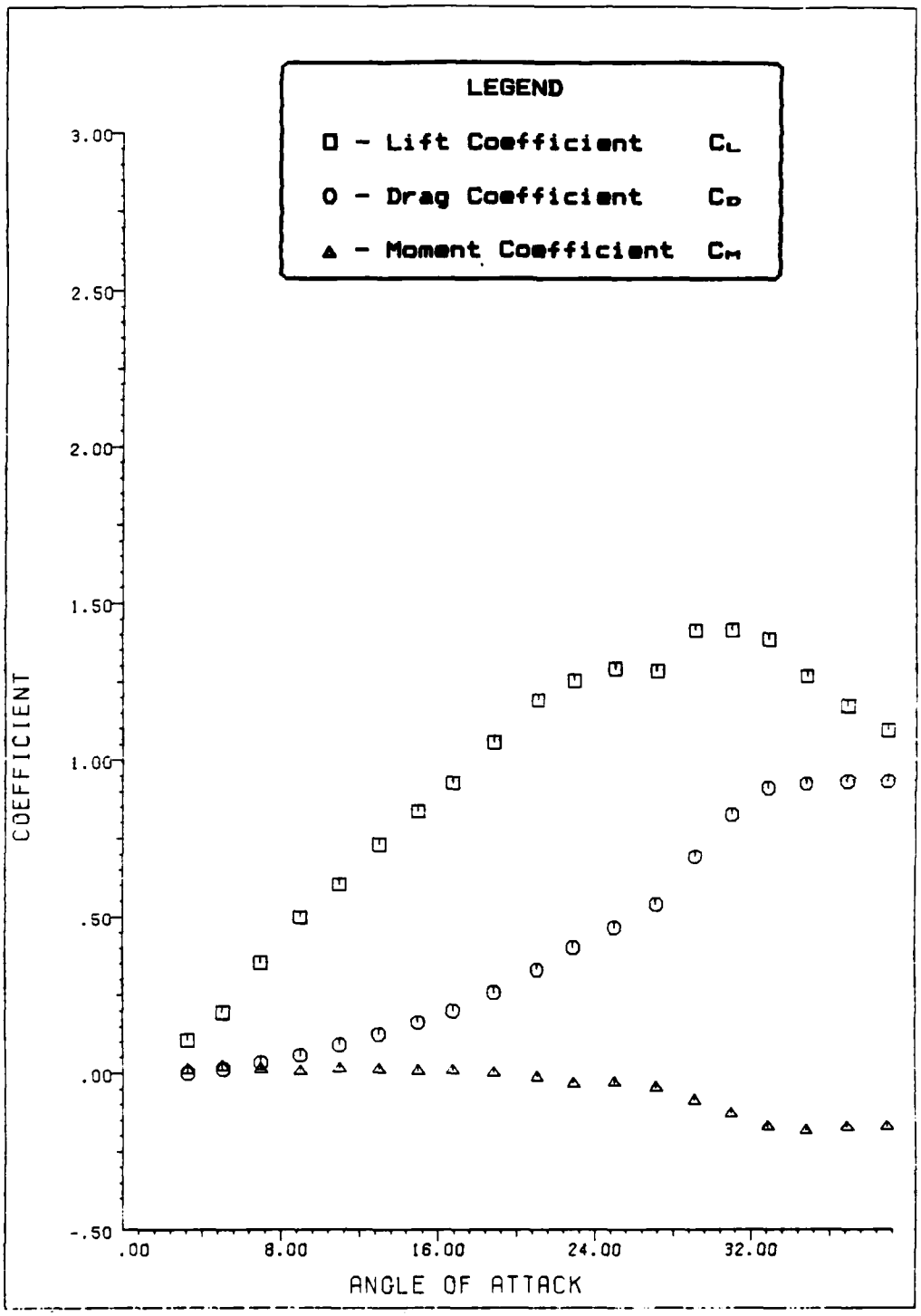

Figure 71. Data From Test Run 3 - 19

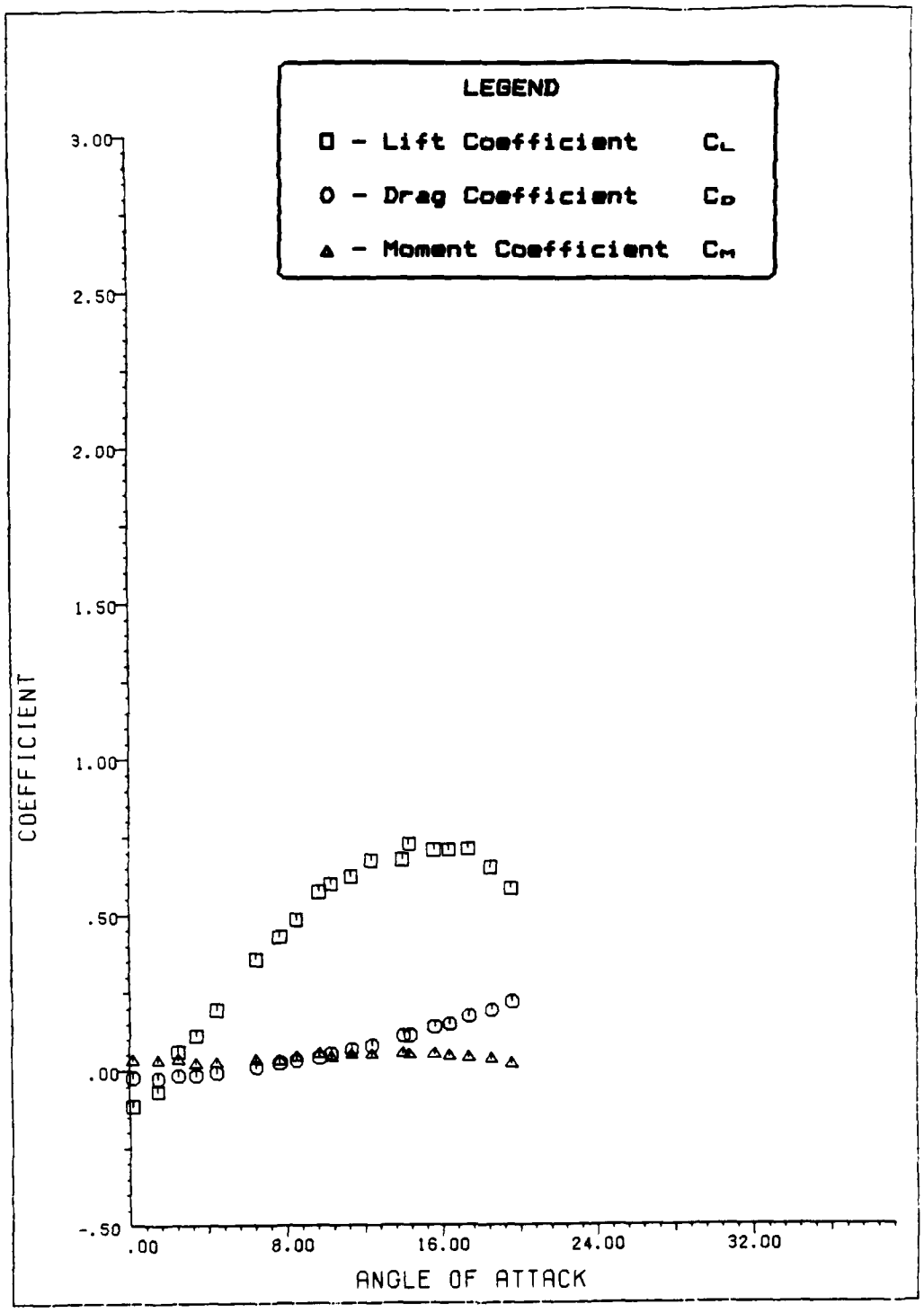

Figure 72. Data From Static Stall Test Runs Pitch Location #3 (.50c), V = 25.6 to 44.1 fps

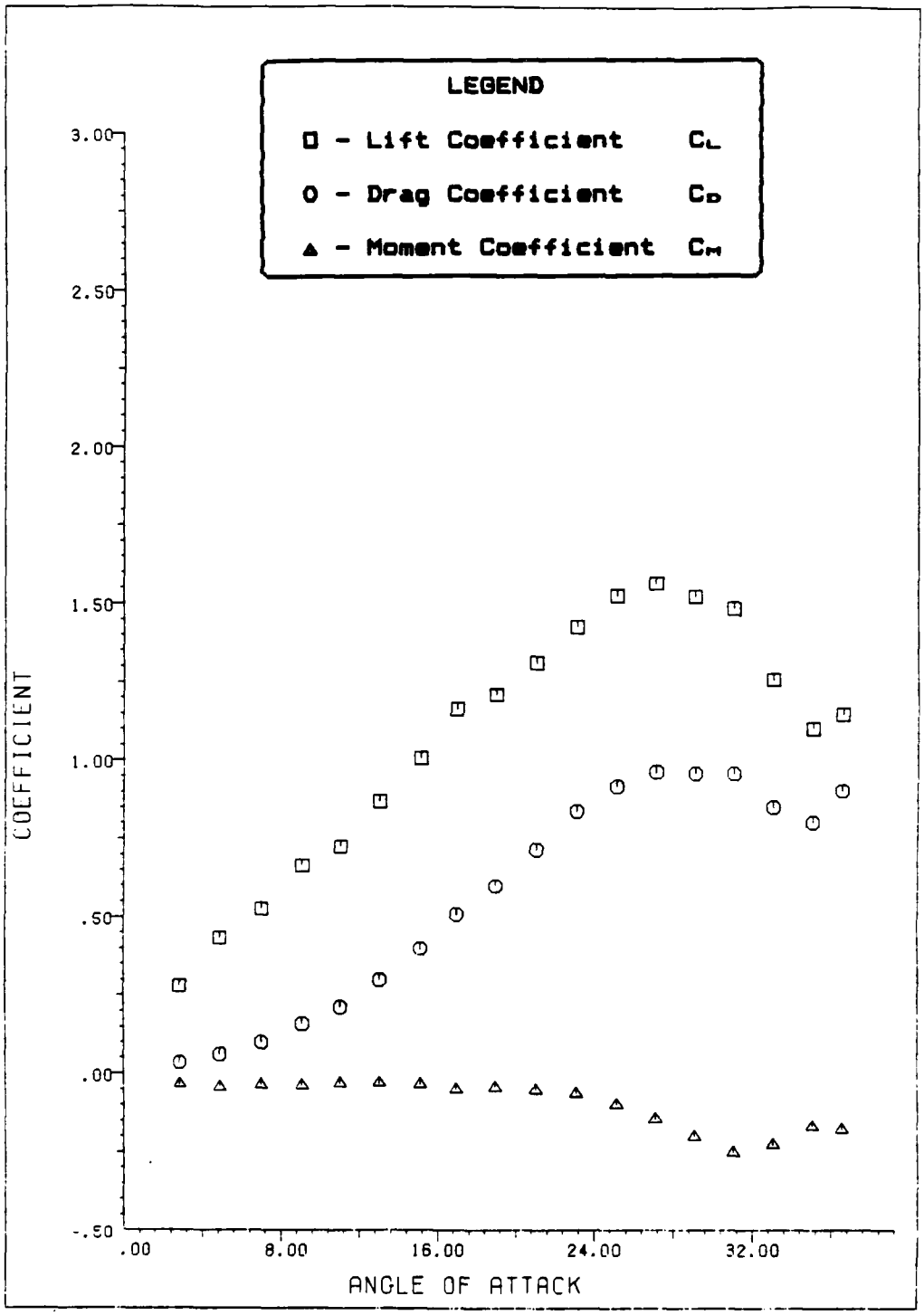

Figure 73. Data From Test Run 4 - 1

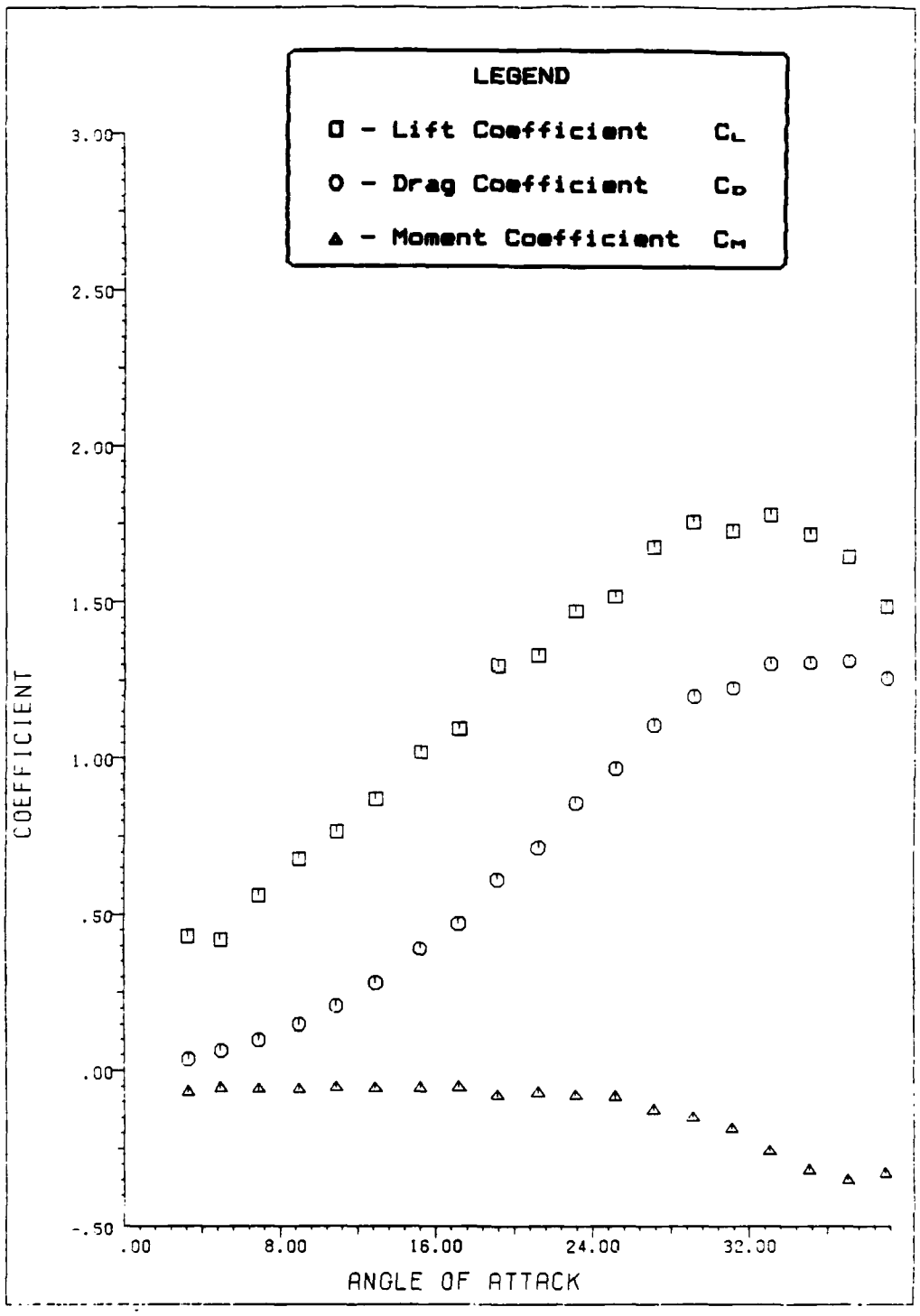

Figure 74. Data From Test Run 4 - 2

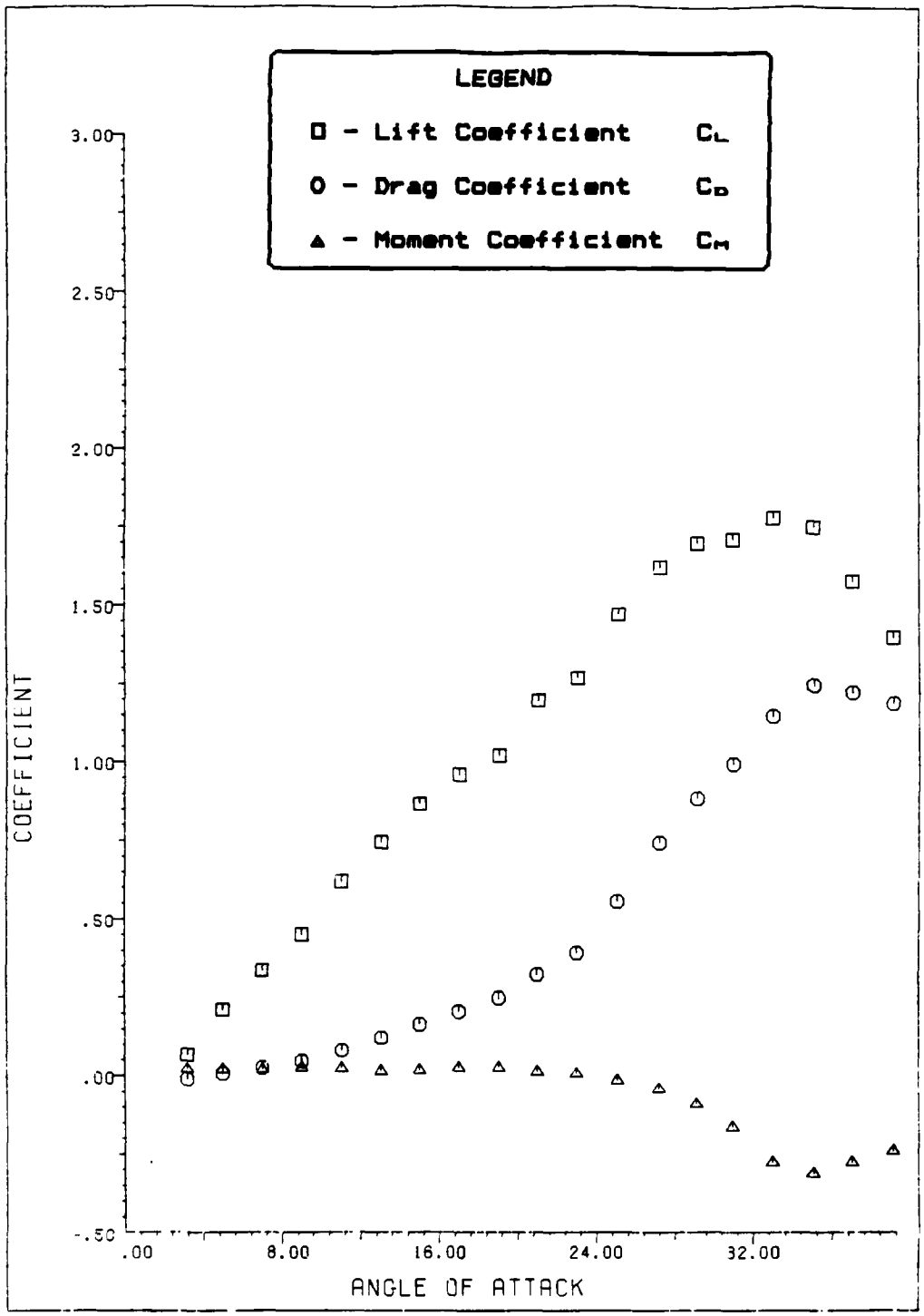

Figure 75. Data From Test Run 4 - 3

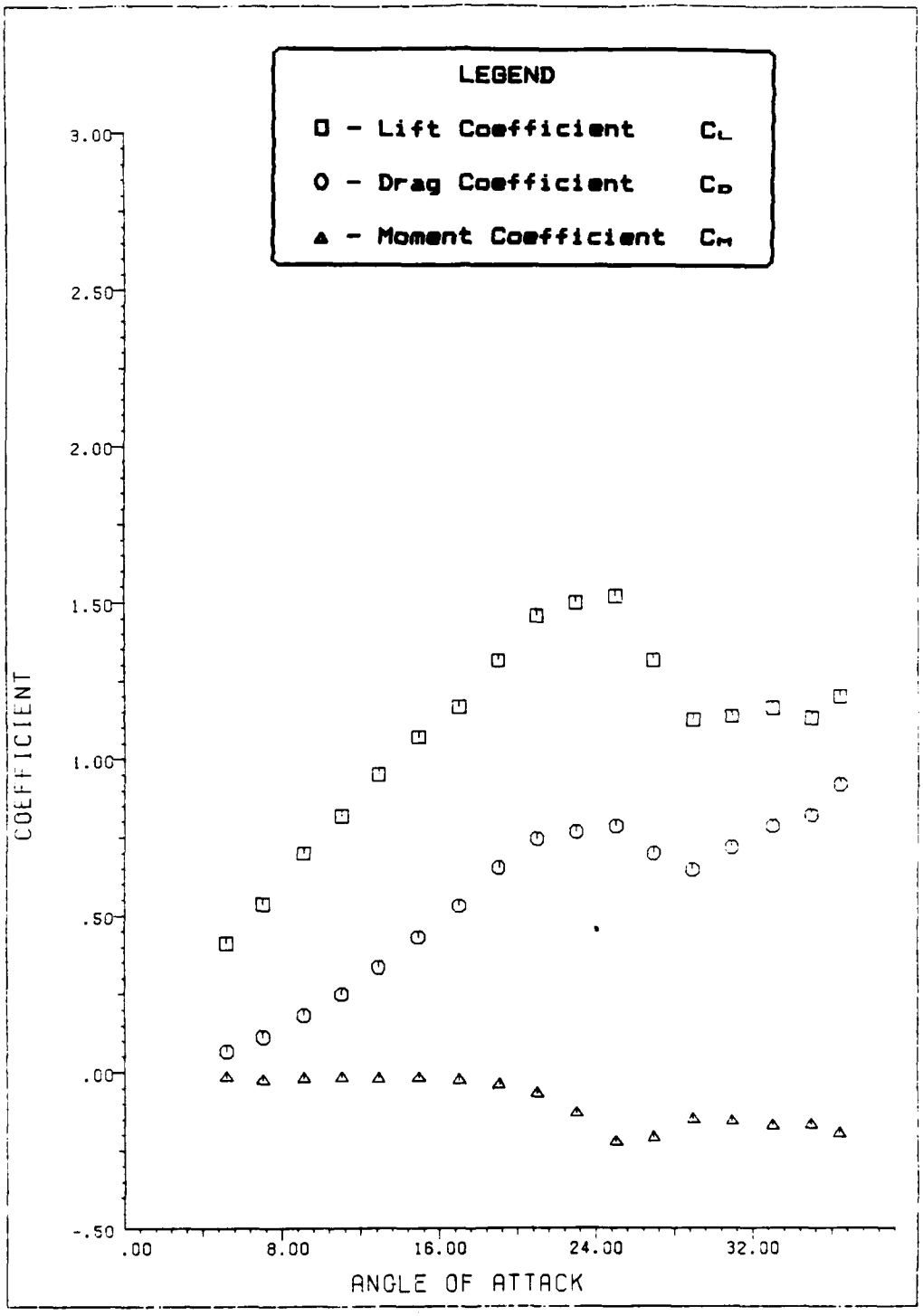

Figure 76. Data From Test Run 4 - 4

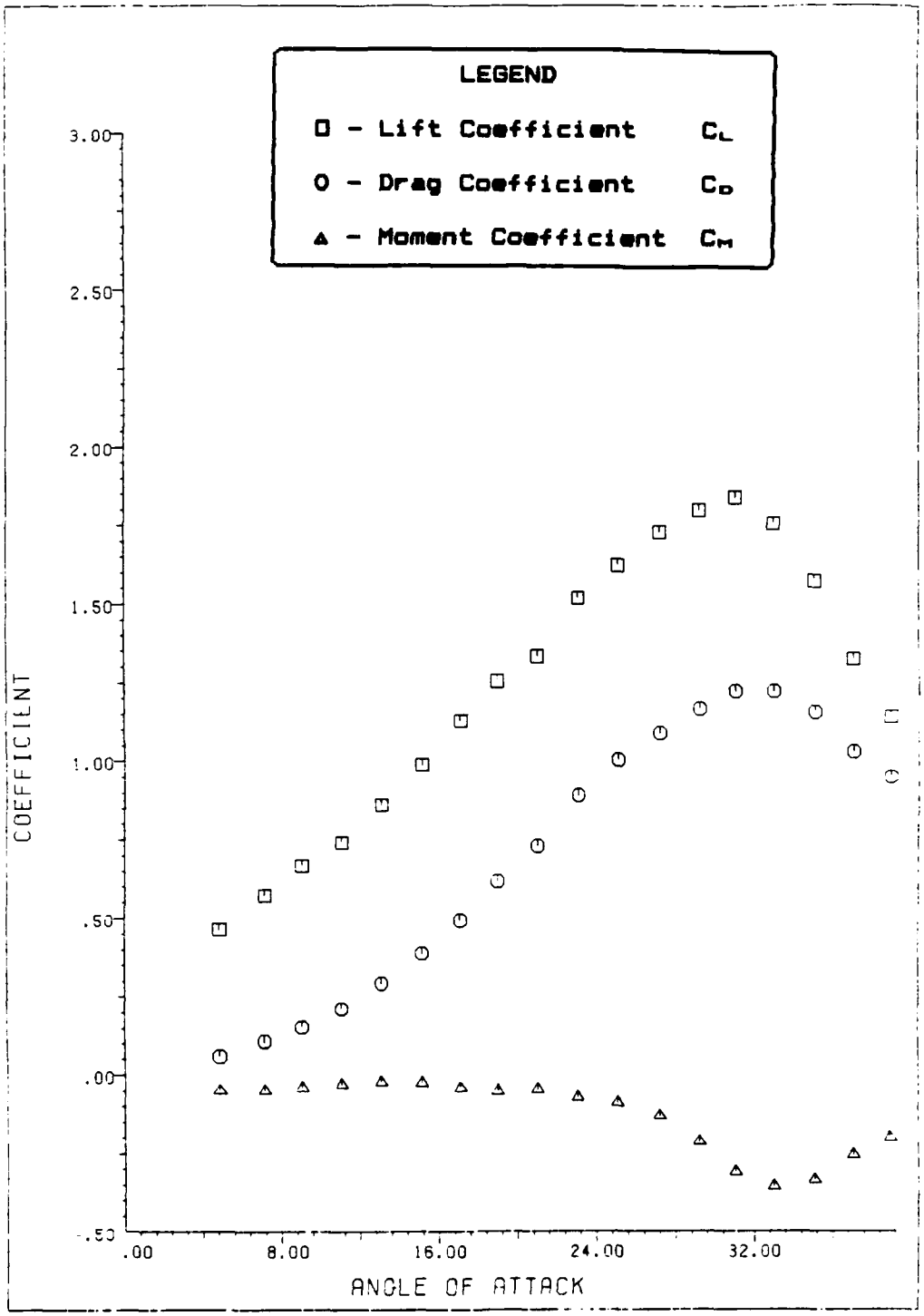

Figure 77. Data From Test Run 4 - 5

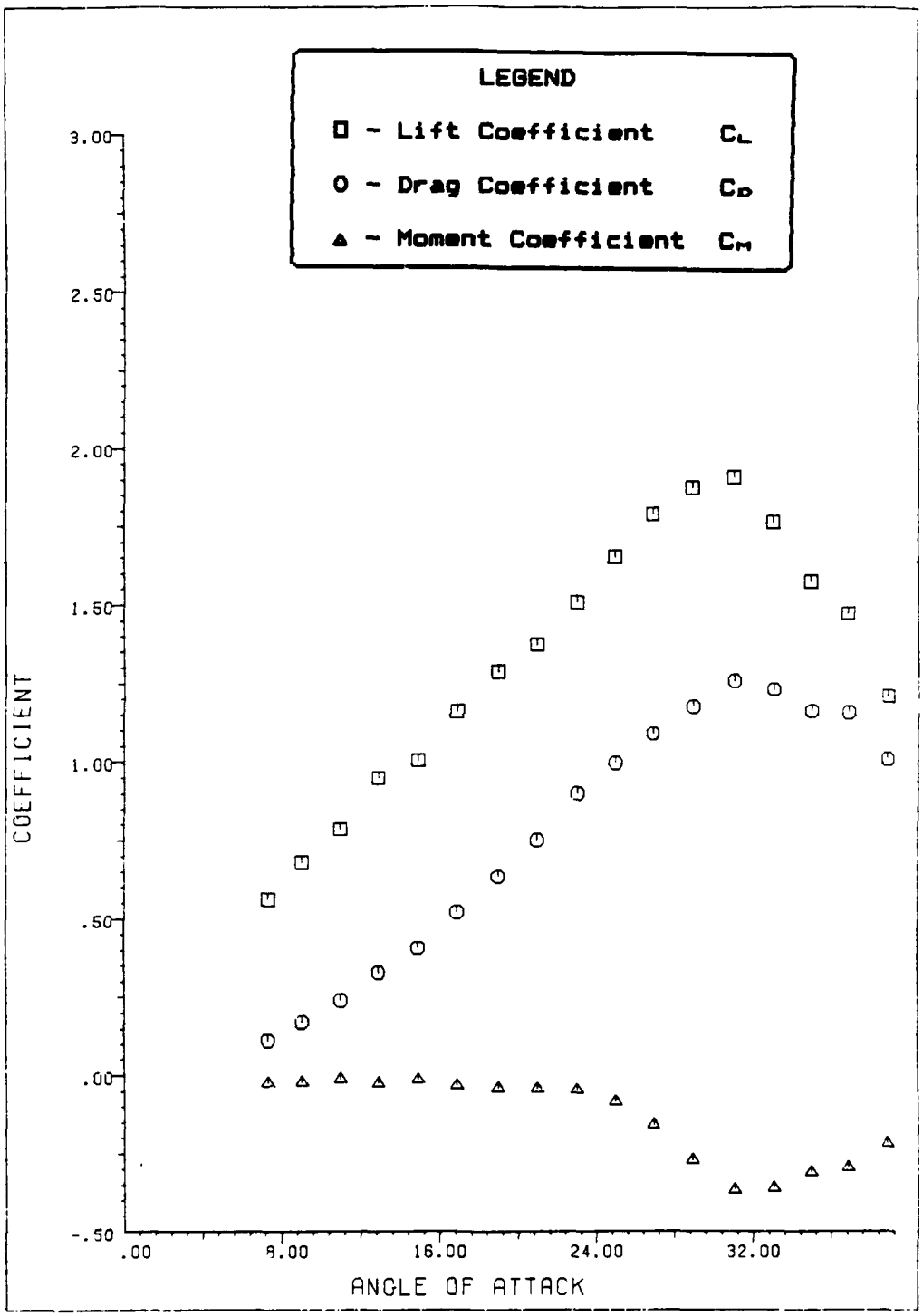

Figure 78. Data From Test Run 4 - 6

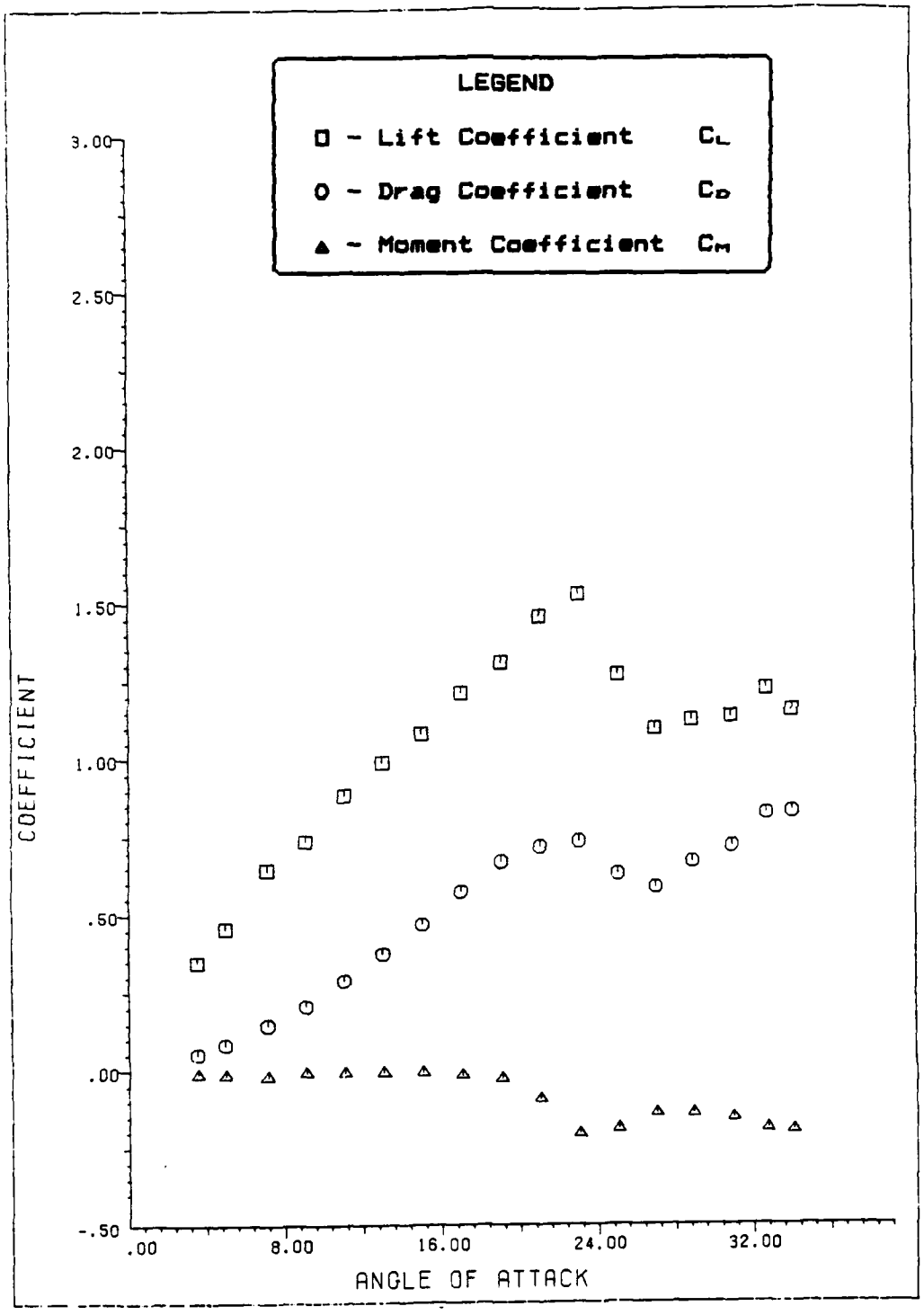

Figure 79. Data From Test Run 4 - 7

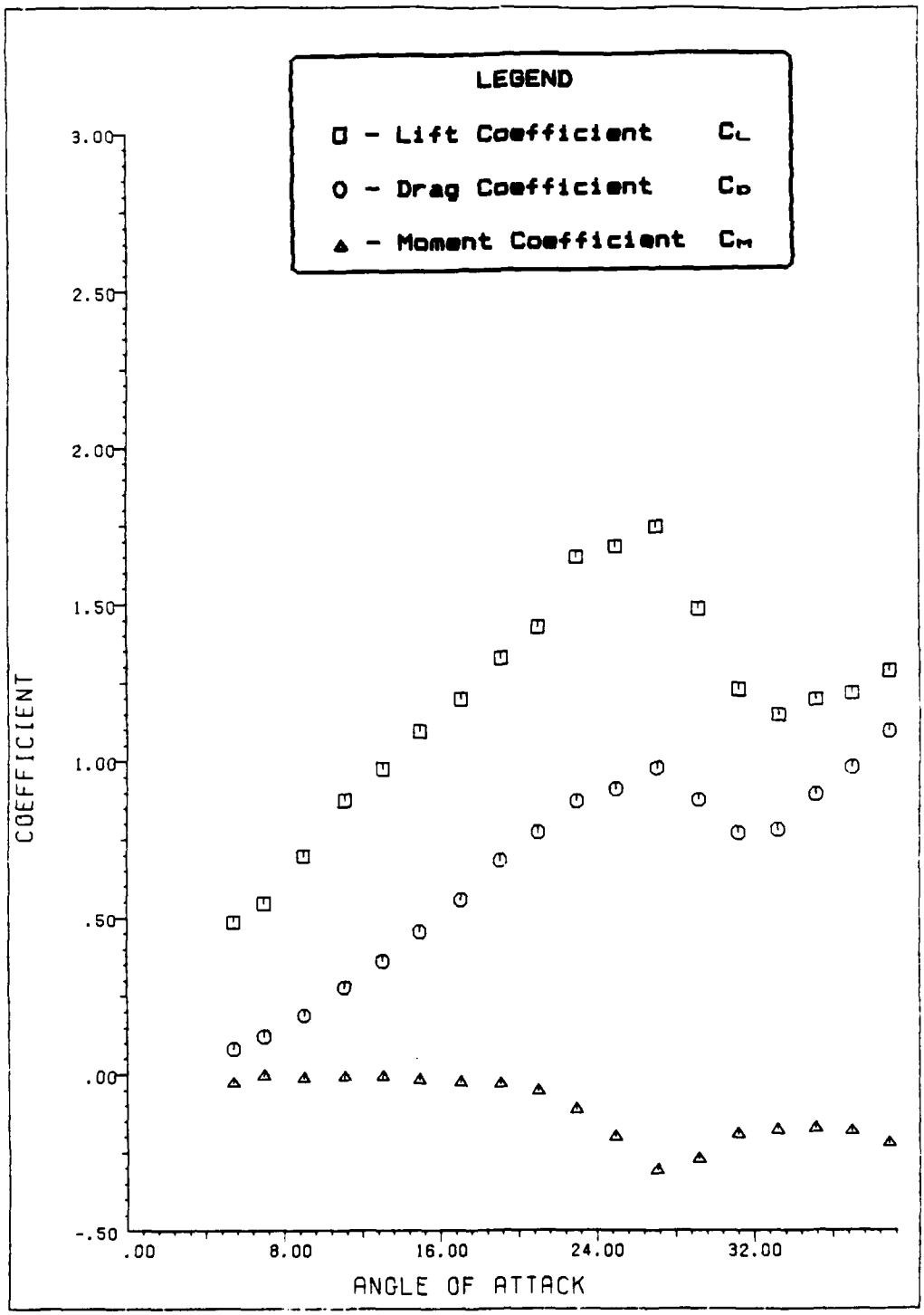

Figure 80. Data From Test Run 4 - 8

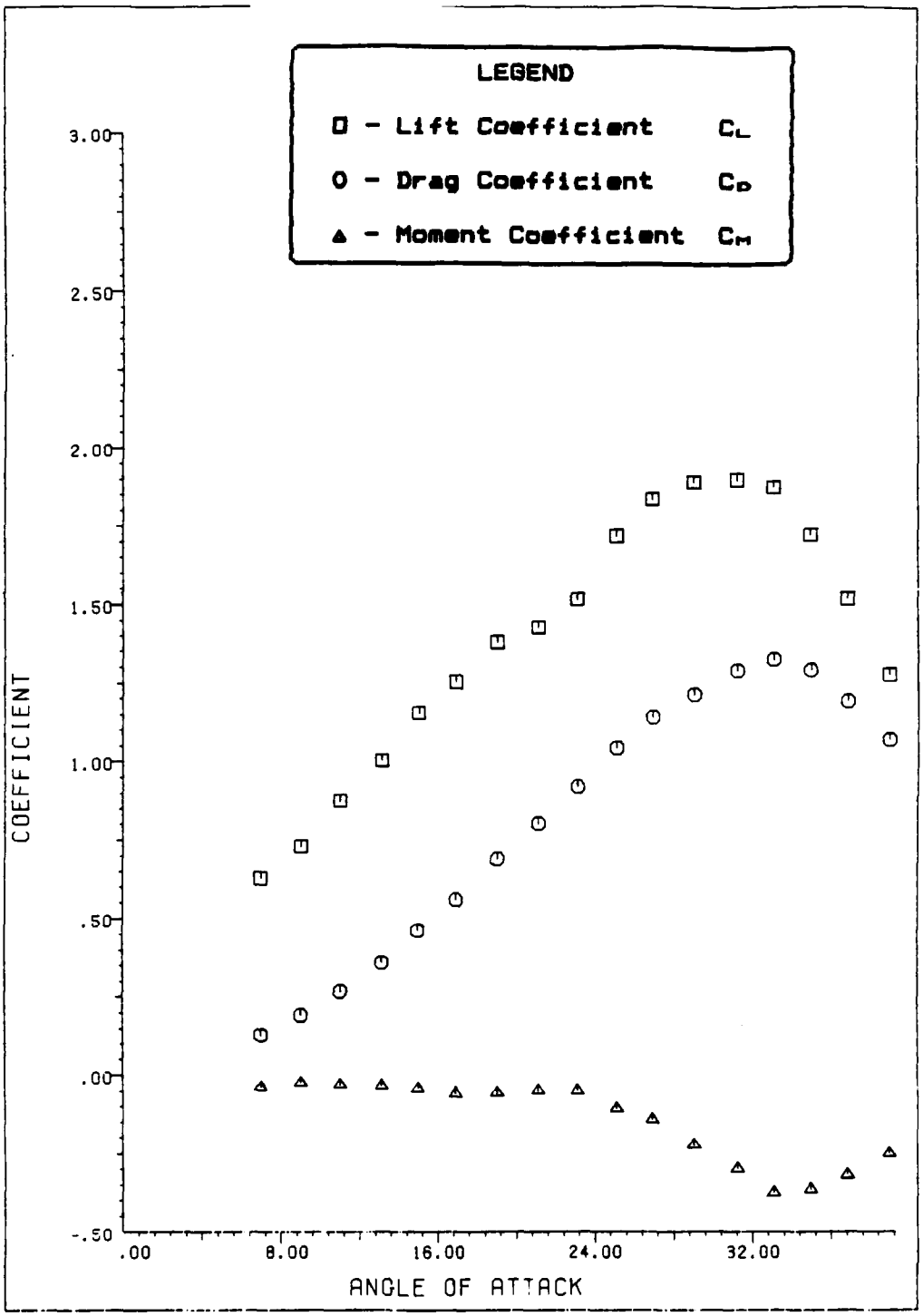

Figure 81. Data From Test Run 4 - 9

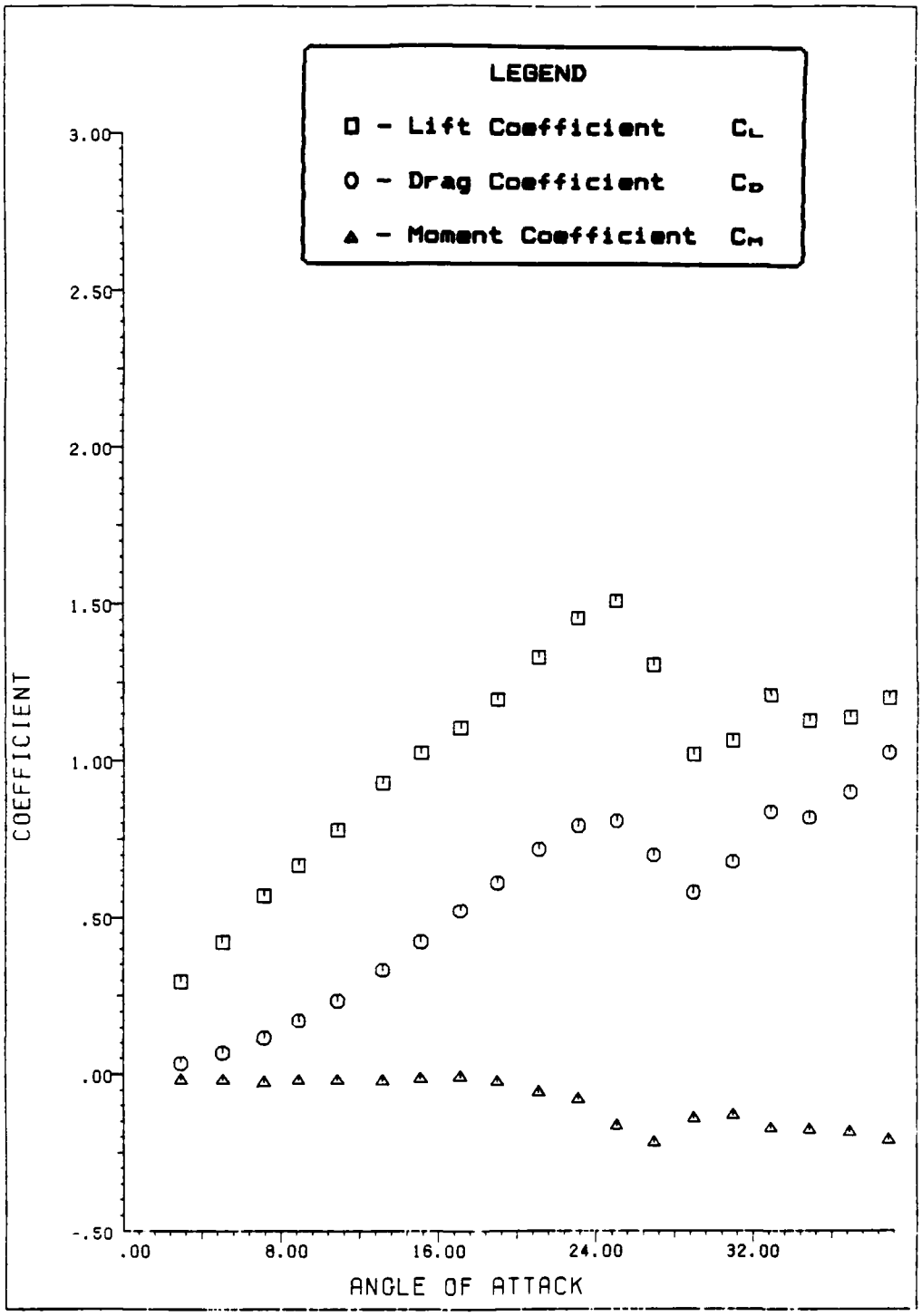

Figure 82. Data From Test Run 4 - 10

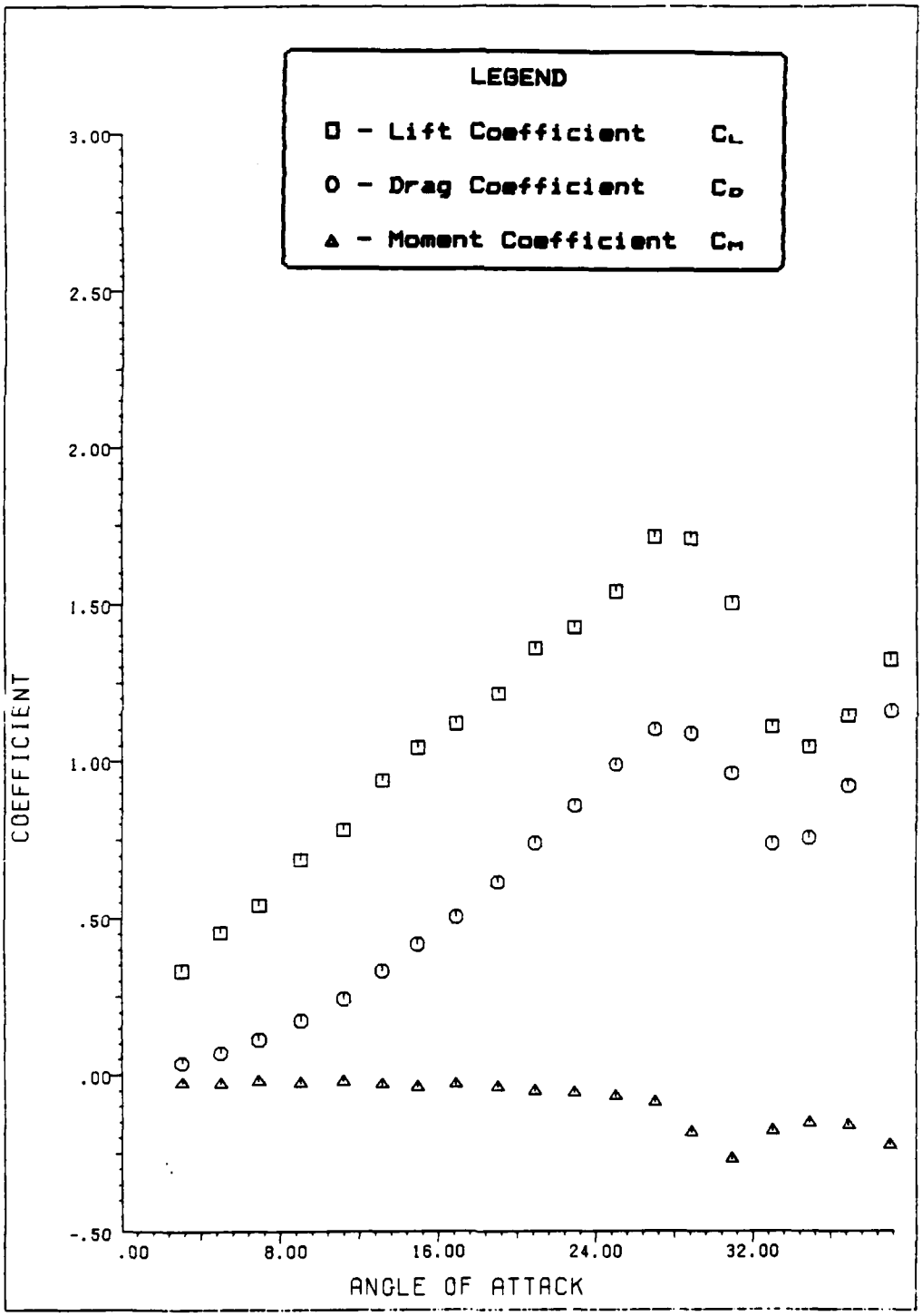

Figure 83. Data From Test Run 4 - 11

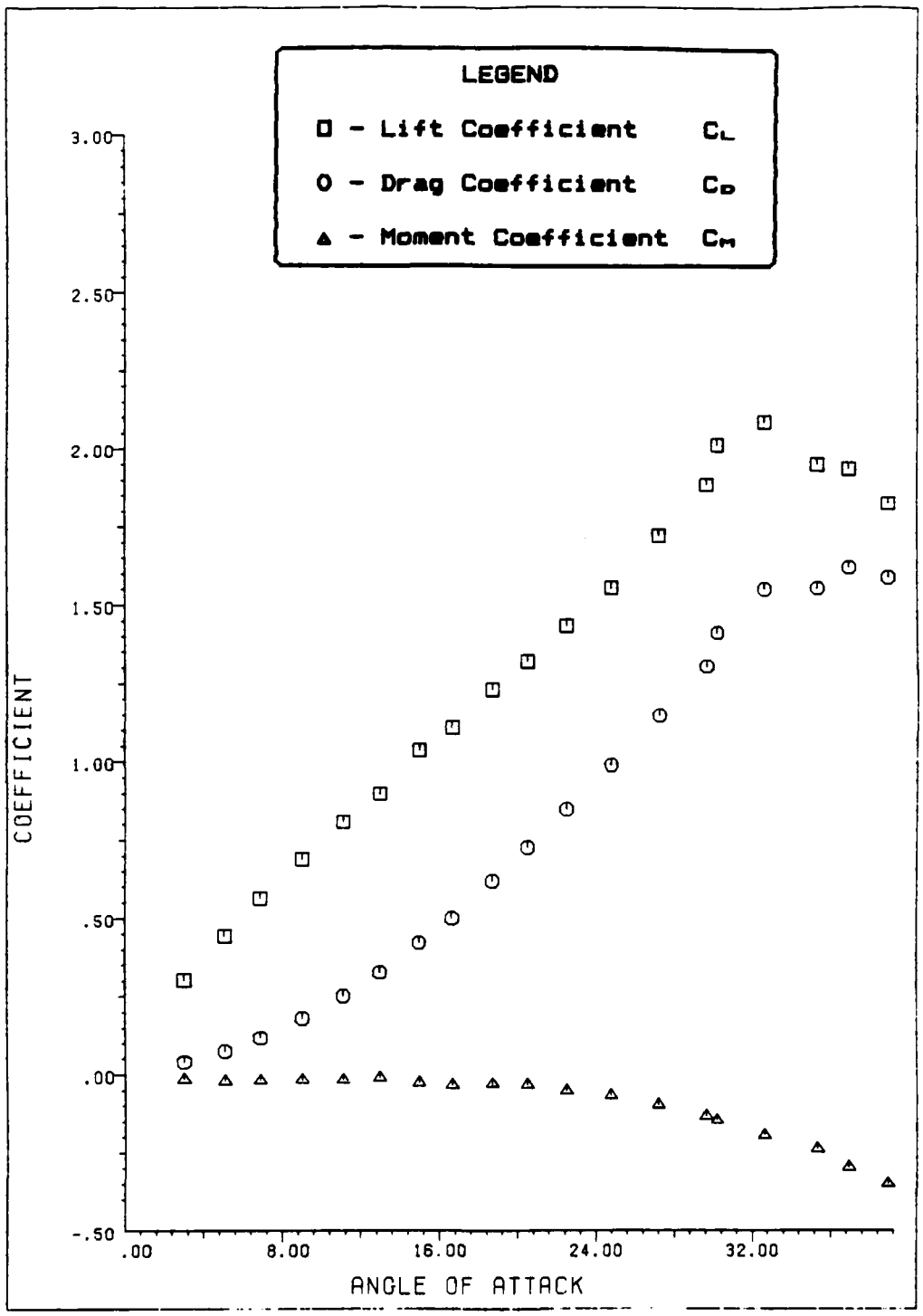

Figure 84. Data From Test Run 4 - 12

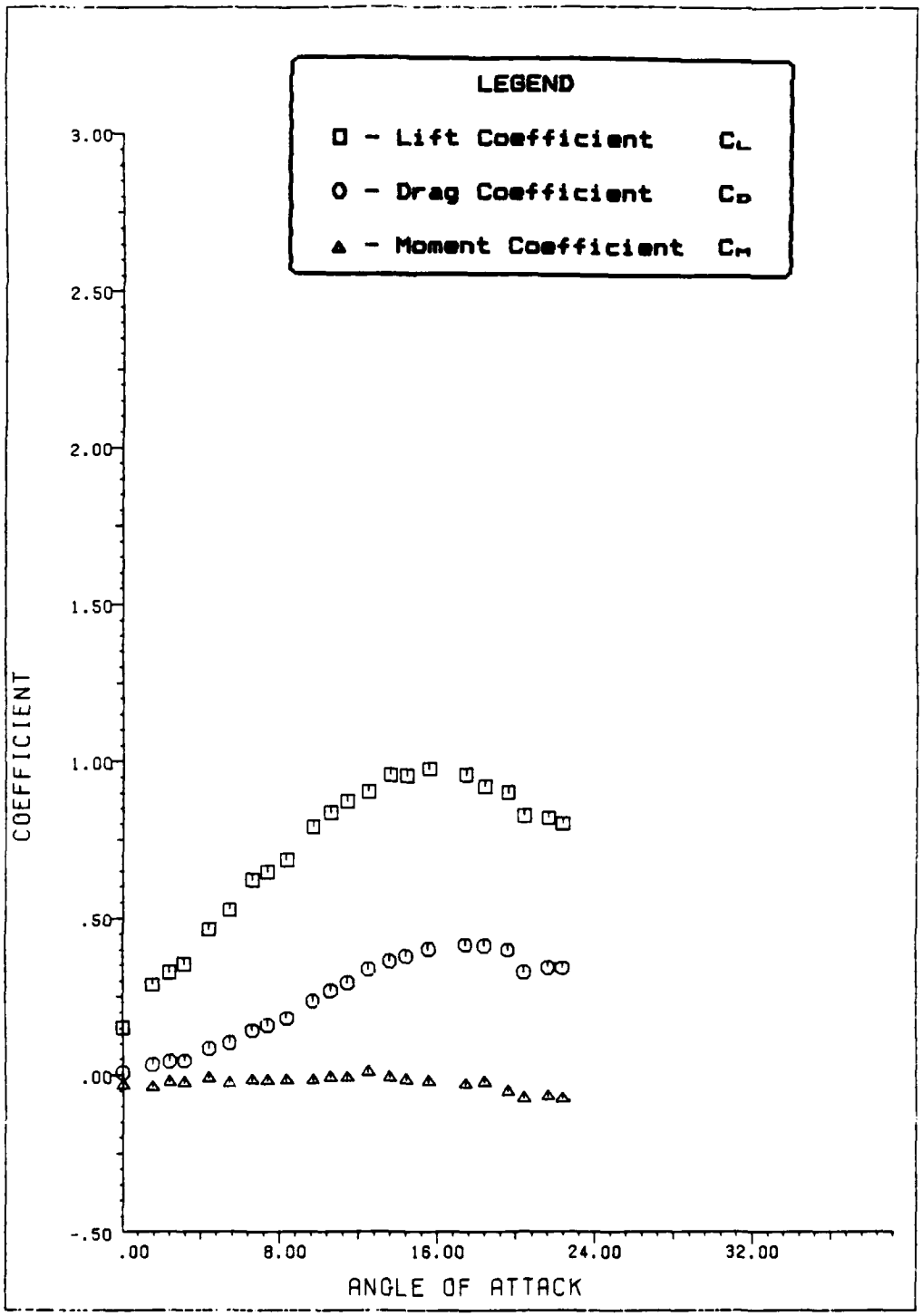

Figure 85. Data From Static Stall Test Runs
Pitch Location #4 (.61c), V = 25.7 to 39.8 fps

VITA

Robert L. Dimmick was born on 31 October 1956 in Cleveland, Ohio. He grew up in Lakewood, Ohio and upon graduation from Lakewood High School in 1974 he received an appointment to the United States Air Force Academy. He graduated from the Academy in 1978 with a Bachelor of Science Degree in Aeronautical Engineering. After graduation, he attended Undergraduate Navigator Training at Mather AFB, followed by KC-135 training at Castle AFB. He was subsequently assigned to Grissom AFB in 1979, where he flew KC/EC-135 aircraft as a navigator. He was reassigned to Wright-Patterson AFB in June of 1984 when he entered the School of Engineering, Air Force Institute of Technology.

Permanent Address: 1254 Virginia Avenue
Lakewood, Ohio 44107

UNCLASSIFIED

SECURITY CLASSIFICATION OF THIS PAGE

AD-A160 322

REPORT DOCUMENTATION PAGE

1a. REPORT SECURITY CLASSIFICATION UNCLASSIFIED	1b. RESTRICTIVE MARKINGS
2a. SECURITY CLASSIFICATION AUTHORITY	3. DISTRIBUTION/AVAILABILITY OF REPORT Approved for public release; distribution unlimited.
2b. DECLASSIFICATION/DOWNGRADING SCHEDULE	
4. PERFORMING ORGANIZATION REPORT NUMBER(S) AFIT/GAE/AA/85D-4	5. MONITORING ORGANIZATION REPORT NUMBER(S)
6a. NAME OF PERFORMING ORGANIZATION School of Engineering 6b. OFFICE SYMBOL (If applicable) AFIT/ENG	7a. NAME OF MONITORING ORGANIZATION
6c. ADDRESS (City, State and ZIP Code) AF Institute of Technology Wright-Patterson AFB, OH 45433	7b. ADDRESS (City, State and ZIP Code)
8a. NAME OF FUNDING/SPONSORING ORGANIZATION 8b. OFFICE SYMBOL (If applicable)	9. PROCUREMENT INSTRUMENT IDENTIFICATION NUMBER
8c. ADDRESS (City, State and ZIP Code)	10. SOURCE OF FUNDING NOS. PROGRAM ELEMENT NO. / PROJECT NO. / TASK NO. / WORK UNIT NO.
11. TITLE (Include Security Classification) See Box 19	
12. PERSONAL AUTHOR(S) Robert L. Dimmick, B.S., Capt, USAF	
13a. TYPE OF REPORT Thesis 13b. TIME COVERED FROM _____ TO _____	14. DATE OF REPORT (Yr., Mo., Day) 1985 December 15. PAGE COUNT 185
16. SUPPLEMENTARY NOTATION	

17. COSATI CODES			18. SUBJECT TERMS (Continue on reverse if necessary and identify by block number)
FIELD	GROUP	SUB. GR.	Stall, Dynamic Stall, Increased Lift, Ramp Angle of Attack, Pitch Location
20	04		

19. ABSTRACT (Continue on reverse if necessary and identify by block number)

Title: PITCH-LOCATION EFFECTS ON DYNAMIC STALL

Thesis Advisor: Eric J. Jumper, Lt Col, USAF

Approved for public release IAW AFR 190-1.
LYNN E. WOLAVER 16 JAN 86
Dean for Research and Professional Development
Air Force Institute of Technology (AFIT)
Wright-Patterson AFB OH 45433

20. DISTRIBUTION/AVAILABILITY OF ABSTRACT UNCLASSIFIED/UNLIMITED ☒ SAME AS RPT. ☐ DTIC USERS ☐	21. ABSTRACT SECURITY CLASSIFICATION UNCLASSIFIED	
22a. NAME OF RESPONSIBLE INDIVIDUAL Eric J. Jumper, Lt Col, USAF	22b TELEPHONE NUMBER (Include Area Code) (513)-255-2998	22c. OFFICE SYMBOL AFIT/ENY

DD FORM 1473, 83 APR EDITION OF 1 JAN 73 IS OBSOLETE.

SECURITY CLASSIFICATION OF THIS PAGE

Experimental investigations were conducted in the AFIT Smoke Tunnel to study the effects of pitch-location on dynamic stall. A NACA 0015 airfoil was rotated about four different locations at a constant angular rate and digital position and pressure information were recorded. This information was then converted into airfoil pressure distributions and integrated numerically to obtain airfoil force coefficients. Results of this investigation showed a direct relationship between the dynamic-stall angle of attack and the non-dimensionalized angular rotation rate, $_{ND}$, defined as one-half the airfoil chord length times the angular rate divided by the freestream velocity. Based on the three rotation points forward of the mid-chord, it was also shown that dynamic stall is delayed as the pitch location is moved aft from the leading edge. Experimental data was obtained for pitch locations of .08c, .25c, .50c and .61c and non-dimensional angular rates between .011 and .065.

END

FILMED

3-86

DTIC